DUMAND-80

PROCEEDINGS of the

1980 INTERNATIONAL DUMAND SYMPOSIUM
July 24 - August 2

HAWAII-DUMAND CENTER

Edited by V.J. Stenger

VOLUME II

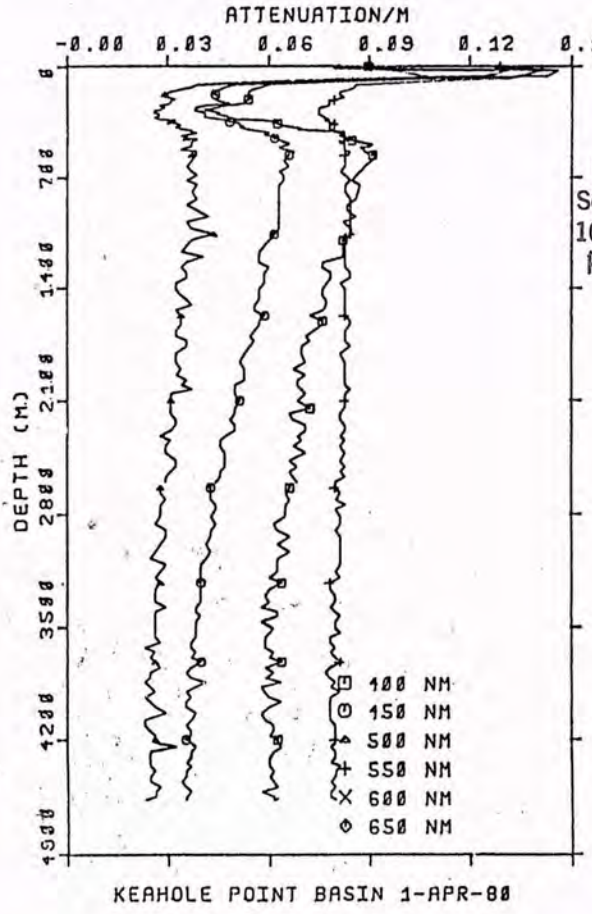

UNIVERSITY OF HAWAII AT MANOA
SEA GRANT COLLEGE PROGRAM
2525 CORREA ROAD, HIG 238
HONOLULU, HAWAII 96822

UNIHI-SEAGRANT-BB-79-02

DUMAND · 80

Proceedings of the

1980 INTERNATIONAL DUMAND SYMPOSIUM
July 24 - August 2

HAWAII-DUMAND CENTER

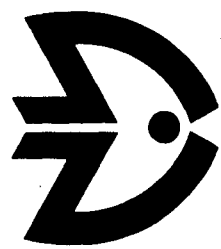

Edited by

V. J. Stenger

VOLUME II

Published by the HAWAII DUMAND CENTER

2505 Correa Road, Honolulu, HI 96822

First Published February, 1981

Hawaii DUMAND Center, University of Hawaii

2505 Correa Road, Honolulu, Hawaii 96822

1980 International Symposium and Workshop at Hawaii DUMAND Center, Honolulu, Hawaii July 24 - August 2, 1980

Sponsored by:

University of Hawaii, Manoa
University of Hawaii Foundation
Marine Affairs Coordinator, State of Hawaii
U.S. Department of Energy - High Energy Physics Program
U.S. National Oceanic and Atmospheric Administration - Sea Grant
U.S. Office of Naval Research

SYMPOSIUM ORGANIZATION

Conference Director: Prof. John G. Learned, Hawaii DUMAND Center

Organizing Committee:

Chairman: Prof. Arthur Roberts, Hawaii DUMAND Center
Prof. V. Z. Peterson, University of Hawaii, Principal Investigator
Dr. Howard Blood, Naval Ocean Systems Center, San Diego
Prof. Ugo Camerini, University of Wisconsin
Prof. David Cline, University of Wisconsin
Prof. David Eichler, University of Maryland
Prof. Robert March, University of Wisconsin
Prof. R. Oakes, Northwestern University
Prof. F. Reines, University of California, Irvine
Prof. D. Schramm, University of Chicago
Dr. M. M. Shapiro, Naval Research Laboratory, Washington
Adm. N. Sonenschein, Global Marine Dev. Co., Newport Beach, CA (ret.)
Prof. L. Sulak, University of Michigan
Mr. H. Talkington, Naval Ocean Systems Center, San Diego

Local Arrangements Committee:

Chairman: Prof. V. Stenger
Prof. J. E. Andrews
Prof. H. Bradner
Prof. J. Learned
Prof. E. Ma
Dr. D. Moore
Prof. A. Parvulescu
Prof. V. Z. Peterson
Prof. A. Roberts
Dr. A. Stockton
Mr. G. Wilkins

DUMAND - Deep Underwater Muon and Neutrino Detector

The Proceedings were prepared at the Hawaii DUMAND Center, Department of Physics and Astronomy, under U.S. DOE Research Contract DE-AC03-76ER00511, with the University of Hawaii, Honolulu, Hawaii USA.

Volume II

Page

V. Underground Experiments

VI. Neutrino Mass and Oscillations

VII. Neutrino Astrophysics and Stellar Collapse

Page

VIII. High Energy Physics and Astrophysics

V. Underground Experiments

The Kolar Gold Field Baryon Stability Experiment

M.R.Krishnaswamy,M.G.K.Menon,N.K.Mondal and V.S.Narasimham
Tata Institute of Fundamental Research,Bomhay,India
and
Y.Hayashi,N.Ito,S.Kawakami and S.Miyake*
Osaka City University,Osaka,Japan
*Institute for Cosmic Ray Research

I. Introduction

In the gold mines at Kolar Gold Fields,Measurements were made over the past two decades to study cosmic ray phenomena i.e. muon and neutrino interactions as well as exotic processes such as Kolar events,anomalous cascades,Muon bundles etc. This has led to a detailed understanding of the intensities and interaction properties of cosmic ray particles in deep underground sites - vital factor in undertaking new,low-counting rate experiments. For a proton-stability experiment to be viable it is also necessary to know how to recognise the background and eliminate it from the sample of events so that the level of sensitivity is increased and the results are unambiguous. The neutrino experiments[1] conducted in KGF during 1965 - 1969 at a depth of 2300 m come in handy for recognition of neutrino backgrounds. These involved simple telescopes with scintillators,striated absorbers and visual detectors as well as magnetic spectrographs, with a total area $\sim 50\ m^2$. In addition to cosmic ray muons and their secondaries, events due to ν -collisions in rock as well as inside the detector were recorded in these experiments; for some of them the momentum of the leading lepton has also been measured. These data provide us with a good experimental base for undertaking large scale experiments in which decay channels of bound nucleons are sought.

A new experiment has been proposed[2] in Jannuary 1980 to look specifically for decay of bound protons and neutrons in the lifetime regions up to 5×10^{31} years. This detector has constructed and started observation at the end of October in 1980.

II. Estimates on lifetimes and decay modes

The currently popular models of Grand Unified theories[3] indicate that the lifetime of protons and bound neutrons, $\tau_{p,n}$ is in the region

10^{30} - 10^{32} years. These are tantalizingly close to the experimental limits derived for specific modes (μ + anything) from the deep underground neutrino experiments. Learned et al[4] have used the data from the South African experiment of late 60's to raise the lower limit to the region of 10^{30} years. A reanalysis[5] of the KGF neutrino data of 1965 - 69 has also yielded a similar value of $> 10^{30}$ yrs. for muonic modes. In this work they have taken advantage of the graininess of the detectors and searched for charged particles at large zenith angle with energy $\gtrsim$ 100 MeV. It is worth noting that both of these experiments were not designed to look for nucleon decay and as such could not provide unambiguous evidence even if a decay event existed in the data.

Since 1970, several experiments were conducted in KGF to study cosmic ray muons, new particle states of high mass etc. In these, one or two examples with characteristics similar to those predicted for nucleon decay (with lifetimes around 10^{30} years) have been recorded but could not provide unambiguous evidence for lack of adequate data on the secondary particles. For this reason one should not foreclose the possibility that the lifetime could be even close to the lower end of the prodicted values.

A general consensus seems to emergy, for SU(5) models, that $P \rightarrow e^+\pi^o$ and $N \rightarrow \pi^- e^+$ are the dominant decay modes. The recent estimates[6] suggest other decay modes and branching ratios.

In Pati and Salam models[3], there are two mechanisms by which nucleons decay depending on $\Delta F \neq 0$ and $\Delta F = 0$ transitions (where F is Fermion number, $F = B + L$). While $\Delta F \neq 0$ transition gives rise to decay modes similar to those described above, $\Delta F = 0$ leads to states involving 3 leptons + mesons.

All these decay channels should be considered only as guidelines for the basic design of a detector, with a flexibility built in so that several parameters could be measured simultaneously on individual secondaries arising from the decay of nucleons.

III. Site and Detector Design

The most important consideration in our design is suppression of unwanted background to the extent feasible. In our experience with large area detectors at shallow depths underground in KGF, there have always been a few unresolved low energy events that could not be understood in terms of normal interaction of muons or of their secondaries. Neutral secon-

daries could also pose severe limitations on the sensitivity of low counting-rate experiments. To circumvent these difficulties, the new detector has been installed at a depth 2300 m underground at a distance of about 30 m from the site of the earlier (1965 - 69) KGF neutrino experiment.

A schematic diagram of the detector is shown in Fig. 1. This comprises 35 layers of proportional counters stacked one above the other and tnterspersed with thin iron plates (1.2 cm). The overall dimensions of the detector are 4 m (width) x 6m (length) x 3.7 m (height). The alternate layers of proportional counters will be arranged in an orthogonal geometry to enable measurement of spatial coordinates to an accuracy of 10 cm in X ,Y and Z directions.

Proportional Counters

The detector has a total of about 1700 sealed proportional counter modules of lengths 4 m and 6 m and of cross-section 10 cm x 10 cm. These are formed from square iron pipes of wall thickness 2.3 mm, with a 100 μm gold coated tungsten wire serving as an anode. They are filled with a mixture of 90% Argon and 10% methane at a pressure equvalent to that of the underground site. These counters are found to exhibit excellent long term stability and good resolution for relativistic particles in an earlier experiment[8] conducted during 1979 at a shallow depth of 600 m. A typical counter exposed to natural radioactivity in the underground site will have a pulse height spectrum with 2 peaks - a sharp one corresponding to fluorescent X-rays of iron at $\sim$ 7 keV and a broad peak at $\sim$ 18 keV due to ionisation in the gas by Compton electrons. This provides an excellent handle for calibration and monitor of counter performance over long periods of time. At an operating voltage of 3 kV, a relativistic charged particle gives rise to a pulse of $\sim$ 5 mV with a risetime of 300 nsec leading to simplicity in trigger circuitry.

Electronics

Each of the counters will be instrumented separately with an amplifier and a discriminator. Pulse widths from thses discriminators are continuously written into individual RAMS (256 bits) and upon the arrival of a trigger pulse all data will be transferred into a system memory serially. The pulse width(time) digitised with a 2 MHz clock,contains information on the total number of relativistic particles traversing each of the counters. The control circuit decides which of the counters in each layer has responded and only these data will be punched on a paper tape. A block diagram of the data acquisition system is given in Fig 2.

Initially the trigger is sufficiently flexible to accommodate all

possible decay modes of nucleons. At the moment,a coincidence of any four layers with more than six discharged counters in total is employed. From the Monte-Carlo simulations it is clear that the most of decay modes will not be missed by this triggering condition.

We make a tacit assumption, that decay characteristics of nucleons bound in nuclei are essentially same as those predicted for free protons except for the consequences of Fermi momentum on the angle and energy distribution of secondary particles and some interactions in the nucleus. In the final analysis, the efficiency of detection depends on how well the expected characteristics stand out against the background. One would therefore use all available data such as (1) the ranges of all tracks and hence the total visible energy (2) coplanarity and (3) track configurations. We feel that the detection efficiency, taking all these factors into account, would be at least 40 %.

Background Estimates

Even at the present depth of 2300 m one has to contend with a substantial background due to cosmic ray muons and neutrinos. In Table 1, the backgrounds due to differenct known processes are listed separately for muon-induced and neutrino-induced reactions.

Cosmic ray muons have an intensity of 10^{-10} $cm^{-2}sec^{-1}st^{-1}$ and an angular distribution $I(\theta) = I(0) \cos^{10} \theta$ at the depth 2300 m. The outer jacket of crossed proportional counters with almost 100 % efficiency, will completely eliminate charged particle background arriving from interactions in rock. The estimated background from neutrals (γ ,n,K^o) in muon interactions in rock, as shown in the table, is a conservative upper limit and can be fully rejected by energy cuts and track configurations of secondary particles.

The neutrino background is essentially constant at all depths underground and their angular distribution is more or less uniform with a slight peaking towards the horizontal direction. In our earlier neutrino experiments[1], in addition to the angular distribution, it was possible to measure the energy of secondary muons by means of magnetic spectrographs. The ν_μ, $\tilde{\nu}_\mu$ interactions are thus well understood,at least to the extent of making reliable background estimates for the present detector. On the other hand the ν_e, $\tilde{\nu}_e$ interactions can pose problems in event identification due to channels such as $\tilde{\nu}_e + p \rightarrow e^+\pi^o n$ etc. The overall background from these processes can be reduced to < 0.3 events/year by imposing cuts on the visible energy to < 2 GeV (using particle ranges and shower information) and by study of track configurations of individual events.

IV. Other Physics Problems

The detector with 24 m^2 area and weight 150 tons will provide a natural extension to our continuing programme of study of new phonomena using cosmic ray beams.

1. New particle phenomena (Kolar events)

Evidence for long-lived ($\gtrsim 10^{-9}$ sec) and massive (> 2 GeV/c^2) particle production has been obtained in our earlier experiments[9] in KGF. The present detector has adequate resolution to study such events in great detail ; it may be recalled that the prominent features of these events are multiple secondaries (mostly penetrating, μ or hadron) with large opening angles.

2. Anomalous cascades

Cascades of very high energy ($\gtrsim$ 1000 GeV) and of nearly isotropic angular distribution were recorded earlier[10] in KGF experiments at depths of 1100 m and 2300 m. Their intensity has been found to be too high compared to those estimated for μ , ν -interactions. The present detector acts as an excellent calorimeter with fine-grained sampling of particle densities over 30 - 40 rediation lengths. This would provide accurate estimation of cascade energies, directions of central cores as well as distinction between soft and hadronic cascades.

3. Multiple muon events

For the first time, muon bundles can be detected at energies of about 20 TeV. This has relevance to the chemical composition of primary cosmic rays as well as the characteristics of hadron collisions at energies $>$ 1000 TeV. Search for high P_t events corresponding to large lateral separations of multiple muons is also possible in view of the large area and good spacial resolution available in this detector.

V. Preliminaly Results

During operation for about 25 days, this new detector recorded 50 single muons , one stopped muons inside the detector, and , one case of double muons parallel to each other. Oct. 1980.

References

1.M.R.Krishnaswamy et al, Proc. Roy. Soc., London A 323 489 (1971)
A 323 511 (1971)

2.V.S.Narasimham,"Test of conservation of baryon no. - proposal for an experiment at KGF", TIFR preprint 1980

3.J.C.Pati and A.Salam, Phys. Rev. D8 1240 (1973)
H.Georgi and S.L.Glashow, Phys. Rev. Lett. 32 438 (1973)
M.Gell-Mann, P.Ramard and S.Slansky, Rev. Mod. Phys. 50 721 (1978)
T.J. Goldman and D.A.Ross, Phys. Lett. 84B 208 (1979)
H. Georgi, H.Quinn and S. Weinberg, Phys. Rev. Lett. 33 451 (1974)

4.J.Learned, F.Reines and A.Soni, Phys. Rev. Lett. 43 907 (1979)

5.R.Cowsik and V.S.Narasimham, TIFR preprint 1979
S.Miyake private communication August 1979

6.J.Ellis, CERN preprint Th-2723,1979

7.M.R.Krishnaswamy et al,Proc. 16th Int. Cosmic Ray Conf., Kyoto paper T 4 - 2 (1979)

8.M.R.Krishnaswamy et al, Pramana 5 59 (1975)
Proc. Int. Neutrino Conf., Aachen 197 (1976)
Proc. 16th Int. Cosmic Ray Conf.,Kyoto, 13 24 (1979)

9.M.R.Krishnaswamy et al, Proc. 16th Int. Cosmic Ray Conf., Kyoto 13 14 (1979)

Table 1

Background for 150 ton detector

Source	Frequency (per Year)	Rejection Criterion
1) Straight through muons	~ 600	VETO JACKET
2) Stopping muons	~ 6	"
3) Multiple muons	~ 10	"
4) Corner clips	< 60	"
5) Muon out of geometry + neutrals (γ, n, K^0 etc.)	$\lesssim 10$	Energy cuts ; track configuration
6) New particle (Kolar) events	~ 2	Track configuration, visible energy
7) Anomalous showers	~ 2	Visible energy
8) ν -interaction in rock	~ 10	VETO JACKET
9) ν -interaction inside the detector (visible energy 0.3 - 2 GeV)		
a) $\nu_\mu, \tilde{\nu}_\mu$ charged current)	$\lesssim 3$	VETO JACKET (Elastic channels)
b) $\nu_\mu, \tilde{\nu}_\mu$ neutral current)		+ Track Configuration (Inelastic channels)
c) $\nu_e, \tilde{\nu}_e$ charged current)	$\lesssim 1$	Track configuration
d) $\nu_e, \tilde{\nu}_e$ neutral current)		"
10) Estimated overall background for decay events	$\lesssim 0.3$	

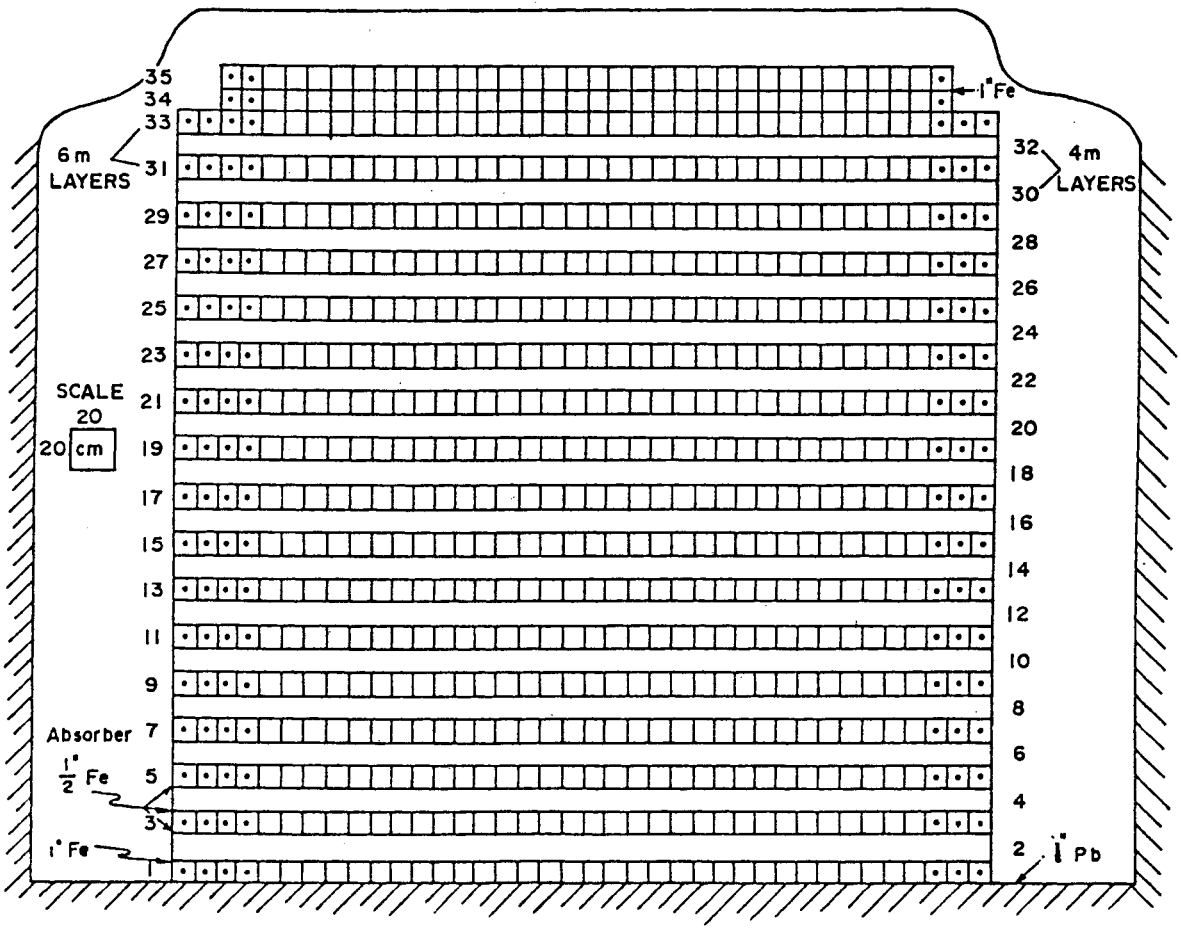

FIG1: FRONT VIEW OF PROTON STABILITY DETECTOR IN K.G.F (7600 FEET)

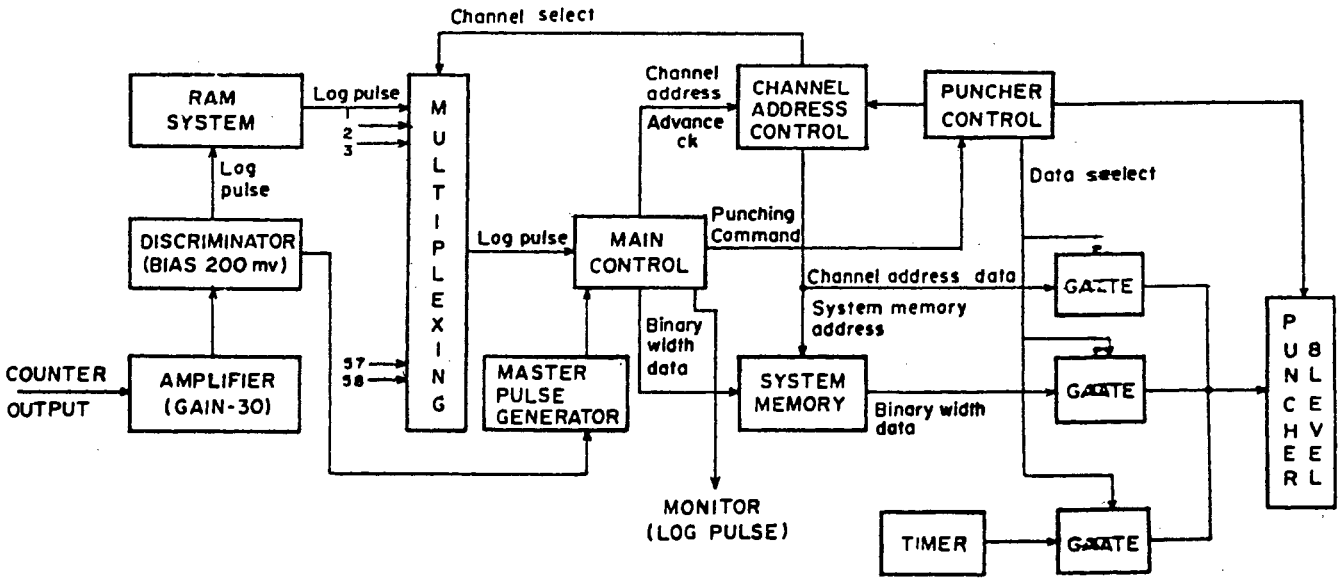

FIG 2: DATA ACQUISITION SYSTEM

FUTURE LARGE EUROPEAN UNDERGROUND EXPERIMENTS (+)

M.Conversi
Istituto di Fisica dell'Università di Roma
Piazzale Aldo Moro, 5 - 00185 Rome, Italy

ABSTRACT

The prospects of the experimental program in possible future European underground laboratories include the development of a modular multikiloton visual detector suitable to "see" and identify most of the expected final states resulting from the nucleon decay. The detector is essentially a fine grain calorimeter, with 3 mm sampling iron plates alternated with flash chambers triggered by limited streamer counters.Its mass could reach the 10 Kt region (about 10^7 flash cells) at a cost still accessible to the European Physics Community.

1. Introduction

The future European program for large-scale underground experiments is not defined as yet. The existing laboratory under the Mont Blanc, at a depth of about 5000 m w.e. (water equivalent) has a limited capacity which at present does not appear realistic to increase. Other locations, for possible future underground laboratories of a much larger capacity, both at an average depth of approximately 4500 m w.e., are: a) in the Frejus tunnel, near the French-Italian border, and b) in the tunnel of the Gran Sasso mountain, at a distance of about 150 km from Rome. The volume forseen for the latter laboratory could reach $5 \cdot 10^4$ m^3. Steps are being made to obtain the permission and the financial support from the competent State Authorities.

Needless to say, a large and deep underground laboratory would allow the European Physics Community to investigate, over a period of presumably several decades, a variety of subjects of great physical and cosmological interest, ranging from the nucleon instability predicted by the so-called grand unified theories[1], to possible processes involving $\Delta B = 2$ transitions[2] (B = baryonic number), possible oscillations of atmospheric neutrinos, neutrino astrophysics[3], etc.. In this report, however, I shall limit the range of these potential applications by discussing only the case of the nucleon instability[4], for which a considerable amount of thinking has been made already in Europe.

As discussed in the course of this Meeting[5] some searches for the proton decay exploit the fact that very massive detectors can be realized at a still reasonable cost using water, where fast charged particles emit Cerenkov radiation at a well detectable level. Other searches are based on the use of "fine grain calorimeters"; but in general the high cost per unit mass of this solution tends to limit the size of the detector.

(+) Up-to-date version of talk given at the 1980 International DUMAND Symposium.

I shall discuss here an approach to the calorimetric solution which should overcome this limitation, making it possible to build a very massive visual detector of comparatively low cost per unit mass, well suited to study the various expected decay modes of the nucleon. This approach has gained consensus in Europe leading to a letter of intent to the Italian Authority[6] and, more recently, to a proposal to the French Authority[7].

2. General features of proposed detector

The general features of this approach can be summarized as follows: The proposed apparatus for the detection of most of the expected decay modes of the nucleon will have a modular structure, expandable up to the 10 Kt region; each module(+) will be essentially a huge track detector, of a mass in the neighbourhood of 1 Kt, allowing vertex reconstruction and particle identification in many instances, with energy determination for most of the final state particles. As the track detector has an intrinsic space resolution of about 4 mm (the size of the "flash cells") and it will contain "sampling" iron plates 3 mm thick which can be eventually magnetized, each module will be somewhat similar to a gigantic heavy liquid bubble chamber of poor space resolution.

The modular structure will make it possible to start the experiment with 1 module of $\sim$ 1 Kt mass, and to develop in time up to 10 Kt or more, depending on the space available in the underground laboratory and funding.

The detector should allow to "see" many of the expected decay modes of the nucleon, to identify possible $\Delta B = 2$ processes, and possibly to observe oscillations of atmospheric neutrinos.

3. Detector components

The detector in each module is composed of:

a) Flash chambers of extruded polypropylene[8], made of tubular cells of $(4\ \text{mm})^2$ square section, of total area $(8\ \text{m})^2$, alternated with
b) 3 mm thick "sampling" iron plates of the same area and, after any 9 such alternations,
c) limited-streamer counters[9], covering the same area, used to trigger the flash chambers with the help of a suitable electronics.

The principle of operation of a plastic flash chamber is identical to that of the "old" glass flash-tube "hodoscope chamber"[10] (principle of "selective electronic trigger", utilized in all subsequent "electrically pulsed chambers": spark chambers, wide gap chambers, streamer chambers, ...). However, using extruded plates of polypropylene with rectangular tubular holes (the "flash cells", of typically 4-5 mm linear dimensions and any arbitrary length) presents a number of advantages: 1) Nearly no dead space; 2) No fragile components; 3) Easiness of construction in large size; 4) Extremely low cost. The only drawback is that gas circulation is required, since the polypropylene walls emanate electronegative impurities which tend to shorten the chamber sensitive time below the minimum acceptable value for a good detection efficiency after the triggering time.

(+) The module described here is quite similar to that described in ref. (7), except for its larger mass which should allow one to reduce appreciably the cost per unit fiducial mass.

While the "old" glass flash tubes have been extensively utilized in cosmic ray physics, the plastic flash chambers have found applications especially in large scale experiments with particle accelerators.

Also the limited streamer counters[9] have been and are being utilized extensively in experiments with particle accelerators, and are characterized by a great stability of operation.

Both techniques appear therefore well suited for large long-running underground installations, also on account of their comparatively low cost.

4. Module description

For a cubic module of 8 m side, $\sim$ 2 g/cm^3 density, the mass is $\sim$ 1 Kt, largely due to the $\sim$ 650 iron plates 3 mm thick. There will be $\sim 10^6$ flash cells per module , contained in $\sim$ 650 flash chamber planes with 90° alternated orientations in order to get two stereoscopic views of the tracks. For such a large number of cells an optical read out is recommended. The out-put light signal from the flash cells is large enough to be recorded(+) on 70 mm film of 400 ASA, via mirrors and Fresnel lenses [7] attached to one of the lateral sides and the top side of the cubic module. An alternative solution is to record the events by TV (plumbicon) systems on magnetic tape[11]. Also a magnetostrictive read-out[12] could be considered in case of severe limitations in the available space of the underground laboratory.

The module just described is sketched in Fig.1. It is essentially a "plastic flash calorimeter" of the type introduced a few years ago[11] and developed on a large scale at York University, Toronto[13], at Fermilab[12], at UC Irvine[14] and elsewhere, for use especially in neutrino physics.

The response of such a calorimeter to high energy electrons, photons and pions has been studied experimentally[12-11] and by Monte Carlo simulations[15] up to energies of 200 GeV. At the energies of interest for the decay products of typical nucleon decays such as

$$p \to e^+\pi^\circ \quad (\to \gamma\gamma) \qquad\qquad n \to e^+\pi^- \qquad\qquad (1)$$

the response can be inferred from that of a shower detector made of layers of 1 cm diameter glass flash tubes alternated with 5 mm thick lead plates, which was exposed[16] to electrons of energies from $\sim$ 50 to $\sim$ 500 MeV. As seen in Fig.2 there is a linear relationship between the energy E_e of the impinging electron and the corresponding average number of flashed tubes, $< N_f >$.

The percent resolution in the energy measurement of the primary electron (or photon) for a plastic flash calorimeter containing metal plates, each of t radiation lengths, is given approximately by[11]

$$\Delta E/E = (12\%)\ \sqrt{t/E_{GeV}}$$

for primary particles impinging perpendicularly on the calorimeter planes with energy E_{GeV} , measured in GeV.

(+) Successful tests have been made at Saclay on 6 m long flash chamber planes made of tubular cells of about (5 mm)^2 square cross section.

A muon emitted in a process such as

$$p \to \mu^+ K^\circ \quad \to \pi^+ \pi^-$$

gives rise in the calorimeter to a single track, and its energy could of course be measured, with a great accuracy (< 3%), by its range. The signature of this process would be unmistakable if the K° decay occurs after a few cm or more from the point of the proton decay.

Trigger of the module chambers by means of the limited streamer counters can be made with an estimated efficiency [7] of 80% and 57% respectively for the two processes (1). Use of a suitable electronics ("magic boxes") would make the trigger logic extremely flexible.

5. Observation of nucleon decay events

Some of the two-body nucleon decay modes which should occur more frequently according to the predictions of most theoretical models[17][18] are listed in Table 1 together with their expected branching ratios. The estimated accuracy[7][19] in the energy determination of the two decay products is given for both particles in the last column, taking into account the Fermi motion of the decaying nucleon and averaging over the emission angle (incident angle onto the calorimeter planes).

Monte Carlo simulations of nucleon decays as they should appear in the two orthogonal views of the calorimeter chambers, have been made[7][19] for most of the decay modes listed in Table 1. Fig. 3 shows as an example one view of an event $p \to e^+\pi^\circ \to e^+\gamma\gamma$ as reported in the French proposal[7].

A sketch of a possible underground installation of 10 modules totalling a 10 Kt mass is shown in Fig. 4. The optical read-out could be made[7] as sketched for the side view of the two first modules in the figure. A similar solution can be applied to the top view of each module. The underground laboratory for such an installation should have an area of approximately 25 m x 50 m and a height of about 20 m.

For a nucleon meanlife of 10^{31} years and an over-all detection efficiency of $\sim$ 50% the 10 Kt detector should record $\sim$ 300 nucleon decay events per year. This is to be compared with an estimated rate of less than $\sim$ 10 background events per year at a depth of $\sim$ 4500 m w.e., mostly due[20] to interactions of atmospheric neutrinos in the detector. A further reduction of this background might be achieved by inserting in the detector modules planes of thin "plate resistive counters" - a new type of fast but low-cost d.c. operated counters being developed in Rome[21] - which provide out-put pulses of $\sim$ 0.3 V amplitude, $\sim$ 1 ns rise time, allowing accurate time-of-flight measurements.

6. Acknowledgments

I wish to thank Drs. R.Barloutaud, A.Grant, E.Iarocci and B.Tallini for discussions on various technical aspects of the project outlined above.

TABLE 1 - "Main" predicted nucleon decay modes[17][18]. The percent branching ratios in parenthesis are from Ref.(18).

Decay mode	Percent br.ratio	Accuracy in en measurement (+) p.1	p.2
$p \to e^+\pi^0$ $\to \gamma\gamma$	31-40 (8)	15%	∿12%
$p \to e^+\omega$ $\to \pi^+\pi^-\pi^0$	18-26 (47)	15%	?
$p \to e^+\rho^0$ $\to \pi^+\pi^-$	2-21	15%	∿30%
$p \to \mu^+K^0$ $\to \pi^+\pi^-$	< 19	∿3% (by range	∿25%
$n \to e^+\pi^-$	45-79 (22)	15%	30%(++)
$n \to e^+\rho^-$ $\to \pi^-\pi^0$	4-49	15%	∿30%

(+) Including Fermi motion and averaging over emission angle (after A.Grant[19]).

(++) From measurements in liquid Ne-H_2 mixture (BEBC).

References

1. See e.g.: H.Georgi and S.Glashow, Phys. Today 30, n.9, 30 (1980).

2. See e.g.: R.E.Marshak and B.N.Mohapatra, Phys. Lett. 91B, 222 (1980); P.R.L. 44, 1136 (1980).

3. K.Lande, Ann.Rev.Nucl.Part.Sci. 29, 395 (1980).

4. For extensive quotations of the theoretical work carried out on this subject and for a detailed discussion of the uncertainties in the proton lifetime ($\tau = \sim 10^{31\pm2}$ years), see the recent paper by J.Ellis, M.K.Gaillard, D.V.Nanopoulos and S.Rudaz, LAPP-TH-14, Ref. TH 2833-CERN, April 28 (1980).

5. See reports by E.Bellotti, D.Cline, J.Learned, S.Myake.
For reviews on planned underground experiments looking for proton decay see e.g.: G.Barbiellini and R.Barlouteaud, Proc. of 1980 "Rencontres de Moriond"; M.Goldhaber, Proc. of 1980 Neutrino International Conference at Erice. See also Phys. Today 33, n.31, 17 (1980).

6. Letter of E.Fiorini, sent on June 17, 1980,to the President of the INFN, on behalf of a Frascati-Milan-Rome-Turin Collaboration.

7. B.Bareyre et al., (proposal October 1980) "Proposition d'une éxperience pour l'étude de l'instabilité du nucléon au moyen d'un détecteur calorimètrique" Orsay, Ecole Polytechnique, Saclay Collaboration.

8. M.Conversi and L.Federici, Nucl. Instr. Meth. 151, 93 (1978).

9. E.Iarocci et al., Nucl. Instr. Meth. 152, 423 (1978); 164, 57 (1979).

10. M.Conversi and A.Gozzini, Nuovo Cimento 2, 189 (1955).

11. L.Federici et al., Nucl. Instr. Meth. 151, 103 (1978).

12. F.E.Taylor et al., Fermilab Conf. 77/100-Exp. (October 1977); J.Walker, private communication.

13. W.R.Frisken et al., (unpublished).

14. H.H.Chen et al., UCI Neutrino n.29 (April 1980);see also S.Burman report at this Meeting.

15. M.Conversi and F.Lacava, Nucl. Instr. Meth. 161, 219 (1979).

16. G.Brosco, Thesis, University of Rome, 1972 (unpublished). The results of Fig. 2 are reported in a review article by the present author, Rivista del Nuovo Cimento 3, 233 (1973).

17. M.Machacek, Nucl. Phys. B159, 37 (1979); B.M.Gavela et al., Orsay preprint LPTHE 80/6 (1980); G.Kane and G.Karl, Intern. Report, University of Michigan (1980); A.Diw et al., Phys. Lett. 91B, 77 (1980).

18. J.F.Donoghue, Phys. Lett. 92B, 99 (1980).

19. A.Grant (private communication) has made a detailed Monte Carlo simulation of the various nucleon decay modes in a detector similar to the module described in Sect. 4. See also A.Grant and B.Tallini, CERN internal report dated 4/2/1980.

20. The muon induced background, discussed by D.H.Perkins (CERN - EP 26 September 1979) and in the "NUSEX proposal" (Frascati, Milan, Turin, Collaboration) is essentially negligible at the depths of the forseen European laboratories. See also: R.Barlouteaud and G.Chardin, CEN Saclay, internal report (1979).

21. R.Santonico and R.Cardarelli, internal report Istituto di Fisica, Università di Roma (November 1980), submitted to Nucl. Instr. Meth.

Figure captions

Fig.1 Sketch of detector module of $\sim$ 1 Kt mass. About 70 planes of limited streamer counters, not shown in the figure, are used to trigger $\sim$650 flash chambers of (8 m)^2 area (about 10^6 flash cells). As proposed in Ref.(7) and shown in the top figure insert, each chamber can be made of two extruded polypropylene plates attached to one inner 3 mm thick Fe plate ("hot electrode") and two outer 1.5 mm thick Fe plates (grounded).(+)

Fig.2 Linear relationship[16] between electron energy E_e and average number of flashed cells $< N_f >$ in a shower detector made of flash-chambers alternated with 0.5 cm thick lead plates (flash-tubes of 1 cm diameter).

Fig.3 Monte Carlo simulated example of decay event $p \to e^+\pi^\circ \to e^+\gamma\gamma$, as it would appear in one of the two orthogonal views of the detector module of Fig. 1.

Fig.4 Sketch of a possible lay-out of 10 detector modules totalling a mass of $\sim$ 10 Kt in an underground laboratory of about 25m x 50m area, $\sim$ 20m height.

(+) Some unavoidable "dead space" between contiguous chambers (not shown in the figure) accounts for the assumed average density of the detector module ($\sim$ 2g/cm^3).

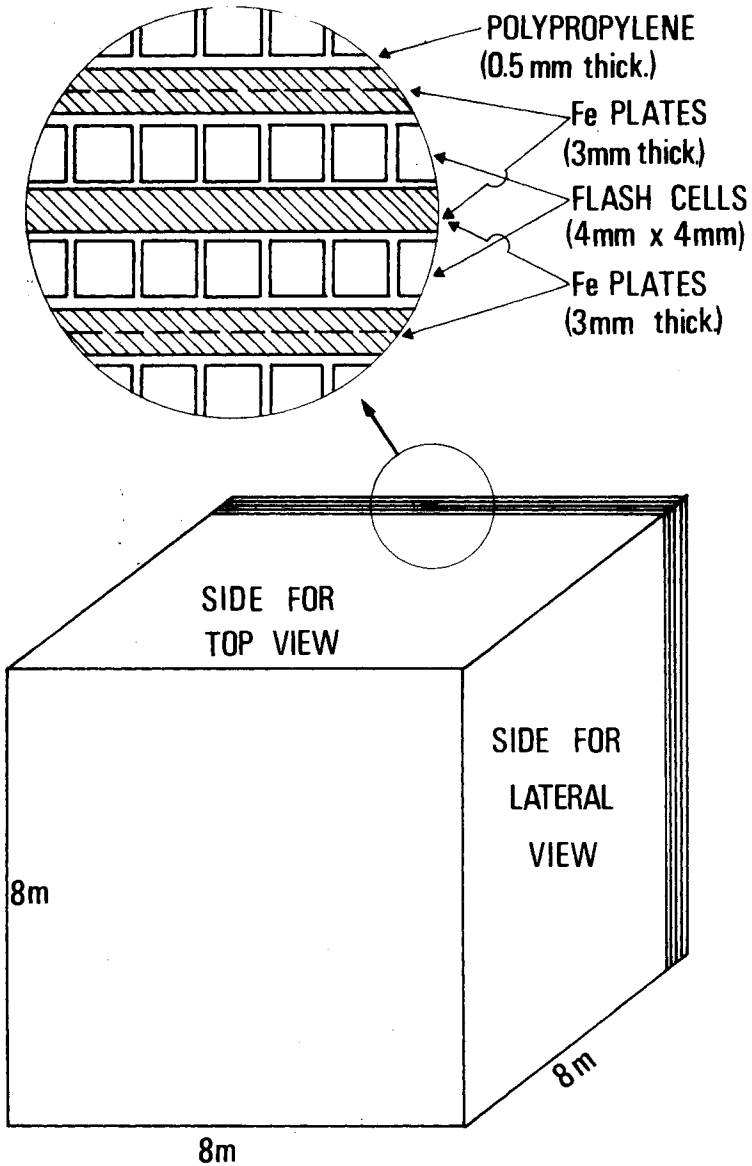
POLYPROPYLENE
(0.5 mm thick.)
Fe PLATES
(3mm thick)
FLASH CELLS
(4mm x 4mm)
Fe PLATES
(3mm thick)
SIDE FOR
TOP VIEW
SIDE FOR
LATERAL
VIEW
8m
8m
8m

fig.1

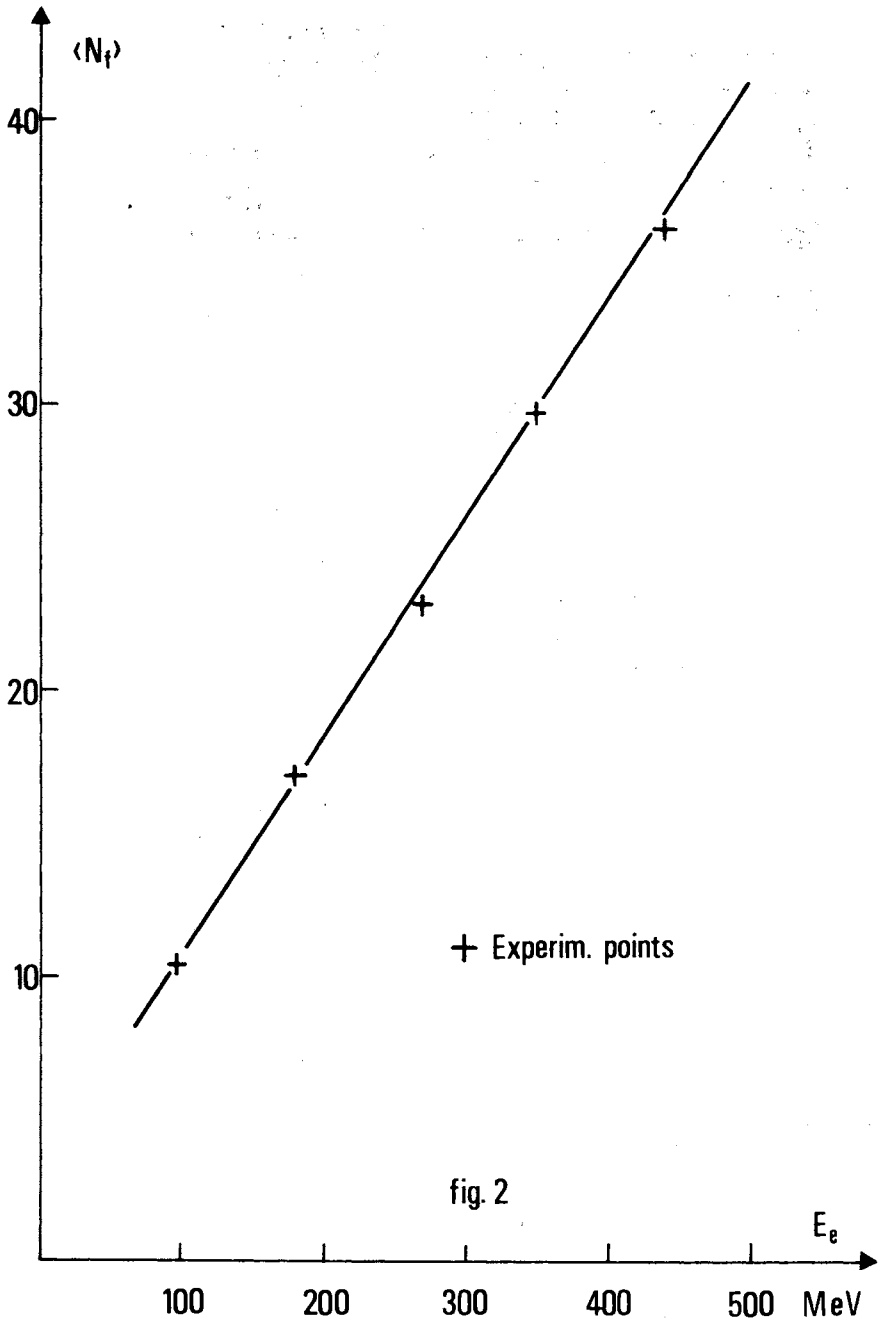

fig. 2

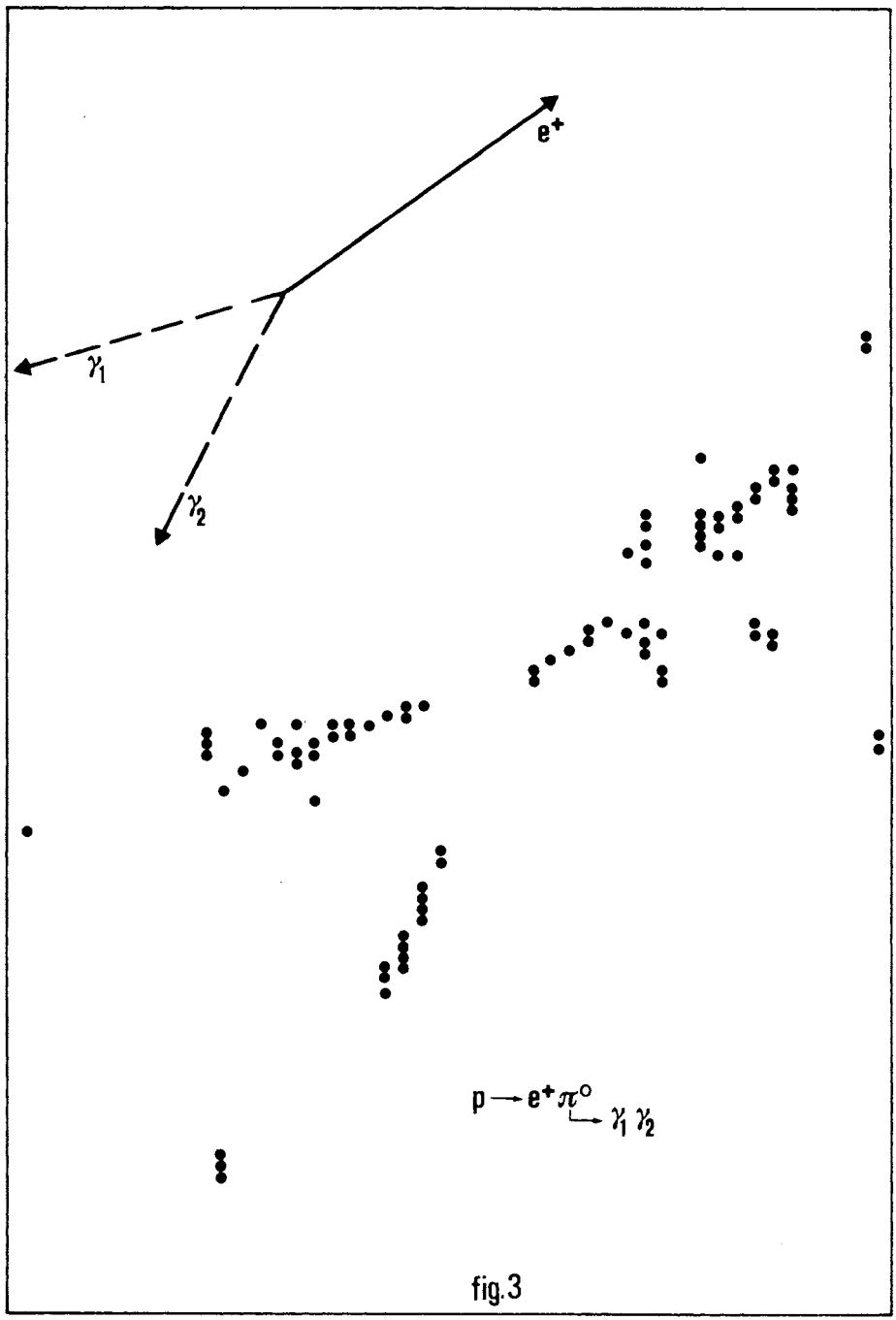

fig.3

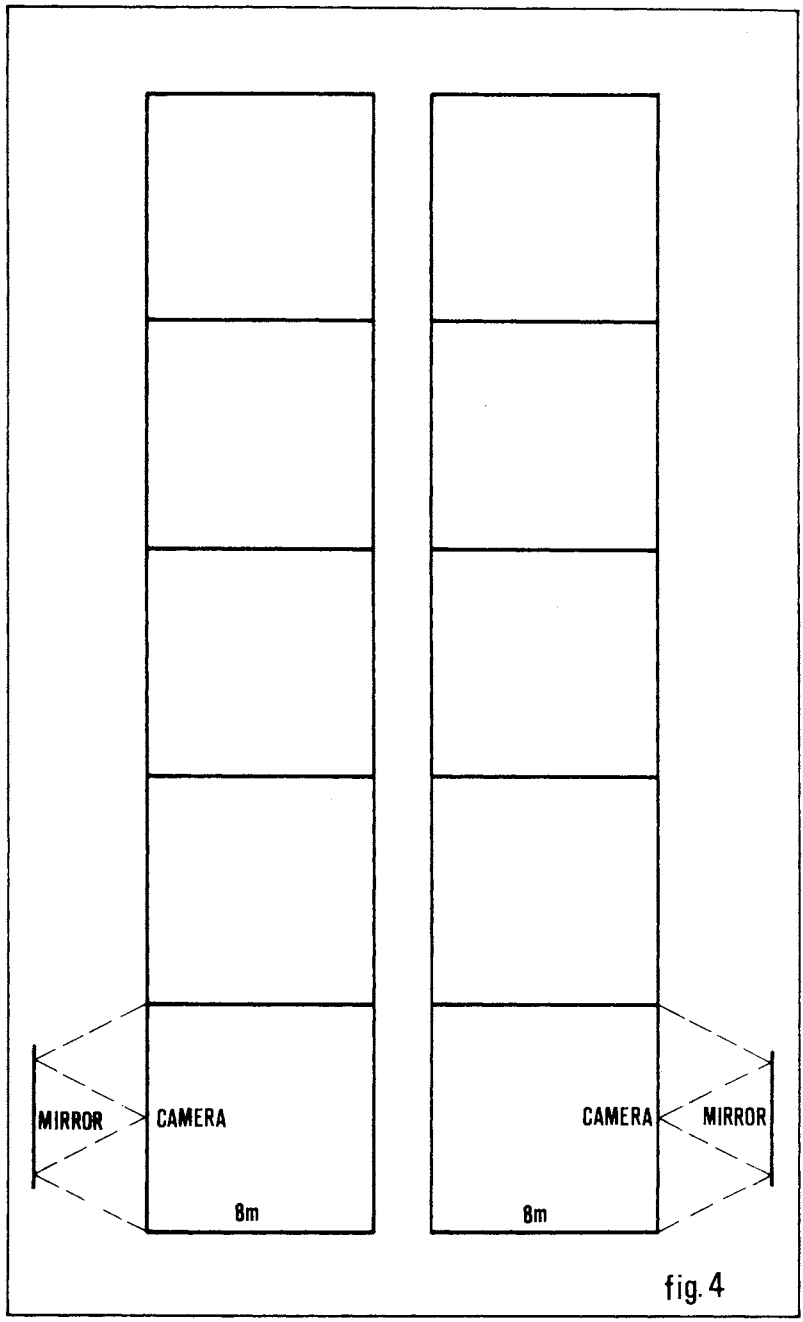

fig. 4

VI. Neutrino Mass and Oscillations

Neutrino Instability

Henry W. Sobel, Frederick Reines, Elaine Pasierb

Presented by Henry W. Sobel

Department of Physics
University of California
Irvine, California 92717

1. Introduction

We have obtained indications of neutrino instability from our data on the processes:

$$\bar{\nu}_e + d \longrightarrow n + n + e^+ \quad \text{(charged current)}$$
$$\bar{\nu}_e + d \longrightarrow n + p + \bar{\nu}_e \quad \text{(neutral current)}$$

Although the deuteron reaction is not the ideal way to search for neutrino oscillations, it has a number of attractive features which allow us to side step many of the problems currently inherent in reactor neutrino studies. The reactor is a good source since it provides a very intense (2×10^{13} $\bar{\nu}_e cm^{-2} sec^{-1}$) pure source of $\bar{\nu}_e$'s at low energies (<10 MeV). The difficulty has been the uncertainty in the $\bar{\nu}_e$ spectrum.

2. Reactor Neutrino Experiments

The Reactor as a Neutrino Source

A power reactor produces neutrinos from the fission of ^{235}U, ^{238}U and ^{239}Pu. The neutrino spectrum of each component is different (Fig. 1). At the Savannah River Project (SRP) reactor where we work, ^{239}Pu produced less than 8% of the fissions during our experiment, and ^{238}U produced less than 4%. At the Grenoble reactor all the fissions come from ^{235}Pu.

Neutron activation of the reactor surroundings can also produce $\bar{\nu}_e$'s but they are less than $\sim$ 1.3 MeV.[1] Neutrino production in this mode is also possible with $\nu_e/\bar{\nu}_e \simeq .0005$ and $E_{\nu_{max}} = 0.8$ MeV.[2] Experimentally, the ratio $\nu_e/\bar{\nu}_e$ has been determined to be < 0.02.[3]

The antineutrino spectrum itself is calculated by adding up the beta decay spectrum of all the fission products. Unfortunately, approximately 30% of the fission products involve unknown decay schemes, and as a consequence, the neutrinos from these decays require extrapolation and modeling. The two newest theoretical predictions for the antineutrino spectrum are shown in Fig. 2. They disagree to a level of about 30% depending on $\bar{\nu}_e$ energy.

$\bar{\nu}_e + p \rightarrow n + e^+$ Experiments

The inverse beta decay reaction has been studied in several different experiments and new experiments are being built. The data so obtained can be

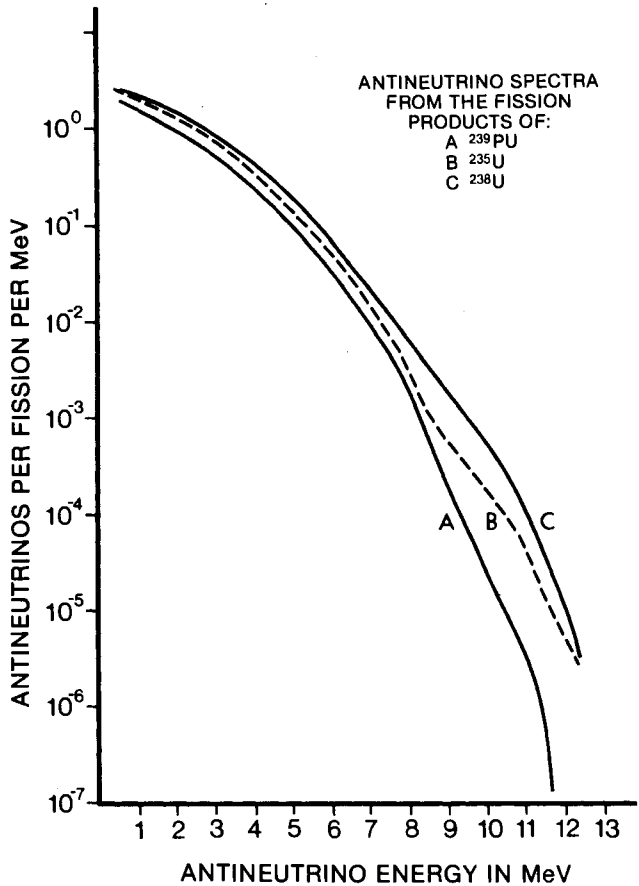

Fig. 1. Antineutrino spectra from fission products.

used in several ways.

1. Since the e^+ takes essentially all of the $\bar{\nu}_e$ energy in the reaction, a measurement of the e^+ spectrum determines the $\bar{\nu}_e$ spectrum. This neutrino spectrum can be used as input in other experiments.

2. The process can be used to study neutrino oscillations.

a. Experimental results can be compared with theoretical prediction: This technique suffers from the uncertainty in the predicted neutrino spectrum in that any observed discrepancies can be attributed to that source.

b. We can compare the results of different detectors at various source to detector distances: These data are just beginning to be available in the required precision and analysis is incomplete.[4]

c. We can compare the results of the same detector taken at different

distances: This clearly is the experiment of choice and two groups are actively pursuing this technique.

There are three data sets available at this time. They are the 6.5 meter data of Nezrick and Reines,[5] the 11.2 meter data of Reines, Gurr, and Sobel,[6] and the 8.7 meter data of the C.I.T.-Grenoble-Munich group.[7] Within one year, additional data are expected from a 38 meter point with the C.I.T.-Munich detector at a 2700 MW reactor near Zurich, a mobile detector at the SRP reactor which will span a 12 to 35 meter distance,[8] and a single point at 15.4 meters from the SRP reactor by a G.I.T.-U.S.C. group.[9]

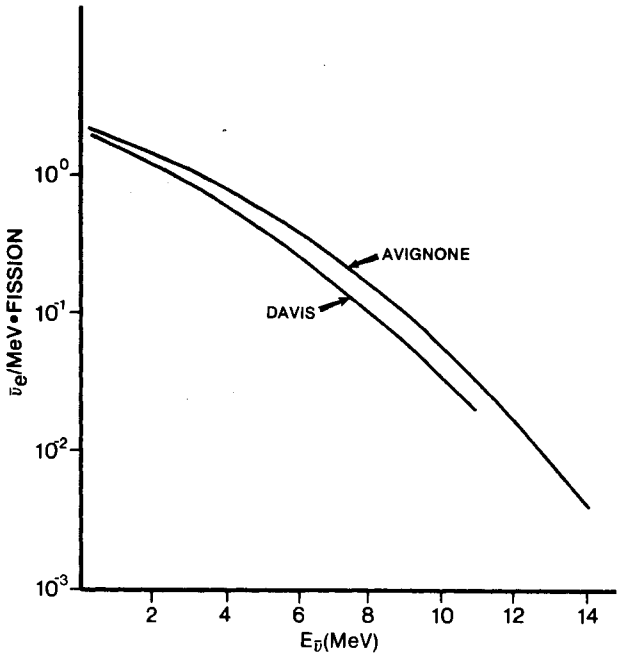

Fig. 2. Predicted $\bar{\nu}_e$ spectrum.

Results from the 11.2 meter data are given in Fig. 3. and compared with the predicted positron spectrum of Avignone et al and Davis et al. We note that the observed data agree with the Davis prediction at β^+ energies $\gtrsim$ 2 MeV but diverge below the prediction at higher energies.

All three experiments are compared in Table I. We list the ratio of the observed rates to those predicted by the Avignone and Davis spectra. In order to interpret these results in terms of neutrino oscillations we assume a simple two neutrino case.

Two Neutrino Approach

In this case a physical neutrino can be written as a super-position of two pure states i.e.:

$$\bar{\nu}_e = \nu_1 \cos\theta + \nu_2 \sin\theta$$

and

$$\bar{\nu}_{\mu/\tau} = -\nu_1 \sin\theta + \nu_2 \cos\theta$$

where θ is the mixing angle. Then, the probability of finding a $\bar{\nu}_\mu$ (or $\bar{\nu}_\tau$) at time t, given that we started with a $\bar{\nu}_e$ is:

$$\text{Prob.} = |a(t)|^2 = \tfrac{1}{2}\sin^2 2\theta \left[1 - \cos \frac{(\Delta)(t)}{2E_\nu \hbar} \right]$$

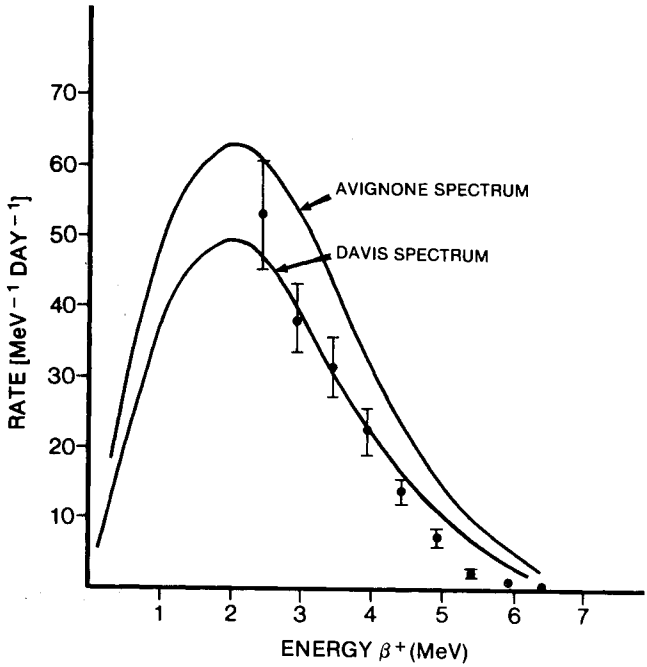

Fig. 3. 11.2 meter data from $\bar{\nu}_e + p \rightarrow n + e^+$.

Table I. Comparison of inverse beta decay results. The ratio of observed/predicted rates are tabulated.

Distance from Core Center (Meters)	Reaction	Neutrino Detection Threshold (MeV)	Ratio	
			Avignone Spectrum	Davis Spectrum
11.2	ccp	4.0	.68 ± .12	.88 ± .15
11.2	ccp	6.0	.42 ± .09	.58 ± .12
6	ccp	1.8	.65 ± .09	.84 ± .12
6	ccp	4.0	.81 ± .11	1.02 ± .15
8.7	ccp	3.0	.68 ± .15	.87 ± .14

where $\Delta = |m_1^2 - m_2^2|c^4$, and the oscillation length

$$\lambda(m) = \frac{2.5E_\nu(MeV)}{\Delta(eV^2)} \quad .$$

For $\bar{\nu}_e$ sensitive experiments, the ratio of counting rates with and without oscillations is given by:

$$R(d) = 1 - \tfrac{1}{2}\sin^2 2\theta \left[1 - \frac{\int N(E_\nu)\sigma(E_\nu)\cos(\frac{\Delta\, d}{2c\hbar E_\nu})dE_\nu}{\int N(E_\nu)\sigma(E_\nu)dE_\nu} \right]$$

where d = distance from source to detector

$N(E_\nu)$ = Neutrino flux

and, $\sigma(E_\nu)$ = Reaction cross section.

We can plot R(d) as a function of $\Delta \cdot d$ using $\sin^2 2\theta$ as a parameter for a particular process and energy interval. The result is a family of curves which can be used to imply Δ for any distance, d. In Fig. 4 for example, we plot such a family for the $\bar{\nu}_e + p$, charged current proton (ccp), reaction with a neutrino energy greater than 6.0 MeV. If we now use the Table I value $0.42 \pm .09$ (11.2 meters, $E_\nu > 6.0$ MeV, Avignone spectrum), Fig. 4 gives, for $\sin^2 2\theta = 1$, $\Delta = .42 \pm .04$ eV^2 and $\Delta = 1.1 \pm .05$ eV^2. We can continue this procedure and generate a plot of Δ vs. $\sin^2 2\theta$, showing a region allowed by this measurement at the one standard deviation level (Fig. 5). Using the same data, if we compare instead to the Davis spectrum we get an allowed region shown in Fig. 6.

From this we can see that the conclusions we reach with this technique depend very strongly on the spectrum we use for comparison.

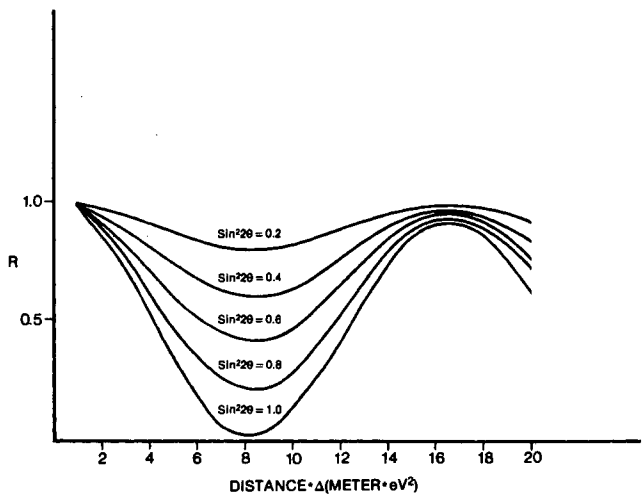

Fig. 4. R as a function of distance times Δ for ccp and $E_\nu > 6.0$ MeV.

3. The Deuteron Experiment

As part of our reactor program, we have been studying the neutral current reaction,[10]

$$\bar{\nu}_e + d \rightarrow n + p + \bar{\nu}_e \quad \text{(ncd)}$$

and its charged current counterpart

$$\bar{\nu}_e + d \rightarrow n + n + e^+ \quad \text{(ccd)}$$

We have recently realized that this experiment could be used as a neutrino oscillation test. The neutral current branch is independent of ν type, while the charged current branch will only occur for incident $\bar{\nu}_e$'s. In addition, while the predicted rates of the individual branches are sensitive to the predicted neutrino spectrum (Fig. 7), the ratio of the predited rates is not (Table II).

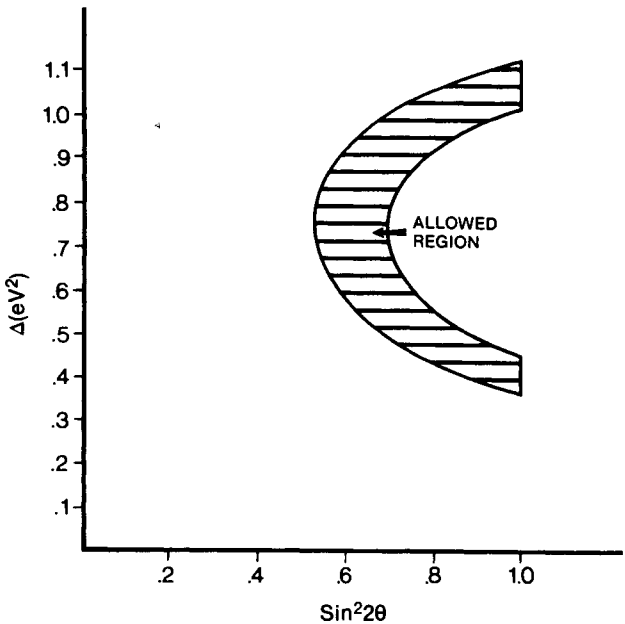

Fig. 5. $\Delta(ev^2)$ vs. $\sin^2 2\theta$ allowed region for 11.2 m ccp data; $E_\nu \geq 6.0$ MeV; Avignone spectrum.

We choose to define the quantity:

$$R = \frac{\left(\frac{ccd}{ncd}\right)_{experiment}}{\left(\frac{ccd}{ncd}\right)_{predicted}} .$$

The denominator of this quantity has the following features:

1. It is independent of the reactor neutrino absolute normalization.

2. It is insensitive to the precise shape of the reactor neutrino spectrum.

3. The ncd process is independent of neutrino type.

4. The ccd process only occurs with $\bar{\nu}_e$'s.

5. Assuming the standard model, the ratio of the coupling constants is known to $\sim$ 5%.[11]

The quantity, R, is expected to be unity. A value of R below unity would signal the instability of $\bar{\nu}_e$ as it traversed the distance (centered in this deuteron experiment at 11.2 meters) from its origin to the detector.

Experimental Approach

We have constructed a shielded volume at the reactor which has a greatly reduced neutron background. This shield made it feasible to search for the

n.c. reaction by looking only at the product neutron, so avoiding the proton background problem of the earlier approaches.[12] The c.c. reaction is identified by detecting both product neutrons in a time window of 2 ms (the neutron capture time in this detector is 300 μs). Those cases in which only one of the two neutrons from the c.c. reaction was detected represented background for the n.c. reaction.

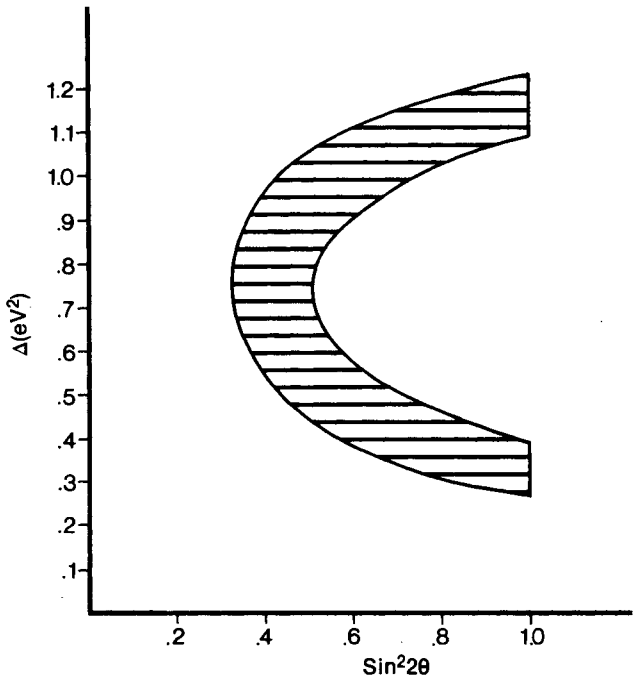

Fig. 6. $\Delta(eV^2)$ vs. $\sin^2 2\theta$ allowed region for 11.2 m ccp data; $E_\nu \geq 6.0$ MeV; Davis spectrum.

Detector Description

The target consists of 268 kg. of D_2O. Immersed in the D_2O are 10 cylindrical, helium-3 filled, neutron proportional counters. A side view of the detector is shown in Fig. 8. The target is enclosed in 10.2 cm of lead, 0.1 cm of cadmium and immersed in a 2200 liter anticoincidence detector. The detector is in turn surrounded by massive lead, concrete and water shielding. Events arise from a neutron capture in the ^3He counters,

$$^3He + n \rightarrow p + {}^3H + 773 \text{ keV}$$

which meet the trigger requirements. All signals from the ^3He counters and the anticoincidence system within 2 ms before and after an event are recorded.

Neutron Detection Efficiency

The neutron detection efficiency was determined using Monte Carlo techniques and a ^{252}Cf source.

1. Monte Carlo. The neutron detection efficiency for our system is dependent on the energy spectrum of the neutrons under consideration. Accordingly, the efficiency is different for neutrons emitted from the ^{252}Cf source and those resulting from the lower energy n.c., c.c. or $\bar{\nu}_e + p \rightarrow n + e^+$ (I.B) background reaction.

The Monte Carlo computer code utilized for these calculations is one written by the Savannah River Laboratory. It has an extensive cross section library. Originally written for reactor geometries, it was modified to simulate the geometry of this experiment. The calculation is two dimensional, assuming an infinitely long array, and therefore a correction due to the loss of

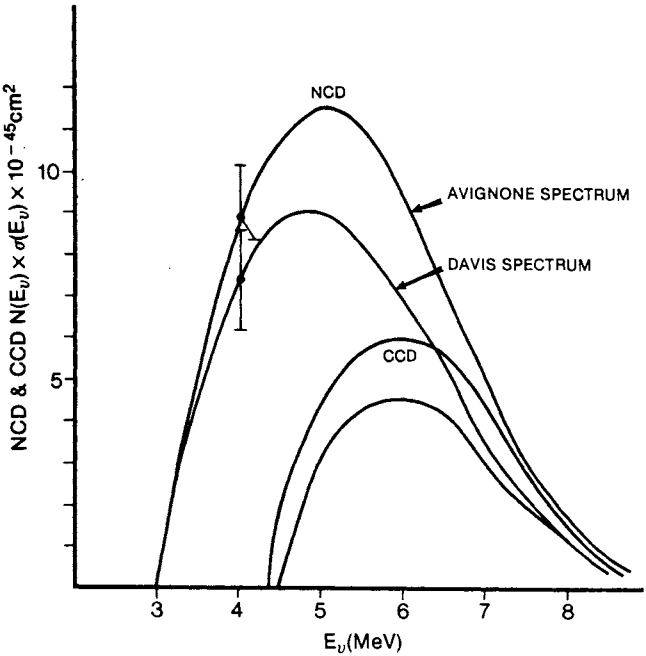

Fig. 7. Flux times cross section for ncd and ccd process as predicted from Avignone and Davis spectra.

Table II. Predicted cross sections for charged current and neutral current reactions, and the ratio of these predictions.		
Cross section (cm^2/fission)	Davis Spectrum	Avignone Spectrum
ncd	2.87×10^{-44}	3.73×10^{-44}
ccd	1.21×10^{-44}	1.64×10^{-44}
Ratio $\frac{ccd}{ncd}$	0.42	0.44

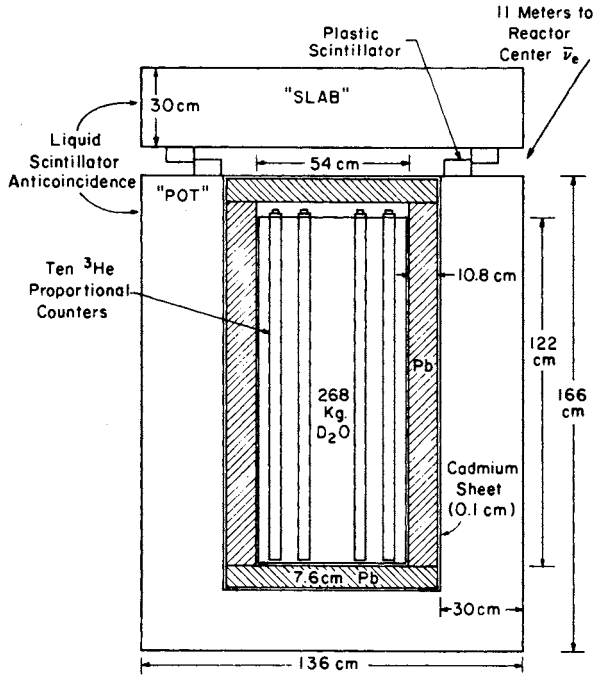

Fig. 8. Schematic diagram of the detector side view.

neutrons from the top and bottom of the detector must be made.

We find that the detection efficiency is relatively insensitive to neutron energy.

2. ^{252}Cf Source. We have checked the results of the Monte Carlo using a ^{252}Cf source positioned at various locations inside the detector.

a. A source calibrated to $\pm$ 3% was counted and the results used to establish efficiency as a function of location.

b. The Cf source is a source of multiple neutrons, emitting on the average 3.73 neutrons per fission.

The numbers of single, double, triple and multiple neutron events were recorded for each source position. The neutron detection efficiency can be determined from ratios of these values without a knowledge of the absolute source calibration.

The efficiencies derived from the Monte Carlo, the direct neutron counting, and the neutron multiplicity method are in agreement within the uncertainties given below. The efficiencies for single neutrons produced uniformly throughout the D_2O are:

$$\bar{\eta}_{n.c.} = \bar{\eta}_{c.c.} = .32 \pm .02$$

$$\bar{\eta}_{^{252}Cf} = .28 \pm .02$$

and,

$$\bar{\eta}_{I.B.} = .36 \pm .02$$

The efficiency for detecting two neutrons in the c.c. reaction is $\overline{\eta^2} = 0.112 \pm 0.009$ where the two neutron efficiency is averaged over the D_2O volume.

During single neutron analysis, we use $\overline{\eta'} = .89\ \bar{\eta}$, the efficiency loss due to a background reduction, cut.

Data

We report the results of two data sets. Each data set consists of a number of reactor on and reactor off sequences alternating in time. Several time groupings were made from these sequences, each consisting of reactor on and off data. Reactor associated (reactor on minus reactor off) single and double neutron rates were obtained for each group. Some of the groups in data set 1 are shown in Table III. From this, we see that we have a reactor associated signal from both single and double neutrons. We now establish that this signal is due to neutrinos, and further, that they are due to the deuteron reactions in question.

Background Tests

1. Neutrons. Our neutron background was established by completely surrounding our detector with an additional neutron shield. The observed change in our signal implied a neutron background of 0.7 ± 0.14 day^{-1}.

2. Gammas. The reactor associated gamma ray spectrum was measured with a 300 kg NaI detector in the same location as the D_2O target.

The background due to the (γ,n) reaction on the deuteron was calculated to be 0.05 day^{-1}.

3. $\bar{\nu}_e$ Background.

a. Our D_2O is not pure. The ratio of the number of protons to the number of deuterons is .0015. Since the inverse beta process has a relatively large cross section, this small contaminant gives a neutron background of 1.6 ± 0.1 day^{-1}.

b. The liquid scintillator anticoincidence detector consists of $CH_{1.8}$ and is therefore a large source of proton targets for the I.B. process. We calculate that about 10^4 day^{-1} are occurring in this detector. Most of the neutrons which are produced are thermalized in the scintillator, and captured on hydrogen or our cadmium shield. The probability of a neutron being seen by the ^3He detectors was calculated via Monte Carlo and measured with a neutron source immersed in the liquid scintillator. This probability varies from .0018 to

Table III. Sample neutron rates in data set 1.

	Group 1	Group 2	Group 3 . . .	Group 7	Weighted Mean
		Single Neutron Rate			
Reactor on (day^{-1})	386.90 ±11.83	387.27 ±11.90	406.31 ±6.72 . . .	439.95 ±6.98	
Reactor off (day^{-1})	323.73 ±7.32	320.01 ±5.09	333.92 ±12.92 . . .	385.61 ±5.68	
On-Off (day^{-1})	63.17 ±13.49	67.26 ±12.94	72.39 ±14.56 . . .	54.34 ±8.90	68.26 ±4.11
		Double Neutron Rate			
Reactor on (day^{-1})	53.51 ±4.40	54.12 ±4.45	58.54 ±2.55 . . .	51.85 ±2.40	
Reactor off (day^{-1})	47.67 ±2.81	51.55 ±2.04	55.87. . . ±4.96	46.81 ±1.98	
On-Off (day^{-1})	5.84 ±5.22	2.57 ±4.90	2.67 ±5.58 . . .	5.04 ±3.11	3.66 ±1.52

.00056 as a function of source location, and implies a background of 34 neutrons per day.

The I.B. process occurs in a live anticoincidence, and as a consequence a large fraction (.77) of the background events are discriminated against by means of the energy deposition of the positron and its annihilation gammas. The residual background is thus 7.9 ± 0.7 day^{-1}.

Deuteron Rates

We can now calculate the c.c.d. rate (R^{ccd}) and the n.c.d. rate (R^{ncd}) from the observed one neutron and 2 neutron signals (S_{1N}, S_{2N}).

$$R^{ccd} = \frac{S_{2N}}{\eta^2} \quad \text{and} \quad R^{ncd} = \frac{S_{1N}^{ncd}}{\eta_{1N}}$$

where: $S_{1N}^{ncd} = S_{1N} - S_{1N}^{(BKGND)} - S_{1N}^{ccd}$

and, $S_{1N}^{ccd} = 2(\eta_{1N})(1 - \eta_{1N})R^{ccd}$

The experimental ratio of ccd to ncd is therefore:

$$r_{exp} = \frac{R^{ccd}}{R^{ncd}} = \frac{\overline{\eta'}\, S_{2N}}{\overline{\eta^2}(S_{1N}-S_{1N}^{BKGND})-2(.89)(\bar{\eta}-\overline{\eta^2})S_{2N}}$$

and the error in r_{exp} is calculated from

$$\sigma^2_{r_{exp}} = (\frac{\partial r}{\partial S_{1N}})^2\sigma^2_{S_{1N}} + (\frac{\partial r}{\partial S_{2N}})^2\sigma^2_{S_{2N}} + \ldots$$

to be $r_{exp} = 0.167 \pm 0.093$.

We had that $R \equiv \frac{r_{exp}}{r_{theory}}$

so, $R_{\substack{\text{Avignone}\\\text{spectrum}}} = \frac{0.167 \pm .093}{0.44} = 0.38 \pm 0.21$

and, $R_{\substack{\text{Davis}\\\text{spectrum}}} = \frac{0.167 \pm .093}{0.42} = 0.40 \pm 0.22.$

These represent a 3.0 to 2.7 standard deviation departure from unity, assuming that the σ_r calculated above is representative of a normal distribution.

In the same way as for the ccp experiments the allowed values of Δ and $\sin^2 2\theta$ are plotted in Fig. 9 for $R = .38 \pm .21$.

Consistency Checks

1. We have mentioned previously another experiment at the 11.2 meter position which measured the ccp process. This positron spectrum has been used to obtain a $\bar{\nu}_e$ spectrum for $E_{\bar{\nu}_e} > 4$ MeV (Fig. 10). The value for R deduced using this spectrum, extrapolated below 4 MeV, is $0.47 \pm .24$, a 2.2 standard deviation effect. If neutrino oscillations occur, with the parameters implied by the deuteron experiment, then the extrapolation of the neutrino spectrum to lower energies would be in error and the value of R reduced.

2. In Table IV we list the individual ccd and ncd rates, and other previously mentioned reactor results compared to the predicted rates using the Avignone spectrum, the Davis spectrum and the measured $\bar{\nu}_e$ spectrum at 11.2 meters.

Unlike the insensitivity of R to the reactor neutrino spectrum, all other ratios of experimentally determined rates to predicted rates are markedly dependent on the spectrum and normalizations. For this reason, we consider the

precise values of these other ratios listed in Table IV to be of less significance. They can however be used to test consistency with R.

a. We note that since our measurement of the neutrino spectrum is only sensitive to $\bar{\nu}_e$ it should enable us to correctly predict the ratio for the charged current branch. Table IV indicates that the preliminary prediction for this ratio using the measured spectrum is 1.3 standard deviations from the expected value of unity. If the difference can be attributed to a normalization error between the two experiments it would have no effect on the ratio R. If, however, the difference is due to a statistical fluctuation and we therefore choose for the charged current the most likely value consistent with the two experiments, then the ratio R would become 0.62 ± 0.16. We note in this case that whereas R has increased, its error has diminished reflecting the greater precision of the prediction based on the measured $\bar{\nu}_e$ spectrum.

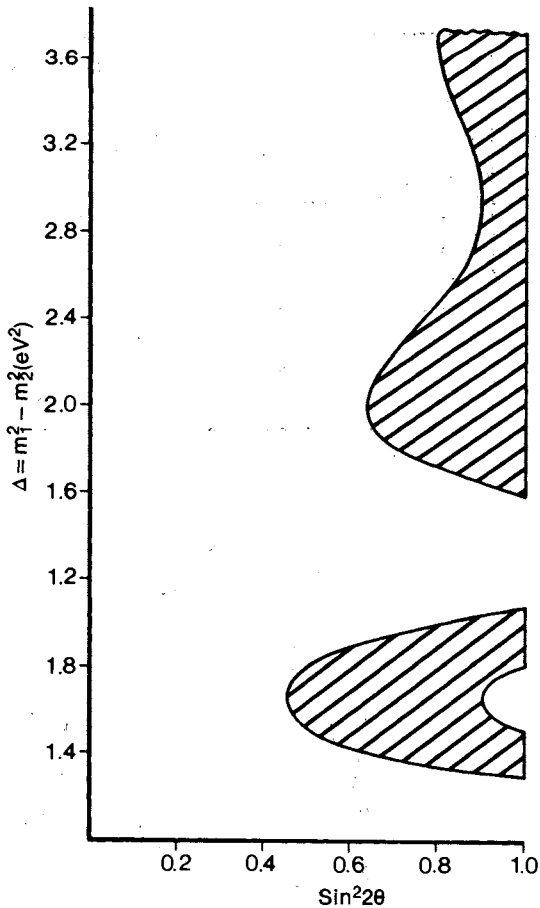

Fig. 9. $\Delta(eV^2)$ vs. $\sin^2 2\theta$ for $R = 0.38 \pm .21$.

b. Allowed regions Δ vs. $\sin^2 2\theta$ can be drawn for each of the ratios listed in Table IV. For the Avignone spectrum there is an overlapping region consistent with all the experiments at 11.2 meters but not with the > 4 MeV data at 6 meters. We note that small changes in the normalization of the 6 meter data could give agreement. This yeilds

$$0.5 \leq \sin^2 2\theta \leq 0.8 \quad (32^\circ > \theta > 22^\circ)$$

and

$$0.7 \leq \Delta(eV^2) \leq 1.0$$

We find that the Davis spectrum yields no overlapping region at the level of one standard deviation. On the other hand it appears to predict more precisely the observed neutral current branch of the deuteron experiment.

Table IV. Summary of Results for the Ratio $\frac{\bar{\sigma}_{expt.}}{\bar{\sigma}_{th.}}$

Distance from Core Center (Meters)	Reaction	Neutrino Detection Threshold (MeV)	Ratio		
			Avignone Spectrum	Davis Spectrum	Measured $\bar{\nu}_e$ Spectrum (preliminary)
11.2	ncd	2.2	.83 ± .13	1.10 ± .16	1.3 ± .22
11.2	ccd	4.0	.32 ± .14	.44 ± .19	.61 ± .29
11.2	ccp	4.0	.68 ± .12	.88 ± .15	≡ 1.0
11.2	ccp	6.0	.42 ± .09	.58 ± .12	≡ 1.0
6	ccp	1.8	.65 ± .09	.84 ± .12	-
6	ccp	4.0	.81 ± .11	1.02 ± .15	1.19 ± .27
8.7	ccp	3.0	.68 ± .15	.87 ± .14	-

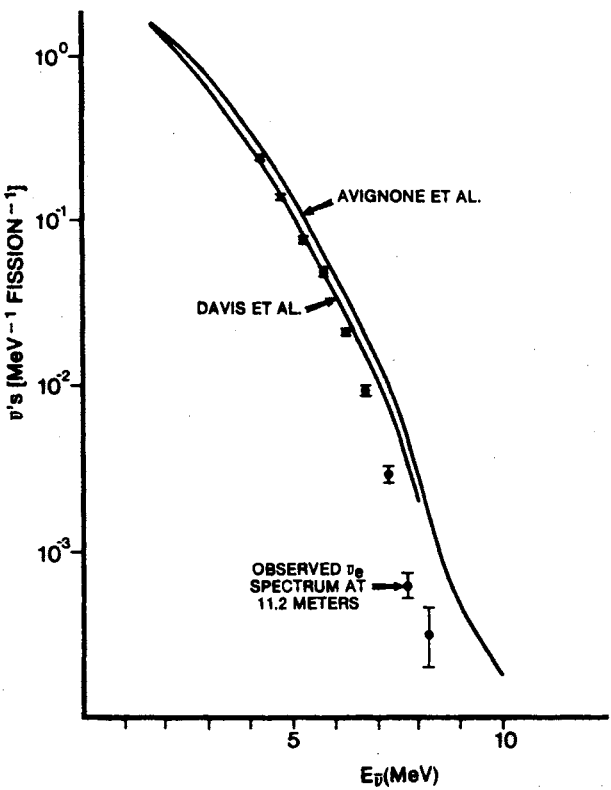

Fig. 10. The observed ν_e spectrum at 11.2 meters compared to Avignone and Davis predictions.

c. If oscillations occur with these approximate parameters, then the observed spectrum at 11.2 meters should show evidence of spectral changes. In Fig. 11 we plot the ratio of the observed 11.2 meter data to the Avignone prediction as a function of neutrino energy. If oscillations do not exist and further if the Avignone spectrum is the correct one, then the ratio should be 1.0 independent of energy. For comparison, the predicted ratio for $\Delta = 1$ eV^2 and $\sin^2 2\theta = 1$ is plotted. The same comparison is made, this time to the Davis spectrum in Fig. 12.

4. Conclusions

The results of a reactor experiment comparing the observed rates of the charged current and neutral current interactions of reactor neutrinos with deuterons gives an indication of neutrino instability at the 2 to 3 standard deviation level.

5. References

1. S. Blankenship - UCI internal report, UCI-10P19-102 (1976).
2. S. Blankenship - UCI internal report, UCI-10P19-104 (1976).
3. R. Davis, Jr., and D.S. Harmer, Bull. Amer. Phys. Soc. (2) 4, 219 (1959).
4. A. Soni and D. Silverman, private communication.
5. F. Nezrick and F. Reines, Phys. Rev. 142, 852 (1966).
6. F. Reines, H.S. Gurr, and H.W. Sobel, Phys. Rev. Lett. 37, 315 (1976).
7. F. Boehm, private communication.
8. UCI internal reports - UCI-10P19-141 (1979), UCI-10P19-132 (1978), UCI-10P19-126 (1977).
9. S. Blankenship, Georgia Institute of Technology, private communication.
10. E. Pasierb, H.S. Gurr, J. Lathrop, F. Reines and H.W. Sobel, Phys. Rev. Lett. 43, 96 (1979).
11. R.M. Ahrens and L. Gallaher, Phys. Rev. D20, 2714 (1979) and private communication (1980). S.L. Glashow, J. Iliopoulos and L. Maiani, Phys. Rev. D2, 1285 (1970).
12. J.H. Munsee and F. Reines, Phys. Rev. 177, 2002 (1969).

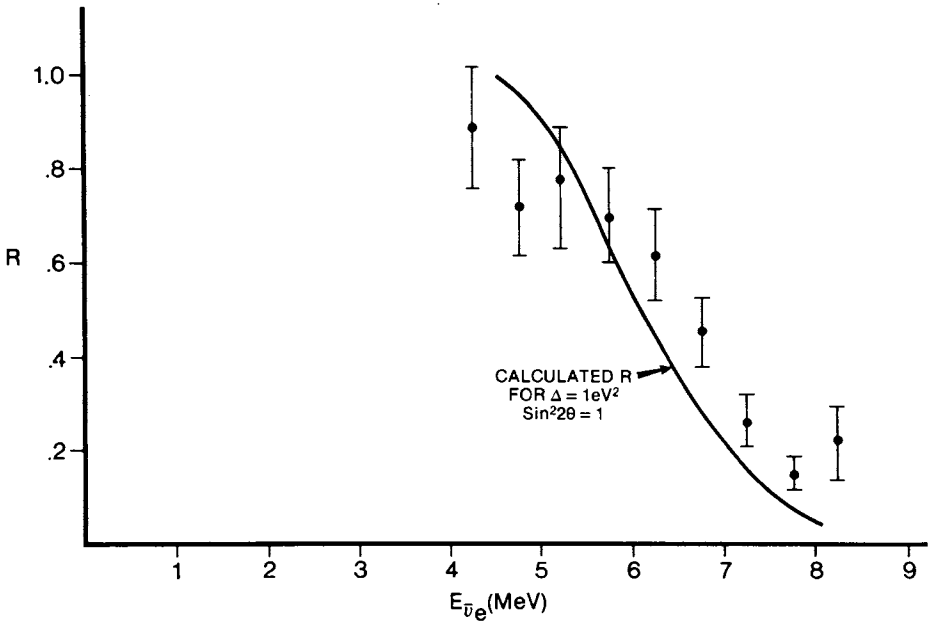

Fig. 11. The ratio of 11.2 meter ccp measured neutrino spectrum to that predicted by Avignone.

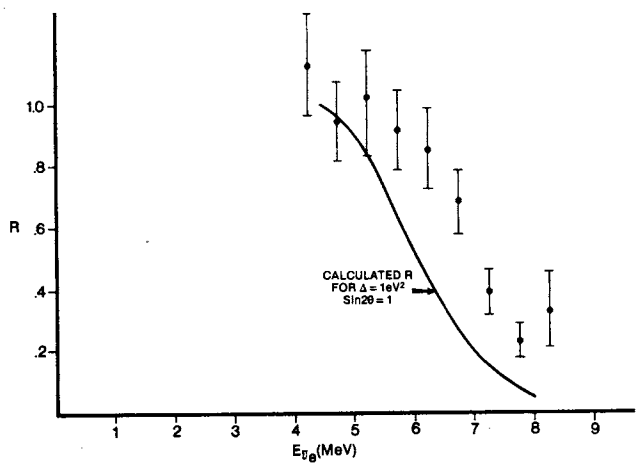

Fig. 12. The ratio of 11.2 meter ccp measured neutrino spectrum to that predicted by Davis.

NEUTRINO OSCILLATIONS IN DUMAND

V. J. Stenger
Department of Physics and Astronomy
University of Hawaii
Honolulu, Hawaii 96822

ABSTRACT

A Monte Carlo simulation of a one-year experiment with a 0.9 km^3 DUMAND Array yields 18,656 expected events with one muon from ν_μ charged-current interactions. It is shown that neutrino oscillations resulting from eigenmass-squared differences in the range .1 to 1000 eV^2 would be detectable as a modulation of the one-muon event rate with zenith angle. Using several proposed models, it is shown that the statistics and measurement precision are adequate to aid in the determination of mass differences and mixing angles and perhaps provide unique information on matter oscillations.

INTRODUCTION

Because of the large range in path length for neutrinos passing through the earth, experiments deep underground or underwater offer unique possibilities in the study of neutrino oscillations. This report considers those possibilities for DUMAND. By means of a Monte Carlo simulation, it is shown that the reaction

$$\nu_\mu N \rightarrow \mu X$$

will be modulated by neutrino oscillations of the type which have been recently considered[1,2]. This modulation would be detectable with sufficient statistics and precision to provide important information on the mass difference and mixing matrix elements involved.

In Fig. 1 we define the zenith angles, θ at the detector and θ^* at the production point in the atmosphere, and show how the path length L is related to θ. Other Monte Carlos[3] have shown that DUMAND is capable of measuring the muon direction and thus θ, to an accuracy of 10 mr for muons above 1 TeV, so L would be well-determined. In particular, we note the large dynamic range in L, from 20 to 12,000 km, which makes this experiment, and the others proposed for deep mines, a powerful probe of neutrino oscillations.

If we consider energies above 1 TeV or so, the range in L/E for DUMAND is $\sim 10^{-3}$ to 10 m/MeV and thus the detectable range of neutrino eigenmass-squared differences is 0.1 to 10^3 eV^2. While this range is not unique and will be explored by a number of upcoming experiments at reactors and accelerators, the energy is considerably higher than what can be studied in the much less massive deep mine experiments and so effects, such as matter oscillations[4], which may depend on L and E separately, might be uniquely studied.

SIMULATION OF EXPERIMENT

For this study one year's supply of events in a 0.6 km^3 array (e.g., DUMAND G2[5]) were generated. The assumptions were:

1. The atmospheric muon neutrino and anti-neutrino flux is given by[6]

$$\Phi(>E_\nu) = 125E_\nu^{-3.8}\sec\theta * km^{-2}s^{-1}sr^{-1}$$

2. $\nu_\mu = 2\bar{\nu}_\mu$[7].

3. The cross section is given by the standard theory, with $M_W = 80$ GeV and QCD effects included.

Measurement errors are simulated by a Gaussian wiggling of the true values with standard deviations of 10 mr for the muon angles θ_μ (which we take to be the zenith θ), and 40% in the muon and hadron energy. These are based on results of array simulations [3].

Applying a cut to the simulated measured neutrino energy E_ν of 1 TeV, we get 15,212 ν_μ and 3,444 $\bar{\nu}_\mu$ charged-current (one-muon) events, or a total of 18,656 for a one-year simulated run.

We then proceed to study these events as if they were real data. All the results presented thus will have statistical and systematic errors which hopefully realistically represent those for actual experiment.

EFFECT OF OSCILLATIONS

A wide range of oscillation possibilities exists, especially in the framework of 3 neutrinos. In order to be able to get some indication of the sensitivity of DUMAND to oscillations specific models which take into account the range of available data from all relevant experiments have been used to calculate the probability $P(\nu_\mu \to \nu_\mu)$[1,2]. These are listed in Table I, along with the mass-squared differences assumed. The matrix elements are not given and the reader is referred to the references for these. However, it is to be remarked that all except Barger et al. Model B suppress ν_μ oscillations for the second mass-squared difference listed in the table.

Table I. Neutrino oscillation models and the mass-squared differences assumed.

Model		δm^2 (eV^2)	
De Rujula et al.[1]		1	100
Barger et al.[2]	A	.05	1
	B	.05	.25
	C	1	50

In this analysis the effects of matter oscillations have been neglected, although these are expected to be important for large L and may, in fact, prove to be very interesting in DUMAND. Also neglected is the possible oscillation of ν_e in the "beam" into ν_μ. Since $\nu_e \ll \nu_\mu$ in the TeV range, because of the large time dilation of the muon lifetime, this is a reasonable assumption and another advantage of DUMAND over lower energy experiments.

RESULTS

In Fig. 2 we present the simulated path length distribution showing what is expected for no oscillations compared with the various models. The strange

shape of the distribution is a result of the rapid variation of L as θ passes through 90° (see Fig. 1).

We see that oscillation effects are evident in the region of $L > 1000$ km, and all models studied are distinguishable. The De Rujula model gives the most dramatic effect, resulting from the large $\delta m^2 = 1\ eV^2$ oscillation. This same oscillation is suppressed in Barger A, but the .05 eV^2 oscillation is just beginning to be evident in the simulated data. The other models, Barger B and C, also show detectable, and distinguishably different, effects.

In Fig. 3 we see the results for the distribution of L/E. Here again the oscillation is evident except for Barger A which shows no effect. It is to be remarked that L is very well determined since it depends only on the well-measured θ, while L/E depends on E which is measured to only 40% precision. Nevertheless effects are still seen in L/E.

The distributions of L and L/E have very pronounced variations which result purely from geometry and the $\sec\theta^*$ distribution of the "beam". When looking for an effect, it is nice to have a variable which is flat in the absence of the effect. Such a variable is defined as

$$\zeta = \ln\cos\theta^*/\ln\cos\theta^*_{max}$$

where θ^* is the zenith angle at the production point in the atmosphere (Fig. 1) and $\theta^*_{max} = 87^{\circ}$ corresponds to $\theta = 90^{\circ}$.

A $\sec\theta^*$ distribution in the neutrino flux will result in a flat distribution in ζ. In Fig.4 the simulated results are shown for the distribution of ζ with conclusions similar to those for L and L/E. The models except Barger A give distinguishable differences with very nice oscillations evident. In particular, note the 3 cycles of oscillation detected for De Rujula's model, and the one full oscillation for Barger B.

OTHER POSSIBILITIES

While the charged current interaction of muon neutrinos is the easiest the detect and study in DUMAND, the mixing angles for neutrino oscillations may be much smaller than those assumed in the models used in this report. In that case the modulation of the charged current event rate may not be detectable. The easiest way to detect a small oscillation is by means of a flavor change, e.g., $\nu_\mu \rightarrow \nu_e$. As Cline has pointed out[8], the flux of electron neutrinos produced in the atmosphere is expected to be about 1% of that of muon neutrinos. For any reasonable sized detector designed for ν_e the event rate will be less than one event per year[9]. Thus any signal of ν_e events is "something interesting", either extraterrestrial or neutrino oscillation. Directional information would be necessary to distinguish between the two.

CONCLUSIONS

If neutrino eigenmass-squared differences on the range $.1 \leq m^2 \leq 1000\ eV^2$ exist, they could be detectable in DUMAND unless they happen to be suppressed by small mixing matrix elements. More than this, the statistics and measurement precision would be adequate to help pin down the parameters of the oscillation. While the region of L/E explored is not unique but will be covered by experiments involving synthetic neutrinos, it is the only experiment proposed which will explore this entire range, 10^{-3} to 10 m/MeV, in one experiment. Finally, the energy is much higher than what will be studied in deep mines so

that effects which depend on L or E separately, such as matter oscillations, might be explored in a unique fashion.

The author is grateful to Sandip Pakvasa for his help on this study. The work was supported in part by the U.S. Department of Energy under Contract DE-AC03-76ER00511.

REFERENCES

1. A. DeRejula, et al., Ref.TH.2788-CERN(1979).

2. V. Barger,K. Whisnant, R.J.N. Phillips, DOE-ER/00181-151(1980).

3. V.J. Stenger, Proc. DUMAND 1979 Workshops at Khabaraovsk and Lake Baikal, p.22 (1980); also see A. Roberts and V.J. Stenger, "Monte Carlo Studies of DUMAND Array Performance", these proceedings.

4. L. Wolfenstein, Phys.Rev.D17,2369(1978).

5. A. Roberts and G.A. Wilkins, "Proposed Modification to DUMAND G: DUMAND G2", these proceedings.

6. O.C. Allkofer et al.,Proc. DUMAND 1978 Symposium and Workshop at La Jolla, Calif.,Vol. I,p.37(1978).

7. A. Okada, ibid.,p.65.

8. D. Cline, "Neutrino Physics Possibilities with a Graded Sensor Array in DUMAND", these proceedings.

9. V.J. Stenger, "The Minimum Detectable Flux of Extraterrestrial Neutrinos", these proceedings.

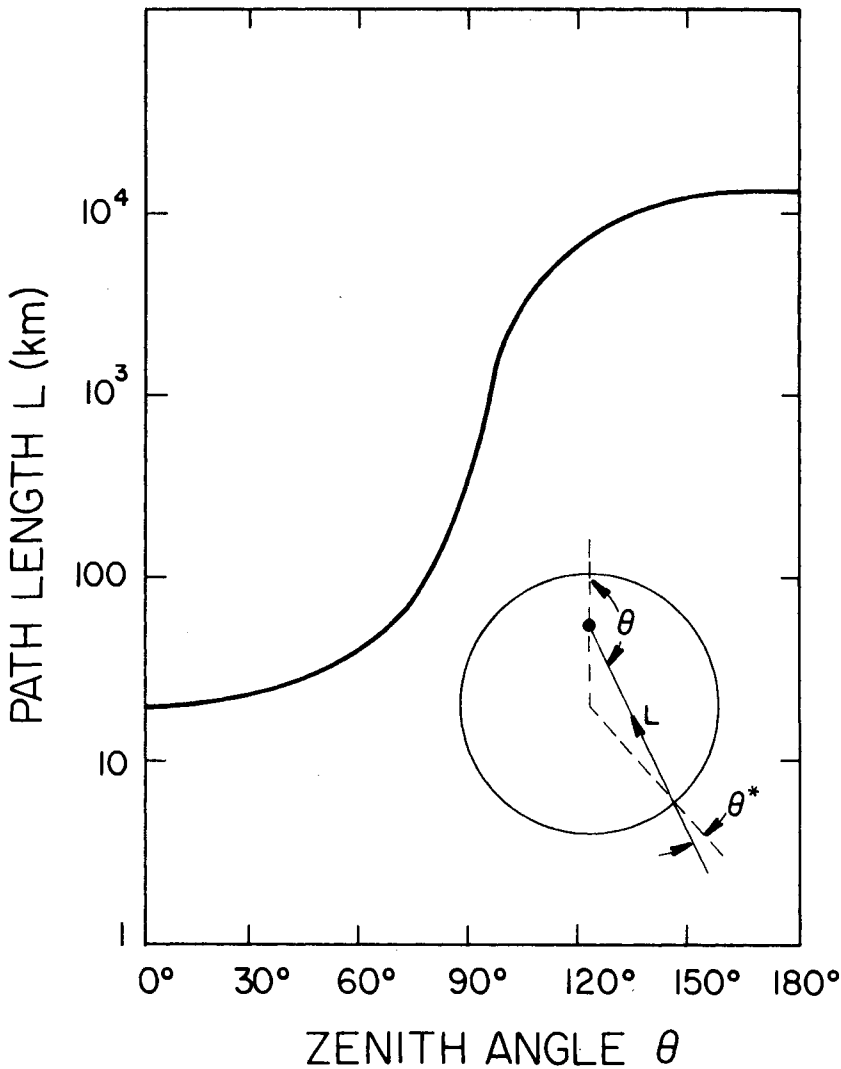

Fig. 1. Neutrino path length through the earth as a function of zenith angle.

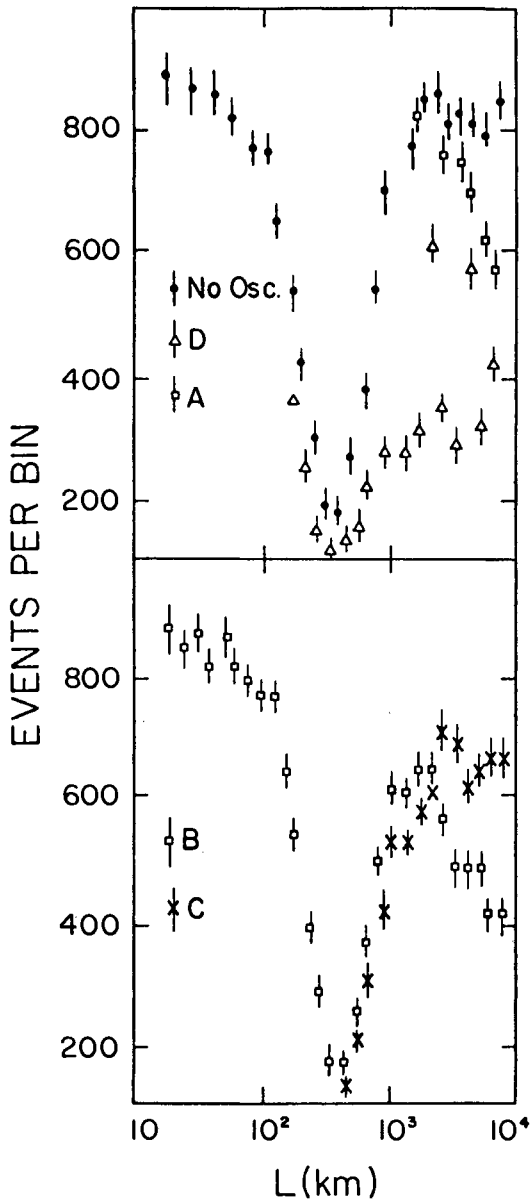

Fig. 2. Path length distribution for a one year simulated experiment. Shown are the results for no oscillations and the four oscillation models discussed in the text: D = DeRujula, et al.[1], A,B,C = Barger et al.[2].

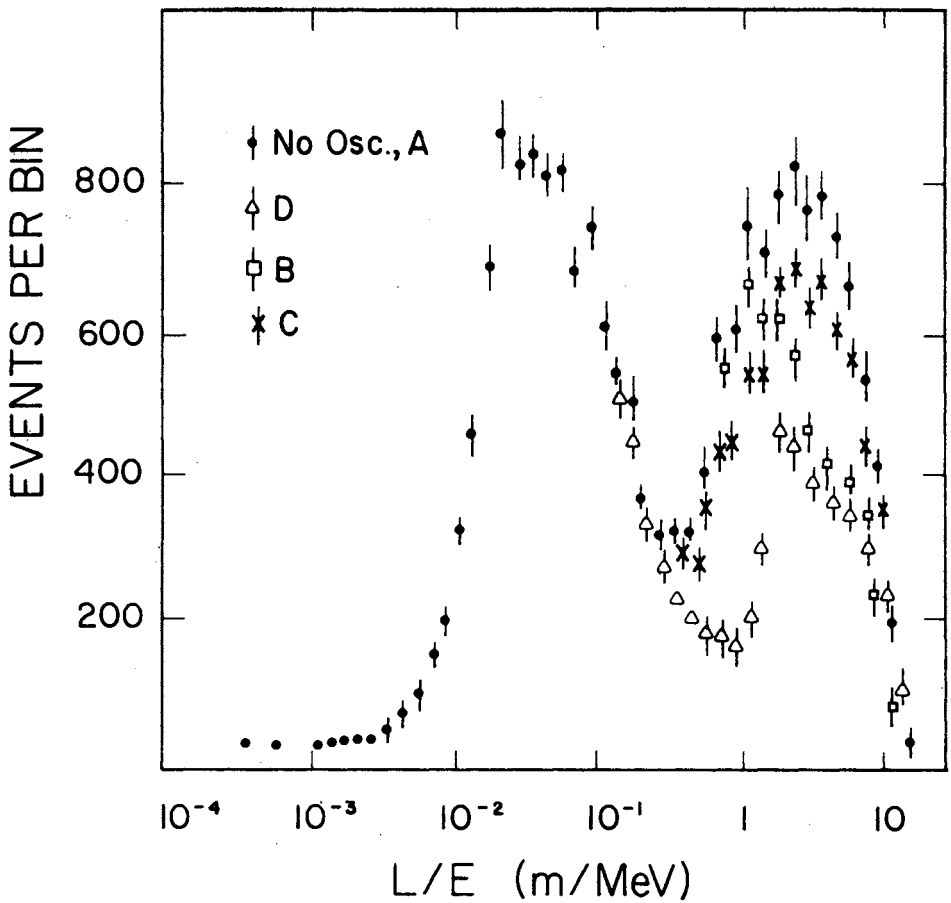

Fig. 3. Distribution of L/E for a one year simulated experiment. Shown are the results for no oscillations and the four oscillation models discussed in the text: D = DeRujula, et al.[1], A,B,C = Barger et al.[2].

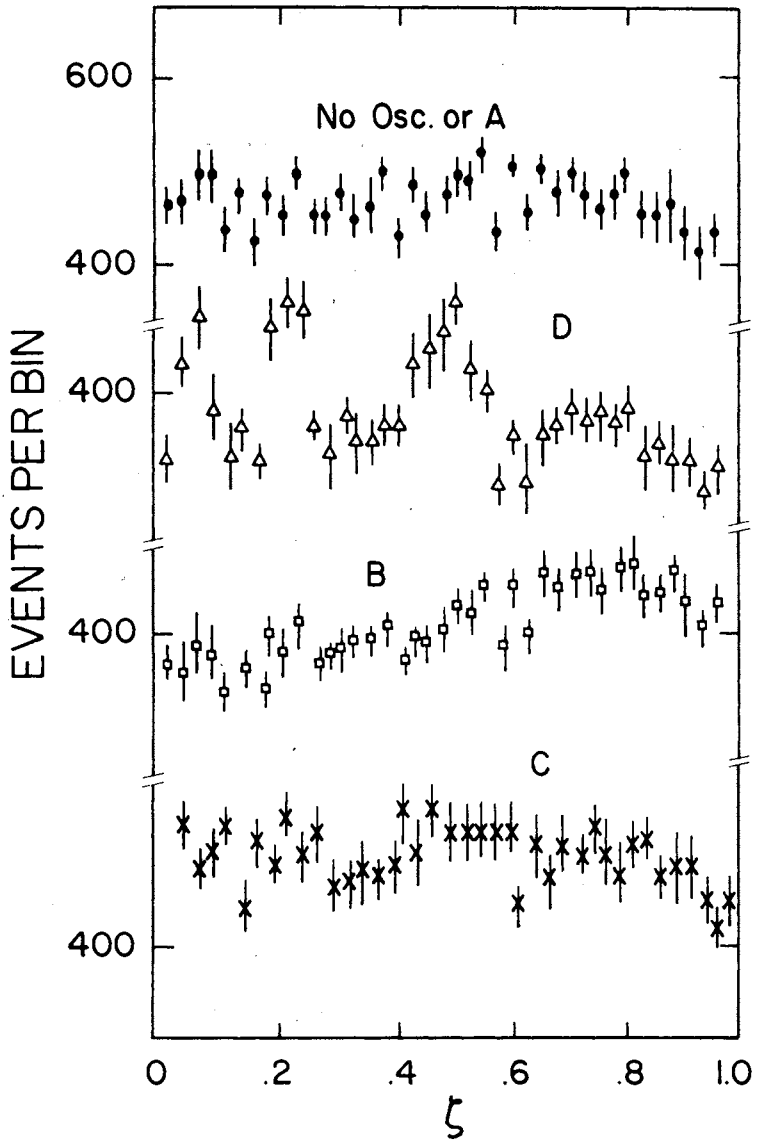

Fig. 4. Distribution of ζ for a one year simulated experiment. Shown are the results for no oscillations and the four oscillation models discussed in the text: D = DeRujula, et al.[1], A,B,C = Barger et al.[2].

NEUTRINO OSCILLATIONS AND MATTER EFFECTS

Sandip Pakvasa
Department of Physics and Astronomy
University of Hawaii
Honolulu, Hawaii 96822

ABSTRACT

The phenomenology of neutrino mixing and oscillations is reviewed, and the importance of effect of matter is discussed.

It seems that high-energy physics community has to be reminded every few years that there is no reason for neutrino masses to be zero, and that in general they will have different masses and mix in the weak current similarly to the quarks. The impetus this time on the theoretical side comes from the fact that unified models such as SO(10), etc., in general lead to non-zero masses for the neutrinos and also the realization that the standard model does not require neutrino masses to be zero (any more than it predicts any other fermion masses). Hence in general there will also be mixing and oscillations. On the experimental side there are several suggestive results: the recent results of the Reines group on Reactor antineutrinos, the new ITEP result on m_{ν_e} from tritium β-ray spectrum and the old problem of solar neutrinos.

There are no firm predictions of neutrino masses or mixings but one can speculate. A wild speculation, e.g., would be based on the long-noticed fact that $m_e/m_\mu \sim 0(\alpha)$ and perhaps

$$m_{\nu_e}/m_e \sim 0(\alpha^2) \tag{1}$$

leading to the expectation that[1]

$$m_{\nu_e} \sim 25 \text{ eV}. \tag{2}$$

A not-so-wild speculation would be to expect a scaling in neutrino masses similar to charged leptons and quarks, e.g.,

$$m_{\nu_e}/m_{\nu_\mu}/m_{\nu_\tau} \sim m_e/m_\mu/m_\tau \sim m_u/m_c/m_t, \tag{3}$$

i.e. proportionality of mass matrices. In this case the mixing matrix is identical for leptons and quarks.

$$U_\ell = U_{KM}. \tag{4}$$

There are half-way decent symmetries one can invent that would predict just this.[2] There are other proposals based on unified schemes such as SO(10) in which ν_R is given a very large mass M ($\sim 10^{14}$ GeV) and then depending on the specific mechanism[3] one can have

$$\begin{aligned} m_\nu &\sim m_q^2/M \\ &\sim 10^{-12} \text{ eV } (\nu_e) \text{ to } 10^{-4} \text{ eV } (\nu_\tau) \end{aligned} \tag{5}$$

or

$$\begin{aligned} m_\nu &\sim m_q m_W/\alpha^2 M \\ &\sim 1 \text{ eV } (\nu_e) \text{ to } 3 \text{ KeV } (\nu_\tau). \end{aligned} \tag{6}$$

In left-right symmetric models, it is possible to relate m_ν to m_{W_R}, e.g.,

$$m_\nu \sim \frac{m_\ell^2}{e\, m_{W_R}} . \tag{7}$$

Various forms for the mixing matrix have also been proposed and discussed.

Let me briefly recall the basic phenomenology[4] of neutrino oscillations although by now everyone is familiar with it. Consider the case of two neutrinos for simplicity--the generalization to three or more is straightforward. The charged weak current for leptons is

$$J_\mu = (\bar{e}\bar{\mu})_L \gamma_\mu \begin{pmatrix} \cos\phi & \sin\phi \\ -\sin\phi & \cos\phi \end{pmatrix} \begin{pmatrix} \nu_1 \\ \nu_2 \end{pmatrix}_L , \tag{8}$$

where ν_1 and ν_2 are mass eigenstates (Dirac or Majorana). Since

$$J_\mu = (\bar{e}\bar{\mu})_L \gamma_\mu \begin{pmatrix} \nu_e \\ \nu_\mu \end{pmatrix}_L \tag{9}$$

by definition; hence

$$\begin{aligned} \nu_e &= \cos\phi\, \nu_1 + \sin\phi\, \nu_2 \\ \nu_\mu &= -\sin\phi\, \nu_1 + \cos\phi\, \nu_2 \end{aligned} \tag{10}$$

and if one could measure the mass of the ν emitted in inverse β-decay, then one would find ν_1 with probability $\cos^2\phi$ and ν_2 with probability $\sin^2\phi$ (assuming equal phase space for both). Consider the wave function of a ν emitted in β^+-decay at t = 0,

$$\psi(0) = \nu_e = \cos\phi\ \nu_1 + \sin\phi\ \nu_2. \tag{11}$$

At a later time t,

$$\psi(t) = \cos\phi\ \nu_1\ e^{-iE_1 t} + \sin\phi\ \nu_2\ e^{-iE_2 t}. \tag{12}$$

The amplitudes and probabilities for finding ν_e or ν_μ at time t are then

$$\begin{aligned} A\ (\nu_e \to \nu_e,\ t) &= \cos^2\phi\ e^{-iE_1 t} + \sin^2\phi\ e^{-iE_2 t}, \\ A\ (\nu_e \to \nu_\mu,\ t) &= \cos\phi\sin\phi\ (-e^{-iE_1 t} + e^{-iE_2 t}), \end{aligned} \tag{13}$$

$$\begin{aligned} P\ (\nu_e \to \nu_e,\ t) &= 1 - \sin^2 2\phi\ \sin^2(\delta E_{12} t/2), \\ P\ (\nu_e \to \nu_\mu,\ t) &= \sin^2 2\phi\ \sin^2(\delta E_{12} t/2). \end{aligned} \tag{14}$$

Generalization to three neutrinos, e.g., is obtained by writing

$$\nu_\alpha = \sum_{i=1}^{3} U_{\alpha i}\ \nu_i$$

$$A\ (\nu_\alpha \to \nu_\beta,\ t) = \sum_i U_{\alpha i}\ e^{-iE_i t}\ U^\dagger_{i\beta} \tag{15}$$

$$P\ (\nu_\alpha \to \nu_\beta,\ t) = |A\ (\nu_\alpha \to \nu_\mu,\ t)|^2$$

where α = e, μ or τ and $U_{\alpha i}$ are elements of a 3x3 unitary matrix.

Going back to the 2x2 case, if the initial state is a momentum eigenstate (a careful treatment with wave packets confirms this) and $p,E \gg m_i$

$$\begin{aligned} \frac{1}{2}\ (E_1 - E_2)t = \frac{1}{2}\ \delta E_{12} t \ &\doteq\ \left(\frac{m_1^2 - m_2^2}{4p}\right) x = \frac{\delta m_{12}^2 x}{4p} = \frac{\delta m_{12}^2 x}{4E} \\ &= 1.27\ \delta m_{12}^2\ (eV^2)\ L(m)/E\ (MeV). \end{aligned} \tag{16}$$

Note that the (vacuum) oscillations are unchaged under $\delta m_{12}^2 \to -\delta m_{12}^2$ and under $\phi \to \pi/2 - \phi$ and hence do not distinguish the dominant component of ν_e.

To observe the effects of oscillations some obvious conditions must be satisfied. E.g., for interference to take place, beam coherence must be

satisfied, i.e., size of the wave packet must be large compared to the separation of the two components.

$$d \gtrsim \lambda \times (v_1 - v_2) \sim \frac{L \delta m_{12}^2}{2E^2} . \qquad (17)$$

Also, to see the actual oscillating behavior, $\frac{\delta m_{12}^2 L}{E}$ must not be too large because otherwise $\sin^2 1.27 \frac{\delta m_{12}^2 L}{E}$ just averages to 1/2. Of course one still sees a change of intensity. A lack of energy resolution at the source or detector has a similar averaging effect. The oscillating behavior is strongest, of course, if δm_{12}^2 L/E is near one, for instance. Some typical values for L/E, δm^2 sensitivity and available ν's for various sources are listed in Table I.

Table I

Experimentally Accessible Ranges of L/E

Source	Beams	L/E (m/MeV)	δm^2 Sensitivity (eV)
Sun	ν_e	10^{10}	$> 10^{-10}$
Deep Mine	$\nu_\mu, \nu_e, \bar{\nu}_\mu, \bar{\nu}_e$	$10\text{-}10^5$	$> 10^{-5}$
DUMAND	$\nu_\mu, \bar{\nu}_\mu, \nu_\tau, \bar{\nu}_\tau$	0.1 to 10^3	10^{-3} to 10
Low Energy Accelerators	$\nu_\mu, \nu_e, \bar{\nu}_\mu\ \bar{\nu}_e$	1 to 7	$\sim$ 0.1 to 1
Reactors	$\bar{\nu}_e$	1 to 15	$\sim$ 0.1 to 1
Meson Factories	$\nu_\mu, \nu_e, \bar{\nu}_\mu, \bar{\nu}_e$	0.3 to 3	$\sim$ 0.1 to 10
High Energy Accelerators	ν_μ, ν_e, ν_τ $\bar{\nu}_\mu, \bar{\nu}_e, \bar{\nu}_\tau$	0.01 to 0.05	$\sim 10^2$

Before summarizing the present indications of non-zero neutrino masses and oscillation effects, I would like to mention two other kinds of neutrino oscillation that can occur in practice. These can arise in the following way. When there is a ν_R, in general, in addition to the usual Dirac mass terms of the type $m_D \bar{\nu}_L \nu_R$, one can also have Majorna mass terms of the type $m_L \nu_L^c \nu_L$ and $m_R \nu_R^c \nu_R$. The result of diagonalizing the 2 x 2 mass matrix is that the original ν_L is a mixture of two Majorana mass eigenstates, ν_1 and ν_2, e.g., $\nu_L = \cos\chi\ \nu_1 + \sin\chi\ \nu_2$. The orthogonal combination being η_L. Another way of thinking about this mixing is doublet-singlet mixing or equivalently to have more neutrinos than charged leptons. As a result of this, a ν_e produced in inverse beta decay oscillates[5] into a mixture of ν_e and η_e as long as m_1, m_2 are both small. And since η_e is essentially sterile (non-interacting), it is lost and $P(\nu_e \to \nu_e, t)$ decreases leading to apparent non-conservation of probability, Specifically,

$$P(\nu_e \to \nu_e, t) = 1 - \sin^2 2\chi \sin^2 \frac{\delta m_{12}^2 L}{4E} . \qquad (18)$$

Because of non-zero mass of the neutrinos and possible admixture of V + A coupling, in this case there is also some "true" neutrino-antineutrino oscillations,[6] i.e., $\bar{\nu}_{e_R}$ with a probability

$$P(\nu_{e_L} \to \bar{\nu}_{e_R}, t) = 4|\alpha|^2|\beta|^2 \sin^2 2\chi \sin^2 \frac{\delta m_{12}^2 L}{4E} , \qquad (19)$$

where

$$4|\alpha|^2|\beta|^2 = \frac{4\epsilon^2}{(1+\epsilon^2)^2} + \frac{(1-\epsilon^2)^2}{(1+\epsilon^2)^2} \cdot \frac{m^2}{E^2} ,$$

ϵ is the ratio of the amount of V + A to V - A coupling and $m^2 = m_1^2\cos^2\chi + m_2^2\sin^2\chi$. In the rest of the discussion we shall ignore such oscillations and concentrate on flavor oscillations of the $\nu_e \leftrightarrow \nu_\mu \leftrightarrow \nu_\tau$ kind. This amounts to assuming a) pure Dirac masses for ν's, or b) pure Majorana masses for ν_L's, or c) that one of the m_1, m_2 is much larger than all masses of interest, or d) that angles χ_i are all essentially zero.

The present indications for non-zero neutrino masses and mixings are:

a) The ITEP result[7] that 14 eV < "m_{ν_e}" < 46 eV from a measurement of electron energy spectrum in Tritium Beta Decay.

b) The celebrated solar neutrino result of Davis et al.[8] viz. that the $\langle\phi\sigma\rangle$ for solar ν's on chlorine is 2.2±1.5 SNU (1 SNU = 1 ν capture/sec/10^{36} Cl).

The latest prediction of the standard model[9] for the sun is 7.5±1.5 SNU. This would suggest that

$$P(\nu_e \to \nu_e,\ t \to \infty) \lesssim 1/3\ (L/E \sim 10^{10}\ \text{m/MeV})$$

if all $\delta m^2 \ll 10^{-10}\ eV^2$. Even if one $\delta m^2 \sim 10^{-10}\ eV^2$, the broad energy spectrum tends to have an averaging effect.

c) The result of the Reines group on measurement of $(\bar{\nu}+n+p \to nne)/(\bar{\nu}+n+p \to \bar{\nu}+n+p)$ with Savannah River reactor beam of $\bar{\nu}_e$ suggests[10] that

$$P(\bar{\nu}_e \to \bar{\nu}_e,\ L/E \sim 2\ \text{m/MeV}) \sim 1/2.$$

d) Deep mine measurements of ν_μ events ($E \sim 1$ to 10 GeVs $L \gtrsim 10^4$m) suggest[11]

$$P(\nu_\mu \to \nu_\mu,\ L/E \sim 50\ \text{m/MeV}) \sim 1/2.$$

There are also stringent limits on other rates from accelerator experiments,[12] e.g., at $L/E \sim 0.04$ m/MeV

$$\begin{aligned} P_o = P(\nu_\mu \to \nu_\mu) &> 0.99 \\ P(\nu_\mu \to \nu_\tau) &< 0.01 \\ P(\nu_e \to \nu_e) &> (0.92\pm0.21)P_o \\ P(\nu_\mu \to \nu_e) &< (1.3 \times 10^{-2})P_o \end{aligned}$$

One can search for a matrix U (Eq. 15) and δm^2_{ij} values that will accommodate all the data, e.g., one such solution is:[13]

$$\delta m^2 = 1\ eV^2, \qquad \delta m^2 = 5 \times 10^{-2}\ eV^2$$

$$U = \begin{pmatrix} 0.64 & 0.66 & 0.38 \\ -0.72 & 0.69 & 0.01 \\ -0.26 & -0.28 & 0.92 \end{pmatrix}. \tag{20}$$

This would predict $P(\nu_e \to \nu_e) \sim 0.4$ for solar neutrinos and $P(\nu_\mu \to \nu_\mu) \sim 0.5$ for deep mine events.

There are many experiments underway, as well as new proposals to measure these transition rates $P(\nu_\alpha \to \nu_\beta, t)$ for various values of L/E which would test these proposals for U and δm^2 in the near future.[14] Two interesting effects are looking for $\nu_\mu e$ event rate in a ν_μ beam which should grow[15] if $\nu_\mu \to \nu_e$ at all and by the same token look for $\nu_e e$ event rate in a ν_e beam which should decrease[16] if ν_e goes into other flavors. The first one is

especially interesting as it distinguishes flavor mixing from doublet-singlet mixing unambiguouly.

Let me consider a grossly simplified experiment looking for events from neutrinos produced by cosmic rays in the atmosphere in either a deep mine or a DUMAND-like set-up. Let me consider only vertical intensity due to neutrinos going downwards (from atmosphere) or upwards (thru the earth). The proper thing to do would be to calculate for all zenith angles and take the zenith angle and energy spectrum into account as for example the Monte Carlo calculations to be presented by Stenger. To simplify further, let me assume that we detect leptons in an energy range where mostly ν_μ's are produced in the atmosphere ($N \equiv N_{\nu_\mu} >> N_{\nu_e}, N_{\nu_\tau}$). Now if all δm^2_{ij}'s are in the range

$$\frac{1}{x_{down}} << \frac{\delta m^2}{4p} << \frac{1}{x_{up}} , \tag{21}$$

since $x_{down} \sim 10^4$ m and $x_{up} \sim 10^7$ m, for E $\sim$ few GeV, this limits δm^2_{ij} to be in the range

$$10^{-3}\ eV^2 << \delta m^2 << 1\ eV^2.$$

Then in the limit of only ν_μ, ν_e mixing we have

$$\begin{aligned} N^d_\mu &= N_o, & N^d_e &= 0 \\ N^u_\mu &= (1 - \tfrac{1}{2}\sin^2 2\phi)N_o, & N^u_e &= (\tfrac{1}{2}\sin^2 2\phi)N_o. \end{aligned} \tag{22}$$

And therefore we have[17]

$$\left(\frac{N_\mu - N_e}{N_\mu + N_e}\right)_{up} \Bigg/ \left(\frac{N_\mu - N_e}{N_\mu + N_e}\right)_{down} = \cos^2 2\phi. \tag{23}$$

So the number of muons and electrons going up and down yield a measurement of the mixing angle. If the electrons are not detected, one has

$$N^{up}_\mu / N^{down}_\mu = 1 - \tfrac{1}{2}\sin^2 2\phi . \tag{24}$$

This can be generalized to many flavors by writing it as

$$\begin{aligned} N^{up}_\mu / N^{down}_\mu &= \cos^4\phi + \sin^4\phi \\ &= U^4_{\mu 1} + U^4_{\mu 2} + U^4_{\mu 3} + \ldots . \end{aligned} \tag{25}$$

Even if all the conditions above were satisfied, a measurement of $N^{up}_\mu / N^{down}_\mu$ is not simply interpreted. This is because the neutrinos, when traveling through matter, can interact coherently with matter[18], and this has to be taken into account in any interpretation.

In traversing through matter the neutral-current couplings of all ν_α are identical, giving an overall phase and hence do not affect the oscillation probabilities. However, ν_e and $\bar{\nu}_e$ have in addition charged-current interaction with the electrons in the matter. This means that the effective δM^2_{ij} and U in matter are different and are to be obtained from a rediagonalization of energy eigenstates in matter. The equation of motion for ν's in matter is

$$i\,\dot{\psi}_i = E_i\psi_i - \sum_j \sqrt{2}\, G\, N_e\, U_{ei}U^*_{je}\psi_j\,, \tag{26}$$

where E_i and U are the vacuum values and N_e = number density of electrons. For $\bar{\nu}$'s the matter term changes sign due to vector nature of the interaction.

First let us consider the two-neutrino case and parameterize the 2 x 2 matrices U, V that relate them to the mass eigenstates ν_i and matter eigenstates ν'_i by

$$\begin{aligned} U_{e1} &= U_{\mu 2} = \cos\alpha\,, \qquad U_{e2} = -U_{\mu 1} = \sin\alpha \\ V_{e1} &= V_{\mu 2} = \cos\alpha'\,, \qquad V_{e2} = -V_{\mu 1} = \sin\alpha'\,. \end{aligned} \tag{27}$$

There is just one mass-squared difference $\delta m^2 = m_1^2 - m_2^2$. As mentioned before, vacuum oscillations of two neutrinos determine only $|\delta m^2|$ and $\sin^2 2\alpha$, leaving the sign of δm^2 and the quadrant of 2α unresolved. By convention we take $\alpha < 45^o$. The ambiguity in the sign of δm^2 is resolved by the effects of matter.

It is convenient to define the oscillation length in vacuum ℓ_V and a characteristic length ℓ_M for matter effects by

$$\ell_V = 4\pi E/\delta m^2\,, \qquad \ell_M = 2\pi/(\sqrt{2}\, G\, N_e)\,. \tag{28}$$

For antineutrinos, the sign of ℓ_M is reversed. We note that ℓ_V or ℓ_M can have either sign. With E in MeV, δm^2 in eV^2, and N_e in cm^{-3}, the oscillation lengths in meters are given by

$$\ell_V = 2.48\, E/\delta m^2\,, \qquad \ell_M = 1.77 \times 10^7\, N_A/N_e\,. \tag{29}$$

For terrestrial matter $N_e \sim 2\, N_A\ cm^{-3} = 1.2 \times 10^{24} cm^{-3}$ in the mantle (3.5×10^6 m $< r < 6.4 \times 10^7$ m) and $N_e \sim 5\, N_A\ cm^{-3}$ in the core ($r < 3.5 \times 10^6$ m).

The solution in the neutrino case is given by[18]

$$\tan 2\alpha' = \sin 2\alpha/[\cos 2\alpha - \ell_V/\ell_M] \tag{30}$$

for the oscillation angle in matter and

$$\delta M^2 = \delta m^2[1 - 2(\ell_V/\ell_M)\cos 2\alpha + (\ell_V/\ell_M)^2]^{\frac{1}{2}} \tag{31}$$

for the matter eigenmass-squared difference. The associated oscillation length in matter is

$$\ell = \ell_V[1 - 2(\ell_V/\ell_M)\cos 2\alpha + (\ell_V/\ell_M)^2]^{-\frac{1}{2}}. \tag{32}$$

The physical consequences are clear.

i) If $|\ell_V| \ll |\ell_M|$, i.e. the vacuum oscillation length is very short on the matter scale, then $\alpha' \lesssim \alpha$, $\delta M^2 \lesssim \delta m^2$ and matter corrections are negligible.

ii) If $|\ell_V| \gg |\ell_M|$, then $\alpha' \lesssim 0$ and the matter corrections damp out all oscillation effects.

iii) At intermediate values $|\ell_V| \sim |\ell_M|$ the matter corrections are very significant, and differ between neutrinos and antineutrinos.[19] Moreover, matter effects resolve the vacuum oscillation ambiguity in the sign of δm^2.

iv) For matter corrections to be observable, the distance traversed in matter must also be an appreciable fraction of ℓ_M. Hence matter corrections are very small in all terrestrial contexts, except when neutrinos traverse a substantial fraction of the earth's diameter and have energies

$$E(\text{MeV}) \gtrsim 10^5 \ |\delta m^2 \ (\text{eV}^2)|. \tag{33}$$

v) For given δm^2 the vacuum oscillation length ℓ_V depends on E, whereas ℓ_M does not; hence there is always some energy range where matter effects are important.

vi) There is always some energy where $\ell_V/\ell_M = \cos 2\alpha$ and hence $\alpha' = 45^\circ$, for either ν or $\bar{\nu}$ depending on the sign of δm^2. Hence there is always some energy where ν or $\bar{\nu}$ matter mixing is maximal. At this energy, the diagonal transition probability vanishes at a distance

$$L = \ell_M/2 \cot 2\alpha. \tag{34}$$

With $\alpha = 22.5^\circ$ and $N_e = 2N_A \ \text{cm}^{-3}$, this distance is $L \sim 5 \times 10^6$ m, which would correspond to deep mine events about 10° below the horizontal direction.

Some of these results are illustrated in Fig. 1, showing the ratio $\delta M^2/\delta m^2$ (describing the correction to the oscillation wavelength) and $\sin^2 2\alpha'$ (describing the oscillation amplitude) versus $E/|\delta m^2|$. This illustration is based on $\alpha = 22.5^\circ$ and $N_e = 2N_A$. As expected, there is little matter correction for $E(\text{MeV}) < 10^5|\delta m^2 \ (\text{eV}^2)|$. The mixing becomes maximal in one channel (ν or $\bar{\nu}$) at one energy; at sufficiently large energy where $\ell_V \gg \ell_M$ the mixing is damped out. When δm^2 changes sign, ν and $\bar{\nu}$ exchange roles. The transition probabilities are given simply by

$$\begin{aligned} P(\nu_e \to \nu_\mu) = P(\nu_\mu \to \nu_e) &= 1 - P(\nu_e \to \nu_e) = 1 - P(\nu_\mu \to \nu_\mu) \\ &= \sin^2(2\alpha')\sin^2(\tfrac{1}{4}\delta M^2 L/E). \end{aligned} \tag{35}$$

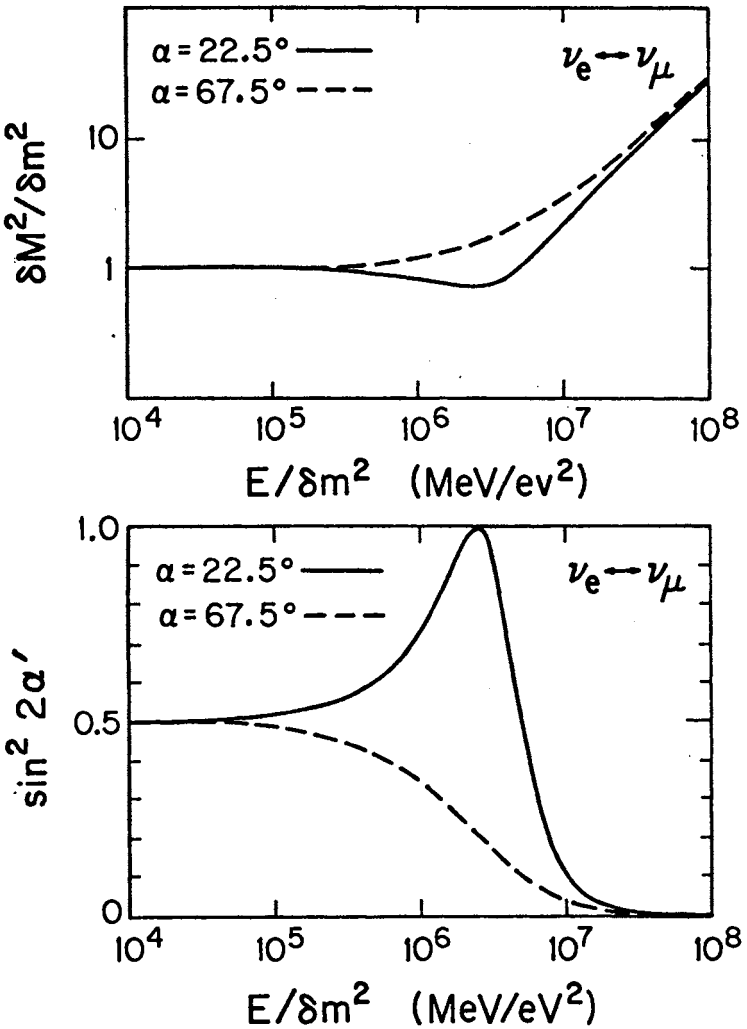

Fig. 1. Matter to vacuum eigenmass-squared difference ratio and matter amplitude $\sin^2 2\alpha'$ for oscillations of two neutrinos with vacuum amplitude $\sin^2 2\alpha = 0.5$ ($\alpha = 22.5^\circ$).

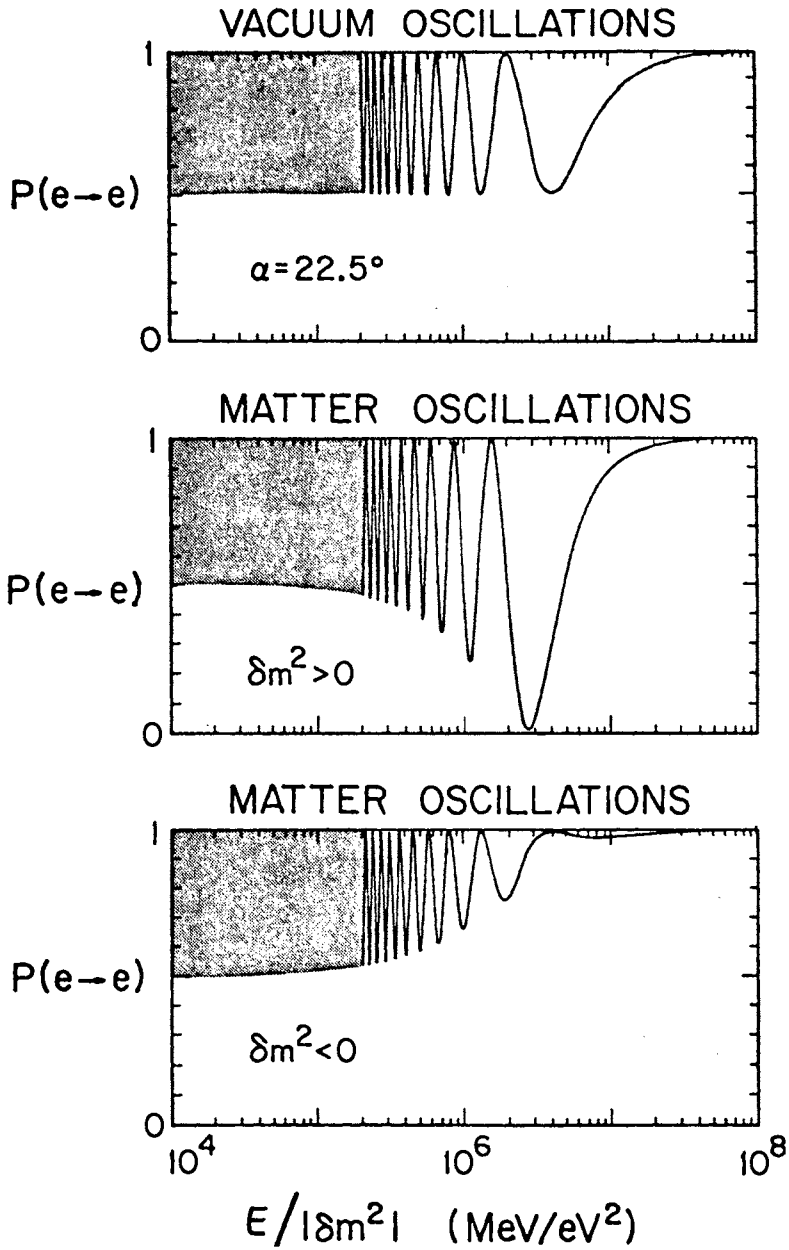

Fig. 2. Comparison of vacuum and matter transition probability P(e→e) for two neutrinos at fixed L = 5 x 10^6 m for density $N_e = 2N_A$.

Figure 2 compares vacuum and matter oscillation results for $P(e \to e)$ in the two neutrino case at a fixed distance $L = 5 \times 10^6$ m.

For constant density N_e, we have algebraically performed the diagonalization of Eq. (26) in the three-neutrino case.[19] Unfortunately, the algebra is impenetrable. It is more fruitful and transparent to construct approximate solutions.

If $\delta m^2_{ij}/2E \gg G\,N_e$ for all δm^2_{ij}, and if $G\,N_e L \ll 1$, then the main effect of matter is to shift the mass differences:

$$\delta m^2_{ij} \to \delta m^2_{ij} - 2\sqrt{2}\,G\,N_e E(|U_{ei}|^2 - |U_{ej}|^2). \tag{36}$$

If, on the other hand, $\sqrt{2}\,G\,N_e \gg \delta m^2_{ij}/2E$, then matter gives ν_e a fast-changing phase and decouples it from the rest.[19] The other ν's oscillate with each other as if in vacuum (subject to conservation of probability), e.g., this condition numerically is

$$\delta m^2(eV^2) \ll E(MeV) N_e(cm^{-3})\, 10^{-31}\ eV^2. \tag{37}$$

In a typical neutron star of mass density 10^{15} gm/cm^3, $N_n \sim 10^{39}$ cm^{-3} and N_p and $N_e \sim 10^{37}$ cm^{-3}. So for neutrinos of energies in MeV range

$$\delta m^2 \ll 10^6\ eV^2.$$

Hence for δm^2 of current interest ($\lesssim 100\ eV^2$) ν_e's emitted from inside a neutron star decouple until they leave the surface of the star and then resume normal vacuum oscillation.[20] For the earth the condition for ν_e to decouple becomes

$$\delta m^2 \ll E(MeV)\, 10^{-7}\ eV^2.$$

So even for $E \sim 1$ TeV, δm^2 has to be $\ll 0.1\ eV^2$ for ν_e to decouple.

To summarize, matter effects on neutrino oscillations are known, calculable and must be taken into account whenever neutrinos pass through matter containing a large number of electrons anywhere.

I am grateful to Vernon Barger, Paul Langacker, Jacques Leveille, Roger Phillips, and Kerry Whisnant for stimulating discussion, collaboration, and counsel, and acknowledge the support of the U. S. Department of Energy under Contract No. DE-AC03-76ER00511.

References

1. Such speculations were made, e.g., by K. Tennakone and S. Pakvasa, Phys. Rev. Lett. 13, 757 (1971), ibid. 15, 1415 (1972).

2. Proportionality of mass matrices would guarantee this and can be accomplished with horizontal symmetries either gauged or discrete (e.g., permutation).

3. T. Yanagida, Proceedings of the Workshop on The Unified Theory and Baryon Number in the Universe, ed. by O. Sawada and A. Soga, KEK (1979); M. Gell-Mann, P. Ramond, and R. Slansky in Supergravity, ed. by P. van Nieumenhuizen and D. Z. Freedman, N. Holland (1979); P. Ramond, Caltech Report 68-703 (1979); H. Georgi and D. Nanopoulos, Nucl. Phys. B155, 52 (1979); E. Witten, Harvard Preprint HUTP-79/A076; R. Barbieri, D. Nanopoulos, and F. Strochhi, CERN TH 2776 (1979); R. Barbieri, J. Ellis, and M. Gaillard, CERN Preprint TH2787; A. Zee, Pennsylvania Preprint UPR-0150T (1980); L. Wolfenstein, CMU Preprint COO-3066-4191 (1980); S. Nandi, K. Milton, and K. Tanaka, Ohio State Preprint (1980); T. Yanagida and M. Yoshimura, KEK Preprint (1980); R. Mohapatra and G. Senjanovic, Phys. Rev. Lett. 44, 912 (1980).

4. The original suggestion of flavor oscillations is due to Z. Maki, M. Nakagawa, and S. Sakata, Progr. Theoret. Phys. 28, 870 (1964) and M. Nakagawa et al., ibid. 30, 258 (1963). See also B. Pontecorvo, J.E.T.P. 53, 1717 (1967) (English translation Sov. Phys. J.E.T.P. 26, 984 (1968)). A comprehensive review with a complete bibliography up to 1978 is S. M. Bilenky and B. M. Pontecorvo, Phys. Rep. 41, 225 (1978).

5. The presence of both Majorana and Dirac masses was discussed by S. M. Bilenky and B. M. Pontecorvo, Lett. Nuov. Cim. 17, 569 (1976). In the context of gauge models, there has been much discussion of this phenomenon recently: V. Barger, P. Langacker, J. Leveille, and S. Pakvasa, Phys. Rev. Lett. 45, 692 (1980); S. M. Bilenky, J. Hosek, and S. Petcov, Dubna Preprint (1980); Wu Dan Di, Harvard Preprint HUTP-80/A032; T. Yanagida and M. Yoshimura, KEK Preprint TH-14 (1980); J. Schechter and J. P. Valle, Syracuse Preprint SU-4217-167 (1980); T. P. Cheng and L. F. Li, CMU Preprint COO-3066-152 (1980); M. Gell-Mann, R. Slansky, and G. Stephenson, unpublished (1980).

6. ν_e to $\bar{\nu}_e$ oscillations were originally suggested by Pontecorvo in 1958 (J.E.T.P. 34, 247 (1958); English translation, Soviet Physics J.E.T.P. 7, 172 (1958)); and a complete phenomenological discussion is given in J. N. Bahcall and H. Primakoff, Phys. Rev. D15, 3463 (1978). The only change to be made in their formulas is to insert the $\sin^2 2\chi$ dependence on the mixing angle ($\chi = 45^\circ$ in their discussion).

7. V. A. Lyubimov, E. G. Novikov, V. Z. Nozik, E. F. Tretyakov, and V. S. Kosik, Phys. Lett. 94B, 266 (1980).

8. R. Davis, these Proceedings.

9. J. N. Bahcall, W. F. Huebner, S. M. Lubow, N. H. Magee, A. L. Merts, P. D. Parker, B. Rozsnyai, R. K. Ulrich, and M. F. Argo, Phys. Rev. Lett. 45, 945 (1980).

10. E. Pasierb, H. Sobel, and F. Reines, UCI Preprint (1980); H. W. Sobel, these Proceedings.

11. M. R. Krishnaswamy et al., Proc. Phys. Soc. Lond. A323, 489 (1971); M. F. Crouch et al., Phys. Rev. D18, 2239 (1978).

12. E. Belloti et al., Lett. Nuov. Cim. 17, 553 (1976); J. Blietschau et al., Nucl. Phys. B133, 205 (1978); S. E. Willis et al., Phys. Rev. Lett. 44, 522 (1980); A. M. Cnops et al., Phys. Rev. Lett. 40, 144 (1978).

13. V. Barger, K. Whisnant, D. Cline, and R. Phillips, Phys. Lett. 93B, 194 (1980); other possible solutions are also given there and in A. de Rujula, L. Maiani, S. Petcov, and R. Petronzio, Nucl. Phys. B168, 54 (1980).

14. V. Barger, Proceedings of XXth ICHEP, Madison, 1980; Talks by R. Burman and by D. Cline, in these Proceedings; B. R. Cortez and L. R. Sulak, Michigan Preprint UM-PD-80-1, to be published in the Proceedings of Europhysics Workshop on Grand Unification, Erice, Italy, March 1980; B. R. Cortez et al., Harvard Preprint (1980).

15. S. P. Rosen and B. Kayser, Purdue Preprint (1980).

16. V. Barger, K. Whisnant, D. Cline, and R. J. N. Phillips, Wisconsin Report COO-881-148 (1980); B. McKellar and L. Hall, Melbourne Preprint (1980).

17. S. L. Glashow, Harvard Preprint HUTP-79/A059.

18. L. Wolfenstein, Phys. Rev. D17, 2369 (1978); see also R. R. Lewis, Phys. Rev. D21, 663 (1980).

19. V. Barger, K. Whisnant, R. J. N. Phillips, and S. Pakvasa, UH-511-397-80.

20. The relevance of this to neutrino fluxes from neutron stars is discussed by R. Sawyer and by T. Mazurek, these Proceedings.

Effects of Oscillations on Neutrinos Generated by Cosmic Rays in the Earth's Atmosphere

R. Silberberg and M. M. Shapiro
Laboratory of Cosmic Ray Physics
Naval Research Laboratory
Washington, DC 20375 USA

ABSTRACT

Recent indications of neutrino oscillations (Reines, Sobel and Pasierb, 1980) would, if confirmed, have certain consequences for the neutrinos generated by cosmic rays in the earth's atmosphere. The intensity of electron neutrinos produced by cosmic-ray interactions in the atmosphere would be considerably enhanced with respect to that of muon neutrinos. Above 100 GeV, this ratio of the two fluxes $R = J(\nu_e + \bar{\nu}_e)/J(\nu_\mu + \bar{\nu}_\mu)$ would be increased by an order of magnitude, reaching unity for the case of maximal mixing. This enhancement is pronounced only for neutrinos that have penetrated through the earth (i.e. "upward" moving neutrinos) up to energies near 10^4 GeV. It is suppressed at higher energies owing to the relativistic dilation of the oscillation length, which then exceeds the characteristic length for phase change between ν_e and ν_μ in matter, as well as the neutrino flight path through the earth. For downward moving neutrinos, however, with their shorter flight paths, the enhancement would already be suppressed at energies $\gtrsim$ 10 GeV. The enhanced value of the ratio R would increase the background against which proton decay experiments must work.

1. Introduction and Theoretical Background

Maki et al. (1962) and Pontecorvo (1967) suggested that neutrinos of different flavors may oscillate (e.g., $\nu_e \leftrightarrow \nu_\mu$) analogously to the oscillation of strangeness in the neutral K-meson system: $K^o \leftrightarrow \bar{K}^o$. The theory of this process has been discussed by Bilenkii and Pontecorvo (1977). In the case of two neutrinos ν_1 and ν_2 with masses m_1 and m_2, and mixing angle θ, we can write

$$\nu_e = \nu_1 \cos\theta + \nu_2 \sin\theta \qquad (1)$$

$$\nu_\mu = -\nu_1 \sin\theta + \nu_2 \cos\theta$$

In the theory of the two-component neutrino, the Hamiltonian can include only the left-handed (L) components of the neutrino fields,

$$\nu_{iL} = \frac{1+\gamma_5}{2}\nu_i$$

thus

$$\nu_{\ell L} = \sum_{i=1,2} U_{\ell\sigma}\nu_{i\sigma}$$

where $\ell = e, \mu$ and γ_5 is given, e.g., in Jauch and Rohrlich (1976).

The orthogonal matrix U has the general form

$$U = \begin{pmatrix} \cos\theta & \sin\theta \\ -\sin\theta & \cos\theta \end{pmatrix} \tag{4}$$

Let $P_{\nu',\nu}(x)$ be the probability of observing ν' at a distance x from the source of ν (where ν' is produced by oscillation of ν). Then

$$P_{\nu',\nu}(x) = P_{\nu,\nu'}(x) = 1/2\ \sin^2 2\theta\ (1-\cos 2\pi \frac{x}{\Lambda}) \tag{5}$$

where Λ is the oscillation length

$$\Lambda = 4\pi \frac{p}{|m_1^2 - m_2^2|} = 250\ \frac{p(\text{MeV})}{\Delta m^2(\text{eV})^2}\ \text{cm}; \tag{6}$$

here p is the momentum of the neutrino.
For the general case of N types of oscillating neutrinos, with

ν_ℓ (ℓ = e, μ, τ...), one obtains

$$\nu_{\ell L} = \sum_{i=1}^{N} U_{\ell i}\nu_{iL} \tag{7}$$

$U_{\ell i}$ is an orthogonal N x N matrix, and

$$P_{\nu_\ell\nu_\ell}(x) = \sum_{i=1}^{N} U^2_{\ell i}U^2_{\ell' i} + \sum_{i\neq i'} U_{\ell i}U_{\ell' i}U_{\ell i'}U_{\ell' i'}\cos 2\pi \frac{x}{\Lambda_{ii'}} \tag{8}$$

where

$$\Lambda_{ii'} = 4\pi \frac{p}{|m_i^2 - m_{i'}^2|} \tag{9}$$

The case of 3 types is discussed by Mann and Primakoff (1977). The oscillation described above (the so called vacuum oscillation) takes place in vacuum as well as in matter. The oscillation length for this type of mixing increases with momentum; for maximum mixing, the intensity (for $x \gg \Lambda$) becomes $I = 1/N$. (10)

Another type of oscillation has been proposed by Wolfenstein (1978). It occurs (even for zero-mass neutrinos) if the coherent forward scattering

is partially off diagonal in neutrino type, i.e. if the scattering interactions of neutrinos in matter are different for the various types of neutrinos. The oscillation length in this case is

$$\ell_o = 2\pi/GN_e \tag{11}$$

where G is the Fermi coupling constant and N_e is the number of electrons per unit volume.

$$\ell_o = \frac{2.7 \times 10^9}{\rho_e} \text{ cm} \tag{12}$$

where ρ_e is the number density of electrons N_e divided by Avogadro's number 6×10^{23} cm ^{3}. For the earth, $\rho_e \approx 3$, thus $\ell_o \approx 9000$ km for neutrinos traversing the earth.

Wolfenstein (1979) has pointed out that the vacuum oscillation mechanism is also affected by matter, because both the charged current and neutral current contribute to the scattering $\nu_e + e \rightarrow \nu_e + e$, while only the neutral current contributes to $\nu_\mu + e \rightarrow \nu_\mu + e$. Here, too, the characteristic length for the phase change of 2π is ℓ_o.

The probability that a ν_μ has oscillated into a ν_e is given by

$$P_{\nu_e,\nu_\mu}(x) = \tfrac{1}{2} \sin^2 2\theta_m \left(\frac{\ell_m}{\Lambda}\right)^2 \left(1 - \cos \frac{2\pi x}{\Lambda}\right) \tag{13}$$

where

$$\ell_m^{\,2} = \Lambda^2 \left[1 + \frac{\Lambda}{\ell_o} - 2\,\frac{\Lambda}{\ell_o} \cos 2\theta\right]^{-1} \tag{14}$$

$\ell_o = 2.7 \times 10^3/\rho_e$ cm. Thus, for high energies or high electron densities, when $\Lambda >> \ell_o$, the vacuum oscillation mechanism becomes ineffective.

Evidence supporting neutrino vacuum oscillations of electron neutrinos near 1 MeV (to ≈ 3 standard deviations) comes from the recent experiment of Reines, Sobel and Pasierb (1980). The experiment was carried out at the Savannah nuclear reactor. These authors pointed out the deep underground neutrino observations of Reines (1979) at much higher energies, imply the oscillation of ν_μ near energies of $\approx$10 GeV (to better than 2 standard deviations).

We shall now proceed to study the striking effects that neutrino oscillations have on the cosmic-ray induced $\nu_e + \bar{\nu}_e$ flux.

2. The Cosmic-Ray Generated Neutrino Flux

At energies between 0.1 and 100 GeV, the neutrino flux at earth is derived mainly from the decay of secondaries produced by cosmic-ray collisions in the

atmosphere:

$$\pi^{\pm} \rightarrow \mu^{\pm} + \nu_{\mu} \; (\bar{\nu}_{\mu})$$

$$\mu^{\pm} \rightarrow e^{\pm} + \bar{\nu}_{\mu}(\nu_{\mu}) + \nu_{e}(\bar{\nu}_{e})$$

However, at higher energies, the production of neutrinos from these sources is suppressed. Due to time-dilation, the decay-length of the pions will exceed the pion interaction length; the pions will suffer nuclear collisions instead. While muons have a much longer interaction-mean-path, their decay is also suppressed at sufficiently high energies. Muons will reach the ground, undergo ionization losses in the dense material, and decay at low energies. At sufficiently high energies, neutrinos are produced in the atmosphere mainly by K-meson decay. The electron neutrinos are generated predominantly by $K^{\pm} \rightarrow e^{\pm} + \pi^{o} + \nu_{e}(\bar{\nu}_{e})$, which has a branching ratio of only 4.8%, and by $K^{o}_{long} \rightarrow e^{\pm} + \pi^{\mp} + \nu_{e}(\bar{\nu}_{e})$. While the latter reaction has an appreciably higher branching ratio (35%), it is inhibited at high energies by collisions, which prevail in the competition with decay:

$\tau_{o}(K^{o}_{long}) = 5.3 \times 10^{-8}$ sec, four times as long as $\tau_{o}(K^{\pm}) = 1.2 \times 10^{-8}$ sec. Thus the $K^{\pm}$ and K^{o}_{long} decays contribute about equally to ν_{e} ($\bar{\nu}_{e}$) production. The predominant source of neutrinos at high energies is $K^{\pm} \rightarrow \mu^{\pm} + \nu_{\mu}(\bar{\nu}_{\mu})$, which has the large branching ratio of 64%. Mainly owing to this large value, the ratio ν_{e}/ν_{μ} without oscillation is 0.03 at energies above $\approx 10^{3}$ GeV (Allkofer et al., 1979).

The energy spectra of $\nu_{e} + \bar{\nu}_{e}$ and $\nu_{\mu} + \bar{\nu}_{\mu}$ from vertical and horizontal directions have been calculated by Cowsik, Pal and Tandon (1966) for $2 \leq E_{\nu} \leq 200$ GeV and by Allkofer et al. (1979) for $10^{3} \leq E_{\nu} \leq 10^{6}$ GeV in the absence of neutrino oscillations. Fig. 1 shows the differential intensity spectra of $\nu_{e} + \bar{\nu}_{e}$ and $\nu_{\mu} + \bar{\nu}_{\mu}$ from the downward and upward directions, assuming oscillations. For brevity, the symbols (ν_{i}) in the figure represent these sums. The curves $(\nu_{e})_{down}$ and $(\nu_{\mu})_{down}$ between 15 and 300 GeV and 15 and 4000 GeV, respectively, are similar to those of Cowsik, Pal and Tandon (1966) and of Allkofer et al. (1979). However, above~10^{3} GeV and $\sim 2 \times 10^{4}$ GeV, respectively, their calculated $(\nu_{e} + \bar{\nu}_{e})_{down}$ and $(\nu_{\mu} + \bar{\nu}_{\mu})$ spectra would be dominated by the prompt neutrino spectra. This assures a production ratio $N(\nu \text{ prompt})/N_{\pi} = 10^{-4}$ at $E_{\nu} = 30$ GeV and 10^{-3} at $E_{\nu} \gtrsim 10^{4}$ GeV on the basis of Fig. 12 of Allkofer's (1979) rapporteur paper. The energy spectra have been calculated assuming three types of neutrinos and maximal mixing. The dotted lines show the transition regions from oscillating neutrinos to non-oscillating ones, for upward and downward directions. The actual transition energies are uncertain by a factor of ~ 3, because of the uncertainty in the (mass^2) difference Δm^2 in the experiment of Reines, Sobel and Pasierb (1980). The dotted curves are based on assuming $\Delta m^2 = 1$ eV^2, and the use of equations 9 and 12, and $\theta = 45^{o}$ with averaging over equations (5) and (13). The choice of 45° is arbitrary; θ is to be determined in future experiments. Above 10 GeV, the neutrinos coming downward from the atmosphere have an oscillation length Λ that is relativistically dilated so that it exceeds the neutrino flight path.

The effects of oscillations then cease, and therefore the downward flux of $\nu_{e} + \bar{\nu}_{e}$ is appreciably less than the upward flux. A measurement of the ratio $(\nu_{\mu})_{up}/(\nu_{e})_{up}$ will yield the mixing angle θ; only for maximum mixing would the ratio be 1, as assumed in constructing Fig. 1. Near 3×10^{3} GeV,

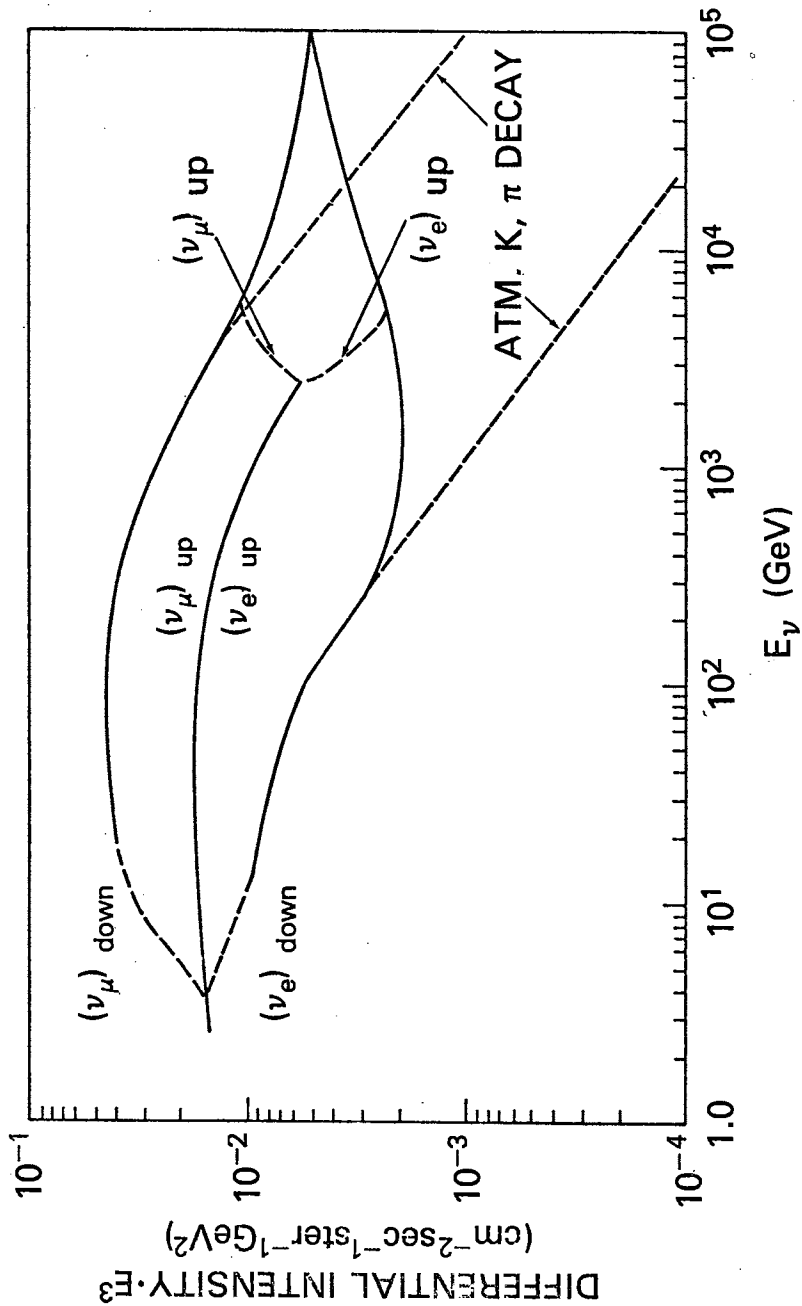
DIFFERENTIAL INTENSITY·E³
(cm⁻²sec⁻¹ster⁻¹GeV²)
10⁻¹
10⁻²
10⁻³
10⁻⁴
1.0
10¹
10²
10³
10⁴
10⁵
E_ν (GeV)
(ν_μ) down
(ν_e) down
(ν_μ) up
(ν_e) up
(ν_μ) up
(ν_e) up
ATM. K, π DECAY

the effects of vacuum oscillations of the neutrinos traversing the earth become suppressed when $\Lambda > \ell_o$ (see eqs. (6) and (12)). Then the fluxes of the atmospheric K-decay neutrinos $(\nu_\mu)_{up}$ and $(\nu_e)_{up}$ diverge, until above 10^4 GeV the prompt neutrinos become dominant. For the prompt neutrinos, a ratio of $\nu_\mu/\nu_e = 1$ has been assumed.

3. Observability in Detectors Under Construction or Under Design

Several large detectors (in the range 100 to 500 tons) have been constructed for the detection of neutrinos from stellar gravitational collapse in our galaxy. (Beresnev et al., 1979; Chudakov et al., 1979; Deakyne et al., 1978). The likelihood of observing the effects of neutrino oscillations (shown in Fig. 1) with these detectors would be marginal.

A more nearly adequate volume is that of a proton decay equipment now under design: 10^4 tons (Sulak 1979, Reines, 1980). With this detector neutrino interactions can be studied at energies up to ~ 100 GeV.

The proposed Mini-DUMAND and DUMAND arrays ($\sim 10^7$ tons and $\sim 10^9$ tons respectively) will permit observations of atmospheric neutrinos up to $\sim 4 \times 10^3$ and $\sim 3 \times 10^4$ GeV, respectively. With such target volumes, it would be possible to search for the suppression of neutrino vacuum oscillations via the mechanism originally proposed by Wolfenstein (1979) for neutrinos of lower energy inside neutron stars. In addition, the production of prompt atmospheric neutrinos could be explored with the full-sized DUMAND array.

4. Effect of Oscillations on the Background in Proton Decay Experiments

An important decay mode of protons is

$$p \rightarrow e^+ + \pi^o$$

with $\pi^o \rightarrow 2\gamma \rightarrow 2e^+ + 2e^-$.

The electron antineutrino can generate similar products $\bar{\nu}_e + p \rightarrow N^* + e^+$ with $N^* \rightarrow n + \pi^o$. Since the production rate of ν_e is lower than that of ν_μ, the numbers of ν_e and $\bar{\nu}_e$ will be enhanced by oscillations. At the low energies of interest, the enhancement is moderate (less than a factor of two). A determination of the energies of e^+ and of π^o, as well as of angular correlations, can help to overcome this background.

References

1. Allkofer, O.C., Rapporteur Paper, 16th International Cosmic Ray Conference, Kyoto, Japan, Vol. 14, 385, 1979.

2. Allkofer, O.C., Kitamura, T., Okada, A. and Vernon, W., Proc. 1978 DUMAND Workshop, 1, 37, Published by DUMAND, Scripps Institution of Oceanography, Code A-010, LaJolla, CA 92093, 1979.

3. Bilenkii, S.M. and Pontecorvo, B.M., Usp. Fix. Nauk., 123, 181, Engl. Transl: Sov. Phys. Usp. 20, 776, 1977.

4. Cowsik, R., Pal, Y. and Tandon, S.N., Proc. Indian Acad. Sci., 43, 217, 1966.

5. Jauch, J.M. and Rohrlich, F., "The Theory of Photons and Electrons," 2nd ed., New York, Springer Verlag, 1976.

6. Maki, Z., Nakagawa, M. and Sakata, S., Progr. Theoret. Phys. 28, 870, 1962.

7. Mann, A.K. and Primakoff, H., Phys. Rev. D15, 655, 1977.

8. Pontecorvo, B.M., Zh. Eksp. Teor. Fix. 53, 1717, Engl. Transl. Sov. Phys. JETP 26, 984, 1967.

9. Reines, F., Proc. 16th Internat. Cosmic Ray Conf., Kyoto, Japan, 14, 60, 1979.

10. Reines, F., Sobel, H., and Pasierb, E., Phys. Rev. Letters 45, 1307, 1980.

11. Wolfenstein, L., Phys. Rev. D17, 2369, 1978.

12. Wolfenstein, L., Phys, Rev. D20, 2634, 1979.

Note on Effects of Neutrino Oscillations on Observability of Neutrinos from Extragalactic Gravitational Collapse

R. Silberberg and M. M. Shapiro
Laboratory for Cosmic Ray Physics
Naval Research Laboratory
Washington, DC 20375 USA

1. Introduction

The search for neutrinos from the gravitational collapse of a star to a neutron star is hampered by two difficulties: For events within our Galaxy, the problem is the infrequency of occurrence—possibly once in 20 years. For extragalactic events, the required detector size and expense present a limitation.

If the time scale of neutrino production is as short as the calculations of Wilson (1976) imply, then neutrino oscillations would permit a reduction of the detector volume. This comes about because the "ease" of observation depends on the reaction $\bar{\nu}_e + p \rightarrow n + e^+$, and the supply of $\bar{\nu}_e$ would be much enhanced by oscillations. The way in which this happens is as follows: the neutronization neutrinos ν_e produced in the process $p + e^- \rightarrow n + \nu_e$ during gravitational collapse, fill the phase space (Schramm 1976) and inhibit $\nu_e + \bar{\nu}_e$ pair production in the subsequent thermal pulse. The supply of $\nu_\mu + \bar{\nu}_\mu$ and $\nu_\tau + \bar{\nu}_\tau$ is, however, unaffected. The suppression of $\bar{\nu}_e$ production makes the detection of gravitational collapse more difficult. Oscillations, however, would permit a change of state of $\bar{\nu}_\mu$ and $\bar{\nu}_\tau$ into $\bar{\nu}_e$, increasing the $\bar{\nu}_e$ flux by a factor of 3 or 4. If, furthermore, the Hubble constant were about 1.5 x the value of 55 km $sec^{-1}Mpc^{-1}$, then a significant reduction of the volume, from 2 x 10^7 tons to 3 x 10^6 tons, would be feasible. On the other hand, the thermal neutrino pulse from the distance of the Virgo cluster would be spread out over $\sim 10^3$ sec if the mass of ν_e were about 10 eV. This would diminish the signal-to-noise ratio.

References

1. Schramm, D.N., Proc. 1976 DUMAND Summer Workshop, p. 87 ff. ed. A. Roberts, Office of Publications, Fermi National Accel. Lab, Batavia, Ill., 1976.

2. Wilson, J.R., private communication to D.N. Schramm, 1976.

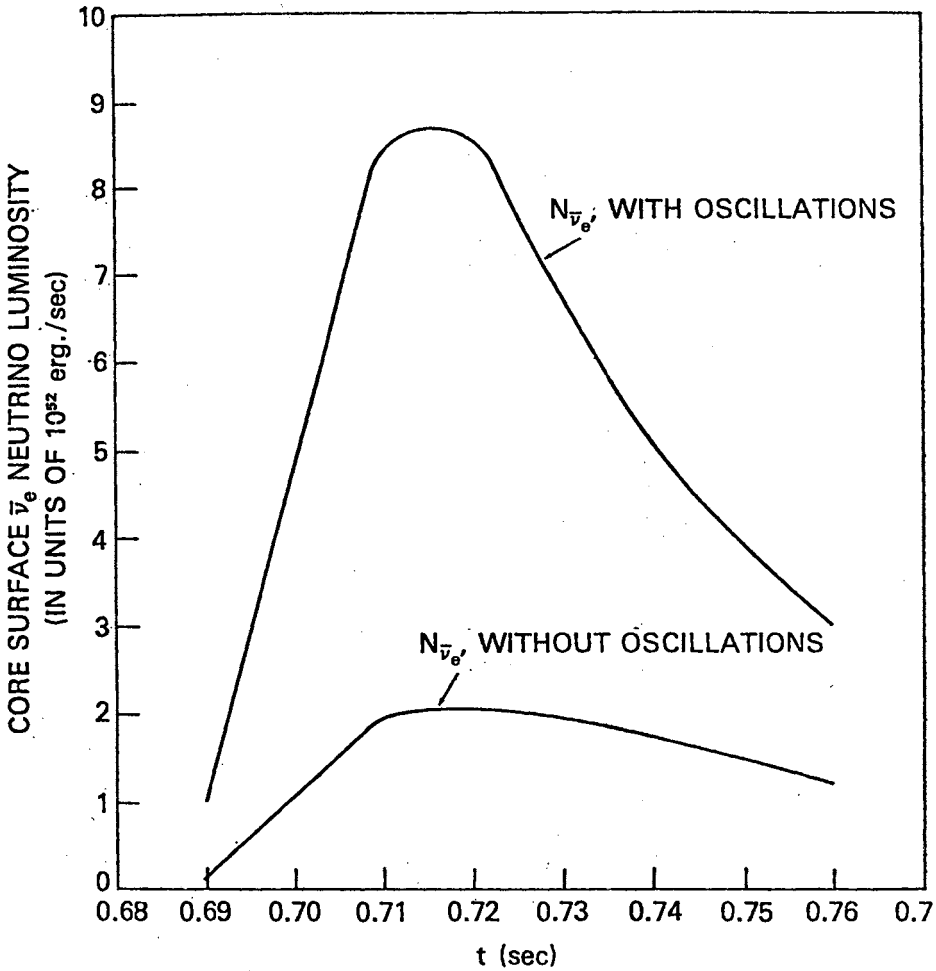

Fig. 1. The luminosity of $\bar{\nu}_e$ vs. time from a calculation of gravitational collapse. The upper curve shows the enhanced luminosity to be expected if neutrinos oscillate.

NEUTRINOS AND COSMOLOGY

David N. Schramm
Astronomy and Astrophysics Center
University of Chicago
Chicago, Illinois 60637

Gary Steigman
Bartol Research Foundation
of The Franklin Institute
University of Delaware
Newark, Delaware 19711

ABSTRACT

It is shown that the cosmological density implied from the dynamics of clusters of galaxies is greater than the upper limit on the density of matter in baryons from big bang nucleosynthesis if the primordial hellium abundance, Y, is ≤ 0.25. If Y is ≤ 0.23 then even the density implied from the dynamics of binaries and small groups of galaxies cannot be in baryons. The solution to these problems comes if neutrinos have a small rest mass. For 3 eV $\lesssim m_\nu \lesssim$ 10 eV, the neutrinos will be trapped on the scale of large clusters. For 10 eV $\lesssim m_\nu \lesssim$ 20 eV, they will be trapped on the scale of binaries and small groups. If neutrinos have a rest mass $\gtrsim$ 10 eV, then the limits on numbers of neutrino types from big bang nucleosynthesis may be relaxed if it is shown that the density of baryon matter is much less than the density implied by binaries and small groups. If neutrinos have rest mass there is no seriuos conflict with big bang nucleosynthesis as long as $Y \gtrsim 0.15$.

1. Introduction

In this paper we will review the arguments on the density of matter in the universe and show that the density implied from large clusters of galaxies may be too large to be consistent with the upper limit on the density of baryons implied from nucleosynthesis. We will use this point to argue that this probably implies that neutrinos have a small rest mass which enables them to be gravitationally bound in large clusters. We will also show that this conclusion is strengthened if the upper limit on the primordial helium abundance, Y, is decreased. We will also review the arguments that big bang nucleosynthesis places on the number of types of neutrinos if neutrinos have a small rest mass.

This paper will in large part draw on the recent work of Schramm and Steigman (1981) and Olive et al. (1981).

For convenience we will express mass densities in terms of the critical density, $\rho_c = 3H_o^2 (8\pi G)^{-1}$, which separates those Friedman models (with $\Lambda = 0$) which expand forever ($\rho < \rho_c$) from those which eventually collapse ($\rho > \rho_c$). For each contribution to the total mass density, ρ_i, we introduce the density parameter, Ω_i, where $\rho_i = \Omega_i \rho_c$. To allow for the large uncertainty in the

present value of the Hubble parameter, we will use $H_o = 100\ h_o(kms^{-1}Mpc^{-1})$ where $0.5 \lesssim h_o \lesssim 1$. In terms of Ω_i and h_o we have

$$\rho_i = 2 \times 10^{-29}\ \Omega_i h_o^2 (gcm^{-3}). \qquad (1)$$

One should note that not all combinations of h_o and Ω_i are allowed in a standard Friedman cosmology since we know that the age of the universe must be greater than the mean age of the elements, 8.7×10^9 yr. This lower limit excludes values of $\Omega \geq 1$ for $h_o > 0.76$ and approximately yields the constraint that $\Omega h_o^2 \lesssim 1$. The lower limit of 8.7×10^9 yr comes from the most conservative combined age constraints of $^{232}Th/^{238}U$ and $^{187}Re/^{187}O$ (see Symbalisty and Schramm, 1980).

To obtain estimates of cosmological densities we will frequently use the mass to light ratio, M/L, for a particular class of objects. If we assume that this class of objects gives a good estimate of the bulk of the mass associated with the light of the universe we can estimate a cosmological mass density by multiplying the M/L by the average luminosity density of the universe, $\mathcal{L}$. From Kirshner, Oemler and Schecter (1979), $\mathcal{L} \approx 2 \times 10^8\ h_o L_\odot\ Mpc^{-3}$. (Note though that Gott and Turner, 1976 used $\mathcal{L} = 1 \times 10^8\ h_o L_\odot\ Mpc^{-3}$ showing that there is at least a factor of 2 uncertainty here.)

As an example of how M/L can be used note that Peebles (1979) has estimated that M/L for the solar neighborhood is 1 to 2 (note that unlike other M/Ls this particular value is independent of h_o since it is based only on local measurements) thus if this were the characteristic mass associated with the light of the universe

$$\rho_s = \frac{M}{L_{S_N}} \cdot \mathcal{L} \approx 1.5 \times 10^{-32}\ \frac{M}{L_{S_N}}\ h_o g/cm^3 \gtrsim 1.5 \times 10^{-32} h_o g/cm^3$$

and thus

$$\Omega_s = \frac{0.0007}{h_o}$$

or for the limiting value of $h_o \lesssim 1$ (Huchra et al., 1980) we obtain

$$\Omega_s \gtrsim 0.0007$$

Since we know there is mass not in the form of stars (e.g. interstellar gas and dust) this is clearly an extreme lower limit on Ω. It is also an extreme lower limit on the density of baryonic matter, Ω_b. Not all density extimates must be baryon matter. In particular, estimates of Ω from dynamics are not necessarily limiting the density of baryons.

2. Density Inferred from Dynamics

Let us now examine the mass density inferred from the dynamics of astrophysical systems of different scales. Here, we will rely extensively upon the data assembled in the excellent review article by Faber and Gallagher (1979).

The inner, luminous parts of galaxies (mainly Ellipticals and SOs for our purposes) which are probably dominated by ordinary matter give

$$(M/L)_{E,SO} \simeq 20h_o$$

which yields

$$\Omega_{E,SO} \simeq 3 \times 10^{-31} \; h_o^2 g/cm^3$$

or

$$\Omega_{E,SO} \simeq 0.012.$$

There is, of course, good evidence that galaxies are considerably more massive than is inferred from studying their inner regions where most of the light originates. Indeed, from studies of the dynamics of Binary galaxies and Small Groups of galaxies, Faber and Gallagher obtain

$$(M/L)_{B,SG} \sim 70 \text{ to } 100 \; h_o$$

which yields

$$\rho_{B,SG} \simeq 1 \text{ to } 1.5 \times 10^{-30} \; h_o^2 g/cm^3$$

and

$$\Omega_{B,SG} \simeq 0.05 - 0.075$$

If we take into account the uncertainty in $\mathcal{L}$ this might go as low as 0.025. As implied by the results of Gott et al. (1974) for reasonable values of H_o on scales up to those of binaries and small groups, most of the inferred mass can be in ordinary matter. There is still a "missing mass" (or rather missing light) problem since the M/L implied from binary and group dynamics is greater than that implied by normal stellar population or that implied by internal galactic motions, however, this problem may be due to non-luminous ordinary matter. However, as mentioned by Schramm and Steigman (1980), if the upper limit on Y is pushed below ~ 0.22 then baryonic matter would no longer be able to satisfy these mass constraints. We will see that for large clusters of galaxies we may already have reached the point where baryonic matter cannot do the job.

After years of extensive investigation using dynamic arguments, the conclusion remains that clusters of galaxies are very massive (Peebles, 1979a, b) with implied

$$(M/L)_c \sim 500 \pm 200 \; h_o$$

yielding

$$\rho_c \sim 7.5 \times 10^{-30} \; h_o^2$$

and

$$\Omega_c \sim 0.4$$

Within the factor of 2 uncertainty in $\mathcal{L}$ and the uncertainties in M/L and other data contributing to this value of Ω_c it is probably true that a value as low as 0.1 cannot be excluded (for example see arguments by Aarseth, Gott and Turner, 1979). (It is also probably true that if one really pushed the data in the other direction Ω as large as unity might not be completely excluded.) However, it is also clear that the current best fit values are somewhat above 0.1.

3. Density Inferred from Nucleosynthesis

During primordial nucleosynthesis the light elements (D, ^{3}He, ^{4}He and ^{7}Li) are formed by two body reactions whose rates depend on nuclear density (c.f. Schramm and Wagoner, 1977 and references therein). High nuclear density results in the production of more ^{4}He and ^{7}Li and less D and ^{3}He since nucleons are conserved (for $T \lesssim 1$ MeV, baryon nonconserving processes are entirely negligible), an upper limit to the present density in nucleons may be inferred from an upper limit to the primordial abundance of deuterium. Since photons are also conserved (with account taken of the extra photons created when electron-positron pairs annihilate as the universe cools below m_e), it is convenient to compare nucleons and photons. For an upper limit to the primordial abundance by mass of ^{4}He, $Y \lesssim 0.25$ (see arguments supporting this upper limit in Yang et al., 1979, hereafter referred to as YS^{2}R) and, for three, two-component neutrinos: ν_e, ν_μ, ν_τ the nucleon to photon ratio is limited by,

$$\frac{n_b}{n_{\gamma_o}} \lesssim 4.2 \times 10^{-10}$$

The number density of black body photons is $n_{\gamma_o} \approx 400\ (T_o/2.7)$ which leads to an upper limit on $\Omega_b h_o^2$, where Ω_b is the fraction of the critical density in the form of baryons.

$$\Omega_b h_o^2 \lesssim 0.014 \frac{T_o^3}{2.7}$$

As pointed out by YS^{2}R this limit is identical with the one which follows from the deuterium abundance and is consistent with (but more restrictive than) the limit from ^{7}Li. A firm upper limit to Ω_b follows using a lower limit to $H_o(h_o \gtrsim 0.5)$ (Branch, 1979) and an upper limit to $T_o(T_o \lesssim 3.0$ K) (Woody et al., 1975).

$$\Omega_b \lesssim 0.12$$

This limit constrains any matter which was in the form of baryons when $T \sim 10^9$ K even if the matter is now locked up in blackholes.

Therefore, if the "best fit" mass inferred from clusters were (at the time of primordial nucleosynthesis) in the form of nucleons (e.g.: today they might be in black holes, neutron stars, etc.), too much ^{4}He and ^{7}Li and too little D would have been produced. Additional support fur such a disparity is provided by the x-ray observations; the temperature of the x-ray emitting gas is a probe for the depth of the potential well in which the gas resides. Using the results of Lea et al. (1973) and assuming the universality of the results yields

$$\Omega_c \gtrsim 0.2.$$

However, again one should be careful with regard to the filling factor of large clusters in the universe. Rather than looking for consistency in the limits of the uncertainties, in this paper we will accept the possibility that Ω_c may be significantly greater than Ω_b and we will assume that the difference is due to the existence at relic neutrinos with a small mass ($m_\nu \approx 5$ eV).

It should be noted that if the upper limit to the Helium abundance, Y, is found to be less than 0.25 as discussed by Stecker (1980) (and references therein) then the upper limit on Ω_b decreases which increases the descrepancy with Ω_c and argues more strongly for the existence of massive neutrinos or some other non-baryonic matter. It should also be noted as pointed out by Olive et al. (1980) that with the lower limit to Ω_b inferred from the inner regions of galaxies yields no serious inconsistency with big bang nucleosynthesis with three neutrino species as long as Y is $\gtrsim 0.15$.

Our selection of low mass neutrinos as the solution to the dark matter problem is a natural consequence of the nucleosynthetic upper limit eliminating such things as low mass stars, rocks, planets, clouds and stellar mass black holes and radiation limits eliminating most reasonable mass ranges for primordial mini-black holes and magnetic monopoles. This leaves only the low mass neutrinos proposed by Cowsik and McClellan (1973) and Marx and Szalay (1973) and the high mass ($\gtrsim$ 106 eV) neutrinos discussed by Gunn et al. (1978). Since high mass neutrinos are more ad hoc and exclude the known ν_e, ν_μ, ν_τ we will concentrate here on low but finite mass neutrinos.

4. Relic Neutrinos

During the early evolution of the universe, all particles, including neutrinos, were produced copiously (c.f. Steigman 1979). Here we focus on the known e^-, μ^- and τ^- neutrinos and entertain the possibility that they have a small but finite mass. Neutrinos with full strength, neutral current, weak interactions were produced by reactions of the type

$$e^+ + e^- \leftrightarrow \nu_i + \bar{\nu}_i;\ i = e,\ \mu,\ \tau.$$

At high termperatures ($kT > m_\nu c^2$), these neutrinos were approximately as abundant as photons.

$$\frac{n_{\nu_i}}{n_\gamma} = \frac{3}{8} g_{\nu_i}$$

where g_ν is the number of neutrino helicity states. For massless spin ½ neutrinos with $\bar{\nu}_e \neq \nu_i$ then $g_\nu = 2$. If the neutrinos have a mass then each spin ½ particle would have 2 helicity states thus for $\bar{\nu}_e \neq \nu$, $g_\nu = 4$ however because known neutrinos appear to be only left handed then, if massive, they may be of the Majorana type ($\nu_i = \bar{\nu}_i$), in which case g_ν is still 2. As for the numerical factor, 3/4 comes from the difference between Fermi-Dirac statistics (neutrinos) and Bose-Einstein statistics (photons); the remaining factor of ½ is from the number of photon spin states ($g_\gamma = 2$).

For light neutrinos ($m_\nu \ll 1$ MeV), equilibrium was maintained until $T \gtrsim 1$ MeV. At lower temperatures the weak interaction rate is too slow to keep pace with the universal expansion rate so that few new neutrinos are produced

and, equally important, few annihilate. Thus, for $T \approx 1$ MeV, the neutrinos decouple; at this stage their relative abundance is given above. When the temperature drops below the electron mass, electron-positron pairs annihilate heating the photons but not the decoupled neutrinos. The present ratio of neutrinos to photons must account for the extra photons produced when the $e^{\pm}$ pairs disappeared (c.f. Steigman 1979)

$$N_\gamma(T < m_e) = \frac{11}{4} N_\gamma(T > m_e); \quad \frac{n_\nu}{n_{\gamma_o}} = \frac{3}{22} g_\nu.$$

From the present density of photons we obtain the present number density of neutrinos; multiplying by the neutrino mass we obtain the neutrino mass density (ρ_ν) which may be expressed in terms of the density parameter,

$$\Omega_{\nu_i} h_o^2 = \frac{g_{\nu_i} m_{\nu_i}}{200} \frac{T_o^3}{2.7}$$

where m_ν is in eV and the sum is over all neutrino species with $m << 1$ MeV. We have implicitly assumed that the neutrinos still exist today and thus have a lifetime greater than the age of the universe for decay into anything other than neutrinos. Because $\Omega h_o^2 \lesssim 1$, this limits the sum of masses

$$\Sigma m_i \lesssim 100 \text{ eV for } g = 2$$

and

$$\Sigma m_i \lesssim 50 \text{ eV for } g = 4$$

For $T_o \lesssim 3$ K and $h_o < 1$ and assuming Majorana mass neutrinos with $g_\nu = 2$ we find that

$$\Omega_{\nu_i} \gtrsim 0.014\, m_{\nu_i}$$

From our limit on Ω_b we obtain the relationship with $g_{\nu_i} = 2$

$$\frac{\Omega_\nu}{\Omega_b} \gtrsim \frac{\Sigma_i m_{\nu_i}}{10}$$

which is independent of h_o and T_o. Therefore if neutrinos have masses of the order of 10 eV or greater then neutrinos are the dominant mass component of the universe today.

Massive neutrinos gravitate and they will have participated in gravitational clustering (see Gunn et al. 1978). However, since neutrinos are non-interacting, their phase space density is conserved and they will cluster only in the deepest potential wells; the slowest moving (i.e.: the heaviest) will cluster most easily.

Tremaine and Gunn point out that neutrinos lighter than ~ 3 eV will not cluster at all due to the fact that their velocities in clusters will be greater than that necessary to escape. Neutrinos with a mass between 3 and 10 eV will

be in clusters of galaxies (the deepest potential wells) but not (significantly) contribute to the mass on smaller scales. But recall, the scale on which the missing light problem truly emerges is that of clusters of galaxies. We propose, therefore, that the dominant contribution to the mass of clusters of galaxies (and to the mass of the universe) is from relic neutrinos with a finite mass $m_\nu \approx 6 \pm 3$ eV.

Obviously, if $\Omega_\nu \approx \Omega_c$ were > 1 the Friedman universe would be closed by neutrinos. As mentioned before, current estimates put $\Omega_c < 1$ and thus Ω_ν would also be constrained to be < 1 however the uncertainties are sufficiently large that colsure by neutrinos cannot be completely excluded. Note that if

$$\Sigma m_{\nu_i} > 100\ h_o^2\ \frac{2.7}{T_o}\ \text{eV}$$

then the Friedman universe with $\Lambda = 0$ is closed.

It is intriguing to note that neutrinos with mass less than 3 eV do not get included in density estimates from cluster dynamics, thus they may provide a smooth background. However, the contribution to Ω from such low mass neutrinos is small. Thus, it is probably true that Ω_ν is constrained by Ω_c.

5. Limits on Neutrino Flavors

YS^2R (and references therein) showed that $Y \lesssim 0.25$ and a lower limit on

$$\frac{n_b}{n_\gamma} \text{ of } \sim 2 \times 10^{-10}$$

set a limit on the number of neutrino flavors. N_ν to be $\lesssim 4$. It has been shown by Olive et al. (1980) that as long as these limits on Y and n_b/n_γ are valid this limit on N_ν holds. However, as Olive et al. point out the limit on n_b/n_γ used above comes from binary galaxies and small groups of galaxies. If these systems are dominated by low mass neutrinos with masses between 10 and 20 eV then one could no longer use that limit on n_b/n_γ. The limit on n_b/n_γ from the central regions of galaxies only yields $n_b/n_\gamma \gtrsim 3 \times 10^{-11}$ when all the uncertainties are included. This limit could allow N_ν to be infinite for $Y \lesssim 0.25$ or to still be extraordinaryily large even for a limit on Y of $\lesssim 0.22$. A less certain lower limit on n_b/n_γ comes from the hot x-ray emitting gas in clusters. This yields $n_b/n_\gamma \gtrsim 10^{-10}$, which in turn limits N_ν to $\lesssim 5$. It is obvious from the above that the strength depends on the mass of the neutrino. If neutrinos have masses $\lesssim 10$ eV then Binaries and small groups of galaxies will not trap neutrinos and the old limits of $N_\nu \lesssim 4$ hold however if $m_\nu > 10$ eV. The lower limits on n_b/n_γ must be revised with a tentative limit on N_ν of ~ 5 but no firm limit being available. The argument for $m_\nu > 10$ eV would be enhanced if Y were found to be $\lesssim 0.23$ since then no 3 ν solution would exist for $n_b/n_\gamma \gtrsim 2 \times 10^{-10}$.

6. Summary

Low mass neutrinos appear to be the most reasonable solution to the missing mass (light) problem in cosmology. The cosmological implications on m_ν place it between 3 eV and 100 eV with the best fit near 10 eV. With these massive

neutrinos consistent big bang solutions are found for Helium mass abundances $\gtrsim 0.15$. If neutrinos have mass $\gtrsim 10$ eV the cosmological limits on N_ν can be loosened.

7. Acknowledgments

We would like to thank Keith Olive, Eugene Symbalisty, Michael Turner and Jim Fry for valuable discussions. This work was supported in part by NSF grant AST 78-20402 and DOE grant DE-AC02-80ER10773 at the University of Chicago and by DOE grant DE-AS02-78ER05007 at Bartol Research Foundation.

8. References

M. Aaronson, J. Mould, J. Huchra, W.T. Sullivan, R.A. Schommer, and G.D. Bothun, Ap. J. (in press).

S. Aarseth, R. Gott, and E. Turner, Ap. J. 228, 664 (1979).

D. Branch, MNRAS 186, 609 (1979).

R. Cowsik and McClellan, Phys. Rev. Lett. (1973).

S.M. Faber and J.S. Gallagher, Ann Rev. Astron. Astrophys. 17, 135 (1979).

R. Gott, J. Gunn, D. Schramm and B. Tinsley, Ap. J. 194, 543 (1974).

R. Gott, E. Turner, Ap. J. 209, 1 (1976).

J. Gunn, B. Lee, I. Lerche, D.N. Schramm, and G. Steigman, Ap. J. 223, 1015 (1978).

R.P. Kirshner, A. Oemler, Jr., and P.L. Schecter, AJ 84 951 (1979).

S.M. Lea, J. Silk, E. Kellogg, and S. Murray, Ap. J. Lett. 184, L105 (1973).

G. Marx and A. Szalay, Proc. of Int. Neutrino Conf. (1973).

K. Olive, D.N. Schramm, G. Steigman, M.S. Turner and J. Yang, Astrophys. J. (submitted).

P.J.E. Peebles, AJ 84, 730 (1979a).

P.J.E. Peebles, in Proc. Les Houces School on Physical Cosmology, ed. Audouze, Balian, and Schramm, (1979b).

B. Pontecorvo, Sov Phys. JETP 26, 984 (1968).

F. Reines, et al., Phys. Rev. Lett. (in press).

D.N. Schramm and G. Steigman, Astrophys. J. (in press).

D.N. Schramm and E.M.D. Symbalisty, Reports on Progress in Physics (in press).

D.N. Schramm and R.V. Wagoner, Ann. Rev. Nucl. Part. Sci. 27, 37 (1977).

F. Stecker, Proc. DUMAND Symposium (1980).

G. Steigman, Ann. Rev. Nucl. Part. Sci. 29, 313 (1979).

E.M.D. Symbalisty and D.N. Schramm, Nature (in preparation).

S. Tremaine and J.E. Gunn, Phys. Rev. Lett. 42, 407 (1979).

D.P. Woody, J.C. Mather, N. Nishioka, and P.L. Richards, Phys, Rev. Lett. 34, 1036 (1975).

J. Yang, D.N. Schramm and R.V. Wagoner, Ann. Rev. Nucl. Part. Sci. 27, 37 (1977).

COSMOLOGICAL LIMITS ON NEUTRINO MASSES

Keith A. Olive

Enrico Fermi Institute
University of Chicago
5640 S. Ellis
Chicago, IL. 60637

Abstract

Limits relating stable neutrino interaction strengths and their masses are derived from the standard big bang model. For light neutrinos ($m_\nu < 1$MeV), the upper limits range from 0.1 - 1.0 KeV depending on their interaction strength. For heavy stable neutrinos, m_ν (GeV) $\gtrsim (G_F/G_{SW})^{0.96}$. An additional constraint is available if there exists a neutrino asymmetry comparable to the baryon asymmetry which implies $m_\nu \lesssim 2.0$ TeV. A brief review of previous limits will also be discussed.

I. Introduction

The growing interest and possibility that neutrinos have mass has once again opened up a window for cosmologists to examine the relationship between particle physics and cosmology. In the past, many authors have set limits on neutrino masses, lifetimes, and flavors.[1-11] Preliminary experimental evidence[12] may imply the existence of massive neutrinos possibly leading to a solution of the "missing light" problem in galaxies.[13] In addition, certain grand unified theories [e.g. O(10)] propose the existence of light left-handed neutrinos as well as heavy (possibly superheavy) right-handed neutrinos.[14]

These right-handed neutrinos necessarily interact more weakly than their left-handed counterparts; and it is the purpose of this paper to extend previous neutrino mass limits to superweakly interacting right-handed neutrinos.

Before specifically addressing the problem concerning superweakly interacting neutrinos, it will be useful to briefly describe some of the previous work constraining the masses of neutrinos. Therefore, in section II, I will discuss the present state of cosmological constraints on ordinary full strength weakly interacting neutrino masses. In section III, the role of superweakly interacting neutrinos will be examined. In section IV, the previous constraints will be extended to include arbitrary interaction strength neutrinos and concluding remarks will be given in section V.

II. Limits on Masses

In the very early stages of the universe, thermal equilibrium was established for all types of particles by either strong, weak, or electromagnetic interactions. In particular, light neutrinos ($m_\nu < 1$ MeV) were kept in thermal equilibrium by neutral current weak interactions such as $e^+ + e^- \leftrightarrow \nu_i + \bar{\nu}_i$ ($i = e,\mu,\tau$, etc.). These neutrinos will remain in equilibrium so long as the weak interaction rate, Γ_w, is greater than the expansion rate of the universe, t^{-1}. When $\Gamma_w \approx t^{-1}$, at a temperature of about 1 MeV, the neutrinos decouple from the thermal background (consisting of $e^{\pm}$'s and photons) and behave as a freely expanding fermi gas. The number density of neutrinos at this time can easily be compared to the number density of photons

$$n_{\nu_i} = (\tfrac{3}{8}) g_{\nu_i} n_\gamma \ , \qquad (1)$$

where g_{ν_i} represents the number of degrees of freedom for neutrino type i, and the factor (3/8) is due to the difference betwen the Fermi and Bose statistics for neutrinos and photons. For massless as well as massive Majorana neutrinos $(\nu_i = \bar{\nu}_i)$, $g_{\nu_i} = 2$. While for Dirac mass neutrinos $(\nu_i \neq \bar{\nu}_i)$, $g_{\nu_i} = 4$.

As the temperature of the universe continues to cool down to $T \approx m_e$, the $e^{\pm}$ pairs annihilate heating up the photons relative to the neutrinos.[15] Thus, for $T < m_e$, $(T_\nu/T_\gamma)^3 = 4/11$ and

$$n_{\nu_i} = (3/8)(4/11)\, g_{\nu_i} n_\gamma. \tag{2}$$

The present number density is then,

$$n_{\nu_i} = (3/22) g_{\nu_i} n_{\gamma_o} \approx 55 g_{\nu_i} \left(\frac{T_o}{2.7}\right)^3 \text{ cm}^{-3}, \tag{3}$$

where T_o is the present temperature of the microwave background. The mass density of the neutrinos today is given by

$$\rho_{\nu_i} = m_{\nu_i} n_{\nu_i} \approx 10^{-31} m_{\nu_i} g_{\nu_i} \left(\frac{T_o}{2.7}\right)^3 \text{ gcm}^{-3}, \tag{4}$$

where m_{ν_i} is measured in eV.

From the constraint $\Omega h_0^2 < 1$ one finds that $\sum_i \rho_{\nu_i} < 2 \times 10^{-29}$ gcm^{-3}. Thus we have the following constraint on the sum of the masses of all neutrinos with $m_{\nu_i} < 1$ MeV,[1,3]

$$\sum_i m_{\nu_i} g_{\nu_i} \lesssim 200 \left(\frac{2.7}{T_o}\right)^3 < 200. \tag{5}$$

Thus, for Majorana mass neutrinos

$$\sum_i m_{\nu_i} \lesssim 100 \text{ eV}, \tag{6a}$$

while for Dirac mass neutrinos

$$\sum_i m_{\nu_i} \lesssim 50 \text{ eV}. \tag{6b}$$

The situation is slightly different when one considers high mass neutrinos ($m_\nu > 1$ MeV). The heavy neutrinos can only maintain their equilibrium number density through annihilations. Thus, the neutrinos effectively decouple at a much higher temperature than the low mass neutrinos, since their annihilation rate Γ_A drops below the expansion rate much earlier than does the neutral current rate Γ_W. So that when $\Gamma_A \approx t^{-1}$ the number of neutrinos is frozen and they are present in greater numbers today then they would have been, had they stayed in equilibrium. The present mass density of these high mass stable neutrinos has been calculated by Lee and Weinberg[2] and is given by

$$\rho_\nu = \frac{4}{11} g_\nu m_\nu T_\gamma^3 F(\mu), \tag{7}$$

where
$$F(\mu) \approx 1.2 \times 10^{-5} \ (\text{cm } {}^\circ\text{K})^{-3} [\mu(\text{GeV})]^{-2.85}, \tag{8}$$

and
$$\mu^3 = C m_\nu^3 N_A \ / \sqrt{N_F}, \tag{9}$$

$C \propto G_F^2$, N_A represents the number of annihilation channels for ν and $\bar{\nu}$, N_F is the number of degrees of freedom in the universe at the decoupling temperature. (The value of N_A depends on m_ν ; see Table 1.)

Table 1

m_ν(GeV)	N_A	m_ν(GeV)	N_A
< 1.5	14	$20 - M_{W_L}$	24
1.5 - 1.8	17	$M_{W_L} - M_{W_R}$	26
1.8 - 5	18	M_{W_R}	28
5 - 20	21		

Thus using $T_\gamma = 2.7^\circ K$ and $g_\nu = 2$ we have,

$$\rho_\nu \approx 3.1 \times 10^{-28} m_\nu^{-1.85} (N_A / \sqrt{N_F})^{-0.95} \text{ gcm}^{-3}, \tag{10}$$

where m_ν is now measured in GeV.

Once again we must require that $\rho_\nu < 2 \times 10^{-29}$ gcm^{-3} so that

$$m_\nu (N_A / \sqrt{N_F})^{.51} > 4.4 \text{ GeV}. \tag{11}$$

and using $N_A = 17$, $N_F = 4.5$, one finds that

$$m_\nu \gtrsim 1.5 \text{ GeV}. \tag{12}$$

One should note, however, that these massive neutrinos may collect together with ordinary matter to form clusters of galaxies.[3] Thus, perhaps a better lower limit on the mass of the neutrino would be obtained by requiring $\rho_\nu < 10^{-30}$gcm^{-3}, the upper limit on the mass density observed in clusters of galaxies. We then have

$$m_\nu (N_A / \sqrt{N_F})^{.51} > 22 \text{ GeV}, \tag{13}$$

and using $N_A = 21$ and $N_F = 4.5$ one finds that

$$m_\nu \gtrsim 6.8 \text{ GeV}. \tag{14}$$

It is possible to add a further constraint on the masses of neutrinos if one assumes that an asymmetry of neutrinos over antineutrinos was produced at the time of baryon generation at a temperature $T \approx 10^{15}$ GeV.[4] If we define η to be the ratio of the number of excess neutrinos to photons then

$$\rho_\nu = m_\nu \eta n_\gamma < \rho_{max}$$

or

$$m_\nu < \rho_{max} / \eta n_\gamma. \tag{15}$$

For $T_o = 2.7^oK$, $N_\gamma = 400\ cm^{-3}$ and $\eta \geq 1.5 \times 10^{-11}$[11],

$$m_\nu \lesssim 93.5\ GeV,\ \rho_{max} = 10^{-30}\ gcm^{-3}$$

or

$$m_\nu \lesssim 1.8\ TeV,\ \rho_{max} = 2 \times 10^{-29} gcm^{-3}. \qquad (16)$$

Thus there exits only two small windows for neutrino masses: $\sum_i m_{\nu_i} < 100$ eV and $1.5\ GeV < m_\nu < 1.8\ TeV$.

III. Superweak Neutrinos

The existence of superweakly interacting neutrinos has been proposed by various unification models such as extended Weinberg-Salam-Glashow-Ward; $SU(2)_L \times SU(2)_R \times U(1)$ [16] or the grand unified model O(10).[14] In both types of models there exists right-handed counterparts for the usual left-hand neutrinos. The right-handed current is mediated by a guage boson designated W_R and the interaction strength can be characterized by $G_{SW} \propto M_{W_R}^{-2}$. Present experimental limits require $M_{W_R} \gtrsim 300$ GeV. (O(10) models predict M_{W_R} as well as m_{ν_R} to be on the order of 10^{13} GeV. In this case, ν_R is probably very unstable and would not be subjected to the constraints presented below.)

Let us assume then, that these right-handed neutrinos interact with an arbitrary interaction strength $G_{SW} < G_F$. The decoupling temperature T_d, of neutrinos is very sensitive to the competition between the expansion rate and the weak (or superweak) interaction rate. If one decreases the coupling strength of the interaction, neutrinos will in general, freeze out at a higher temperature. That is, the decoupling temperature of superweakly interacting neutrinos will be greater than that of ordinary full strength neutrinos. Hence, their number densities will be reduced by a factor $(T_{\nu_R} / T_{\nu_L})^3$ due to the annihilations of more massive particles such as $\mu^\pm$, $\pi^\pm$ etc. For example, if the decoupling temperature of the superweak neutrinos is, say,

greater than the muon mass, the annihilation energy of the $\mu^{\pm}$ pairs will be shared among the photons and full strength neutrinos and not by the decoupled neutrinos. Thus, the temperature of the superweak neutrinos will be lower than that of the full strength neutrinos, just as in the case of the effect of $e^{\pm}$ annihilation on the ratio of the photon temperature and the ordinary neutrino temperature. (See references 9 and 10 for a detailed description of this factor.)

To calculate the relationship between G_{SW} and T_d, consider a superweak process such as $\nu_R + e \rightarrow \nu_R + e$. The cross-section for this process can be scaled by a generalization of the normal weak cross-section[3] so that

$$\sigma_{SW} \approx 5.1 \times 10^{-44} (G_{SW} / G_F)^2 T^2 \text{cm}^2. \tag{17}$$

The density of electrons can be written as

$$n_e \approx 2.4 \times 10^{31} T^3 \text{ cm}^{-3}, \tag{18}$$

where all temperatures are measured in MeV. The superweak interaction rate is then

$$\lambda = \sigma_{SW} n_e c \approx 3.6 \times 10^{-2} (G_{SW} / G_F)^2 T^5 \text{ sec}^{-1}. \tag{19}$$

The expansion rate of the universe is just

$$\frac{1}{2} t^{-1} = 0.29 N_F^{1/2} T^2 \text{ sec}^{-1}, \tag{20}$$

where once again N_F is the total number of degrees of freedom. To determine the decoupling temperature we then use the condition

$$2\lambda t \approx (G_{SW} / G_F)^2 T_d^3 / 8 N_F^{1/2} = 1. \tag{21}$$

Thus we have

$$G_F / G_{SW} \approx 0.35 \, T_d^{3/2} / N_F^{1/4} . \tag{22}$$

We are now in a position to extend the limits on full strength neutrino masses to account for arbitrary interaction strength neutrinos.

IV. Limits on Superweak Neutrino Masses

As in the case of full strength neutrinos, the limits on superweak neutrino masses must also be treated separately for low mass (< 1 MeV) and high mass neutrinos, as well as distinguishing between Dirac and Majorana neutrinos. Let us begin, therefore, with the limits on low mass neutrinos.

In building models with several types of low mass, relatively stable ($\tau > 1$ sec) neutrinos, one must take care not to exceed the upper limit on neutrino flavors, N_ν, from primordial nucleosynthesis. N_ν, however, strongly depends on the present nucleon density of the universe.[11] For example, if the universe today is dominated by nucleons, using the lower limit on the nucleon density $\rho_N \geq 2 \times 10^{-31} \text{gcm}^{-3}$ [17] (corresponding to $\Omega_N \geq .04$, $h_0 \geq 1/2$), one obtains[8] $N_\nu \leq 3$. This implies that if the three neutrinos (ν_e, ν_μ, ν_τ) do in fact have mass, they are required to be either Majorana neutrinos or in the case of Dirac neutrinos, their right-handed components must interact with a strength $G_{SW} / G_F \lesssim 3 \times 10^{-3}$.[9,10] On the other hand, if the universe is not dominated by nucleons but rather by massive neutrinos[13], so that perhaps the nucleon density may be as low as $2.5 \times 10^{-32} \text{gcm}^{-3}$ (corresponding to $\Omega_N \geq .005$, $h_0 \geq 1/2$), the upper limit on N_ν can be quite large and three Dirac mass neutrinos can be accomodated with no conflict with primordial nucleosynthesis.[11]

With these provisions in mind, let us then proceed to calculate the upper limit on the mass of a light Dirac neutrino. (These calculations as well as those which follow were done by Michael Turner and myself.[18]) Let us assume

that these neutrinos have left-handed components which interact with full strength weak interactions. The right-handed components, however, are allowed to interact with an arbitrary interaction strength $G_{SW} < G_F$. Since the right-handed components interact more weakly, their decoupling temperature is higher and hence they will be present in lower abundances than their left-handed counterparts. The present number density of the left-handed component is given by equation (2) with $g_{\nu_i} = 2$. The density of the right-handed neutrinos is

$$n_{\nu_{R_i}} = 2\,(3/8)(4/11)(T_{\nu_R} / T_{\nu_L})^3\, n_\gamma \,. \tag{23}$$

The values for T_{ν_R} / T_{ν_L} as a function of G_F/G_{SW} are shown in Figure 1.[10]

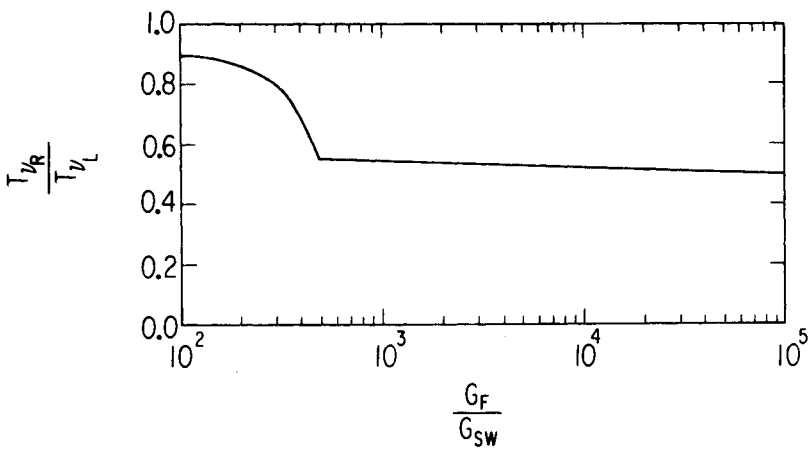

Figure 1

The total present mass density of each neutrino type is given by

$$\rho_{\nu_i} \approx 2 \times 10^{-31}\, m_{\nu_i} [1 + (T_{\nu_R} / T_{\nu_L})^3]\ \text{gcm}^{-3}, \tag{24}$$

where m_{ν_i} is measured in eV. Demanding once again that

$\sum_i \rho_{\nu_i} < 2 \times 10^{-29}$ gcm^{-3}, we have the following constraint on $\sum_i m_{\nu_i}$:

$$\sum_i m_{\nu_i} \lesssim 100 \text{ (eV)}/[1 + (T_{\nu_R}/T_{\nu_L})^3]. \tag{25}$$

The allowed region in the neutrino mass-coupling strength plane is shown in the low mass region by the dashed curve in Figure 2. The dotted curve assumes a nucleon dominated universe with three neutrino types, hence $\log(G_F/G_{SW}) > 2.55$ from nucleosynthesis arguments[9,10]. It should be noted that for the case of an extremely weak coupling constant, the upper limit on $\sum_i m_{\nu_i}$ is 93 eV.

These limits are slightly altered when one considers low mass Majorana neutrinos which interact superweakly. Let us assume that these particles are distinct from the normal full strength neutrinos which may or may not have mass. One should bear in mind, however, that in most models in which these types of particles exist, they aquire a fairly large mass $O(M_{W_R})$ while at the same time, the normal left-handed neutrinos aquire a very small mass $m_{\nu_i} \approx \frac{m_i^2}{g\, m_{W_R}}$, [19] where g is the $SU(2)_R$ gauge coupling. The limits for high mass right-handed neutrinos will be given below. For the moment, assume the righthanded neutrinos, ν_R, have mass $m_{\nu_R} < 1$ MeV. Equation (23) then becomes

$$\sum_i m_{\nu_{L_i}} + \sum_i m_{\nu_{R_i}} (T_{\nu_R}/T_{\nu_L})^3 < 100\text{eV} \tag{26}$$

For simplicity, assume thats $m_{\nu_{L_i}} \approx 0$. The constraint on the mass of the superweakly interacting light Majorana neutrino becomes

$$\sum_i m_{\nu_{R_i}} \lesssim 100(T_{\nu_L}/T_{\nu_R})^3 \text{ eV} \tag{27}$$

The allowed mass-coupling strength region is shown for low masses by the solid curve in Figure 2. Since we are assuming that ν_R is distinct from ν_L, the

nucleosynthesis argument will also apply here. The limit for extremely weak coupling in this case is $\sum_i m_{\nu_{R_i}} < 990$ eV.

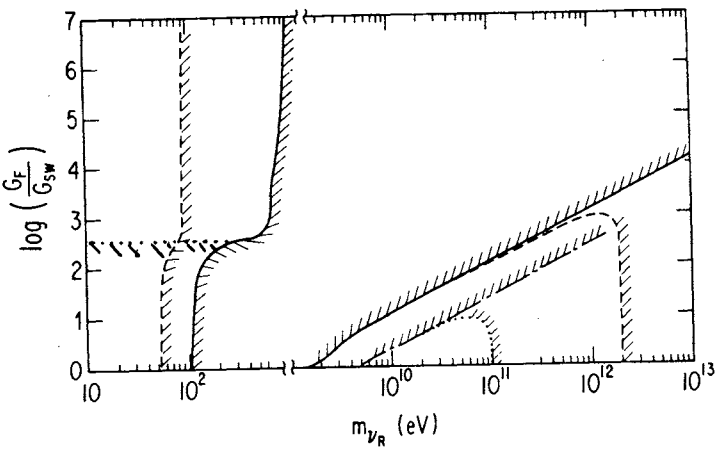

Figure 2

In order to generalize the limits in equations (12) and (14) for high mass neutrinos, we must scale the coupling strength in equation (9). Just as in the case for full strength neutrinos, the higher the mass of the neutrino, the more efficient the annihilation rate becomes. However, if we decrease the coupling strength of the interaction, we are forced to higher masses in order to ensure enough annihilation so that the mass density remains below the maximum allowed density. (The following discussion on high mass neutrinos, will be restricted to Majorana neutrinos for reasons explained in Section V.) Let us redefine μ in equation (9) so that

$$\mu^3 = (G_{SW}/\, G_F)^2\, C\, m_\nu^3\, N_A/\sqrt{N_F}\ . \tag{28}$$

Equation (10) then becomes

$$\rho_\nu \approx 3.1 \times 10^{-28} m_\nu^{-1.85} (G_F/\, G_{SW})^{1.9} (N_A/\sqrt{N_F})^{-.95} (T_{\nu_R}/\, T_{\nu_L})^3\ \mathrm{gcm}^{-3}, \tag{29}$$

where once again the factor T_{ν_R} / T_{ν_L} is due to a higher freeze-out temperature of the superweak neutrinos (ν_R) relative to the full strength neutrinos (ν_L) (see Figure 1). The freeze-out temperature is obtained from[2]

$$y^{1/2}e^{y} = 1.35 \times 10^{7}\ N_A N_F^{-1/2} m_\nu^3 (G_{SW}/\ G_F)^2, \tag{30}$$

where $y = m_\nu/KT_f$ and in general $y \approx 20$. The values for N_A have been displayed in Table 1 and the values for N_F range from 4.5 to ~ 55 depending on the freeze-out temperature[10].

Using the constraint $\rho_\nu < \rho_{max}$, we find that

$$(G_F/\ G_{SW}) < m_\nu^{.97} N^{1/2} N_F^{-1/4} (T_{\nu_R} / T_{\nu_L})^{-1.58} (\rho_{max}/3.1 \times 10^{-28}\ gcm^{-3})^{.53}, \tag{31}$$

where ρ_{max} is either 2×10^{-29} or $10^{-30}\ gcm^{-3}$. The allowed high mass regions are shown in Figure 2. The solid curve corresonds to $\rho_{max} = 2 \times 10^{-29}\ gcm^{-3}$ and the dotted-dashed curve corresponds to $\rho_{max} = 10^{-30}\ gcm^{-3}$.

By utilizing the probably asymmetry of neutrinos over antineutrinos, we can again obtain a firm upper limit on the mass of heavy neutrinos. As before, define $\eta = (n_\nu - n_{\bar{\nu}})/n_\gamma > 1.5 \times 10^{-11}$,[11] so that the contribution to the mass density due to the asymmetry is $m_\nu \eta n_\gamma$. This quantity must now be added to the density due to insufficient annihilation which gives a total mass density for neutrinos

$$\rho_\nu = m_\nu \eta n_\gamma + 3.1 \times 10^{-28} m_\gamma^{-1.85} (N_A/\sqrt{N_F})^{-.95} (G_F/G_{SW})^{1.9} (T_{\nu_R}/T_{\nu_L})^3\ gcm^{-3} \tag{32}$$

The condition $\rho_\nu < \rho_{max}$ becomes

$$(G_F/G_{SW}) < 3.8 \times 10^{14} (\rho_{max} - m_\nu \eta n_\gamma)^{.53} m_\nu^{.97} N^{1/2} N_F^{-1/4}\ (T_{\nu_R}/T_{\nu_L})^{-1.58}$$

or (33)

$$(G_F/G_{SW}) < \left(\frac{\rho_{max}}{3.1 \times 10^{-28} gcm^{-3}} - 3.45 \times 10^{-5} m_\nu\right)^{.53} m_\nu^{.97} N_A^{1/2}\ N_F^{-1/4} (T_{\nu_v}/T_{\nu_L})^{-1.58}$$

where m_ν is measured in GeV. These results are shown in the high mass region in Figure 2. The dashed curve corresponds to $\rho_{max} = 2 \times 10^{-29}$ gcm^{-3} and the dotted curve corresponds to $\rho_{max} = 10^{-30}$gcm^{-3}.

V. Summary and Discussion

The previous limits on the masses of neutrinos have been generalized to include the effects of arbitrary interaction strength neutrinos. In particular, the previous low mass limits of $\sim$ 100 eV and $\sim$ 50 eV, for Majorana and Dirac neutrinos, respectively, may be as high as $\sim$ 1 KeV and $\sim$ 90 eV for extremely weak interacting neutrinos. The main reason for the difference in these limits is due to the fact that more weakly interacting particles will decouple from the thermal background earlier at a higher temperature. Hence their present temperature will be reduced relative to the full strength neutrinos due to the annihilation of various particle species. Thus, they will be present in lower abundances and are allowed a greater mass.

While the effect of reducing the interaction strength for low mass neutrinos serves to increase the allowed mass ranges, for high mass neutrinos, one is forced to larger, more restricting masses. For full strength weak interactions, neutrinos are required to have a mass larger than $\sim$ 1.5 GeV. However, if we decrease the interaction rate, annihilations become less efficient so that more neutrinos are left over when the interaction freezes out. To compensate for this, we must increase the neutrino mass so that $m_\nu \gtrsim (G_F/G_{SW})^{0.96}$. Thus, the weaker the interaction, the more restricive the cosmological limits become. These arguments for high mass neutrinos, however, only apply to Majorana neutrinos. The reason being that for Dirac neutrinos, by the time the right-handed components cease to annihilate, they are already

very non-relativistic and one no longer has a well defined helicity state. Thus, they may continue to annihilate as full strength left-handed particles and the previous limit of ~ 1.5 GeV is left unchaged. Majorana neutrinos, however, always maintain a well defined helicity state (save perhaps for a very small amount of mixing with a lighter left-handed neutrino) and cannot proceed to annihilate after freeze-out.

The additional limit due to an asymmetry of neutrinos over antineutrinos has also been generalized to include superweakly interacting particles. The upper limits of ~ 93 GeV and ~ 2 TeV (depending on the maximum allowed mass density) remain firm upper limits on the masses of heavy stable neutrinos.

VI. Acknowledgements

I would like to thank J. Preskill and D.N. Schramm for valuable discussions and in particular, my collaborator, M.S. Turner, with whom these results were calculated. This work was supported in part by NSF grant 78-20402, and the Fannie and John Hertz Foundation Fellowship at the University of Chicago.

References

1. R. Cowsik and J. McClelland, Phys. Rev. Lett. 29, (1972), 669;
A.S. Szalay and G. Marx, Astron. Astrophys. 49, (1976), 437.

2. P. Hut, Phys. Lett. 69B, (1977), 85;
B.W. Lee and S. Weinberg, Phys. Rev. Lett. 39, (1977), 165.

3. J.E. Gunn, B.W. Lee, I. Lerche, D.N. Schramm, and G. Steigman,

Astrophys. J. 223, (1978), 1015.

4. P. Hut and K.A. Olive, Phys. Lett. 87B, (1979), 144.

5. D.A. Dicus, E.W. Kolb and V.T. Teplitz, Phys. Rev. Lett. 39, (1977), 168.

6. S.W. Falk and D.N. Schramm, Phys. Lett. 79B, (1977), 511.

7. G. Steigman, D.N. Schramm, and J.E. Gunn, Phys. Lett. 66B, (1977), 202.

8. J. Yang, D.N. Schramm, G. Steigman, and R.T. Rood, Astrophys. J. 227, (1979), 697.

9. G. Steigman, K.A. Olive, and D.N. Schramm, Phys. Rev. Lett. 43, (1979), 239.

10. K.A. Olive, D.N. Schramm and G. Steigman, submitted to Nucl. Phys. B., (1980).

11. K.A. Olive, D.N. Schramm, G. Steigman, M.S. Turner, and J. Yang, submitted to Astrophys. J., (1980).

12. F. Reines, H.W. Sobel, and E. Pasierb, (preprint 1980).

13. D.N. Schramm and G. Steigman, submitted to Astrophys. J., (1980).

14. H. Georgi, and D.V. Nanopoulos, Nucl. Phys. B155, (1979), 52.

15. S. Weinberg, Gravitation and Cosmology, John Wiley and Sons, (1972), New York.

16. V. Barger, W.Y. Keung, and E. Ma, Phys. Rev. Lett. 44, (1980), 1169.

17. J.R. Gott, J.E. Gunn, D.N. Schramm, and B.M. Tinsley, Astrophys. J. 194, (1974), 543.

18. K.A. Olive and M.S. Turner, submitted to Phys. Lett. B, (1980).

19. R.N. Mohapatra and G. Senjanovic, Phys. Rev. Lett. 44, (1980) 912.

MASSIVE NEUTRINOS

AND

COSMOLOGICAL NUCLEOSYNTHESIS

Ira Wasserman, Stuart L. Shapiro and Saul A. Teukolsky
Center for Radiophysics and Space Research
Cornell University
Ithaca, NY 14853

ABSTRACT

We show that finite neutrino rest masses, $m_\nu \sim 10$eV, would not alter primordial element abundances produced in the early Universe. Even though massive Dirac neutrinos could occupy up to twice as many spin states as massless neutrinos, weak interactions via the standard Weinberg-Salam-Glashow theory couplings never proceed sufficiently rapidly to produce a thermal population of positive helicity neutrinos.

1. Introduction

In recent years, theoretical speculations about particle physics at ultra-high energies ($E \sim 10^{15}$GeV) and cosmology at very early epochs ($t \sim 10^{-36}$sec) have become increasingly inter-related. The validity of the standard Big Bang model[1] of the early Universe, which predicts a primordial He^4 abundance, Y, in substantial agreement with the observed values, is one of the basic theoretical assumptions on which the union of high energy physics and cosmology is based. Assuming the standard model and given the observed values of Y physicists have derived meaningful constraints on the number and properties of elementary particles (cf. Ref. 2 and references therein). In particular, if $Y \lesssim 0.25$[3] and $\Omega_B h^2 \gtrsim 0.01$[4], where Ω_B is the present-day baryon density in units of the closure density

$$\rho_c = \frac{3H_o^2}{8\pi G}$$

and h is Hubble's constant, H_o, in units of 100km $s^{-1}Mpc^{-1}$, the stan-

dard model can tolerate the existence of at most 4 flavors of massless neutrinos[2] i.e. ν_e ν_μ, ν_τ plus at most one more flavor.

Experimental evidence for neutrino oscillations[5], if confirmed, would require that neutrinos have finite rest masses m_{ν_j}[6]. Massive neutrinos with $m_{\nu_j} \sim 10eV$ could solve the missing mass problem for clusters of galaxies, and would contribute most of the rest mass density of the present-day Universe[7].

At first sight, it would appear that finite rest masses could pose problems for the standard model of the early Universe. In the Weinberg-Salam-Glashow (WSG)[8] theory of weak interactions only the chiral left-handed part

$$\nu_L = \frac{1}{2}(1 + \gamma_5)\nu$$

of the neutrino spinor ν appears in the interaction Lagrangian. For massless neutrinos this is enough to guarantee the existence of negative helicity (h=-1) neutrinos only. However, chiral left-handedness does not imply negative helicity for massive neutrinos. One might therefore expect that massive neutrinos in thermal equilibrium would populate both helicity states, h=±1, equally. Three flavors of extremely relativistic massive neutrinos would therefore be equivalent to 6 flavors of massless neutrinos, which would contradict the standard model limit, $N_\nu \leq 4$ massless neutrino flavors.

We examine and resolve this apparent contradiction below: The inclusion of finite neutrino rest masses does not invalidate the standard Big Bang model of the early Universe.

2. Neutrino Masses in the WSG Theory

Neutrino masses in the WSG theory can arise from $SU(2)_L \times U(1)$

invariant couplings of (chiral) left-handed $SU(2)_L$ doublets
($f_L = \frac{1}{2}(1 + \gamma_5)f$; $f_R = \frac{1}{2}(1 - \gamma_5)f$),

$$\psi_L = \begin{pmatrix} \ell_L^- \\ \nu_{\ell,L} \end{pmatrix} ,$$

Higgs fields, H, and right-handed lepton singlets, ℓ_R^- and $\nu_{\ell,R}$, where ℓ^- is any charged lepton and ν_ℓ its associated neutrino. After symmetry is broken and mass matrices are diagonalized there are two possible types of massive neutrinos:

(1) Majorana neutrinos, which are represented by 2-component spinor wave functions that are CP eigenstates in the neutrino rest frame, can arise from $\nu_R\nu_R$ terms in the symmetric Lagrangian. Majorana mass terms do not conserve lepton number so there is no. Majorana antineutrino[6].

(2) Dirac neutrinos, which are represented by 4-component spinor wave functions that are C and P eigenstates in the neutrino rest frame, can arise from Higgs couplings of the form

$$g(\nu\text{-}H)[\bar{\psi}_L H \nu_R + \text{h.c.}] \qquad (1)$$

in the symmetric Lagrangian[9]. Dirac mass terms

$$m_\nu(\bar{\nu}_R\nu_L + \bar{\nu}_L\nu_R) \qquad (2)$$

conserve lepton number, so there are both Dirac neutrinos and Dirac antineutrinos. From equations (1) and (2), and the vacuum expection value of the Higgs field, $\langle H \rangle = (2\sqrt{2}G_F)^{-1/2}$, it follows that[9]

$$m_\nu(G_F\sqrt{2})^{1/2} , \qquad (3)$$

a result we make use of below.

3. State Counting

Assuming the WSG theory, and explicitly excluding the possibility of broken left-right symmetry resulting in hyperweak right-handed couplings with extremely massive right-handed gauge bosons[10] in addition to the usual weak left-handed couplings and gauge bosons, what is the maximum number of neutrino states, g_ν, occupied per neutrino momentum and flavor?

For massless neutrinos only negative helicity states can be populated in the WSG theory. Therefore

$$[g_\nu]_{\text{massless}} = 1 \times 2 = 2$$

where the first factor is the number of allowed helicity states (=1 for massless neutrinos) and the second factor takes into account both neutrinos and antineutrinos.

For Majorana neutrinos both h=+1 and h=-1 states are allowed but there is no antineutrino so

$$[g_\nu]_{\text{Majorana}} = 2 \times 1 = 2 \quad ,$$

the same as $[g_\nu]_{\text{massless}}$. Therefore, in complete thermal equilibrium at $kT >> m_\nu$

$$[\rho(T)]_{\text{Majorana}} = [\rho(T)]_{\text{massless}} \quad . \tag{4}$$

For Dirac neutrinos both h=+1 and h=-1 states can be populated, and there are both neutrinos and antineutrinos so

$$[g_\nu]_{\text{Dirac}} = 2 \times 2 = 4$$

i.e. $[g_\nu]_{\text{Dirac}} = 2 \times [g_\nu]_{\text{massless}}$. In complete thermal equilibrium at

$kT >> m_\nu$

$$[\rho(T)]_{Dirac} = 2[\rho(T)]_{massless} \quad . \tag{5}$$

4. Cosmological Nucleosynthesis

The key result of detailed calculations of cosmological nucleosynthesis is that the final element abundances depend on the neutron to proton abundance ratio, n/p, when the neutrons freeze out of equilibrium[1]. This happens when the rates for the neutron producing and destroying reactions

$$p + e^- \leftrightarrow n + \nu_e$$

$$p + \nu_e \leftrightarrow n + e^+$$

$$n \leftrightarrow p + e^- + \bar{\nu}_e \quad ,$$

which are roughly $\propto T^5$, become slower than the expansion rate

$$\Gamma_{exp} \sim (G\rho)^{1/2} \propto T^2 \quad ,$$

where ρ is the total energy density of all extremely relativistic particles[1].

In the standard model with 3 massless neutrino flavors, neutrons freeze out at $kT_f \sim 1MeV$, with a relative abundance

$$\left(\frac{n}{p}\right)_f \simeq \exp\left[\frac{-(m_n - m_p)}{kT_f}\right] \quad .$$

If ρ were actually larger than it is in the standard model then, since $\Gamma_{exp} \propto \sqrt{\rho}$, (1) neutrons would freeze out earlier - at a higher temperature T_f - so that $(n/p)_f$ would be larger, and (2) free neutron decay would have less time to occur before the neutrons bind into

He^4. Both of these consequences of increasing ρ lead to a larger value of Y.[2]

From equation (4) we see that the energy density of 3 flavors of extremely relativistic Majorana neutrinos is the same as the energy density of 3 flavors of massless neutrinos, so that the computed heavy element abundances in the standard model are unchanged if massive neutrinos are of the Majorana type. However, from equation (5) we see that the energy density of 3 flavors of extremely relativistic Dirac neutrinos in thermal equilibrium is the same as the energy density of 6 flavors of massless neutrinos, two more than can be tolerated in the standard model, unless both allowed helicity states are not equally populated at $T \gtrsim T_f$.

Neutrinos maintain thermal contact via interactions like

$$f^- + \bar{f}^+ \leftrightarrow \nu + \bar{\nu}$$

$$f^- + \nu \rightarrow f^- + \nu, \text{ etc.} \qquad (6)$$

where f^- is any extremely relativistic charged fermion[1]. For massive neutrinos there are two f-ν couplings: interactions involving intermediate vector boson ($W^{\pm}$, Z^0) exchange, and interactions involving Higgs boson (H) exchange[8,9].

Intermediate vector boson couplings involve only the chiral left-handed parts of the neutrino spinors. For h=-1 neutrinos (or h=+1 antineutrinos) only in the initial and final states at $T \lesssim 10^2 \text{GeV}(\sim m_W, m_Z)$ the rates for the various ν-f reactions given in equation (6) are all of order

$$\Gamma_{-1,-1} \sim n_f \sigma_{-1,-1} \sim G_F^2 T^5 \qquad (7)$$

where $n_f \sim T^3$ is the number density of extremely relativistic fer-

mions, $\sigma_{-1,-1} \sim G_F^2 T^2$, G_F is Fermi's constant and we have adopted units in which $\hbar=c=k=1$. (Reactions involving non-relativistic fermions are ignored because their number densities are suppressed by Boltzmann factors, $e^{-m_f/T}$.) The expansion rate is

$$\Gamma_{exp} \sim \sqrt{G}\, T^2 \qquad (8)$$

in the same units, so

$$\frac{\Gamma_{-1,-1}}{\Gamma_{exp}} \sim \frac{G_F^2\, T^3}{\sqrt{G}} \quad . \qquad (9)$$

From equation (9) we get the familiar result that h=-1 neutrinos (and h=+1 antineutrinos) decouple at[1]

$$T_D \sim G^{1/6}\, G_F^{-2/3} \sim 1\text{MeV} \quad .$$

For spin flipping interactions in which, for example, an h=-1 neutrino in the initial state is converted to an h=+1 neutrino in the final state

$$\sigma_{-1,+1} \sim \frac{m_\nu^2}{E_\nu^2} \times \sigma_{-1,-1}$$

for extremely relativistic neutrinos, $E_\nu >> m_\nu$, so that

$$\frac{\Gamma_{-1,+1}}{\Gamma_{exp}} \sim \frac{G_F^2\, m_\nu^2\, T}{\sqrt{G}} \quad . \qquad (10)$$

Since $\sigma_{-1,-1}$ no longer increases like E_ν^2 for $E_\nu \gtrsim m_w$[8,9], $\Gamma_{-1,+1}/\Gamma_{exp}$ decreases with increasing temperature above $T \sim 10^2$GeV. Therefore

$$\frac{\Gamma_{-1,+1}}{\Gamma_{exp}} \lesssim 10^{-7}\, m_\nu^2(\text{eV}) \qquad (11)$$

which is << 1 for $m_\nu \sim 10eV$. Intermediate vector boson couplings are therefore too weak to keep positive helicity neutrinos in equilibrium.[11,12]

To lowest order in m_ν/E_ν, Higgs couplings always induce spin flips because they couple right-handed $SU(2)_L$ singlets to left-handed doublets (cf. equations (1) and (2)). For ν-f interactions (equation (6)), the cross-sections for spin flips via Higgs exchange are

$$\sigma^H_{-1,+1} \sim \sigma_{-1,-1} \times \frac{m_\nu^2\, m_f^2}{(m_H^2 + T^2)^2} \tag{12}$$

where m_f and m_H are the fermion and Higgs masses respectively, and the Higgs propagator has been explicitly included. That $\sigma^H_{-1,+1} \propto m_\nu^2\, m_f^2$ is a consequence of the fact that all fermions in the theory acquire mass via the Higgs mechanism, which requires that the coupling constants in all $\bar{\psi}_L H f_R$ terms in the symmetric Lagrangian are $g(f\text{-}H) = m_f \sqrt{G_F}$ (cf. equation (3)). From equations (7), (8) and (12) we get

$$\frac{\Gamma^H_{-1,+1}}{\Gamma_{exp}} \sim \frac{G_F^2\, m_\nu^2\, m_f^2}{\sqrt{G}} \frac{T^3}{(m_H^2 + T^2)^2} \quad . \tag{13}$$

For $T \lesssim m_H$ equation (13) becomes

$$\frac{\Gamma^H_{-1,+1}}{\Gamma_{exp}} \sim \frac{G_F^2\, m_\nu^2\, m_f^2\, T^3}{\sqrt{G}\, m_H^4} \quad . \tag{14}$$

For extremely relativistic fermions, $m_f \lesssim T$. Using this inequality plus the requirement that $T \lesssim m_H$ gives the upper bound

$$\frac{\Gamma^H_{-1,+1}}{\Gamma_{exp}} \lesssim \frac{G_F^2\, m_\nu^2\, m_H}{\sqrt{G}} \quad .$$

Perturbative calculations of the Higgs effective potential, which must be valid in the WSG theory, break down unless $m_H < 10^3$GeV.[13] Therefore, for $T \lesssim m_H$,

$$\frac{\Gamma^H_{-1,+1}}{\Gamma_{exp}} \lesssim 10^{-6}\, m_\nu^2(\text{eV}) \quad , \tag{15}$$

which is $\ll 1$ for $m_\nu \sim 10$eV.

For $T \gtrsim m_H$ equation (13) becomes

$$\frac{\Gamma^H_{-1,+1}}{\Gamma_{exp}} \sim \frac{G_F^2\, m_\nu^2\, m_f^2}{\sqrt{G}\, T} \quad . \tag{16}$$

Since $T \gtrsim m_f$ for extremely relativistic fermions we get the upper bound

$$\frac{\Gamma^H_{-1,+1}}{\Gamma_{exp}} \lesssim \frac{G_F^2\, m_\nu^2\, m_f}{\sqrt{G}} \quad .$$

Unitarity bounds and stability of the vacuum require[14] $m_f < 800$GeV, which in turn implies

$$\frac{\Gamma^H_{-1,+1}}{\Gamma_{exp}} \lesssim 10^{-6}\, m_\nu^2(\text{eV}) \tag{17}$$

for $T \lesssim m_H$, which is once again $\ll 1$ if $m_\nu \sim 10$eV. From inequalities (15) and (17) we conclude that Higgs couplings are too weak to maintain an equilibrium population of positive helicity neutrinos.[12]

5. Conclusions

We can draw a number of conclusions from the above calculations.[12] First, an equilibrium population of negative helicity neutrinos cannot generate an equilibrium population of positive helicity neutrinos. Second, even if an equilibrium distribution of

positive helicity neutrinos is produced at very early epochs ($T \sim 10^{15}$GeV?) it cannot be maintained by Higgs or left-handed intermediate vector boson couplings alone. Third, the requirement[2] that any positive helicity neutrinos decouple at $T > 0.2$GeV is overwhelmingly satisfied. Finally, we emphasize that arguments based on cosmological nucleosynthesis cannot be used to decide whether massive neutrinos are Majorana or Dirac particles.

6. Acknowledgments

We thank O. Alvarez, E. Farhi, K. Gottfried, W. Press, D. Schramm, G. Steigman, H. Tye and S. Weinberg for discussions. We also thank D. Stewart for aid in preparing the manuscript. S.L.S. acknowledges the support of an Alfred P. Sloan Foundation Research Fellowship. I.W. acknowledges the support of a Chaim Weizmann Postdoctoral Fellowship. This research was supported in part by NSF Grants AST 78-20708 and PHY 78-09795.

7. References

1. P.J.E., Peebles, Physical Cosmology (Princeton Univ. Press, Princeton, N.J., 1971). S. Weinberg, Gravitation and Cosmology (Wiley, New York, 1972).

2. G. Steigman, K.A. Olive, and D.N. Schramm, Phys.Rev.Lett. 43, 239 (1979).

3. J. Lequeux, M. Peimbert, J.F. Rayo, A. Serrano and S. Torres-Peimbert, Astron.Astrophys. 80, 155 (1979).
J. Yang, D.N. Schramm, G. Steigman and R.T. Rood, Astrophys.J. 227, 697 (1979).

4. D.N. Schramm and G. Steigman, preprint (1980).

5. F. Reines, H.W. Sobel and E. Pasierb, preprint UCI-10P19-144 (1980).

6. see S.M. Bilenky and B. Pontecorvo, Phys.Rep. 41C, 225 (1978).

7. R. Cowsik and J. McClelland, Phys.Rev.Lett. 29, 669 (1972). S. Tremaine and J.E. Gunn, Phys.Rev.Lett. 42, 407 (1979). See also Ref. 4.

8. S. Weinberg, Phys.Rev.Lett. 19, 1264 (1967). A. Salam, Proc. 8th Nobel Symposium, edited by N. Svartholm (Almquist and Wiksells, Stockholm, 1968). S.L. Glashow, Nuc.Phys. 22, 579 (1961).

9. See, for example, J.C. Taylor, Gauge Theories of Weak Interactions (Cambridge Univ. Press, Cambridge, 1976).

10. See M.A. Bég, R.V. Budny, R. Mohapatra, and A. Sirlin, Phys. Rev.Lett. 38, 1252 (1977) and references therein.

11. A. Dolgov and Ya. B. Zel'dovich, preprint (1980).

12. S.L. Shapiro, S.A. Teukolsky and I. Wasserman, Phys.Rev.Lett. 45, 669 (1980).

13. See M.K. Gaillard, Fermilab-Conf-79/87-THY and references therein.

14. Unitarity breaks down in the Born approximation in the Higgs sector for $m_f \gtrsim$ 1TeV since $g(f\text{-}H) = m_f \sqrt{G_F}$ in models with only one Higgs field. Radiative corrections would cause the Higgs potential to become negative at large $\langle H \rangle$ for $m_f \gtrsim$ 800GeV, in which case the vacuum would become unstable. See Ref. 13.

VII. Neutrino Astrophysics and Stellar Collapse

SOLAR NEUTRINO EXPERIMENTS AND A TEST FOR NEUTRINO OSCILLATIONS WITH RADIOACTIVE SOURCES

Bruce T. Cleveland, Raymond Davis Jr., and J. K. Rowley
Brookhaven National Laboratory, Upton, New York 11973

ABSTRACT

The results of the Brookhaven solar neutrino experiment are given and compared to the most recent standard solar model calculations. The observations are about a factor of 4 below theoretical expectations. In view of the uncertainties involved in the theoretical models of the sun we do not consider the discrepancy to be evidence for neutrino oscillations. The status of the development of a gallium solar neutrino detector is described.

Radiochemical neutrino detectors can be used to search for ν_e oscillations by using megacurie sources of monoenergetic neutrinos like ^{65}Zn. A quantitative evaluation of possible experiments using the Brookhaven chlorine solar neutrino detector and a gallium detector is given.

INTRODUCTION

In this report we will give the results of the Brookhaven solar neutrino experiment that has been operating for 12 years. This experiment has always observed a solar neutrino capture rate in ^{37}Cl below the rate expected from standard solar models. In recent years the observed rate has been approximately a factor of four below theoretical expectation. Among the various explanations advanced for the low solar neutrino (ν_e) flux is neutrino oscillation. We will discuss this question briefly and point out that the dominant solar neutrino flux signal expected to be observed by the ^{37}Cl experiment according to the standard solar model arises from ^{8}B decays in the sun, and that the flux of these neutrinos may not be reliably calculated. Therefore one should exercise great caution in using results of the ^{37}Cl solar neutrino experiment as evidence for ν_e oscillations. Since the flux of low energy neutrinos from the chain initiating proton-proton reaction can be reliably calculated, observing the flux of this component of the solar neutrino spectrum could give more direct information on the question of neutrino oscillations. A radiochemical solar neutrino detector based upon the neutrino capture reaction $^{71}Ga(\nu_e,e^-)^{71}Ge$ has a sufficiently low energy threshold to observe p-p neutrinos. A gallium solar neutrino experiment can search for oscillations of electron neutrinos with an average energy of 300 keV over distances of one astronomical unit (1.5×10^{11} m). Progress on and the status of the development of a gallium solar neutrino detector will be described.

Radiochemical solar neutrino detectors can also be used to search for ν_e oscillations by using a source of neutrinos of well-defined energy such as ^{65}Zn. Plans for carrying out experiments

along these lines using the Homestake chlorine detector and a small gallium detector will be described in a later section.

THE BROOKHAVEN SOLAR NEUTRINO EXPERIMENT

An experiment designed to observe the neutrinos from the sun has been operating since 1967 in the Homestake Gold Mine (depth 4400 hg/cm^2). A radiochemical technique is used that depends upon observing radioactive ^{37}Ar recovered from 615 tons of perchloroethylene (C_2Cl_4).[1] Neutrino detection depends upon the neutrino capture reaction $^{37}Cl(\nu_e,e^-)^{37}Ar$ and the calculated neutrino capture cross-sections.[2] The results from a series of 40 measurements over the period 1971 through 1979 are given in Figure 1. The values for the individual runs were obtained from argon gas samples removed from the liquid and counted for periods of 150 to 250 days, a sufficient time to distinguish a component decaying with the 35 day half-life of ^{37}Ar from the counter background. The counting data was treated by a maximum likelihood statistical method. The ^{37}Ar production rates are given for 40 individual experiments. The periods of exposure are indicated by the horizontal bars, and the errors given correspond to the 67 percent confidence level. The errors shown are statistical, and the fluctuations are in accordance with expected fluctuations obtained by Monte Carlo simulations.

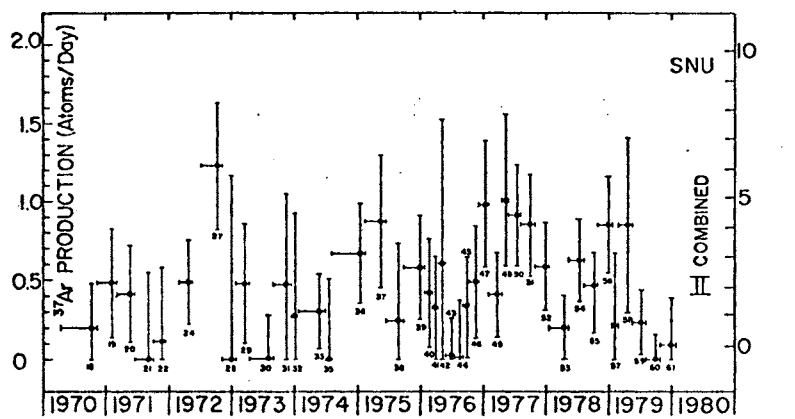

Figure 1

Combining the data for all runs gives a most likely ^{37}Ar production rate of 0.47 ±0.05 atoms per day. There is a background production of ^{37}Ar in the liquid resulting from cosmic ray muon interactions. This muon background is evaluated by measuring the ^{37}Ar production rate in perchloroethylene at shallow depths (300-1100 m.w.e.) and extrapolating these measured values to determine the rate in the solar neutrino detector (4400 m.w.e). We will use a background of 0.08 ± 0.03 ^{37}Ar atoms/day estimated by this method.[3] Experiments are in progress by E. L. Fireman[4] to evaluate this critical background by measuring the depth dependence of muon photonuclear interactions in potassium by the process $^{39}K(\mu^{\pm},\mu^{\pm}n,p)^{37}Ar$. Subtracting the muon background we obtain the following result:

Average ^{37}Ar production rate	=	0.47 ± 0.05 atoms/day
Background from muons	=	0.08 ± 0.03
^{37}Ar production possibly attributable to solar neutrinos	=	0.39 ± 0.06 atoms/day

Possible solar neutrino rate = 5.31 x (0.39±0.06) = 2.1±0.3 SNU

where 5.31 is the appropriate factor for converting the rate in atoms per day in a detector containing 2.18 x 10^{30} atoms ^{37}Cl to SNU (SNU = solar neutrino unit = neutrino captures per second per ^{37}Cl atom x 10^{36}).

The above rate is to be compared to the neutrino capture rate of 7.8 SNU predicted using the standard solar model.[5] This model will be discussed by John Bahcall at this conference. The calculated rate depends upon a number of assumptions associated with the standard solar model. For example, it is assumed that the sun was initially homogeneous with the composition presently observed in its photosphere, and that the sun is non-rotating, spherically symmetrical, and constant in mass. This calculation uses a mixing length theory for turbulent convective energy transport and a modified ideal gas equation of state.[6] A large amount of input data is used in the calculations, some of which is well known and accurately determined (mass, age, and luminosity of the sun), some that is not as well measured or requires extrapolation to obtain relevant values (solar composition, and nuclear reaction rates) and other information that must be calculated or assumed (opacities, turbulent mixing processes). Because of the diverse nature of the input data alone it is difficult to assess the errors involved in the calculated neutrino fluxes. The stated error is 1.5 SNU for this most recent model with a total ^{37}Cl capture rate of 7.8 SNU. Another very important consideration in interpreting the ^{37}Cl solar neutrino experiment is that the major contribution to the rate is from the ^{8}B neutrinos, and this source of neutrinos is very sensitive to various parameters and assumptions used in the solar model. Table 1 lists the neutrino sources in the sun, the calculated cross sections and standard solar model fluxes. It can be noticed that 6.3 SNU is attributed to the ^{8}B neutrino flux alone.

Table 1

SOLAR NEUTRINO FLUXES* AND CROSS SECTIONS**

$\nu + {}^{37}Cl \rightarrow e^- + {}^{37}Ar^* \rightarrow {}^{37}Ar$

Neutrino Sources & Energies	Flux on Earth ϕ in $cm^{-2}\ sec^{-1}$	Cross Section σ in cm^2	Capture Rate ^{37}Ar $\phi\sigma \times 10^{36}\ sec^{-1}$ SNU
$H + H \rightarrow D + e^+ + \nu$ (0-0.42)	6.1×10^{10}	0	0
$H + H + e^- \rightarrow D + \nu$ (1.44)	1.5×10^{8}	1.56×10^{-45}	0.23
^{7}Be decay	4.1×10^{9}	2.38×10^{-46}	0.98
^{8}B decay	5.85×10^{6}	1.08×10^{-42}	6.31
^{15}O decay	3.7×10^{8}	6.61×10^{-46}	0.24
^{13}N decay	2.6×10^{8}	1.66×10^{-46}	0.04

$\Sigma\phi\sigma = 7.8$ SNU

* J. N. Bahcall, W. F. Heubner, S. H. Lubow, N. H. Magee, A. L. Mertz, P. D. Parker, B. Rozsnyai and R. K. Ulrich

** J. N. Bahcall, Rev. Mod. Phys. 50, 881 (1978)

A number of non-standard models have been calculated that give solar neutrino capture rates in ^{37}Cl in the range 1 to 2 SNU. Various features are introduced in these models that lead to lower internal temperatures and thereby yield lower ^{8}B and ^{7}Be production rates.[7] Although most of these models do agree with the results of the chlorine experiment, they are not generally accepted because some of the mechanisms invoked do not seem to be reasonable or they lead to consequences that are in conflict with observations. Of these various models one of the most reasonable simply assumes that the heavy element composition in the interior of the sun is a factor of ten below the accepted photospheric value. The lower heavy element composition reduces the opacity, which gives lower internal temperatures, and leads to a capture rate in ^{37}Cl of about 1.5 SNU.

There are many uncertainties in the theoretical calculations of the solar neutrino spectrum and the errors are difficult to evaluate properly. Therefore, the difference between our result of 2.1 ± 0.3 SNU and the rate of $7.8 \pm (\sim 1.5)$ estimated from the standard model could easily be ascribed to our incomplete or

incorrect knowledge of the solar interior. Neutrino oscillations could of course account for the discrepancy, a factor of 3.6 ± 0.9, or a part of it, depending upon the value of the mixing angle and oscillation length.

NEW SOLAR NEUTRINO EXPERIMENTS

There is great interest in performing additional experiments directed toward observing the solar neutrino spectrum. At this conference there will be a report by R. S. Raghavan on the development of a direct counting neutrino detector based upon the $^{115}In(\nu,e^-)^{115}Sn^* \rightarrow ^{115}Sn$ reaction. Another approach to observation of the solar neutrino spectrum is to perform a set of measurements with radiochemical detectors having different threshold energies and sensitivities to the neutrino flux.[2] The radiochemical detectors considered for this purpose are based upon the following reactions: $^{71}Ga(\nu,e^-)^{71}Ge$, $^{7}Li(\nu,e^-)^{7}Be$, $^{81}Br(\nu,e^-)^{81}Kr$, and $^{37}Cl(\nu,e^-)^{37}Ar$. Table 2 compares these

Table 2

COMPARISON OF RADIOCHEMICAL SOLAR NEUTRINO DETECTORS

Percent of signal from various solar neutrino sources, standard model.

Neutrino Source	^{37}Cl-^{37}Ar	^{7}Li-^{7}Be	^{71}Ga-^{71}Ge	^{81}Br-^{81}Kr
$H + H \rightarrow D + e^+ + \nu$	0	0	65	0
$H + H + e^- \rightarrow D + \nu$	3	22	2	8
^{7}Be decay	12	10	27	69
^{13}N decay	1	3	1	4
^{15}O decay	3	21	3	10
^{8}B decay	81	44	2	9
$\Sigma\phi\sigma$	7.8	41	100	6.3
Tons Element for 1 ν-capture/day	356	3.5	34	495

detectors. It shows the $\sum\phi\sigma$ and the tons of the element required for one ν-capture per day according to the standard solar model.[5] The main body of the table gives the percent of the signal contributed by the various neutrino sources in the sun. The pp reaction rate in the sun is very well calculated and is essentially independent of the usual input data. The major energy producing reactions in the sun are those of the predominant p-p I chain, $H(H,e^+,\nu)D(H,\gamma)^3He(^3He,2p)^4He$, that includes only this one neutrino producing reaction. Therefore, the p-p reaction rate is related very directly to the solar luminosity and, if the sun is indeed producing energy by hydrogen fusion, the p-p rate is established. If a measurement of the total capture rate in ^{71}Ga is made, it should be between 67 and 100 SNU, the lower limit being the p-p flux contribution alone. If we have confidence in this argument, then a signal lower than 67 SNU could be evidence for neutrino oscillations. A gallium solar neutrino experiment has great potential for testing whether the lower than expected solar neutrino capture rate in ^{37}Cl is a result of incorrect solar structure or input data or is a consequence of a property of the neutrino such as oscillation or decay.

A gallium solar neutrino detector is being developed through a joint program of several laboratories: the Max-Planck Institute at Heidelberg, the Weizmann Institute, Institute for Advanced Study, the University of Pennsylvania, and Brookhaven National Laboratory.[8] The product, ^{71}Ge, is separated from the target, a water solution of $GaCl_3$ with added hydrochloric acid, as $^{71}GeCl_4$ by a helium purge. A pilot detector that uses 1.3 metric tons of gallium is now in operation. Extraction of ^{71}Ge is essentially quantitative, and it is clear that a 50 ton solar neutrino experiment is indeed feasible. The next step in development is the calibration of a gallium detector with a megacurie radioactive source of monoenergetic neutrinos. This source calibration can serve as a test for neutrino oscillations, as will be described in the next section.

OBSERVING NEUTRINO OSCILLATIONS WITH MEGACURIE RADIOACTIVE SOURCES

This section deals with possible radiochemical experiments that can test for the existence of short range neutrino oscillations. This type of experiment follows the original suggestion of L. W. Alvarez to use a ^{65}Zn source to measure the neutrino absorption cross-section of ^{37}Cl.[9]

The general principles of an oscillation experiment are quite straightforward: a strong source of a radioactive isotope that decays primarily by electron capture is prepared. The shielded source is placed deep underground within or near to a target material that is able to capture the emitted neutrinos by an inverse beta decay process that leads to a moderately long-lived product isotope. This product is extracted from the target by chemical means and then counted by detecting the beta decay back to the original target isotope. Possible sources include ^{51}Cr and ^{65}Zn; possible target isotopes are ^{7}Li, ^{37}Cl, ^{71}Ga, ^{81}Br, etc.

Some of the advantages of radiochemical neutrino oscillation experiments are:

1. The neutrinos are monochromatic
2. The neutrinos are of the electron type for which oscillations have been reported by Reines et al.[10]
3. The source can be made quite compact
4. The source strength can be accurately calibrated
5. The neutrino absorption cross-section is well-known
6. Background production rates due to α-particles, neutrons, and muons can be made negligibly small. There is only a minor residual background effect from solar neutrinos.
7. Different neutrino oscillation lengths can be sampled by placing concentric detectors about the source.

The principal difficulaty in experiments of this type is that very large source strengths are required. With the strongest available reactor flux an irradiation time of approximately one year is needed. Even then, large targets are required (1-10 m in diameter) and the neutrino capture rates are low (less than 5 per day).

We shall now outline the procedures used in the calculation of the expected capture rate and then present two radiochemical experiments that are feasible at the present time.

Consider a point source that emits s neutrinos per second and an extended absorber that contains n atoms/cm^3 of a neutrino absorbing isotope. From the definition of the cross-section σ, the neutrino capture rate R is given by $R = A \cdot G$ where $A = ns\sigma$ depends on the physical properties of the source and absorber and

$$G = \frac{1}{4\pi} \int_{\text{absorber}} \frac{dV}{r^2} \qquad (1)$$

depends only on the source and absorber geometry (r here is the distance from the source to an arbitrary point in the absorber). The factor A is given in Table 3 for cross-sections calculated by Bahcall.[2] The geometrical factor G can be expressed in closed form for simple geometries such as a sphere or a cylinder, and can be easily evaluated for more complex geometries or for an extended source by Monte Carlo techniques.

Table 3

Absorber	Source	Detected Isotope	A (cm^{-1} Mc^{-1})
C_2Cl_4	^{65}Zn	^{37}Ar	0.0112
7.1 M $GaCl_3$	^{51}Cr	^{71}Ge	0.0284
7.1 M $GaCl_3$	^{65}Zn	^{71}Ge	0.0367

We suppose that the electron type neutrinos emitted by the source oscillate into one other type and that the probability of no oscillation at the distance r (cm) from the source is given by the standard formula,

$$P(r) = 1 - \sin^2(2\alpha_m) \sin^2(0.0127\ \delta m^2 r/E) , \qquad (2)$$

where α_m is the mixing angle, δ_m^2 is the neutrino mass difference in eV^2, and E is the neutrino energy in MeV. The neutrino capture rate in the presence of oscillations is then easily calculated by including P(r) from eq (2) into the integrand of G in eq (1).

Two possible experiments will now be considered. The first involves placing a 1 Mc source of ^{65}Zn inside a tube that extends to the center of the 100,000 gallon C_2Cl_4 detector in the Homestake mine. Two obvious advantages of this experiment are that the detector presently exists and that the background has been well determined. The dependence of the capture rate on δm^2 for the case of maximal mixing is given in Figure 2. Without oscillations the capture rate of neutrinos from the source is 4.2 per day and there is also present a background production rate of 0.5 per day. The error bars indicated on this figure are at the 68% confidence level and are due only to random effects. These errors have been calculated by a simulation of the entire process of ^{37}Ar production, extraction, and counting for a set of experimental conditions that are believed to be realizable in practice. The production rate due to the neutrino source was extracted from the simulated counting times by a maximum likelihood method. It is evident from Figure 2 that for $\delta m^2 > 0.2\ eV^2$ the production rate at the 90% confidence level falls below the predicted rate in the absence of oscillations. The lower limit on δm^2 that is obtained for other choices of the mixing angle is presented in Figure 3.

Another possible experiment employs a target of a water solution of $GaCl_3$.[8] All of the procedures for extraction, purification, and counting of the ^{71}Ge that is produced by neutrino capture have been well developed. Background effects due to neutrons and α-particles are known and can be controlled by suitable choice of location and materials of construction. The muon produced background is much less severe than for C_2Cl_4 and is less than 0.1 per day for depths greater than 1800 hg/cm^2. The background effect due to solar neutrinos is believed to be 0.2 to 0.3 per day for the approximately 10 tons of Ga that is needed for a neutrino source experiment. In this case since an experiment can be designed specifically to search for neutrino oscillations, it can be made in two different zones. An experimental configuration that could be built consists of a central tank that forms the inner zone surrounded by six close-packed tanks as the outer zone. With a 2 Mc source of ^{65}Zn in a central annulus the capture rates in the inner and outer zones of a 10.6 ton Ga detector are given as a function of δm^2 in Figures 4 and 5, respectively. This again is for maximal mixing and the error bars are at the 68% confidence level for a reasonable schedule of experimental operations. A zero background has been assumed in both zones. If we compare these predicted rates in the two zones, there are two regions of δm^2 over

which the rates differ by more than two standard deviations. These regions are plotted for this and for other mixing angles with a dashed line in Figure 6. These regions happen to overlap to a considerable extent with the regions suggested by the reactor ν_e experiment of Reines et al.[10] We can also look at only the rate in the outer zone, and, in a manner similar to that for the Cl experiment, obtain the lower bound for δm^2 given by the solid line in Figure 6.

It is apparent from these figures that interesting neutrino oscillation experiments can be performed with a ^{65}Zn source and either a gallium or chlorine target. Such experiments, sensitive to oscillation lengths of the order of several meters, are logical steps to be taken on the way to a full-scale gallium solar neutrino experiment. They would settle the question of the possible oscillations suggested by the Reines experiment. In addition, if it is shown that such oscillations do not exist, the calculated neutrino capture cross sections of these targets can be confirmed. Then a full scale gallium solar neutrino experiment could be confidently undertaken which would yield critical information about the reason for the present discrepancy between the results of the chlorine experiment and the predictions made by the standard solar model.

Figure 2

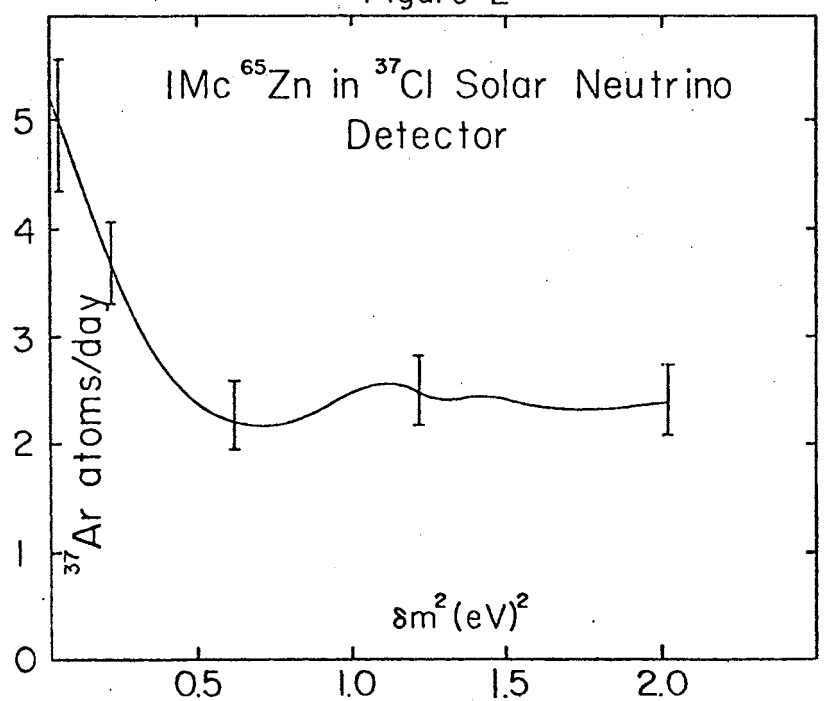

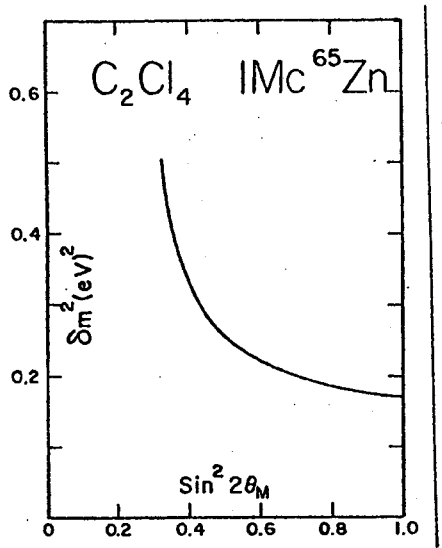

Figure 3

Figure 4

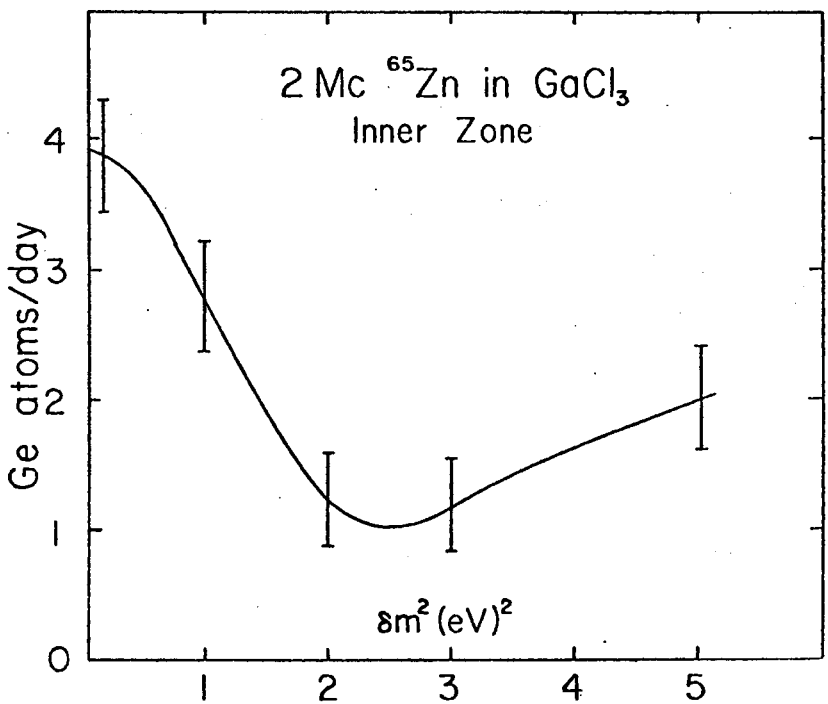

Figure 5

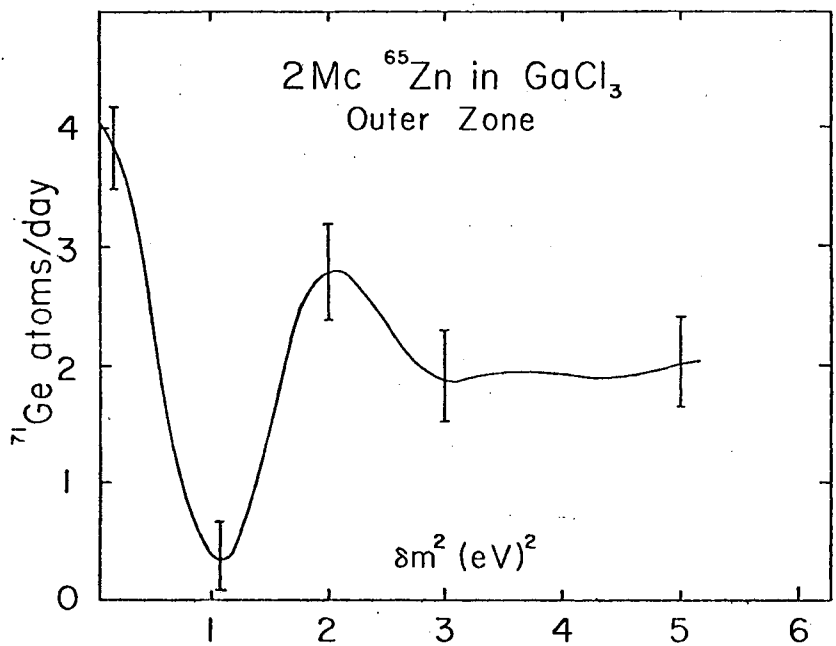

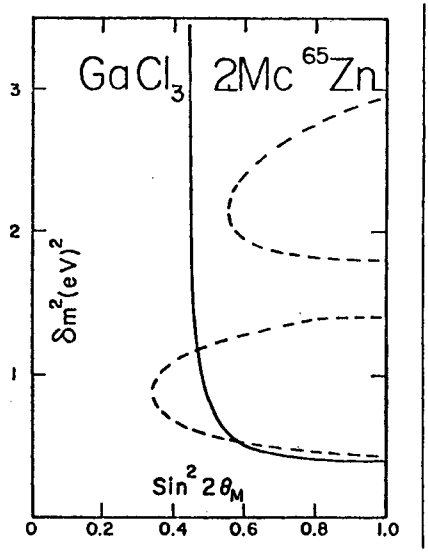

Figure 6

REFERENCES

1. R. Davis Jr., K. C. Hoffman, and D. S. Harmer, Phys. Rev. Letters 20, 1205 (1968); R. Davis Jr., Proc. Informal Conf. on Status and Future of Solar Neutrino Research (BNL 50379) 1, 1, G. Friedlander, Editor.

2. J. N. Bahcall, Rev. Mod. Physics 50, 881 (1978).

3. A. W. Wolfendale, E. C. M. Young and R. Davis, Nature Physical Sci. 238, 1301 (1972); G. A. Cassidy, Proc. 13th Int. Conf. on Cosmic Rays, Denver, Vol 13, p 1958 (1973).

4. E. L. Fireman, Proceedings 16th International Cosmic Ray Conference, Kyoto, Vol. 13, 389 (1979).

5. J. N. Bahcall, S. H. Lubow, W. F. Huebner, N. H. Magee Jr., A. L. Merts, M. F. Argo, P. D. Parker, B. Rozsnyai, and R. K. Ulrich, Phys. Rev. Letters 45, 945 (1980).

6. G. Friedlander (editor), Proceedings Informal Conference on Status and Future of Solar Neutrino Research (1978), BNL 50879, Volume I, see reports by J. N. Bahcall p 55, P. D. Parker p 77, W. F. Huebner p 107, S. H. Lubow and R. K. Ulrich p 157, and I. W. Roxburgh p 207.

7. Ibid, Vol I, R. T. Rood p 175.

8. J. N. Bahcall, B. T. Cleveland, R. Davis Jr., I. Dostrovsky, J. C. Evans, Jr., W. Frati, G. Friedlander, K. Lande, J. K. Rowley, R. W. Stoenner and J. Weneser, Phys. Rev. Letters 40, 1351 (1978).

9. L. W. Alvarez, Memo no. 767, Lawrence Radiation Laboratory, Univ. of California, March 23, 1973.

10. F. Reines, H. W. Sobel and E. Pasierb, Phys. Rev. Letters 45, 1307 (1980).

Solar Neutrino Calculations: An Update

B. W. Filippone
Argonne National Laboratory, Bldg. 203
9700 S. Cass Avenue
Argonne, IL 60439 USA

and

The University of Chicago, Chicago, IL 60637

ABSTRACT

Preliminary calculations of the capture rate in two solar neutrino detectors—^{37}Cl and ^{71}Ga—are reported. The assumptions needed to generate a standard solar model and the input required are discussed. New experimental and theoretical work on the input physics has increased the expected rates from previous values, but has also complicated the question of uncertainties in the prediction. Best estimates for the mean values and uncertainties are 7.1 ± 3 SNU for ^{37}Cl and 110 ± 10 SNU for ^{71}Ga. The possibility of observing neutrino oscillations in solar neutrino detectors is also discussed.

1. Introduction

The search for electron neutrinos from the sun has been at once both discouraging and intriguing. Originally intended as a confirmation of nuclear energy generation in the sun, the discrepancy between theory and experiment has resulted in one of the most puzzling problems in astrophysics. Figure 1 traces the history of the problem, with the disagreement ranging roughly from a factor of two to a factor of ten.

While the number of observed solar neutrinos appears to be lacking, the number of attempts to account for their absence certainly is not. Modifications of the input physics, the standard assumptions, or basic neutrino properties have all been suggested as the cause. The purpose of this paper however is to discuss, within the standard model of the sun, recent changes (in some cases outside of previously quoted errors) in several of the input parameters of the model and the resulting predicted neutrino flux. Particular attention will be paid to uncertainties in the prediction as an indication of how well one can calculate the properties of presumably the most well-understood astrophysical entity.

Fig. 1.

Published values of the experimental and theoretical capture rate of solar neutrinos in the ^{37}Cl experiment of Davis (Ref. 1).

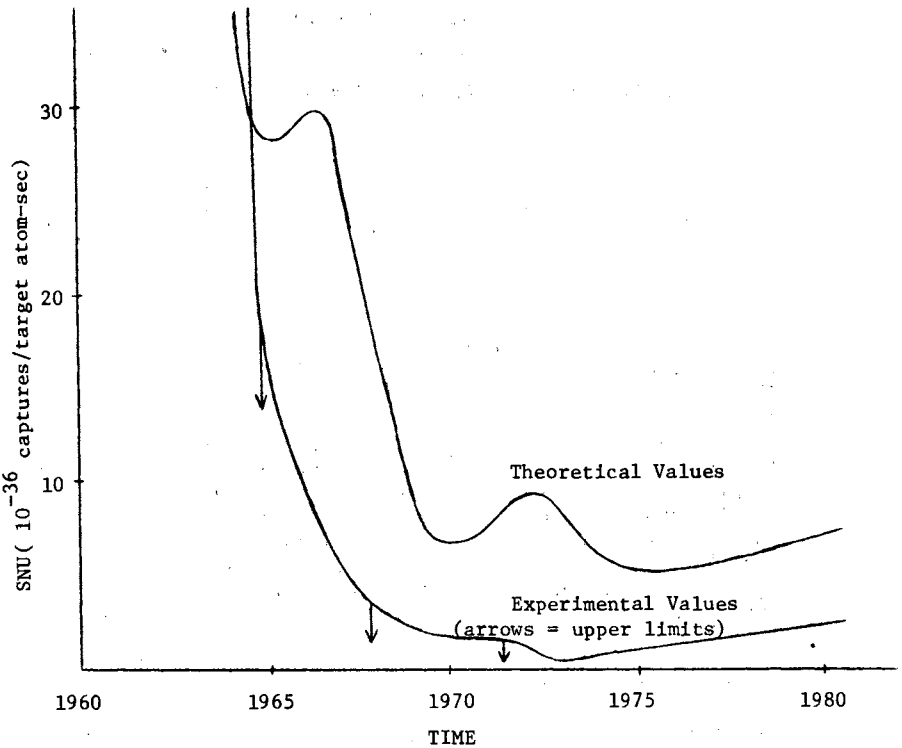

2. Production and Detection

Any discussion of solar neutrinos must begin at the source: the p-p chain of nuclear reactions. Figure 2 shows the basic reactions involved and the characteristics of the resulting neutrinos (an additional set of reactions involving C, N, and O provide a few percent in both energy generation and capture rate). The reactions are important to the discussion of input parameters while the neutrino energies dictate which reactions are observable in the neutrino detectors.

Capture rates in two detectors will be discussed here: the on-line ^{37}Cl experiment (with threshold = 0.814 MeV) of Davis[1] and the proposed ^{71}Ga experiment.[2] The ^{37}Cl experiment is chiefly sensitive to the high energy neutrinos from ^{8}Be decay due to an isobaric analog state in ^{37}Ar at 4.98 MeV (neutrino threshold = 5.79 MeV), the transition to which is superallowed.

Fig. 2.

Proton-proton chain of nuclear reactions. Neutrino energies and fluxes for a mean standard model (from the present work) are included.

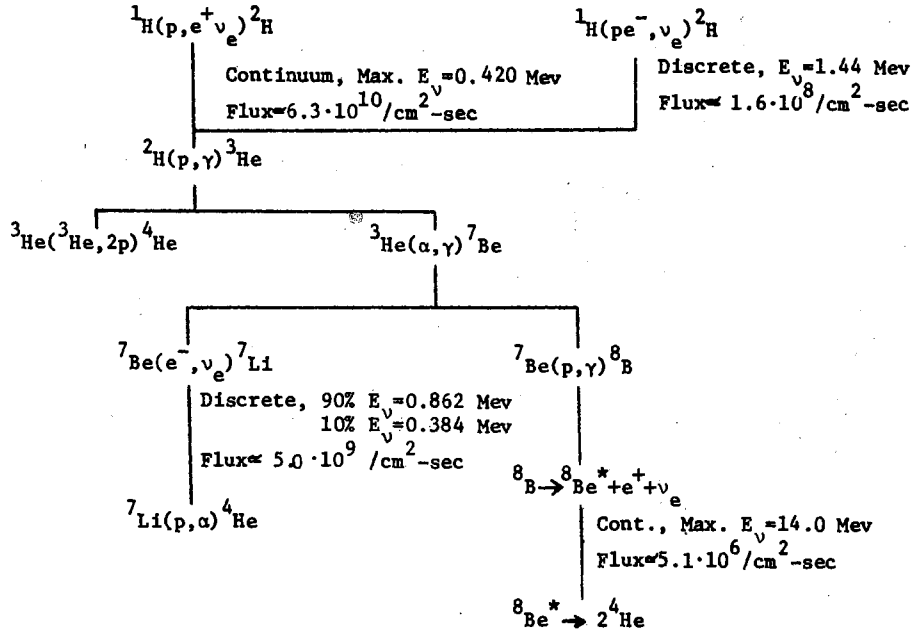

Unfortunately the rate of formation of ^8B via $^7Be(p,\gamma)^8B$ is very sensitive to conditions in the solar core, such that small uncertainties in conditions can lead to large uncertainties in the ^{37}Cl capture rate. In contrast, ^{71}Ga (threshold = 0.236 MeV) is an example of a detector sensitive to the high flux of low-energy neutrinos from $^1H(p,e^+\nu_e)^2H$. This weak reaction is the slowest of the p-p chain and therefore is tied to the energy generation rate and the luminosity. Thus core conditions have much less effect on the ^{71}Ga capture rate.

The latest results[1] from the ^{37}Cl experiment of Davis indicate a value of 2.2 ± 0.4 SNU (1 SNU = 10^{-36} neutrino captures/target atom-sec) above known background. The present work obtains for a mean standard model a value of 7.1 SNU, while Bahcall[3] calculates a best estimate of 7.3 SNU. Discussions of the assumptions involved in calculating a standard model and assigning an error to the prediction comprise the remainder of this paper.

3. Method

In general when calculating a standard solar model the following are assumed.

1) The sun is a sphere, the gravitational constant is time-independent, rotational effects are small, magnetic pressure is negligible, and very little mass loss occurs.

2) No major mixing has occurred except in surface convection regions.

3) The initial elemental composition of the sun was homogeneous and equal to the present observed surface abundances.

4) There are no surprises in the weak interaction.

The first set of assumptions has been tested and it appears that in order to significantly change the flux of neutrinos, very large and usually observable deviations would be required. The second and third are related for if the initial heavy element abundance is much lower than the present surface abundance (through mixing or initial inhomogeneities), the neutrino flux can be drastically reduced.[4] While violation of 2 and 3 are presently not in favor, they cannot be ruled out completely.

Contrary to assumption 4, recent reactor[5] and β-decay[6] experiments have shown that surprises in the weak interaction are fast becoming the rule rather than the exception. In fact the solar neutrino problem has been used as evidence in support of neutrino oscillations.[7] The relevance of the new calculations to the question of neutrino oscillations will be discussed in the conclusions.

Along with the assumptions listed above, an additional three provide the necessary differential equations to solve the problem.

1) Hydrostatic equilibrium is maintained at all points within the sun by a balance between the gravitational force and the pressure gradient.

2) The rate of energy production is given by the reactions of the p-p chain (with a few percent from CNO).

3) Energy is transported to the surface via radiation and convection; which one dominates in a particular region being determined by local conditions.

So far we have considered only the recipe for a solar model; now come the ingredients:

1) mass, luminosity, and age (from observations)

2) ideal-gas equation of state with small corrections (Coulomb effects and electron degeneracy)

3) nuclear cross sections (to determine reaction rates)

4) opacity of material (to characterize the radiative transport)

5) initial X, Y, and Z (mass fraction of H, He, and all elements heavier than He, respectively)

With $X + Y + Z = 1$ and Z determined from photospheric abundances, Y is varied until a model with the present observed luminosity is generated.

4. Key Input Parameters

a) Nuclear

The rate of energy, neutrino, and isotopic production in stars depends intimately on the rate of nuclear processes. Stellar reaction rates are determined from the formula

$$R_{ij} = \frac{n_i n_j}{1 + \delta_{ij}} \langle \sigma v_{ij} \rangle_{M-B}$$

where n_i and n_j are the number densities of the particles in the entrance channel, δ_{ij} is the Kronecker delta to account for identical particles, and $\langle \sigma v_{ij} \rangle_{M-B}$ is a suitable Maxwell-Boltzman average of the energy-dependent cross section multiplied by the relative velocity of the two particles. Measurement of these cross sections should then give the reaction rates as a function of temperature. The situation is complicated however by the relatively low thermal energy in the sun.

In the solar core kT $\simeq$ 1.3 keV, which is far below the Coulomb barrier for any nuclear reaction. Thus the quantum-mechanical penetration probability plays an important role in the rates. Figure 3 shows an example of the penetration probability for the reaction $^3He(\alpha,\gamma)^7Be$. This steeply-falling

Fig. 3.

Relative penetration probability for $\ell = 0$ in the reaction $^3He(\alpha,\gamma)^7Be$. Arrow indicates energy where most reactions take place in the sun.

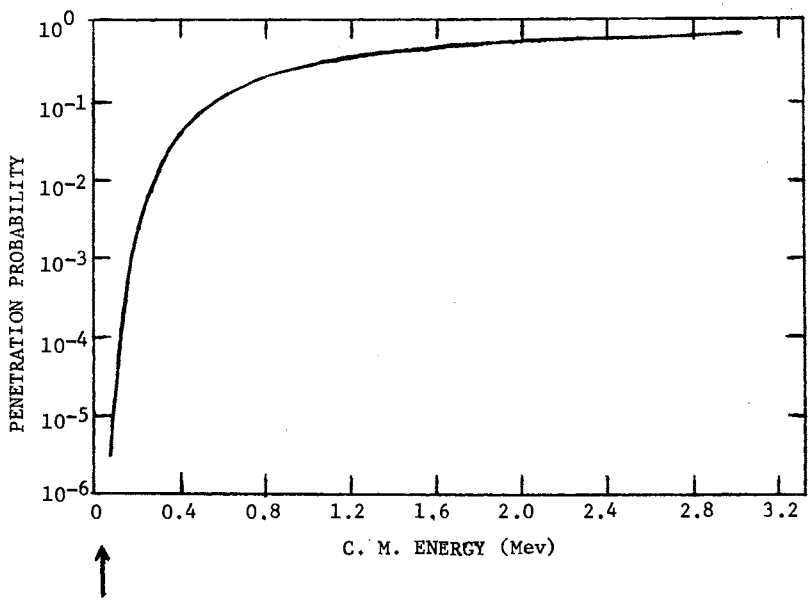

probability causes the reaction to take place mainly in the Maxwell-Boltzman high-velocity tail. The product of these two effects (decreasing probability to interact at lower energies due to the Coulomb barrier, and the decreasing number of particles at higher energies due to the M-B distribution) results in a most-favorable reaction energy. But this energy is still only a few tens of keV in the sun. How then can the cross sections be determined so far below the Coulomb barrier?

To begin, the non-nuclear energy dependence can be factored out of the cross section. Below the Coulomb barrier

$$\sigma_{ij}(E) = \frac{S_{ij}(E)}{E} e^{-2\pi\eta}$$

where $\eta \equiv Z_i Z_j e^2/\hbar v_{ij}$, the 1/E factor is from the usual λ^2 term, and the exponential accounts for the penetration probability. $S_{ij}(E)$ is the astrophysical S-factor [i and j are the atomic masses of the particles in the incoming channel—eg. S_{34} for $^3He(\alpha,\gamma)^7Be$] which contains all the nuclear energy dependence of the cross section. Far from any resonance S(E) should be nearly linear. The standard procedure is to determine S(E) experimentally as low in energy as is possible and extrapolate to zero energy (using theory or a polynomial fit) to determine S(0) and dS/dE, and pray there are no unseen resonances.

There is recent evidence that two of the S-factors—S_{34} and S_{11}—may differ considerably from their previously accepted values.

Two low-energy measurements[8] of the $^3He(\alpha,\gamma)^7Be$ reaction had yielded $S_{34}(0) = 0.61 \pm 0.06$ keV-barns and $dS_{34}/dE = -5.8 \cdot 10^{-4}$ barns from a polynomial fit to the data. In addition, both early[9] and more recent[10] radiative-capture calculations show good agreement with these data. However, there are some preliminary measurements by Rolfs,[11] made at even lower center-of-mass energy than the previous experiments, that imply S_{34} may be smaller by nearly a factor of two with zero slope at low energy. Also, a recent reanalysis of the old data by Parker[12] using radiative-capture calculations to determine the slope yields a slightly lower value of S_{34}, while if the slope is assumed flat (as indicated by Rolfs), he obtains $S_{34} = 0.33$ keV-b. for the Parker and Kavanagh data[8] and $S_{34} = 0.51$ keV-b. for the Nagatani et al.[8] data. Clearly more experimental work is needed for this important cross section.

New experimental work has also affected S_{11} which is used to calculate the rates of both $^1H(p,e^+\nu_e)^2H$ and $^1H(pe^-,\nu_e)^2H$. Since these reactions essentially convert a proton to a neutron, it is not surprising that S_{11} depends sensitively on the neutron half-life.[13] Two recent measurements[14] of the half-life are in considerable disagreement (nearly three standard deviations between them—however one is in good agreement with an earlier measurement[15]). Since the ^{37}Cl capture rate $\propto S_{11}^{-2.4}$ (from the present calculation) this disagreement can result in a large ($\sim$20%) range in the capture rate.

b) Opacity

Most of the energy produced in the nuclear core of the sun is transported to the surface via radiation. The rate of transport is determined by the opacity. Solar opacities are not accessible to experiment and must be calculated from first principles. This makes their uncertainties the most

difficult to quantify of all solar model input. Recent refinements in the calculations have resulted in the most significant contribution to the new ^{37}Cl capture rate.[3]

For a more detailed look at the input parameter choices and their uncertainties, see Filippone and Schramm.[16]

5. Results

Using the solar-model code of Eggleton,[17] new nuclear data,[18] the latest opacities (for an approximate solar composition) from the Huebner astrophysical opacity library of Los Alamos, and neutrino absorption cross sections from Bahcall[19] we have generated a mean standard model that gives 7.1 SNU for ^{37}Cl and 110 SNU for ^{71}Ga.

The effects of the new opacity and the range in the two nuclear parameters discussed on the capture rate in ^{37}Cl and ^{71}Ga are shown in Figures 4 and 5. F_{pp} is a factor multiplying S_{11} to show effects of different neutron half lives. For ^{37}Cl there is a very large range in SNUs, with the curve using the old opacity and S_{34} = 0.35 keV-b. (and zero slope) as suggested by Rolfs nearly overlapping with the experimental limits. In contrast, the results for ^{71}Ga show very little difference when the old and new opacities are used. The small difference for the two values of S_{34} is due to the ^{7}Be neutrinos, which give $\sim$25% to the ^{71}Ga capture rate.

To get a more quantitative picture of the uncertainties, the effects of individual parameter uncertainties on the capture rates in a mean standard model have been investigated. Each parameter uncertainty σ_{pi} results in a corresponding capture rate uncertainty σ_{ci}. If all uncertainties are assumed independent (generally true) then the total capture rate uncertainty is given by

$$\sigma_{tot} = \left(\sum_i \sigma_{ci}^2 \right)^{\frac{1}{2}} .$$

When uncertainties in age, luminosity, nuclear parameters, opacity, heavy element abundance and neutrino absorption cross sections are considered, the results are

$$\sigma_{tot}/R \simeq 45\% \text{ for } ^{37}Cl$$

$$\sigma_{tot}/R \simeq 10\% \text{ for } ^{71}Ga$$

where R is the capture rate. The details of this calculation will be discussed elsewhere.[16]

6. Conclusions

To address the question of neutrino oscillations consider the ratio of theoretical to experimental capture rate

$$\beta = R_T/R_E .$$

Fig. 4.

Capture rate in a ^{37}Cl detector as a function of F_{pp} (see text). Five models (with the present observed luminosity) are generated for each curve. Shown at the bottom is the value of F_{pp} corresponding to three measured values of the neutron half life and the error associated with each measurement.[14,15]

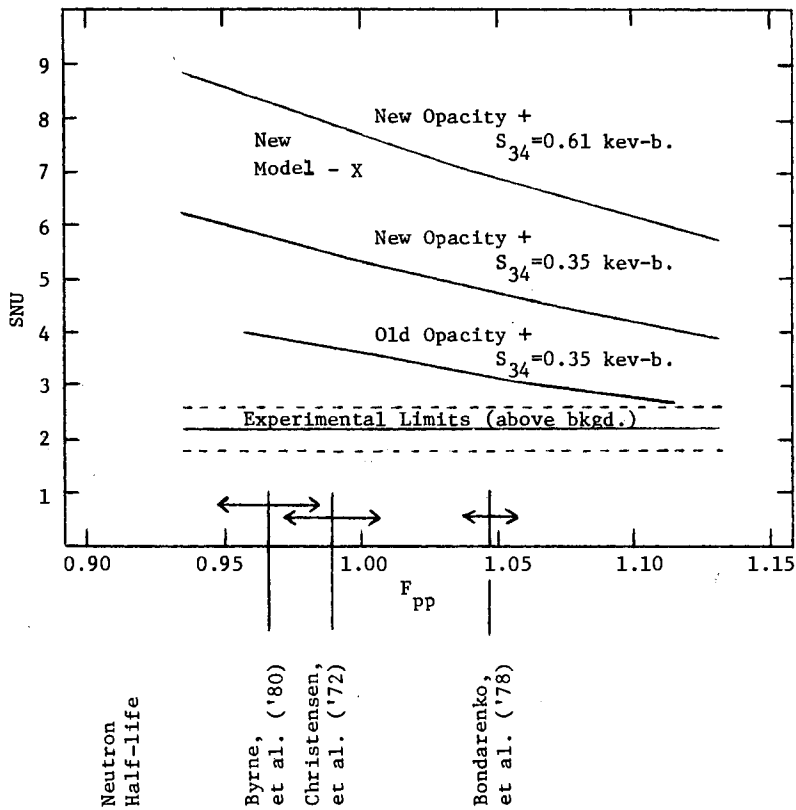

For the present ^{37}Cl results (this calculations and the value of Davis[1])

$$\beta_{^{37}Cl} = 3.2 \pm 1.5.$$

If $\beta = 1$ there would be no evidence for neutrino oscillations, thus the present results are 1.5 standard deviations away from no oscillations. It should be stressed that the theoretical errors discussed here are only for the standard model of the sun. Various non-standard models suggested from time to time could significantly alter these results depending on the magnitude of the non-standard effects. The sensitivity of a ^{71}Ga experiment can be studied by assuming some value for β. If $\beta \equiv 3$ (for 2 neutrinos oscillating with ν_e and oscillation length << earth-sun distance) and a ^{71}Ga experiment of similar precision to ^{37}Cl,

Fig. 5.

Capture rate in a ^{71}Ga detector as a function of F_{pp} (see text).

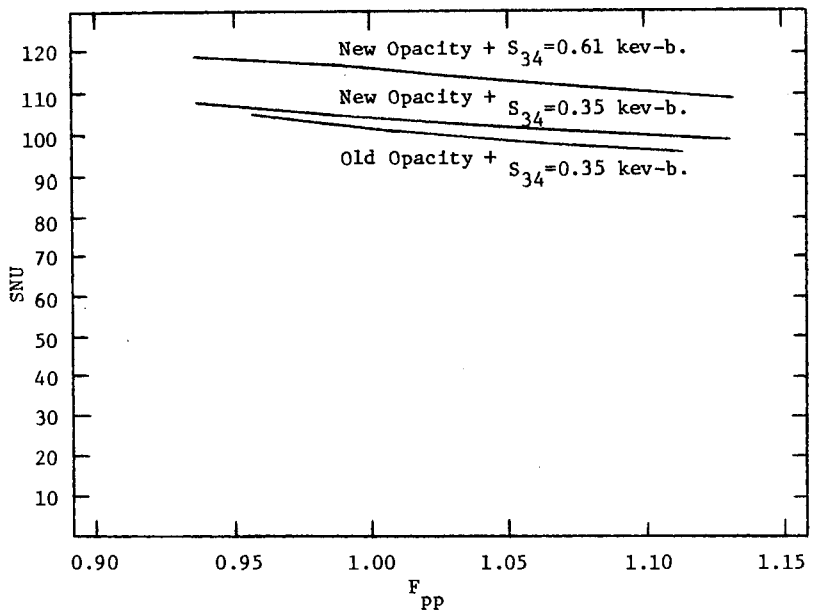

$$\beta_{^{71}Ga} = 3.0 \pm 0.7$$

or 3 standard deviations from the result for no oscillations.

Overall then, nuclear physics questions and the difficulty in determining an error for the opacity make the ^{37}Cl experiment questionable for observing neutrino oscillations. While the nuclear parameter uncertainties can (and should) be improved, the opacity and also the heavy element abundance (not discussed here, but an important effect) will still remain as problems.

However, due to its relative insensitivity to core conditions ^{71}Ga still holds promise in confirming stellar nuclear energy generation and possibly in observing neutrino oscillations.

Acknowledgment

The authors would like to thank A. Cox for furnishing the Los Alamos opacity tables. Useful discussions with D. N. Schramm, W. A. Fowler, C. N. Davids, and L. Aller are gratefully acknowledged. This work was performed under the auspices of the U. S. Department of Energy.

References

1. R. Davis, Jr., Proceedings of the Brookhaven Solar Neutrino Conference, BNL 50879, 1, 1 (1978);
R. Davis, Jr., Proceedings of the International DUMAND Symposium (1980).

2. J. N. Bahcall, B. T. Cleveland, R. Davis, Jr., I. Dostrovsky, J. C. Evans, Jr., W. Frati, G. Friedlander, K. Lande, J. K. Rowley, R. W. Stoenner, and J. Weneser, Phys. Rev. Lett. 40, 1351 (1978).

3. J. N. Bahcall, S. H. Lubow, W. F. Huebner, N. H. Magee, Jr., A. L. Merts, M. F. Argo, P. D. Parker, B. Rozsnyai, and R. K. Ulrich, Phys. Rev. Lett. 45, 945 (1980).

4. J. N. Bahcall and R. K. Ulrich, Astrophys. J. 170, 593 (1971);
J. N. Bahcall, W. F. Huebner, N. H. Magee, Jr., A. L. Merts, and R. K. Ulrich, Astrophys. J. 184, 1 (1973).

5. F. Reines, H. Sobel, E. Pasierb, Phys. Rev. Lett. (to be published) (1980).

6. V. A. Lubimov, E. G. Novikov, V. Z. Nozik, E. F. Tretyakov, and V. S. Kosik, Phys. Lett. 94B, 266 (1980).

7. A. DeRujula, M. Lusignoli, L. Maiahi, S. T. Petcov, and R. Petronzio, Nucl. Phys. B168, 54 (1980);
V. Barger, K. Whisnant, D. Cline, and R. J. N. Phillips, Phys. Lett. 93B, 194 (1980).

8. P. D. Parker and R. W. Kavanagh, Phys. Rev. 131, 2578 (1963);
K. Nagatani, M. R. Dwarakanath, D. Ashery, Nucl. Phys. A128, 325 (1969).

9. T. A. Tombrello and P. D. Parker, Phys. Rev. 131, 2582 (1963).

10. B. T. Kim and K. Nagatani, Phys. Rev. C (to be published) (1981).

11. C. Rolfs, Proceedings of the International Workshop VII, Hirschegg, Austria (1979).

12. P. D. Parker, private communication (1980).

13. J. N. Bahcall and R. M. May, Ap. J. 155, 501 (1969).

14. L. N. Bondarenko, V. V. Karguzon, Yu, A. Prokof'ev, E. V. Rogor, and P. E. Spivak, JETP Lett. 28, 303 (1978);
J. Byrne, J. Morse, K. F. Smith, F. Shaikh, K. Green, and G. L. Greene, Phys. Lett. 92B, 274 (1980).

15. C. J. Christensen, A. Nielsen, A. Bahnsen, W. K. Brown, and B. M. Rustad, Phys. Rev. D 5, 1628 (1972).

16. B. W. Filippone and D. N. Schramm (to be published).

17. P. P. Eggleton, M.N.R.A.S. 151, 351 (1971);
P. P. Eggleton, M.N.R.A.S. 156, 361 (1972).

18. W. A. Fowler, G. R. Caughlan, and B. A. Zimmerman, Ann. Rev. Astron. Ap. 13, 69 (1975);
F. Ajzenberg-Selove, Nucl. Phys. A392, 1 (1979);
F. Ajzenberg-Selove, Nucl. Phys. (to be published) (1981).

19. J. N. Bahcall, Rev. Mod. Phys. 50, 881 (1978).

"NEUTRINO ACCELERATION IN SUPERNOVA SHOCKS"*

Donald Ellison
Catholic University of America and
NASA/Goddard Space Flight Center

Demosthenes Kazanas**
NASA/Goddard Space Flight Center
Greenbelt, MD 20771

ABSTRACT

A Monte Carlo method is employed to study particle acceleration in the presence of shocks. The method is quite general and applicable to many astrophysical situations where shocks are present (i.e., the Earth's bow shock supernovae explosions and remnants, accretion onto compact objects). In particular, it is presently applied to study "neutrino acceleration" in supernova shocks. The neutrinos diffusing ahead of the shock (when the latter is at densities $\rho \sim 10^{12}$ g cm^{-3}) can suffer energy gains (via a first-order Fermi acceleration mechanism) in a way quite similar to that considered for the acceleration of cosmic rays. The calculated emerging neutrino spectra show a power law dependence in agreement with theory. The excess energy thus imparted to neutrinos ($\sim 10^{50}$-10^{51} ergs) and the fact that it is distributed in a way increasing the average neutrino energy (by about a factor of 2) can make the neutrino detection of a supernova more likely. Furthermore, the neutrino spectra could potentially provide information about the physics of such shocks.

1. Introduction

Over the past few years there has been a flurry of activity associated with the acceleration of cosmic rays and attempts to account for their observed power law spectra. (See for example Bell (1978a,b), Blandford and Ostriker (1978) and Axford, Leer, and Skadron (1977)). As a result it became progressively clear that astrophysical shocks could be the potential sites of such acceleration.

The idea of particle acceleration in shocks was introduced several years ago (Fisk 1971). Particles (cosmic rays in this case) diffusing upstream in a shock region can suffer fractional energy gains of the order of $\Delta u/V$ (Δu is the velocity difference across the shock and V the particle's thermal velocity). As a result, the individual particle's energy increases exponentially with the number of crossings. Random walk arguments can then show that the probability that a given particle crosses the shock a certain number of times decreases exponentially with the number of crossings. Folding of this exponentially

* Presented to the DUMAND International Symposium by D. Kazanas

** Also NAS/NRC Resident Research Associate

decreasing probability with the exponentially increasing energy with the number of crossings leads naturally to a power law in energy for the cosmic ray spectrum.

The presented acceleration mechanism is quite general and the arguments apply to any situation where a shock is present, i.e., the Earth's bow shock, supernovae remnants, accretion onto compact objects, etc. We presently examine its effects on the neutrinos which are produced in gravitational collapse (presumably resulting in a supernova explosion) and "accelerated" in the ensuing outgoing shock. These shocks originate in the collapse and bounce of sufficiently massive stellar cores which undergo gravitational collapse after the exhaustion of their thermonuclear fuel (Arnett 1977). The bounce occurs when the central core density becomes $\rho \geq 2.10^{14}$ g cm^{-3}. A shock then forms at the edge of the homologously collapsing core (Van Riper 1978) at densities $\rho \sim 10^{13}$ g cm^{-3} which propagates outward in the direction of the density gradient.

The physical conditions are such that the material is optically thick to neutrinos which are copiously produced during the collapse process (via $e^- p \rightarrow \nu n$). Although these neutrinos are trapped in the fluid (i.e., by $\tau_{diffusion} \gg \tau_{dynamical}$) their mean free paths are large enough to allow diffusion ahead of the expanding shock which could lead to substantial acceleration before they reach the optically thin regions of the core and escape by the first order effect described above.

2. Assumptions and Calculations

Following the above discussion it may appear that such a transient phenomenon would hardly be effective in significantly accelerating any neutrinos (it takes $\sim 10^{-3}$ sec for the shock to reach the neutrino's optically thin region). However, due to the increase of the weak interaction cross sections with energy ($\sigma \propto E_\nu^2$) neutrinos tend to scatter more and increase their energy at a higher rate the more energetic they become. This tends to increase their optical depth and therefore prolong their "acceleration" process which may in turn not be as inefficient as one might think. In addition, higher energy neutrinos are a lot easier to detect, thereby increasing the probability of detecting a supernova explosion. They could also carry important information about the physics of such shocks (i.e., their velocity, temperature and density).

Due to its complicated space and time dependence (the shock propagates in a high density gradient medium, particles are lost when they reach the optically thin regions) and to the similarity of the acceleration mechanism to random walk, the problem has been attacked as such by the use of a Monte Carlo method.

The entire process of neutrino acceleration and escape has been directly simulated, trying at the same time to incorporate, in steps, as much of the relevant physics as possible. The shock was considered to propagate in a configuration of decreasing density similar to that of Arnett's (1977) model. The shock velocity was held constant as well as the velocity difference across the shock. The shock was also treated as a discontinuity as far as neutrinos were concerned i.e., neutrino mean free paths $\gg \Delta x$ shock (see, however, Kazanas 1980).

Since the neutrino mean free paths are much smaller than the radius of the

stellar core at the position of the shock, a plane geometry was used. The neutrinos were released just behind the shock and were allowed to scatter towards and away from it randomly with equal probability. Due to the overall outward density gradient and fluid motion, they of course preferentially moved outward and eventually escaped. The particles and shock coordinates were followed in detail during the diffusion process. Each time a particle crosses the shock its energy was increased by a factor

$$f = \frac{1+(\Delta u/c)\cos\theta}{\sqrt{1-(\Delta u/c)^2}}$$

representing a blue shift, consistent with a first-order Fermi acceleration mechanism (θ is the angle at which particles cross the shock). Once the particle crosses in the upstream region, it is convected towards the shock front with the supersonically infalling material thus increasing the crossing probability.

At each scattering the particle's optical depth is checked. If found less than one, the particle is considered to have escaped. Its energy is registered and the whole process repeated starting at the same initial conditions with another particle. Figs. 1a,b,and c, show the integral spectra of emerging neutrinos from such a calculation. The density profile used was $\rho=\rho_0\, e^{-x/h}$ with $\rho_0=10^{13}$ g cm^{-3} and $h = 2.5.10^6$ cm. The starting position of the shock was $5.5.10^6$ cm and the initial neutrino energy 8, 10^{15}, MeV, typical of the preshock neutrinos at these densities (Arnett 1977). The composition of the fluid in this test run was assumed to be entirely Fe (A=56) with coherent scattering ($\nu A \rightarrow \nu A$) as the only neutrino opacity source. The post shock velocity was assumed to be $u_2 = 3.10^9$ cm s^{-1} while $\Delta u = u_1 - u_2 = 3.10^9$ cm s^{-1}. The resulting spectra depend on the neutrino optical depth at injection, τ_i, and result in greater "acceleration" (flatter spectrum) for larger initial optical depth.

The same calculation was repeated with a different density profile, namely, $\rho = \rho_0\, 2.7/r_7^3$ ($r_7 = R/10^7$ cm). The resulting spectra appear to depend qualitatively on the initial optical depth, τ_i, as in the previous case, and are given in figs. 2 a,b,c, and d for different values of this parameter. They are a little flatter compared to those corresponding to the exponential density profile for the same τ_i, (compare fig. 1b to 2a) especially at the lower and higher energies. Despite this fact, it is doubtful if one can differentiate between the two density profiles from these spectra. The emitted spectra should, however, give an estimate of τ_i and/or Δu due to the rather strong dependence of the acceleration mechanism on these parameters. (Contrast figs. 2a, 2c.)

Looking at the bulk properties of the acceleration process it is interesting to estimate the rate at which the shock does work on the neutrinos. If t_ν is the neutrino mean free time, then the rate of energy increase close to the shock due to the first-order acceleration mechanism is:

$$\frac{dE}{dt} \sim \frac{E_\nu}{t_\nu}\,\frac{\Delta u}{c} \text{ erg cm}^{-3}\text{ s}^{-1}$$

The neutrinos effectively accelerated are those within a few mean free paths from the shock, i.e., those within a volume $V \sim \ell \cdot 4\pi R_s^2$. Therefore,

$$\frac{dE}{dt}tot \sim E_\nu \, \Delta u \, 4\pi R_S^2 \text{ erg s}^{-1}$$

Where E_ν is the neutrino energy density, R_S the shock radius, ℓ the neutrino mean free path and Δu the velocity difference across the shock. Using Wilson's (1979) values for the temperature ($T \sim 5.3$ MeV), velocity jump across the shock ($\Delta u \sim 6.10^9$ cm s^{-1}) and shock radius ($R \sim 7.10^6$ cm) and assuming $E_\nu = \frac{7}{8} aT^4$ one obtains

$$\frac{dE}{dt}tot \sim 4.10^{53} \text{ erg s}^{-1}.$$

At earlier times when $R \sim 3.10^6$ cm, $\Delta u \sim 9.10^9$ cm s^{-1} and $T \geq 10$ MeV this rate is actually an order of magnitude higher. Consequently, the average total energy acquired by the neutrinos from the shock acceleration over a time scale $t \sim 10^{-3}$ sec, that the mechanism is operative, can be of the order of $E_{tot} \sim 10^{51}$ erg which is comparable to the energy emitted in neutrinos at the emergence of the shock through the neutrino photosphere (Bethe et al. 1980).

Similar estimates can also be made from the calculated spectra. Assuming a power law fit, the integral spectra can be expressed as

$$N(E>E_0) = N_0 \left(\frac{E}{E_0}\right)^{-q}$$

Consequently, the differential spectrum will be

$$\frac{dN}{dE} = q \frac{N_0}{E_0} \left(\frac{E}{E_0}\right)^{-(q+1)}$$

and the total energy output, E_{out}, is

$$E_{out} = \int \frac{dN}{dE} E \, dE = N_0 E_0 \frac{q}{q-1} = E_{in} \frac{q}{q-1}$$

Where $E_{in} = N_0 E_0$ is the total input energy in the calculation. The shock, therefore, acts as an engine with efficiency $\eta = \frac{q}{q-1}$. In the case of fig. 2a, $q/q-1 \simeq 2.9$. So if $T \sim 10$ MeV, then the energy within a few mean free paths from the shock is $E_{in} \sim 2.10^{50}$ erg and hence $E_{out} \sim 6.10^{50}$ ergs in accordance with the previous estimate.

At this point it is not clear whether this mechanism would influence the dynamics of the supernova scenario. However, it could certainly affect the neutrino observational aspects of it since, as indicated by the Monte Carlo calculations, there is more energy available in the high energy neutrinos. Furthermore, more energy in neutrinos will be emitted at the emergence of the shock through the neutrino photosphere, i.e., in a pulsed form. This form of emmision is most favorable for detection (Lande 1980).

The Monte Carlo simulation, up to this point, has been quite simplified in the sense that neutrino nucleon scattering was considered to be the only opacity source. This simplification is not bad as far as the preshock material is concerned since due to its high A (=56) the nuclei opacity is the dominant one. Behind the shock the nuclei are dissociated to free nucleons and the electron contribution to opacity becomes significant. However, those electrons are quite hot ($T \simeq 5$-15 MeV) and scattering off them can lead to neutrino energy gains for energies up to $E_\nu \simeq 4kT$ (Tubbs and Schramm 1975). Electron scattering,

in general, is expected to modify the spectrum presented in figs. 1 and 2. (Probably by flattening it and introducing a cutoff at $E_\nu \geq 4kT$ as preliminary results show.) However, the argurments concerning the total excess energy acquired by the neutrinos and its observational consequences should still be valid.

Figure Captions

Fig. 1a. The neutrino integral spectrum for initial energy E_i = 8 MeV and optical depth $\tau_i \simeq 5.4$. The simulation was performed with the exponential density profile ($\rho = \rho_0 e^{-x/h}$) and with $x_i = 5.5.10^6$ cm, $h = 2.5.10^6$ cm and $\rho_0 = 10^{13}$ g cm^{-3}.

Fig. 1b. Same as Fig. 1a with E_i = 10 MeV and τ_i = 8.4.

Fig. 1c. Same as Fig 1a with E_i = 15 MeV and τ_i = 19.

(The break is not real and due to the details of the numerical simulation.)

Fig. 2b. The neutrino integral spectrum for initial energy E_i = 8 MeV and optical depth $\tau_i \simeq 8.68$. The calculation was performed with the power law density profile ($\rho = \rho_0\ 2.7/r_7^3$) with $\rho_0 = 1.62.10^{12}$ g cm^{-3}, $r_7 = 0.55$.

Fig. 2b. Same as fig. 2a with E_i = 8 MeV and $\tau_i \simeq 5.4$.

Fig. 2c. Same as fig. 2a with E_i = 10 MeV and $\tau_i \simeq 3.4$.

Fig. 2d. Same as fig. 2a with E_i = 8 MeV and τ_i = 2.2.

References

Arnett, W. D., 1977, Ap. J., 218, 815.
Axford, W. I., Leer, E. and Skadron, G. 1977, 15th International Cosmic Ray Conference (Plovdiv, Bulgaria).
Bell, A. R., 1978a, M.N.R.A.S., 182, 147.
Bell, A. R., 1978b, M.N.R.A.S., 182, 443.
Bethe, H. A., Applegate, J. H., and Brown, G. E., 1980, preprint.
Blandford, R. D., and Ostriker, J. P. 1978, Ap. J. (Letters), 221, L29.
Fisk, L. A., 1971, JGR, 76, No. 7, 1662.
Kazanas, D., 1980, Ap. J., 238, 998.
Lande, K., 1980, These proceedings.
Tubbs, D. L., and Schramm, D. N., 1975, Ap. J., 201, 467.
Van Riper, K., 1978, Ap. J., 221, 304.
Wilson, J. R., 1980, Ann of N.Y. Acad of Sciences, 336, 358 (Proc. of 9th Texas Symposium on Rel. Astroph.)

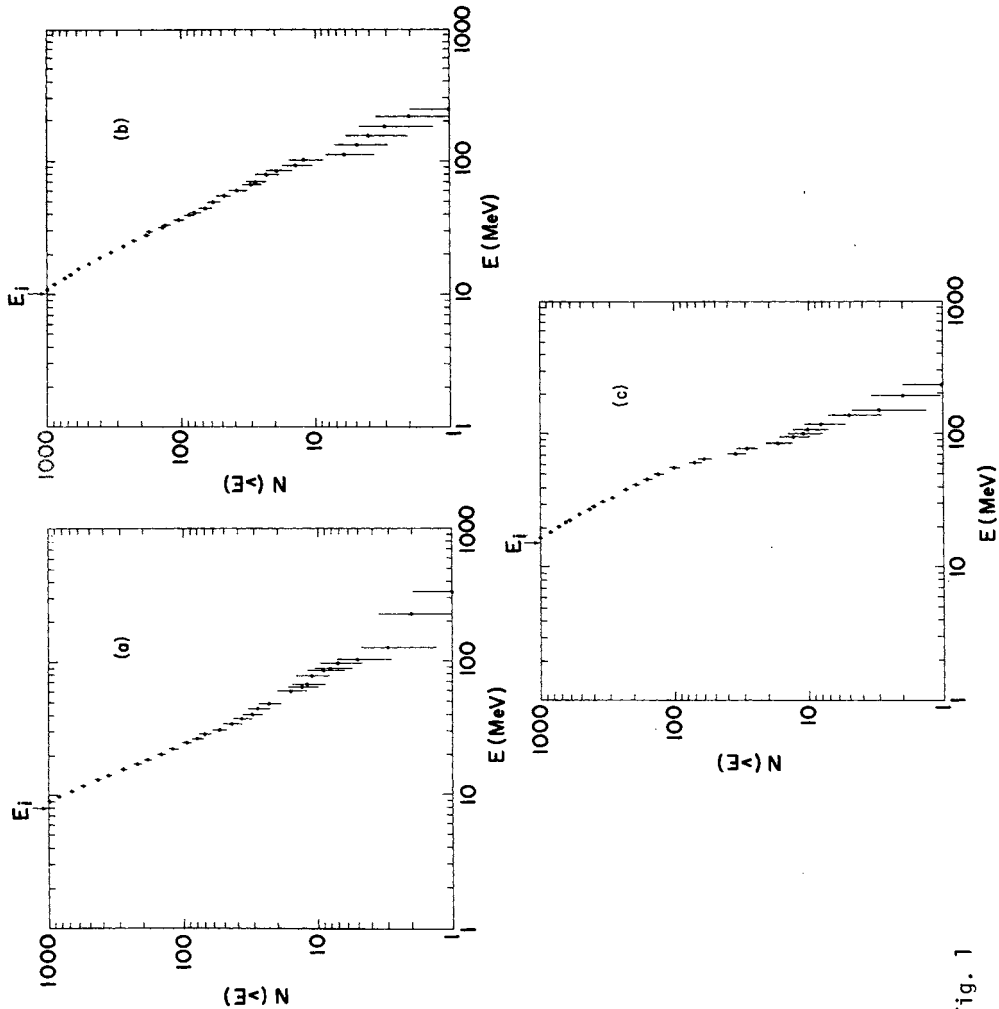

Fig. 1

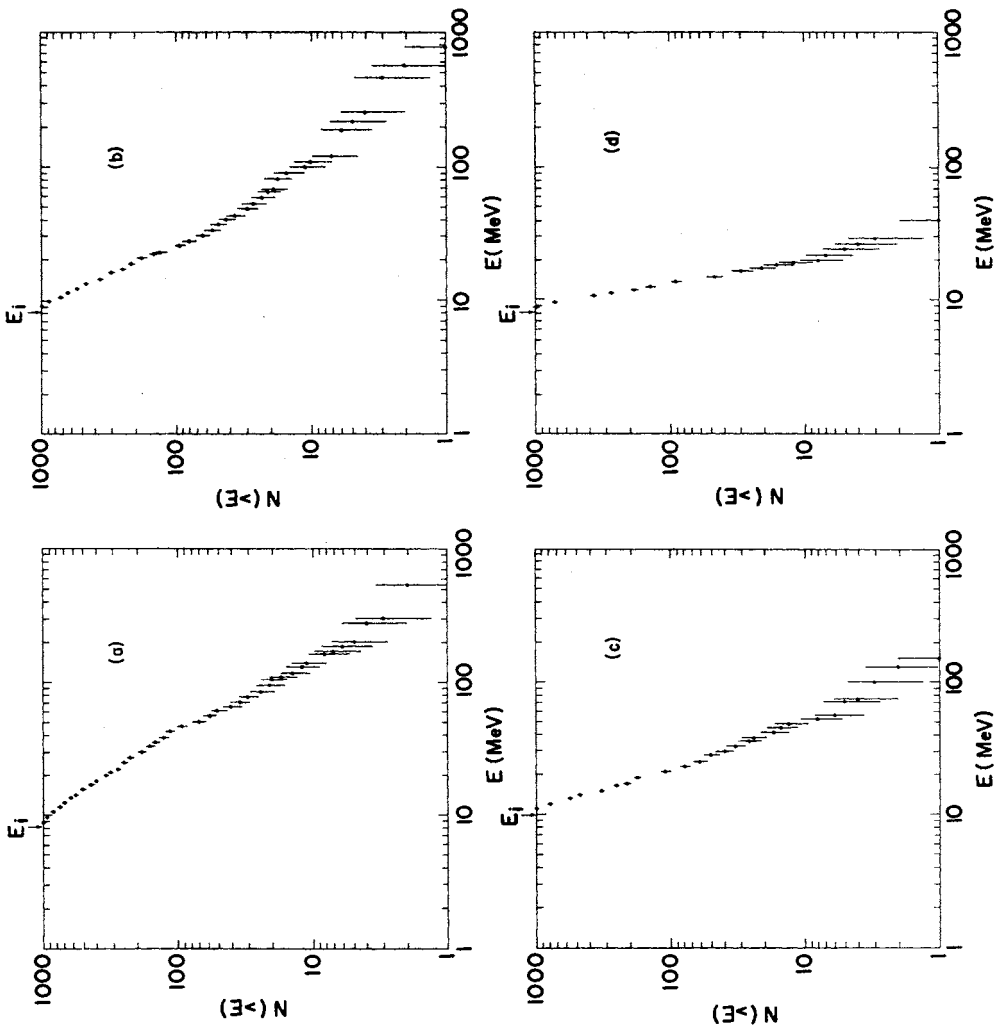

Fig. 2

NEUTRINOS AND SUPERNOVA COLLAPSE

by

Stirling A. Colgate and Albert G. Petschek
New Mexico Institute of Mining and Technology
Socorro, NM 87801
and
University of California
Los Alamos Scientific Laboratory
P.O. Box 1663
Los Alamos, NM 87545

ABSTRACT

The neutrino emission resulting from stellar collapse and supernova formation is reviewed. The electron capture and consequent neutronization of the collapsing stellar matter at the end of evolution determines both the initial adiabat of core collapse as well as the trapped lepton fraction. The initial lepton fraction, $Y_\ell = .48$ supplies the pressure for neutral support of the star at the Chandrasekhar limit. High trapping values, $Y_\ell = .4$, lead to soft core collapses; low values to harder collapses. The value of Y_ℓ is presently in dispute. The neutrino emission from initial electron capture is relatively small. A strong core-bounce shock releases both electron neutrinos as well as thermal μ and τ neutrinos. Subsequent neutrino emission and cooling can sometimes lead to an unstable buoyancy gradient in the core in which case unstable core overturn is expected. Calculations have already shown the importance of the largest possible eddy or equivalently the lowest mode of overturn. Present models of low lepton trapping ratio lead to high entropy creation by the reflected shock and the stabilization of the core matter against overturn. In such cases the exterior matter must cool below an entropy of approximately $s/k \cong 2$ to become unstable. This may require too long a time, approximately one second for neutrino cooling from a neutrinosphere at $\rho \cong 2 \times 10^{12}$ g cm^{-3}. On the other hand, high values of Y_ℓ such as .4 lead to softer bounces at lower density and values of the critical stabilizing entropy of 3 or higher. Under such circumstances, core overturn can still occur.

INTRODUCTION

Supernovae (SN) are believed to occur primarily due to the collapse of an evolved star to a neutron star. Some of the gravitational binding energy of the neutron star is transferred to the outside of the star which is ejected. The bulk of the binding energy of the neutron star is emitted as neutrinos. These neutrinos from galactic as well as extragalactic SN are one of the major possible sources of signal for Dumand. An alternate explanation of SN is that the pre-SN evolved star contains a carbon-oxygen core that burns or detonates with sufficient energy to disrupt and disperse the whole star. Such events would emit roughly 10^{-3} of the neutrino flux of a collapse event. The neutrino flux would be just that due to beta decay of the thermonuclear reaction products. This is a small fraction of the beta decay expected during collapse. If such events explain SN, then one must postulate that there exist more numerous "silent" events that form neutron stars without either light or mass emission because the frequency of occurrence of neutron stars equals or exceeds conservative estimates of visual SN

events. The total neutrino emission from such a "silent" event would nevertheless be comparable to that from a "standard" collapse model SN because the neutron star binding energy is the source of the neutrinos in either case. The rate of neutrino emission is, however, sensitively dependent upon the model of collapse and explosion. Presently there is no widely accepted model that explains in a convincing fashion the mechanism of a collapse SN event. Because of this, the expected neutrino pulse is subject to large uncertainty.

There are four phenomenologically separable sources of neutrinos in "standard" SN collapse model. These are:

1. Electron capture by heavy nuclei resulting from the increasing Fermi level during the initial unstable collapse from 10^{9} to 10^{11} g cm^{-3} density. Leptons are trapped during further collapse due to the large neutral current cross sections of heavy nuclei. The lepton number fraction (Y_ℓ leptons per baryon) is established by the low energy, slow ($\lesssim$ 1 s), early collapse phase. Since Y_ℓ decreases in this phase from .48 to variously 0.4 to 0.3, the corresponding electron neutrino emission can be estimated.

2. The strong shock wave from the elastic bounce of the homologous core. These neutrinos are primarily thermal in origin so that all types are emitted from the shock wave, provided $\rho \lesssim 10^{12}$ g cm^{-3}. Their emission cools and weakens the shock wave. The strength of this shock critically determines both mass ejection as well as neutrino flux. The strength of the shock wave depends sensitively upon details of the model.

3. Overturn (if it occurs) which will release the neutrinos trapped in the core in several milliseconds. The residual inner core has a high pressure due to the presence of degenerate leptons ($\gtrsim$ 100 MeV Fermi level) and so, as the outer core emits leptons, the possibility exists that the core could overturn violently not only releasing the neutrinos trapped in the core but also turning gravitational and internal energy of the core into kinetic energy. This effect depends critically upon the entropy and hence relative buoyancy of the deleptonized matter of the outer core remaining from the core-bounce shock wave.

4. Diffusion of neutrinos out of the cooling core which requires only seconds even in the absence of violent overturn.

NEUTRINO OSCILLATION AND COLLAPSE

Neutrino oscillations (Wolfenstein 1978) can affect hydrodynamic collapse of the core because they reduce the pressure of lepton trapped matter. The initial lepton number Y_ℓ of the trapped matter is established by both the rates of electron capture on heavy nuclei as well as neutrino diffusion during the initial collapse. Both processes are somewhat uncertain so that estimates of Y_ℓ (in the core) vary between 0.42 and 0.25. This large variation will in turn cause an uncertainty in core collapse and subsequent phenomena greater than that due to neutrino oscillations alone. To understand this we give estimates of the fractional pressure of the trapped matter for various assumptions of oscillations and Y_ℓ. The fractional support pressure is the ratio of pressure to the pressure that would exist if all leptons remained electrons starting with iron, i.e., $Y_\ell = Y_e = 0.48$. The latter pressure is the pressure that will just support a mass of $1.4\,M_\odot$ (Chandrasekhar mass) in neutrally stable, hydrostatic equilibrium. This is the presumed starting condition of the pre-SN core. Neutral support implies

equilibrium at any radius and any average density and is possible because the relativistic degenerate adiabatic index has the value 4/3. The fractional support pressure is both a measure of the degree of free-fall collapse as well as a measure of the fractional mass of the homologous core. We calculate this at a density less than nuclear density but high enough that the neutron proton mass difference can be neglected relative to the lepton energy. Then the fractional support pressure is:

$$(1 + 2^{1/3}\, nf^{4/3})(1 + nf)^{-4/3}\ (Y_\ell/.48)^{4/3}$$

where $Y_\ell = Y_e + \sum_i Y_{\nu i}$ and n is the number of neutrino types of assumed one helicity. The parameter f measures the suppression of electron neutrinos due to the chemical potential of the excess neutrons. This suppression results in values of f of about 0.15 (Bethe, Applegate and Brown 1980). Table I shows the fractional support pressure for various Y_ℓ's as well as for various assumption of neutrino types.

TABLE I

Fractional Support Pressure for f = 0.15, Various Values of Y_ℓ and Neutrino Oscillation Characteristics

P_ℓ/P_e	Y_ℓ	No.	ν's
≅0.91	0.48	1	full trapping
0.46	0.29	1	60% trapping
0.79	0.48	3	Majorana mass
0.40	0.29	3	Majorana mass
0.68	0.48	6	Dirac mass

One sees that the uncertainty in Y_ℓ leads to a greater variation in the pressure defect than does increasing the number of neutrinos. Thus, in order to calculate SN collapse, we will certainly have to understand the possible neutrino types; nevertheless at the present state of uncertainty neutrino oscillations are not the dominant question. Furthermore it has been pointed out by Wolfenstein (1978) that neutrino oscillations are suppressed in matter whose density is as great as 10^{13} g cm^{-3} because the index of refraction is different for electron neutrinos than for μ or τ neutrinos.

TRAPPING ENERGY

The difference in binding energy of the collapsed and initial core is available energy. Presumably a fraction of this energy produces the presently observable effects of SN and the remainder is available as neutrino emission.

Gudmundsson and Buchler (1980) have calculated this energy for various trapped lepton fractions Y_ℓ (Fig. 1). One sees that for the typical homologous core of .75 $M_\odot$, the binding energy is roughly 20 MeV per nucleon for a typical trapping value of $Y_\ell = 0.3$. This energy is available to form the core-bounce shock and the

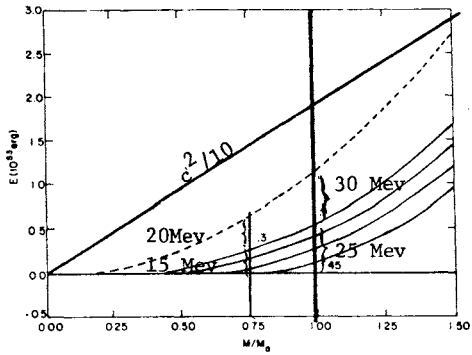

Fig. 1. The binding energy of a neutron core for various lepton trapping ratios using the Baym et al (1971) equation of state and as calculated by Gudmundsson and Buchler (1980). We have added an energy scale that emphasizes the binding energy per nucleon for equilibrium matter (cold neutron star) and a trapping ratio of $Y_\ell = 0.3$ for core masses of 0.75 $M_\odot$ and 1.0 $M_\odot$.

fast burst of neutrinos. The further binding energy available when $Y_\ell \to 0$ is approximately 20 MeV per nucleon also. Larger cores have larger specific energies available. If this further energy were to diffuse out of the core as neutrinos, the time required would be several seconds, long compared to hydrodynamic times of milliseconds. Therefore, diffusive release of neutrinos would not contribute to the SN mass ejection. Instead we have proposed that the residual energy of lepton trapping become observable and contributes to the SN mechanism by a process of violent unstable core overturn, (Fig. 2). (Colgate and Petschek 1980; Livio, Buchler, and Colgate 1980; Bruenn, Buchler, and Livio 1979). As the trapping fraction Y_ℓ increases beyond .3 the fraction of energy available from overturn exceeds that available for the core-bounce shock. The question of overturn may then be critical to SN.

There are two primary questions concerning the possibility of sudden core overturn.

1. Does an unstable buoyancy gradient exist at any time, lasting long enough to permit unstable overturn?

2. Will the lowest mode, L=2, corresponding to overturn dominate, the convective motions above smaller scale convection despite the existence of an unstable atmosphere covering many density or pressure scale heights?

The original concept of Epstein (1979) took question 1 more or less for granted. However, a combination of high exterior entropy values ($S/k \gtrsim 3$) in some present numerical calculations from the core-bounce shock as well as from degenerate electron capture has led to serious doubts that a global unstable gradient will occur before a time of roughly a second. (Convection will start in the mantle much earlier.) By the time of one second collapse will have terminated and diffusive release of trapped leptons will have dissipated the stored energy and excess buoyancy (Mazurek and Lattimer 1980). We will go into this problem more deeply, but first we will answer the second question in the affirmative.

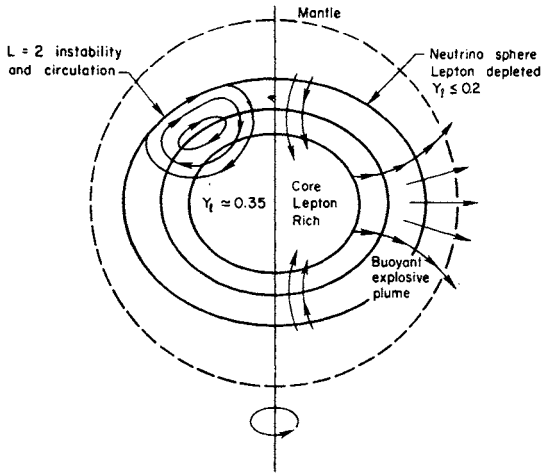

Fig. 2. Two extreme limits of the fluid flow expected from the unstable overturn of the partially de-leptonized neutron-star core during formation. The circulation shown on the left occurs if the $\ell = 2$ instability grows with a relatively small unstable potential difference. The explosive plume on the right occurs if the instability potential is large, i.e., the difference in potential energy between inner and outer core is comparable to the internal energy of the de-leptonized outer core.

A numerical calculation of overturn with a global unstable gradient has been completed by Livio, Buchler, and Colgate (1980) and demonstrates as in Figs. 3 and 4 the overturn of the neutron star matter. In Fig. 4 the "swallowing" of a higher mode convective element (L=8) by a slower growing, but dominating L=2 mode is demonstrated.

These calculations were done with a different equation of state than the one currently considered most likely, and hence, the bounce occurred at lower densities ($\cong 2 \times 10^{13}$ g cm^{-3}) than in calculations using the equation state by Bethe, Brown, Applegate and Lattimer (1979). We note parenthetically that a soft equation of state implies low pressure at a given density which delays the bounce and produces a strong outgoing shock. Thus soft equation of state implies hard bounce and vice-versa. This core-bounce shock wave produces a high entropy in the envelope that stabilizes the mantle against overturn with the core. Another two dimensional calculation of convective overturn starting from a one dimensional calculation of collapse was completed by Smarr, Wilson, Barton, and Bowers (1980). The 1-D calculations produced a strong core-bounce shock and high entropy ($s/k \gtrsim 4$) in the outer $\frac{1}{2}$ $M_\odot$ of the core. Only a small fraction ($\cong \frac{1}{4}$ $M_\odot$) of the distribution was unstable relative to an inner $\frac{1}{4}$ $M_\odot$, which in turn was supported by a stable 3/4 $M_\odot$ core. The two $\frac{1}{4}$ $M_\odot$ regions indeed "violently" overturned and further substantiated the previously envisaged predominance of the largest possible eddy size. Nevertheless, Smarr et al (1980) cite their calculations as conclusive evidence against overturn.

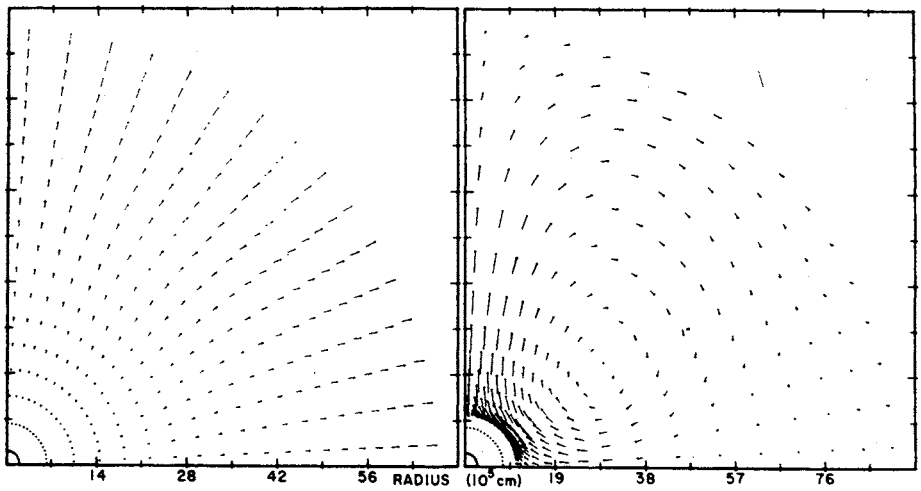

Fig. 3. (a) Velocity field for $\ell = 2$ perturbation 20 ms after the first bounce. Largest velocity of the order of 10^9 cm s^{-1}. Squares denote arrow tails. (b) Velocity field for $\ell = 2$ perturbation 31 ms after the first bounce. Largest velocity of the order of 3×10^9 cm s^{-1}. Squares denote arrow tails.

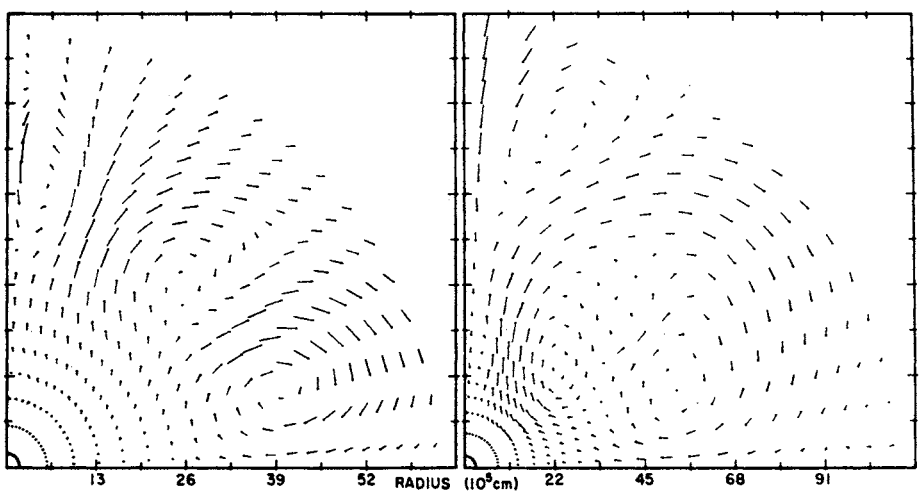

Fig. 4. (a) Velocity field for $\ell = 2$ and $\ell = 8$ perturbations 21 ms after the first bounce. Largest velocity of the order of 5×10^8 cm s^{-1}. Squares denote arrow tails. (b) Velocity field for $\ell = 8$ perturbations 28 ms after the first bounce. Largest velocity of the order of 1.6×10^9 cm s^{-1}. Squares denote arrow tails.

ENTROPY, LEPTON, AND STABILITY GRADIENTS

If the entropy distribution initially and after bounce remains sufficiently high on the exterior relative to the trapped low entropy interior core, then a stable buoyancy gradient may exist. That is

$$\left(\frac{1}{\rho}\frac{d\rho}{dr} - \frac{\gamma}{P}\frac{dP}{dr}\right) \text{ may be negative everywhere.} \qquad (2)$$

Then, of course, the core will remain stable and not overturn. The question of the time evolution of stability is difficult to answer.

The original objection to core overturn based upon stabilizing entropy gradients was proposed by Mazurek and Lattimer (1980). They showed that a core of density around 10^{14} g cm^{-3}, a trapped value of $Y_\ell = .3$ and low core entropy $S/k = 1.2$ was stable against interchange with matter at larger radius, lower density, depleted in leptons to $Y_\ell \leq 0.1$ and having relatively modest entropies ($s/k \gtrsim 2$). Let us explain further what this means. The instability in question presumes that cold lepton trapped matter has a higher pressure at a given density (or conversely lower density at a given pressure) than external matter which has emitted its leptons by electron capture and neutrino escape. This difference in buoyancy is due to the presence or absence of the degenerate pressure of the trapped leptons. However, as Mazurek and Lattimer (1980) pointed out, one can substitute thermal pressure for degenerate lepton pressure in the lepton depleted matter. The question is how much entropy or thermal pressure is required to substitute for the degeneracy pressure?

We assume that the interchange or "overturn" is adiabatic and hence entropy is conserved in the process. Indeed condition (2) is based on just such an adiabatic interchange of two fluid elements. Hence, the question of entropy stabilization must start with an analysis of the magnitude of the entropy required to stabilize the interchange of dense, cold, lepton trapped matter and hot, lepton depleted matter.

We have completed such an analysis from B^{2}AL for this conference with particular emphasis upon the high density region $\rho \geq \rho_{nuc} = 2.7 \times 10^{14}$ g cm^{-3}. Unfortunately, the initial treatment of this problem (Mazurek and Lattimer 1980) was for densities $\leq 10^{14}$ g cm^{-3}, which therefore did not include the core region where the gravitational potential is largest and where the most energy can be generated by an interchange. The strong core-bounce shock and resulting high entropy in the exterior matter occurs when the central density is $\gtrsim$ nuclear density because only then is the pressure increase great enough to reverse the collapse abruptly. Our initial analysis is pessimistic, in that it requires little entropy to stabilize a partially lepton trapped core against overturn.

We ask how much entropy is required to make up for the pressure defect caused by reducing the lepton number at a given density. Then this entropy is the critical stabilizing entropy. We assume the initial entropy is not zero (cold) but finite ($s/k = 1.2$) corresponding to values calculated for initial collapse models (B^{2}AL). We similarly assume that the depleted lepton matter does not correspond to $Y_\ell = 0$, but instead is only partially depleted ($Y_\ell = 0.1$). In this fashion, we expect some nuclear binding to exist in the neutron rich matter. Then following

B^2AL, the nuclear pressure is proportional to $T^2 \propto s^2$ and the pressure at entropy s_2 becomes

$$P(s_2) = P(s_1) \quad s_2^2/s_1^2 \ . \tag{3}$$

Using this and the figures given in their tables 5 and 6, we estimate the values of critically stabilizing entropy s/k in our Table II. In this analysis, we have neglected the relatively minor contribution to the pressure of the heat added to the leptons. The slight variation of s/k with ρ is due to deviations of the equation of state from a perfect gas.

TABLE II

Critical Stabilizing Entropy for Material with $Y_\ell = 0.1$ with Respect to Core Material of $Y_\ell = 0.3$, s/k = 1.2 and density ρ_o

ρ_0/ρ_{nuc}	s/k
1	2.25
1.5	2.0
2	2.0

We see that $s/k \cong 2$ is sufficient to stabilize the dense core against overturn for initial $Y_\ell \lesssim 0.3$.

Mazurek and Lattimer (1980) predict that at lower densities significantly higher entropies are required for stabilization (i.e. s/k = 3 to 4). A strong shock will give still greater entropies (s/k = 7 to 8). Thus we see that the most likely remaining circumstance for convective core overturn is that conditions result in a weak shock similar to those already calculated by Livio et al (1980).

The core-bounce shock deposits an entropy of $s/k \cong 10$ at the neutrino sphere at density = 10^{12} gm^{-3} and T $\cong$ 10 Mev (Van Riper 1980). We would interpret this high entropy as more than sufficient to stabilize against overturn with core lepton-trapped matter. Here we have assumed that the core-bounce shock, although very strong is still insufficient to eject the supernova mantle. Then we must consider cooling. The low density matter ($\rho \lesssim 10^{12}$) cools slowly to $\cong$ 2 Mev where $s/k \lesssim 2$ because electron pair neutrino emission is weak ($\propto T^9$) and nuclear excited state emission (Kolb and Mazurek 1979) is inhibited because nuclei are thermally decomposed to free nucleons. Instead we consider matter at higher density ($\rho \cong 2 \times 10^{13}$ g cm^{-3}) where an entropy of s/k = 2 correspond to T = 6 Mev. Then the cooling time is very short - several milliseconds and neutrino diffusion to the neutrinosphere surface governs the time constant. This time constant very roughly calculated is less than a few 10's of milliseconds. If thermal neutrinos are emitted fast enough to cool the matter to an entropy that permits overturn, then the excess electron neutrinos can similarly escape. Thus we see an unstable gradient developing much as we envisaged in Colgate and Petschek (1980). Then if a relatively strong core-bounce shock derived from a high central density bounce

is insufficient to create the SN mass ejection, we expect subsequent cooling and deleptonization of the sub-neutrinosphere matter will still permit explosive core overturn.

SOFT BOUNCE

If the trapped lepton fraction is increased to $Y_\ell > 0.4$ then the bounce becomes much softer, lower density and closer to the the conditions calculated by Livio et al. Furthermore, the stabilizing entropy increases because of the larger initial degenerate pressure. Under these circumstances we expect core overturn. There is already some speculation of a larger trapped lepton fraction because of the reduced electron capture beta decay rate in very heavy nuclei because of shell structure (Fuller, Fowler, and Newman 1980). If this turns out to be so, then convective core overturn again becomes feasible.

ACKNOWLEDGEMENT

We are indebted for help and conversations with Ted Mazurek, Jim Lattimer, Robert Buchler, Larry Smarr, Jim Wilson, Richard Bowers, and Ken Van Riper. This work was supported by DOE and the National Science Foundation, Division of Astronomy.

REFERENCES

Baym, G., Pethick, C. J., and Sutherland, P., 1971, Ap. J. 170, 299.
Bethe, H. A., Brown, G. E., Applegate, J., and Lattimer, J. M., 1979, Nucl. Phys. A324, 487 BBAL.
Bethe, H. A., Applegate, J. H., and Brown, G. E. 1980, preprint.
Bruenn, S. W., Buchler, J. R., and Livio, M., 1979, Ap. J. 234, L183.
Colgate, S. A. and Petschek, A. G., 1980, Ap. J. Lett 236, L115.
Epstein, R. 1979, M.N.R.A.S., 188, 305.
Fuller, G. M., Fowler, W. A., and Newman, J. M., 1980, to be published.
Gudmundsson, E. H. and Buchler, J. R., 1980, Ap. J. 238, 717.
Kolb, E. W. and Mazurek, T. J. 1979, Ap. J. 234, 1085.
Livio, M., Buchler, J. R., and Colgate, S. A. 1980, Ap. J. Lett. 238, L139.
Mazurek, T. and Lattimer, J., "Stellar Collapse, Supernovae, and Neutron Star Formation" Conference, May 6, 1980, Santa Barbara, CA.
Smarr et al, "Stellar Collapse, Supernovae, and Neutron Star Formation" Conference, May 6, 1980, Santa Barbara, CA.
Smarr, L., Wilson, J. R., Barton, R. T., and Bowers, R. L., 1980, preprint LLL, to be published.
Van Riper, K. A. 1980, private communcation.
Wilson, J. R., 1979, "Neutrino Flow and Stellar Collapse."
Wolfenstein, L., 1978, Phys. Rev. D, 17, 2369.

SAC/rep:4G

NEUTRINOS AND STELLAR COLLAPSE*

T.J. Mazurek and J. Cooperstein
Department of Physics
State University of New York at Stony Brook
Stony Brook, N.Y. 11794

and

S. Kahana
Brookhaven National Laboratory
Upton, N.Y. 11973

ABSTRACT

Detailed calculations of the collapse of stellar cores and the attendant neutrino emission are presented. A critical summary of input physics required for such calculations is given. Present uncertainties in the latter and their potential effects are discussed. The influence of initial starting conditions for collapse is examined. It is found that the dynamic results are not overly sensitive to these, and the collapsed stellar structure is fairly unique. None of the calculations give mass ejection. The neutrino production processes are summarized. Detailed results on the prompt neutrino burst from collapse are given. It is found that electron-type neutrinos dominate the emission. However, for sufficiently high entropies from the shock the mu and tau neutrino emission can become appreciable. The well established features of stellar collapse are abstracted and the most pressing uncertainties in the dynamic calculations are examined. Finally, some comments are presented on possible effects of neutrino oscillations.

1. Introduction

Present hydrodynamic calculations appear to be converging on a common picture for the collapse of cores in massive stars. Electron-degenerate cores become unstable to collapse when their masses approach $\sim 1.5\ M_{\odot}$. Nuclear dissociation and electron capture initiate the dynamic collapse. The leptons continue to dominate the pressure because neutrinos become trapped at high densities. This results in the formation of a cool inner core that collapses homologously. At about nuclear densities, the pressure from nucleons increases rapidly. This halts the collapse, giving a core bounce. A shock forms at the surface of the inner core and propagates into the infalling envelope. Such basic features have emerged in hydrodynamic studies of collapse by various researchers.[1]

It is the propagation of the shock and the post-shock characteristics determine the observable signatures of stellar collapse. A burst of neutrinos is produced when the shock reaches the transparent regions. A plateau of

*Supported in part by USDOE at the State University of New York at Stony Brook (Contracts DE-AC02-80ER10719 and DE-AC02-76ER13001).

constant emission then ensues as the post-shock regions become transparent during expansion. The details of shock propagation are determined by the hydrodynamics of the cool inner core that collapsed homologously. These in turn are determined by physical processes at high densities.

In this contribution to the DUMAND proceedings, we describe results of our detailed hydrodynamic calculations of stellar collapses as well as the input physics used in this numerical work. Calculations with different initial configurations at the start of collapse were performed. The results show salient features of collapse that are essentially independent of starting configurations. Indeed most of the features are common to various studies[1] performed by different researchers. Taken as a whole, these features comprise the currently canonical scenario for core collapse. We also examine the neutrino production, transport, and emission. The electron-type neutrino pulse obtained in our numerical calculations is presented, and estimates for the mu and tau neutrino emission are given.

2. Input Physics

Hydrodynamic codes require as input an equation of state that is in general a function of density, temperature, and composition of the matter. Results of dynamic calculations depend critically on the equation of state. The baryonic component of the matter forms a gas that is in nuclear statistical equilibrium whose composition is determined by the electron fraction in transparent regions, and by the total lepton fractions in regions where the neutrinos are trapped. Electron capture produces neutrinos, reducing the electron fraction. The neutrinos produced can redistribute the energy and lepton fractions within the matter. For a given hydrodynamic calculation these processes couple with and feed back into the dynamics to such an extent that dynamic results cannot be interpreted independently of the thermodynamic and transport processes.

For the neutrino transport we use the diffusion approximation[2] suitably modified by flux-limiting procedures[3] to give free streaming in transparent regions. In addition, we assume that diffusing neutrinos are in thermodynamic equilibrium with the matter. This should be a good approximation since more detailed studies[4] have shown that the neutrino distribution function is close to the Fermi-Dirac distribution in the regions where appreciable coupling between neutrinos and matter exists. We follow explicitly only the transport by electron-type neutrinos. This means that our results underestimate the energy losses due to neutrino emission, and hence favor the possibility of mass ejection. We estimate the additional neutrino losses that can be expected from electron-pair annihilation and find that they may be comparable to the loss through transport of electron-capture neutrinos (see below).

The opacities[5] include contributions from coherent scattering by nuclei, elastic scattering by nucleons, and absorption of neutrinos on neutrons. We use the currently accepted value of $\sin^2\theta_W \approx \frac{1}{4}$, where θ_W is the Weinberg angle. The effects of variations in density and lepton fraction on the mean mass number of the heavy nuclei have been included for transport proposed using a low temperature approach.[6]

The equation of state uses numerically exact expressions for Fermi particles for the leptons and nucleons. The alpha particles and heavy nuclei are assumed to behave as Boltzmann particles. Below nuclear densities we solve the nuclear Saha equation for the matter composition. The method uses one heavy nucleus with average properties determined on the basis of a large equilibrium network

calculation. Above nuclear densities, the alpha particles and nuclei disappear. Here we use the Fermi expressions for a non-interacting gas and add to it a zero-temperature nuclear interaction energy.[7] Additional restrictions are required to determine the transition density between matter in nuclear statistical equilibrium and a pure nucleon composition. We determine this density by requiring that the pressure and entropy be continuous through the transition. While the actual conditions for the transition are a bit more complex[8], the transition densities we derive (nearly that of nuclear matter) differ little from those obtained in more detailed considerations. We also have varied the transition density in our hydrodynamic calculations. There were no noticeable differences in the dynamics of collapse and bounce.

The electron capture during collapse is expected[9] to occur initially on the heavy nuclei. Then as the nuclei become neutron rich the nucleon shells giving rise to the super allowed beta transitions become occupied, and the capture on free protons dominates. In our hydrodynamic calculations we use only the capture on free protons. We have varied the rate of this capture over a reasonable range and have found no noticeable effects on the hydrodynamics.

3. Hydrodynamics of Core Collapse

Our calculations begin with initial models that are on the verge of instability against dynamic collapse. We have used the published models of Arnett[10] and the more recent ones of Weaver, Zimmerman, and Woosley.[11] We have also used models[12] corresponding to detonated carbon/oxygen cores with sufficiently large central densities to give collapse. While differences in the thermodynamic characteristics of these various models can be pronounced, we found the overall hydrodynamic behaviors to be quite similar in all cases. Thus we summarize only the results obtained for a core[11] that corresponds to a star with a total mass of 15 $M_\odot$ and 1.6 $M_\odot$ within the core.

The dynamic collapse begins when the central density is around several times 10^9g cm^{-3}. Degenerate electrons overwhelmingly dominate the pressure and the matter is transparent to neutrinos. As electron-capture proceeds in the central regions the rate of core collapse accelerates. A central inner region where the collapse is homologous forms. The size of this region continuously decreases in mass. When densities around 10^{11}g cm^{-3} are reached the matter becomes increasingly more opaque to neutrinos. At a density around a few time 10^{11}g cm^{-3} the neutrinos can no longer escape from the core on collapse time scales and they are trapped. Their chemical potential grows until beta equilibrium is established between electron capture on protons and neutrino absorption on neutrons. The trapped leptons continue to dominate the pressure until nuclear densities are reached. However, they cannot halt the collapse at a lower density since they are extremely relativistic and have adiabatic indices of 4/3. Thus collapse can only be halted above nuclear densities when the nuclei disolve and the pressures due to the non-relativistic nucleons become important. This occurs at central densities around 4×10^{14}g cm^{-3} in our calculations.

Fig. 1 shows the dynamic collapse of the core where we have used 100 zones of equal mass. This fine zoning insured that a change of a decade in density occured over at least five mesh points outside of the shock transition region. Thus the calculation should be able to reproduce adequately the propagation of the shock in the infalling envelope. In Fig. 1 the radial positions at various core masses are plotted as functions of time. The separation

Figure 1

Time evolution of radii at given core mass points (given in units of $M_\odot$ at right of diagram). The propagation of the shock front (dashed line) and the position of the neutrinosphere (hatched line) defined as the point at which the optical depth for neutrinos at the mean energy drops below unity are also shown.

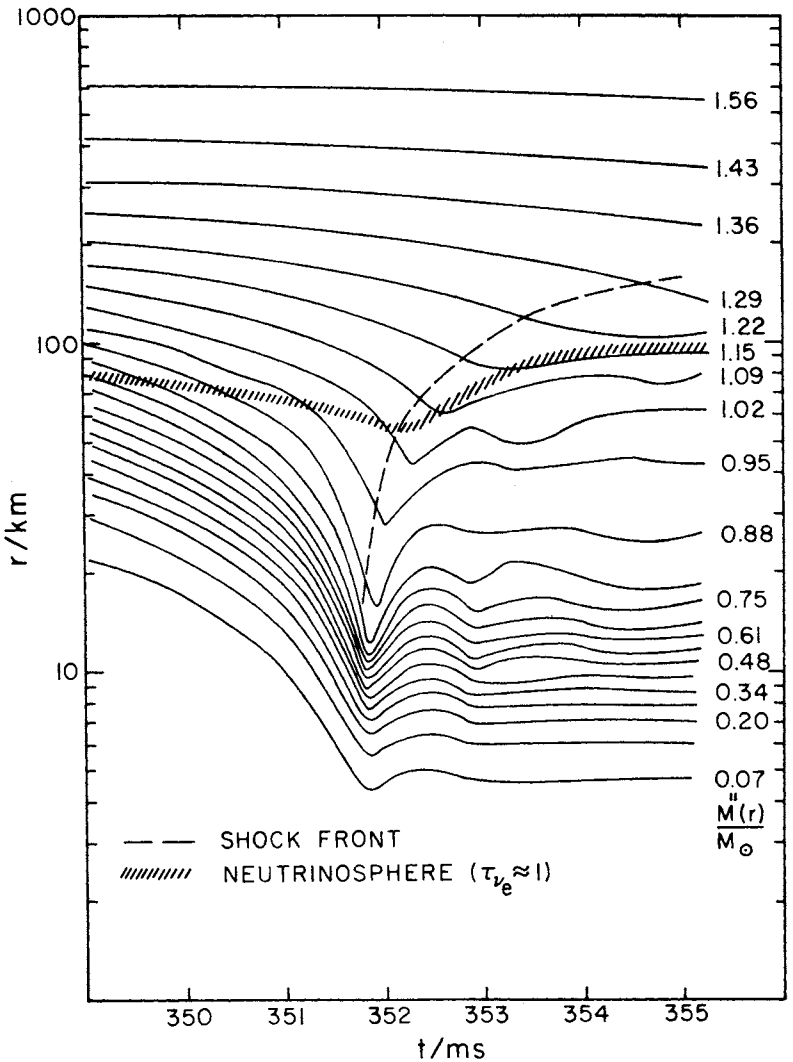

Figure 2

Structure of hydrostatic core at the end of the calculation. The lepton fraction X_ℓ, density ρ, and temperature T are given as functions of radius. The density profile has ticks at various points that are labeled by the total mass at higher densities (in units of $M_\odot$).

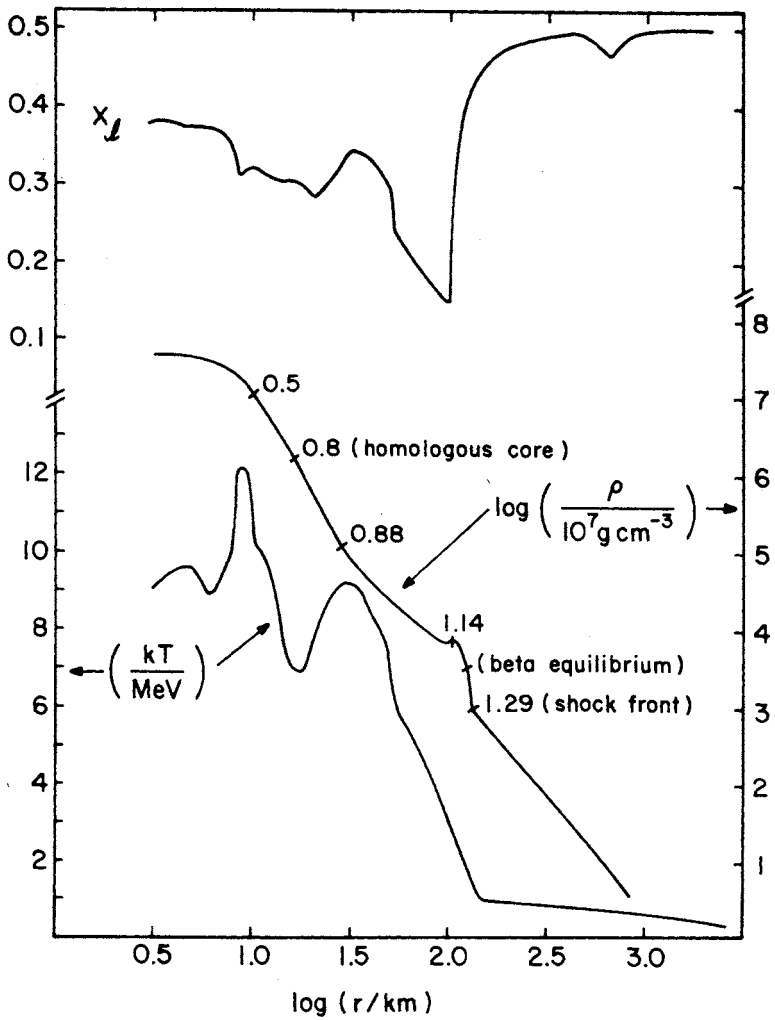

between an inner core in homologous collapse and a roughly stationary surrounding envelope is clearly shown. The bounce of the inner core occurs just before 352 ms (arbitrary starting point for time). From the figure it is seen that at bounce the homologous region contains around .75 to .80$M_\odot$. The reversal of collapse at the mass point of .82$M_\odot$ clearly is at a later time than that of the interior regions which bounce simultaneously.

The shock is indicated by a dashed line in Fig. 1. It is seen that the shock forms at the surface of the core somewhat before the actual bounce occurs. It propagates outward to a radius of about 130 km, where it then becomes a roughly stationary accretion shock. Since it was clear than no mass ejection would occur the calculation was terminated at this point.

The bounce of the inner core clearly is not homologous. The surface regions expand by nearly a factor of two, while the expansion in the center is less than 20%. It is seen that the inner core establishes a rough hydrostatic equilibrium after about one millisecond. The adjustment to equilibrium in the shocked regions is somewhat longer, but not much more than a few milliseconds after shock passage. At the end of the calculation the structure interior to the shock was essentially hydrostatic. It consisted of a cool inner region of $\sim$ .8$M_\odot$ and a hot outer envelope of $\sim$ 0.5$M_\odot$. The time required for the remaining .3$M_\odot$ of envelope to rain is around several hundreds of milliseconds. On such long time scales, the trapped leptons will be able to leak out. This may lead to violent convection[13] in the core that could have some implications for mass ejection. However, the entropy in the shocked envelope is so high (see below) that on the dynamic times of our calculations the effects of convection are negligible.[14]

The density, temperature, and lepton distributions with radius at the end of our calculation are shown in Fig. 2. The density profile is labeled by the interior mass (in $M_\odot$) at several points. The homologous core of $\sim$ .8$M_\odot$ lies at densities above a few times 10^{13}g cm^{-3}. At this point the shocked envelope extends to $\sim$ 1.29 $M_\odot$. Note that the density increases by around a factor of five across the shock transition so that the accretion shock is quite strong. In our numerical treatment which uses the pseudo-viscosity method to follow the shock, beta equilibrium is established within the shock. In reality, the shock transition should be much thinner, and beta equilibrium would occur only after shock passage. However, this should not alter the results appreciably. The temperature profile has two peaks. The peak at $\sim$ 10 km may or may not be real. These regions have undergone the phase transition between nucleons and nuclear statistical equilibrium matter twice. Our approximate treatment of the phase transition may not give the temperature reliably. However at the high densities in these regions thermal pressures are small. Thus differences in temperature of the order of 10% would modify the pressure by less than 1%. Small errors in temperature therefore have negligible dynamical effects. The temperature peak at around 30 km is brought about by the shock propagation down the density gradient and subsequent cooling by neutrino emission. We believe this peak to be real. The lepton fraction is shown at the top of the figure. Note the big dip at about 100 km where the matter is transparent to neutrinos.

All of our calculations to date have given similar results. They provide an almost unique structure for the study of the subsequent deleptonization of the core. The cool inner core at an entropy between 1 to 2 (per baryon in units of Boltzmann's constant k) typically contains between .6 to .8$M_\odot$. At the point when the shock becomes an accretion shock, the hot envelope at entropies between

5 and 8 typically contains .5 to .7$M_\odot$ of matter. Such structures need to be investigated through deleptonization to determine the final outcome of stellar collapse.

Let us now consider the evolution of the entropy profile during collapse. Figure 3 shows the entropy distribution with mass for various times in Fig. 1. Also shown in the entropy profile near the beginning of our calculation at 174 ms. It is seen that the central regions ($M \lesssim .25\ M_\odot$) remain at a very low entropy throughout the collapse. The entropy here is < 1.5, agreeing quite well with analytic estimates.[6] However, in the regions between .25 and .75 $M_\odot$ the entropy rises to ~ 2. This is due to energy deposition by escaping neutrinos. The center-most regions do not experience a large neutrino flux through them while becoming opaque. They thus are quite cool. The outer regions not only get heated by neutrinos from electron capture but also by the flux of diffusing neutrinos from the inner regions. Hence they are heated to a higher entropy.

The profile at 352 ms is just before bounce and shock formation. The mass point at which the shock formed is shown clearly by the rapid rise in entropy above $\sim .75\ M_\odot$ for the two later times shown in the figure. It is seen that the post-shock entropy in this calculation is large. This would preclude any convective overturn[13,14] of the entire core on dynamic time scales. At the latest instant shown in the figure, the entropy decreases outward with mass beyond $\sim .9M_\odot$. These regions are unstable against thermally-driven convection. However, electron-pair production of neutrinos which was not explicitly accounted for would tend to eliminate this instability.

The evolution in time of the lepton fraction over the core is shown in Fig. 4. Before the point of shock formation, the lepton fraction profile has a minimum at roughly half of the homologous inner-core mass. The higher lepton numbers there are due to lower entropies. The lower entropies give smaller proton abundances in the transparent regions, and hence lower rates of electron capture. However the regions at low entropies with a decreasing lepton fraction outward are highly unstable against lepton-driven convection.[13,14] Thus one would expect decreasing gradients to be smoothed out during collapse. The effects of such smoothing on the dynamics may be small. Calculations[15] which include it give results quite similar to ours. Once the shock builds up to its peak strength (post shock entropies ~ 8), there is set up a flow of neutrinos both inward and outward from the hottest regions. This is clearly shown by the lepton profile at 353 ms. It is seen that the diffusion of neutrinos from regions around $1M_\odot$ has produced an inner peak and an outer one. The outer peak is caused by neutrinos diffusing up to the shock front where they are stopped by the high coherent opacity of undissociated matter. We will see below that this peak produces a large burst of energetic neutrinos when the shock reaches the transparent regions. It disappears after this as can be seen in the 355 ms profile of Fig. 4. The depletion of leptons by electron-capture in the transparent regions ($M \sim 1.15M_\odot$ in Fig. 4) results in a steady plateau in the neutrino luminosity.

4. Neutrino Emission

The processes which dominate the neutrino production in stellar collapse are summarized in Table 1. For all practical purposes only electron-capture neutrinos and those from electron-pair annihilation need to be considered. Production of neutrinos by electron capture totally dominates all other processes

Figure 3

Time evolution of the entropy profile (s in units of k per baryon) of the mass of the core. Profiles are given at the beginning of the calculation (174 ms), just before shock formation (352 ms), when the shock is in opaque regions (353 ms), and at the end of the calculation (353 ms).

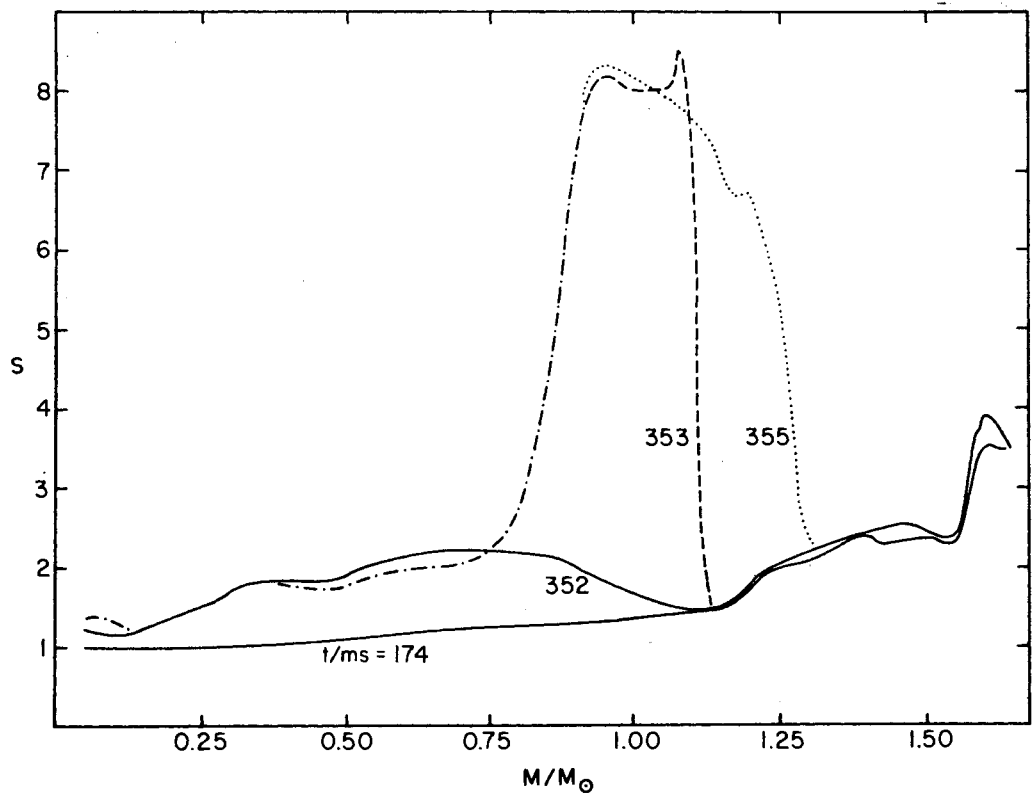

Figure 4

Time evolution of the profile of total lepton fraction X_ℓ over the mass of the core. Profiles are given at the beginning of the calculation (174 ms), just before shock formation (351 ms), when the shock is in opaque regions (353 ms), at the end of the calculation (353 ms), and some intermediate times are shown.

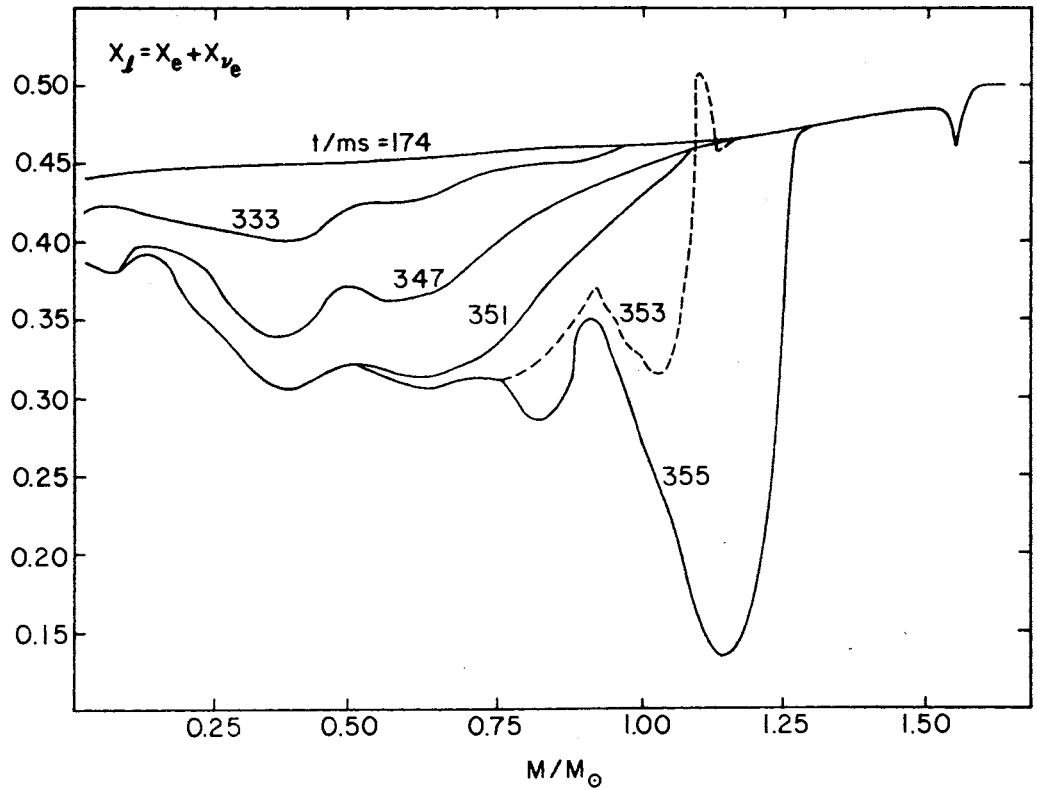

Table 1

Dominant Processes in Neutrino Production (in order of importance)

Process	ν_e	ν_μ, ν_τ	Comment
Electron Capture[6,9,12] $e^- + (A,Z) \rightarrow \nu_e + (A,Z-1)$ $e^- + p \rightarrow \nu_e + n$	✓		Dominates pre-shock production of neutrinos.
Electron Pair Annihilation:[16] $e^+ + e^- \rightarrow \nu + \bar{\nu}$	✓	✓	Is significant only after shock forms. Emission is comparable to electron capture for s ∿ 7 to 8.
Decay of Excited Nuclei:[17] $(A,Z)^* \rightarrow (A,Z) + \nu + \bar{\nu}$	✓	✓	Is dominant in pre-shock production of ν_μ and ν_τ.
Electron Bremsstrahlung:[18] $e^- + (A,Z) \rightarrow e^- + (A,Z) + \nu + \bar{\nu}$	✓	✓	Is negligible relative to Nuclear de-excitation process above.
Photo and Plasma Neutrinos:[16] $\gamma + e^- \rightarrow e^- + \nu + \bar{\nu}$ $\gamma \rightarrow \nu + \bar{\nu}$	✓	✓	Are negligible
Meson and Lepton Decays:[19] π, μ, τ	✓	✓	Are negligible

before the shock forms. Note that in this phase the production of mu and tau neutrinos is dominated by the decay of highly excited nuclear states. However, the electron-type leptons are extremely degenerate, and their pressures totally overwhelm any contributions from the other types. After the shock forms then the entropy it leaves in its wake determines whether or not pair annihilation is significant. Specifically, the entropy near the neutrino-sphere must be around 7 to 8 for appreciable neutrino luminosities from pair annihilation. This is the case for the model discussed above.

Our hydrodynamic presently does not include the pair annihilation process and transport due to mu and tau neutrinos. To estimate the effects of these processes on the basis of our current results we use the following procedure. Using our post shock temperatures and nucleon opacities[5] we estimate that mu and tau neutrinos can escape on millisecond timescales from regions at densities as high as 10^{12}g cm^{-3}. Therefore we make the simplifying assumption that all regions below this density are totally transparent to neutrinos while those above are totally opaque. The pair neutrino emission of our core can then be calculated at any given time from the rates given by Dicus (with $\sin^2\theta_\omega = \frac{1}{4}$). This procedure may overestimate the emission of neutrinos from pair annihilation.

The neutrino particle luminosities of our model are shown in Fig. 5. The top curve shows the results given by the hydrodynamic calculation. We have smoothed out variations that are introduced by the finite zoning of the model. The peak in the emission occurs when the diffusing neutrinos that are trapped behind the shock (cf Fig. 4 and discussion above) reach the transparent regions. The maximum emission occurs after the shock passes through the neutrino sphere. This however may be an artifact of the finite zoning where the shock is spread out artificially over a few zones. After the large initial burst of neutrinos, the emission levels off on a plateau that decreases slowly. This plateau is due to electron capture in the transparent regions that depletes the lepton fractions there. The mean particle energies are shown in the top curve of Fig. 6. It is seen that this energy increases rapidly to $\sim$ 18 MeV at the peak of the neutrino burst. It then decreases to values of around 10 MeV.

The particle luminosities of the pair annihilation neutrinos are given by the lower curve of Fig. 5. These increase rapidly to a peak when the shock enters the neutrino sphere. Subsequently, as the shocked envelope expands and the temperature decreases, the luminosities go down. The results in the figure indicate that the pair emission of electron-type neutrinos may be comparable to the emission from electron capture. However, since our method for computing the pair annihilation effects is likely to exaggerate their importance, it is not clear that this is actually the case. The mean energy of the neutrinos from the pair process are given by the lower curve in Fig. 6. They are significantly below the peak energies of the diffusion burst since mu and tau neutrinos cannot be degenerate.

Of paramount importance to DUMAND is the emission of high energy neutrinos from stellar collapse. The neutrino distribution with energy is roughly given by the Fermi-Dirac distribution evaluated at the temperature and chemical potential in the neutrinosphere. Typically the neutrino chemical potentials are much lower than kT (where T is the temperature) in the post shock neutrinosphere. If we neglect the effects of the neutrino chemical potentials, the mean particle energy is just 3kT. Thus the ratio of particles at high energies to those at the mean energy is roughly given by

$$\frac{n(\varepsilon_\nu)}{n(\bar{\varepsilon}_\nu)} = \left(\frac{\varepsilon_\nu}{\bar{\varepsilon}_\nu}\right)^2 \frac{1 + e^{+3}}{1 + e^{3\,\varepsilon_\nu/\bar{\varepsilon}_\nu}} \simeq \left(\frac{\varepsilon_\nu}{\bar{\varepsilon}_\nu}\right)^2 e^{-3\left(\frac{\varepsilon_\nu}{\bar{\varepsilon}_\nu} - 1\right)} \qquad (1)$$

where $n(\varepsilon_\nu)$ is the number of particles per unit energy interval at energy ε_ν.

In summary, our hydrodynamic calculations indicate the existence of a prompt burst of neutrinos at the bounce of the core. For electron-type neutrinos the particle luminosity at peak is $\sim 10^{59}$ s^{-1}. The mu and tau neutrino luminosities are typically a factor of five below this. The most intense burst of ν_e lasts for a few tenths of a millisecond. It then levels off and decreases slowly over several milliseconds. The mu and tau neutrino emission is most intense for around one millisecond. Following this burst one can expect a sustained emission over time scales of seconds as trapped neutrinos diffuse out. The characteristics of the long term emission are discussed in R. Sawyer's contribution to these proceedings.

Figure 5

Neutrino particle emission $\mathcal{N}_\nu$ as a function of time. See text for discussion.

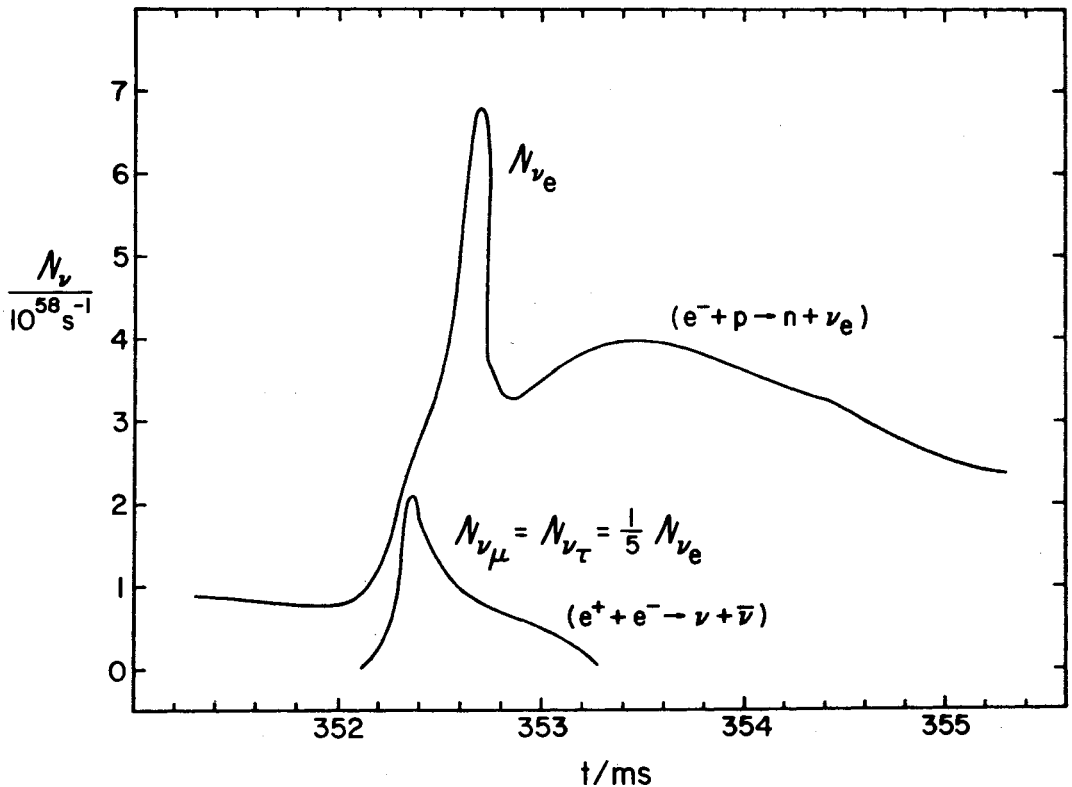

Figure 6

The mean escaping neutrino energy ϵ_ν as a function of time. See text for discussion.

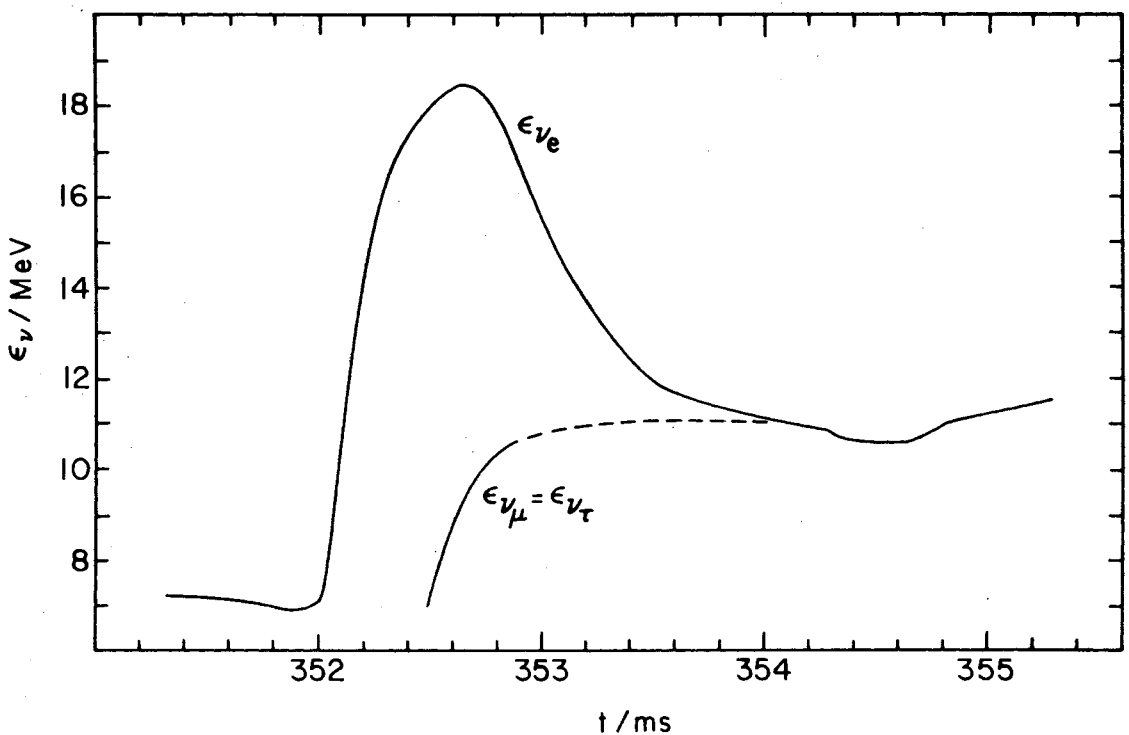

5. Discussion

We now summarize the features of stellar collapse which we think are well established. Then we discuss problems in theoretical work on stellar collapse which are still outstanding. Developments on these problems could change the picture presented above considerably. Finally, we speculate on the effects that neutrino oscillations may have on stellar collapse.

The structure of the inner core that collapses homologously is fairly well established in the absence of neutrino oscillations. Its mass M_h depends only weakly on the initial model for the collapse. Our various calculations have given masses in the range $.6 \leq M_h/M_\odot \leq .8$ and trapped lepton fractions in the range $.29 \leq X_\ell \leq .38$. The differences in results were most strongly dependent on rates of electron capture and neutrino opacities which were varied within reasonable limits. The entropy in the shocked envelope depends somewhat on the homologous inner core mass, but typically is in the range between 5 and 8.

Outstanding problems whose solution could change the results above include shock propagation, the equation of state above nuclear densities, and the subsequent evolution of the collapsed core through deleptonization. The use of pseudoviscosity to follow the propagation of shocks in numerical calculations is always troublesome. The shock is spread out unphysically over a few zones and the electron capture and neutrino transport are distorted. However, the results of the 100-zone model discussed above agree quite well with a computation that used one-fourth as many zones. Thus it's not obvious that finite zoning creates problems but more work in this area is necessary. The equation of state at and above nuclear densities is not very well known. Should it prove to differ significantly in stiffness, the nature of the core bounce could be different. And finally we need to know what occurs in the core as the leptons leak out. At present no detailed investigation of the core evolution during deleptonization exists.

Finally, let us speculate on the joker that may be dealt to the theory of stellar collapse by the existence of neutrino oscillations. First consider the case when the oscillation time scale is long relative to those of dynamic collapse. Here the trapped lepton fraction would not change. However, on longer times the oscillations would result in the presence of degenerate e, mu, and tau neutrinos of equal Fermi energies in beta equilibrium with the electrons. This would slightly lower the lepton degeneracies and decrease the proton fraction somewhat. However, the overall modification would be small.[20] Now lets consider the situation where the oscillation timescale is short relative to that of collapse. This is the case that is implied by present experiments.[21] Here the trapped lepton fraction could be appreciably affected since the oscillations could considerably increase the size of the low energy window[2,4] where neutrinos escape. If the trapped lepton fraction is decreased appreciably, the collapse may be more violent. The central density at core bounce and the shock structure could also be very different. At present the effects of such rapid oscillations on collapse are not known. An additional complication comes from the fact that vacuum oscillations can be suppressed[22] in dense matter. Thus even if neutrinos oscillate in vacuum this may have no implication for stellar collapse.

References and Footnotes

1) Results of hydrodynamic work on stellar collapse were discussed during the May 1980 meeting at the Institute for Theoretical Physics in Santa Barbara. Many of the researchers that are presently conducting hydrodynamic studies of collapse were present, including D. Arnett, S. Bludman, R. Buchler, S. Colgate, W. Hillebrandt, I. Lichtenstadt, T. Mazurek, K. Van Riper, and J. Wilson. A general consensus on the collapse to bounce and initial shock formation was apparent. However, there was no agreement on the question of final outcome. Whether or not the shock ejects matter to create a supernova is a question that has not been resolved at present.

2) T.J. Mazurek, Astrophys. Space Sci., 35, 117 (1975).

3) M.L. Alme and J.R. Wilson, Ap. J., 186, 1015 (1973).

4) W.D. Arnett, Ap. J., 218, 815 (1977); D.L. Tubbs, Ap. J. Suppl., 37, 287 (1978); and W.R. Yueh and J.R. Buchler, Ap. J. Lett., 211, L121 (1977).

5) D.L. Tubbs and D.N. Schramm, Ap. J., 201, 467 (1975).

6) H.A. Bethe, G.E. Brown, J. Applegate and J.M. Lattimer, Nucl. Phys., A324, 487 (1979).

7) G. Baym, H.A. Bethe, and C.J. Pethick, Nucl. Physics, A175, 225 (1971).

8) G. Baym, Presentation at the May 1980 meeting at the Institute for Theoretical Physics in Santa Barbara.

9) G. Fuller, Presentation at the May 1980 meeting at the Institute for Theoretical Physics in Santa Barbara.

10) W.D. Arnett, in Explosive Nuclear Synthesis, eds. D.N. Schramm and W.D. Arnett (University of Texas Press, Austin).

11) T. Weaver, G.B. Zimmerman, and S.E. Woosley, Ap.J., 225, 1021 (1978).

12) T.J. Mazurek, J.W. Truran, and A.G.W. Cameron, Astrophys. Space Sci., 27, 261 (1974).

13) See S. Colgate's contribution to these proceedings.

14) See the contribution of J.M. Lattimer and T.J. Mazurek to these Proceedings.

15) J.R. Wilson, Presentation at the May 1980 meeting at the Institute for Theoretical Physics in Santa Barbara.

16) D.A. Dicus, Phys. Rev., D6, 941 (1972).

17) E.W. Kolb and T.J. Mazurek, Ap. J., 234, 1085 (1979).

18) D.A. Dicus, E.W. Kolb, D.N. Schramm, and D.L. Tubbs, Ap. J., 210, 481 (1976).

19) T.J. Mazurek, in Neutrinos-78, ed. E.C. Fowler (Purdue Univ. Press, 1978).

20) T.J. Mazurek, in Neutrinos-79, eds. A. Haatuft and C. Jarlskog (Univ. of Bergen Press, 1979).

21. F. Reines, H.W. Sobel, and E. Pasierb, 1980 preprint.

22. L. Wolfenstein, Phys. Rev., D20, 2634 (1979).

STELLAR IMPLOSION SHOCKS AND CONVECTIVE OVERTURN*

J.M. Lattimer
Department of Earth and Space Sciences
State University of New York
Stony Brook, New York 11794

and

T.J. Mazurek
Department of Physics
State University of New York
Stony Brook, New York 11794

ABSTRACT

Rayleigh-Taylor overturn in stellar collapse is examined from a thermodynamic point of view. At sufficiently high entropies leptonic gradients alone cannot give instability. The characteristics of shocks in the infalling envelope are examined. For shock strengths that are typical of current hydrodynamic calculations the entropy is sufficiently high to prevent large-scale overturn of the entire core. In addition, the condition of beta equilibrium at lower densities and entropies insures a stable lepton gradient. Thus overturn powered solely by lepton gradients must be limited to the dense shocked mantle of the collapsed core. This suggests that lepton-overturn may not be able to induce stellar explosions, and that the enhancement of neutrino emission due to convection is not likely to be dramatic.

I. Introduction

The core overturn mechanism for supernovae suggested by Colgate and Petscheck[1] has important implications for the expected neutrino emission from stellar collapse, if it can occur. In their model, lepton gradients destabilize the collapsed core leading to global overturn and a dredging up of neutrinos from the very center of the core to its surface. This release of trapped neutrinos increases dramatically the stress that they exert or the in-falling matter, and under favorable circumstances can lead to an explosion.[2] In the process, the dredged up neutrinos escape on dynamic time scales of milliseconds giving a burst that is enhanced considerably over that expected in the absence of core overturn. These significant theoretical and observational consequences of core overturn make it of paramount importance to determine if it indeed can occur during stellar collapse.

The basis of the instability is discussed by Epstein.[3] He notes that lepton gradients which are sufficient to give Rayleigh-Taylor instability can form during stellar collapse. Thus energy transport need not be restricted solely to the diffusion mode but may also occur via convective overturn. Presently, Wilson[4] includes a local approximation to the convective transport in his numerical calculations and finds that it has little effect due to the

*Supported in part by USDOE (Contracts DE-AC02-80ER10719 and DE-AC02-76ER13001).

fact that the convection is self-limiting. It mainly acts to smooth out destabilizing gradients. However, Colgate and Petscheck[1] argue that the local approximation to convective overturn breaks down since the core is unstable globally. Numerical calculations supporting the latter view are presented by Livio, Buchler, and Colgate.[5] A recent fillip has been added by a similar numerical study performed by Smarr, Wilson, Barton, and Bowers.[6] They find that convection does not penetrate the core but is limited to the outer mantle. Thus at present there is no agreement on the form of convective overturn that would occur in the presence of destabilizing lepton gradients.

Some ambiguity in the results is unavoidable due to the simplifications that must be made to simulate the little understood process of convection. To the extent that the discrepancy of results arises from numerical modelling, it will not be resolved readily. However, the question of stability against overturn is independent of the details of the convective process. A given equation of state determines uniquely the stability or instability of a particular stellar configuration. Thus one may hope to deleneate in a model independent way between stable and unstable situations. Once this is done the modelling dependent problems can be addressed.

In his contribution to this DUMAND conference Sterling Colgate gives an excellent review of the implications and problems of convective overturn as well as the question of initial Rayleigh-Taylor instability. We are studying the latter question with the equation of state due to L^2PR.[7] In this contribution we present some detailed numerical results on the question of lepton-driven instability to compliment Colgate's discussion on this point. In addition, we are studying the properties of shocks in the mantle of the collapsed core. The post-shock entropy is determined by the fluid velocity difference across the shock front and the Ronkine-Hugoniot equations. Our results show that the entropy increase due to shocks for the velocity differences that are typically obtained in hydrodynamic calculations are sufficiently large to prevent core penetration by convection. Neutrino cooling cannot remove this shock entropy on dynamic time scales. Thus convection is limited to the shocked mantle.

2. Criteria for Convective Instability

Standard linear stability theory[3,5] can be used to test for the occurence of convective overturn. The testing procedure displaces a fluid element in the stellar structure under consideration while keeping it isolated and in pressure equilibrium with its surroundings. The density contrast between the fluid element and the ambient medium then determines stability. Note that this approach is valid only in regions where the neutrinos are either strongly trapped or nonexistent. In regions where neutrinos can transport energy readily between the fluid element and its surroundings the assumption of an isolated displacement breaks down. However, for simplicity such complications are ignored.

The criterion for instability can be expressed in terms of the parameter

$$a \equiv \rho^{-1}\left[\left(\frac{dp}{dr}\right)_o - \left(\frac{dp}{dr}\right)_{iso}\right] = -\rho^{-1}\left(\frac{dp}{dp}\right)_{iso}\left\{\left(\frac{\partial p}{\partial s}\right)_{\rho,X_\ell}\left(\frac{ds}{dr}\right)_o + \left(\frac{\partial p}{\partial X_\ell}\right)_{s,p}\left(\frac{dX_\ell}{dr}\right)_o\right\}, \tag{1}$$

where ρ is the density, r the radius, p the pressure, s the entropy per baryon in units of Boltzmann's constant k, X_ℓ the lepton fraction per nucleon, and the subscript o refers to the ambient medium while iso refers to the variation due to the isolated displacement. The right-most expression is obtained by the use of pressure equilibrium between the fluid element and its surroundings, and expansion of dp/dr in terms of the independent variables ρ, s, and X_ℓ. The condition for instability is given by a > o. Equation (1) can be put in the more useful form

$$a = -\rho^{-1} \left(\frac{d\rho}{dp}\right)_{iso} \left(\frac{dp}{ds}\right)_{\rho,X_\ell} \left(\frac{dX_\ell}{dr}\right)_o \left\{ \left(\frac{ds}{dX_\ell}\right)_o - \left(\frac{\partial s}{\partial X_\ell}\right)_{\rho,p} \right\} , \qquad (2)$$

via the identity $(\partial s/\partial X_\ell)_{\rho,p} = -(\partial p/\partial X_\ell)_{\rho,s}/(\partial p/\partial s)_{\rho,X_\ell}$. The first term in the curly brackets represents the effects of entropy gradients. While in principle it may also drive convective overturn, typical results of hydrodynamic calculations indicate that entropy increases with radius. Hence in practice this term tends to stabilize the core against convective overturn. The lepton gradient effects are contained in the last term in the curly brackets. In the usual case in which a lepton-induced instability develops $(dX_\ell/dr)_o<0$. Since $(d\rho/dp)$ iso $(dp/ds)_{\rho,X_\ell}>0$, lepton-driven convection is possible only if $(\partial s/\partial X_\ell)_{\rho,p}<0$.

Using the L^2PR equation of state, we have computed isobars in the (s,X_ℓ) plane at various fixed densities. Our results are shown in Fig. 1. It is seen that the $s(X_\ell,p_o,\rho_o)$ curves cease to be monotonic at some minimum entropy and a region with $(\partial s/\partial X_\ell)_{\rho,p} > o$ developes. The regions where this occurs are shaded in the figure. From our previous discussion, convective overturn cannot be driven by lepton gradients in these areas.

These areas of stability against leptonic convection occur only in regions with essentially pure nucleonic composition. We have shown from the equation of state of such a gas that $(\partial s/\partial X_\ell)_{\rho,p}>0$. We will make further use of this figure to discuss the possibility of large-scale overturn of the entire core in Section 4 below. Since the shock entropy enters in a critical way we will first require the results of the following section on shocks.

It should be noted that Figure 1 can be used to test the stability of any given model against convection. To do this, one plots the model's $s(X_\ell)$ trajectory in one of the constant density diagrams. The model is unstable if the regions at lower (higher) densities than that of the diagram have lower (higher) pressures than the region at the density of the diagram.

3. Shocks and Entropy

Convective instability in general depends on both entropy and lepton gradients. Hydrodynamic calculations show that during collapse the entropy is uniform over $\sim .7M_\odot$ of the core which implodes homologously. The entropy in this region is low, being below ~ 2. At the point where the shock forms, a steeply increasing entropy gradient with radius results. This tends to stabilize the central regions against convective overturn. The details of shock propagation in the infalling matter determine the entropy profile in the cores mantle. This mantle has two distinct regions, i.e., one that is opaque

Figure 1

Isobars in the entropy-lepton fraction plane for various densities. The dashed line in each figure indicates the boundary between pure nucleon and nuclear statistical equilibrium matter with appreciable heavy elements (defined by the composition being 90% free nucleons). Regions where lepton gradients cannot drive convective overturn are shaded in. See text for discussion.

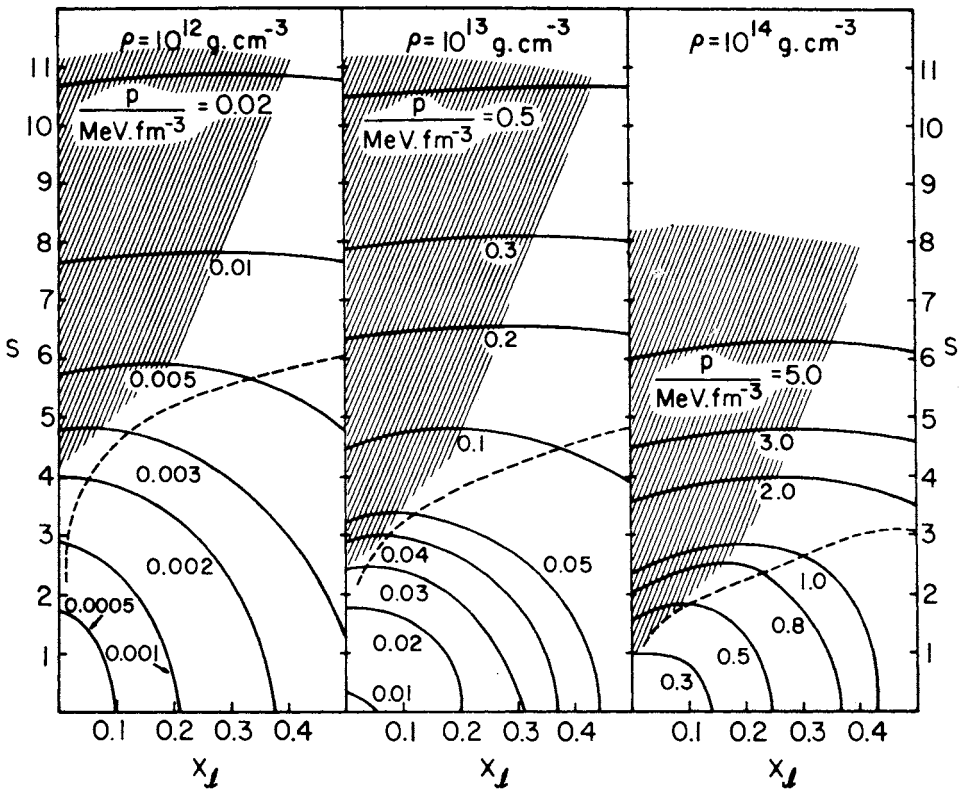

to neutrinos and one that is transparent. In the opaque regions the leptons are trapped. Assuming that beta equilibrium obtains, one can solve the Rankine-Hugoniot relations to determine the post-shock characteristics as a function of the velocity difference across the shock. In regions transparent to neutrinos the problem becomes more complex since lepton number need not be conserved across the front. However, we will see below in Section 4 that at low entropies (the prerequisite for lepton-driven convection) the requirement of beta equilibrium establishes a lower limit to the electron fraction. This limit is not much different from the pre-shock lepton fraction at densities below $\sim 10^{11}$g cm^{-3}. Thus the escape of neutrinos would have little effect on the shock. Such is not the case at high entropies where the electron fraction can drop to very low values. However, we see from Figure 1 that at high entropies the pressure dependence on lepton number is minimal.

The Rankine-Hugoniot relations[8] can be reduced to

$$\frac{\sigma_o}{2}\left(\frac{p}{p_o} - 1\right)\left(1 - \frac{\rho_o}{\rho}\right) = \alpha \ , \tag{3}$$

$$e - e_o = \frac{\sigma_o}{2}\left(\frac{p}{p_o} + 1\right)\left(1 - \frac{\rho_o}{\rho}\right) \ , \tag{4}$$

$$\alpha = \frac{1}{2} N_o^{-1} (u-u_o)^2 \ , \text{ and } \sigma_o = N_o^{-1} p_o \rho_o^{-1} \ , \tag{5}$$

where e is the specific energy per baryon, u is the matter velocity, the subscript o indicates the preshock conditions, and N_o is Avergado's number. We have solved equations (3) and (4) for the post-shock conditions as a function of α using the L^{2}PR equation of state. Our results are shown in Fig. 2 for the typical trapped lepton number of 0.3 and preshock entropy of 1.

The figure gives the variation of the post-shock entropy as a function of ρ/ρ_o for various values of the preshock density. Curves of constant α are superposed on the entropy plots. Thus for a given α and ρ_o one can determine the post-shock entropy from Fig. 2. The similarity of the entropy curves as a function of ρ/ρ_o for different initial densities suggests that the increase in entropy is only a function of ρ/ρ_o. It can be shown on the basis of a simplified equation of state that ρ/ρ_o is only a function of α/σ_o, and hence so in the entropy. Indeed, numerical fitting of the detailed results gives the following rough relation

$$\Delta s = s - s_o \overset{\sim}{=} \frac{1}{2}\frac{\alpha}{\sigma_o} \ . \tag{6}$$

The implications of these results for the problem of convective overturn are discussed in the next session.

4. Implications

Let us first examine the shock propagation in the infalling envelope. The shock forms outside the central core that collapses subsonically. This means that the infall velocities must exceed sound speed. The results of various numerical studies show that the ratio of this infall velocity to the sound speed c_o is in the range $2.0 \lesssim u_o/c_o \lesssim 3.0$. Typical post-shock expansion velocities tend to be around 50% of those of infall. Thus one has $3 \lesssim (u-u_o)/c_o \lesssim 4.5$. Since the relativistic leptons dominate the pressure,

Figure 2

The post-shock entropy as a function of density enhancement across the shock for various initial densities (solid lines) with an initial entropy of unity and lepton fraction of 0.3. Curves of constant values of the square of the velocity difference across the shock divided by Avogodro's number, or α, are given by dashed lines. See text for discussion.

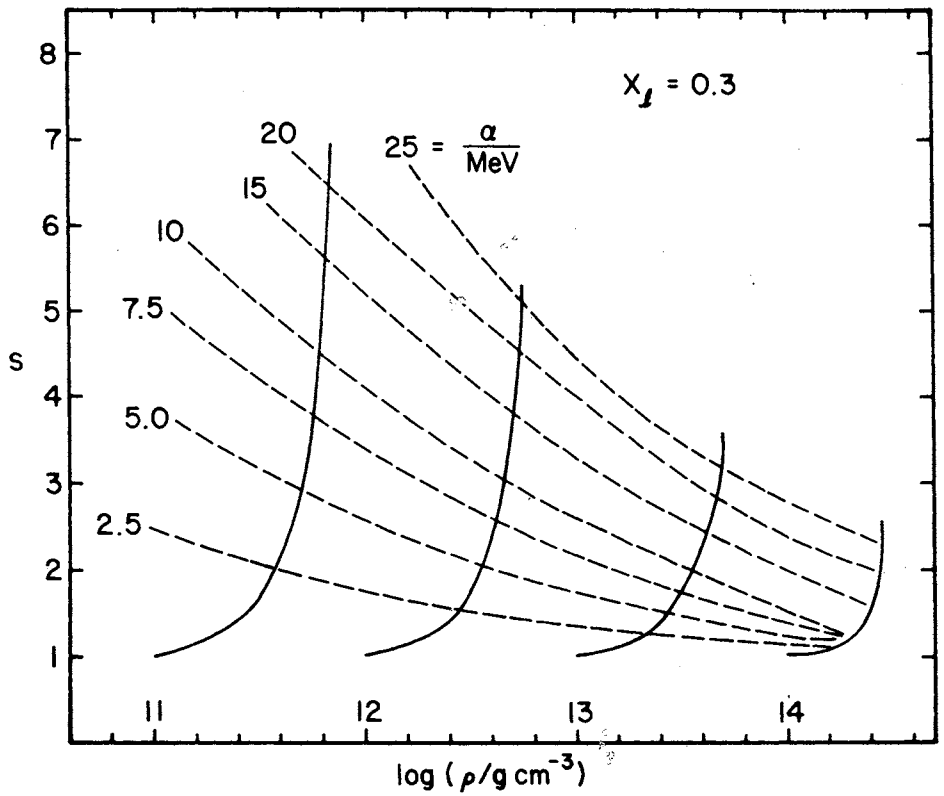

$c_o^2 = (4/3)\sigma N_o$. Hence, an entropy increase in the range $3 \lesssim \Delta s \lesssim 7$ is indicated by equation (6). This means that the entropies in the shocked mantle will lie in the range $4 \lesssim s \lesssim 8$.

Let us now consider the possibility of core penetration by fluid elements from the shocked envelope. The unshocked core[9] has an entropy that is below 2 and a trapped lepton fraction around .35. Essentially all of the cool core lies at densities above 10^{14}g cm^{-3}. Using Fig. 1, one sees that any fluid element that reaches this density from the shocked envelope ($s \gtrsim 4$) has a pressure much above the ambient one, and it must therefore rise due to its bouyancy. This means that the central core must be stable against convective overturn for as long as the entropies in the shocked mantle do not drop appreciably below their initial values.

The next question that one needs to answer is how long does it take to cool the mantle to the entropies of the core. The maximum rate of cooling occurs in regions where the matter is just becoming transparent to neutrinos at densities around 10^{12}g cm^{-3}. At an entropy of 4, the temperature in the matter is around 3 MeV for this density. To get to an entropy of ~ 2, the temperature must be reduced by around a factor of two. One can ask what is the time scale required to accomplish this. If heavy elements are present, the most rapid production of neutrinos occurs via de-excitation of high energy states.[10] In reality, at $s \sim 4$ the heavy element mass fraction is below 0.1. However a lower limit to the cooling time is obtained by assuming the matter to be purely heavies. The cooling rate[10] per gram is

$$\varepsilon_{\nu\nu} \simeq 5\times10^{13}\ A^{-1}\left[3.4\ \left(\frac{kT}{MeV}\right) - 2.3\right]^7 \text{ erg g}^{-1}\text{s}^{-1}\ , \qquad (7)$$

where we have taken the nuclear Fermi energy to be 36 MeV. The time required to reduce the temperature by a factor of two is thus

$$t_{cool} > \frac{3}{4}\frac{N_o kT}{A\,\varepsilon_{\nu\nu}} \simeq 23 \text{ ms}. \qquad (8)$$

This absolute lower limit for cooling is already about a factor of 4 greater than the dynamic time of shock propagation into the envelope. A more careful analysis shows that at entropies around 4, the heavy element abundance is less than 10% by mass. Thus a factor < 0.1 is introduced in the cooling rates, while the factor of A^{-1} in the energy constant is replaced by a number > 0.9 due to the dominance of nucleons in the composition. This increases the cooling time by a factor of ~ 500 for $A \sim 50$. Thus the required cooling times are of the order of thousands of milliseconds. This shows that core overturn is not possible on dynamic times. In addition, for time scales of the order of a second the trapped leptons in the core will have time to leak out. We believe that this will result in heating[11] the outer mantle; however, detailed evolutionary calculations are needed to determine whether the diffusive heating or neutrino pair cooling dominates.

The above considerations show that at least initially any convective overturn is restricted to the shocked mantle. We now point out another restriction on lepton convection at low densities for the case of weak shocks. Let's for the moment assume that beta equilibrium is maintained, giving the condition $\mu_n - \mu_p = \mu_e - \mu_\nu$. Now in the transparent regions the neutrinos will

escape without establishing thermal equilibrium. However, there is no mechanism for generating an excess of antineutrinos, and one has the condition $\mu_\nu \geq 0$. Thus for any given density and entropy a lower limit to the lepton fraction is obtained with the usual beta equilibrium condition assumed for neutron stars ($\mu_\nu = 0$). This should be valid over long timescales ($\sim$100 ms).

We have computed the lepton fraction that result using the L^2PR equation of state. The results are shown in Fig. 3, where contours of constant X_ℓ are plotted in the (ρ,T) plane (solid lines). Contours of constant s are also shown (dashed lines). At entropies below unity essentially all of the matter is in the form of nuclei and dripped neutrons. The electron fraction is determined by exactly the same considerations as those used in the theory of cold neutron stars, i.e., a sea of degenerate electrons is required to prevent the decay of the neutron-rich nuclei. For higher entropies more neutrons drip out of nuclei. This decreases the electron Fermi energy that is required to prevent beta decay. Consequently, the electron fraction decreases with increasing entropy. This does not continue indefinitely. At sufficiently high temperatures lepton pairs appear and μ_e/kT and $\mu_\nu/kT \to 0$. The nucleons form a Boltzmann gas so $(\mu_e-\mu_\nu)/kT = (\mu_n-\mu_p)/kT = \ell n(X_n/X_p) \to 0$. Thus $X_e \to 0.5$ and there must be an absolute minimum to X_e as a function of s for any density.

Now let us consider lepton gradients for the case of neutral entropy gradients (ds/dr = 0). Leptonic driven convection is most effective only at low entropies around 3. Fig. 3 shows that for matter at this entropy, X_e must increase with decreasing density along an adiabat for regions with densities below 10^{12}g cm^{-3}. These regions therefore are stable against convective overturn due to lepton gradients. Thus at low shock entropies leptonic convection is restricted to dense mantle regions between 10^{12}g cm^{-3} and 10^{14}g cm^{-3}. As the shock entropy goes up the lower end of this density range can be expanded. At s $\sim$ 10 it drops to $\sim 10^9$g cm^{-3}. However, at such high entropies the dependence of the pressure or lepton fraction becomes negligible (cf. Fig. 1), and leptonic convection must become inefficient. We thus conclude that the most efficient leptonic convection is restricted to the opaque regions of the shocked mantle, even at late times.

These considerations lead to some caveats on the possibility of mass ejection due to neutrino release from lepton-induced overturn. Bruenn, et al.[12] show that under very favorable circumstances lepton overturn can give mass ejection. Generally, they find that convective mixing must proceed far beyond the regions of neutrino trapping for an explosion to occur. In cases where they restrict mixing to the trapped regions no explosion results. However, our results above show that much of the transparent regions must be stable against convective overturn powered by lepton gradients. The required mixing for explosion cannot be motivated physically on the basis of lepton gradients, and if it is to occur it must be driven by gradients in entropy.

In closing, we summarize the salient results of our analysis of lepton driven overturn, based primarily on the features of the L^2PR equation of state. The efficiency of leptonic convection depends critically on the post-shock entropy:

Figure 3

Characteristics of beta equilibrium with $\mu_\nu = 0$. The solid lines indicate curves of constant X_e. The dashed curves give contours of constant entropy. See text for discussion.

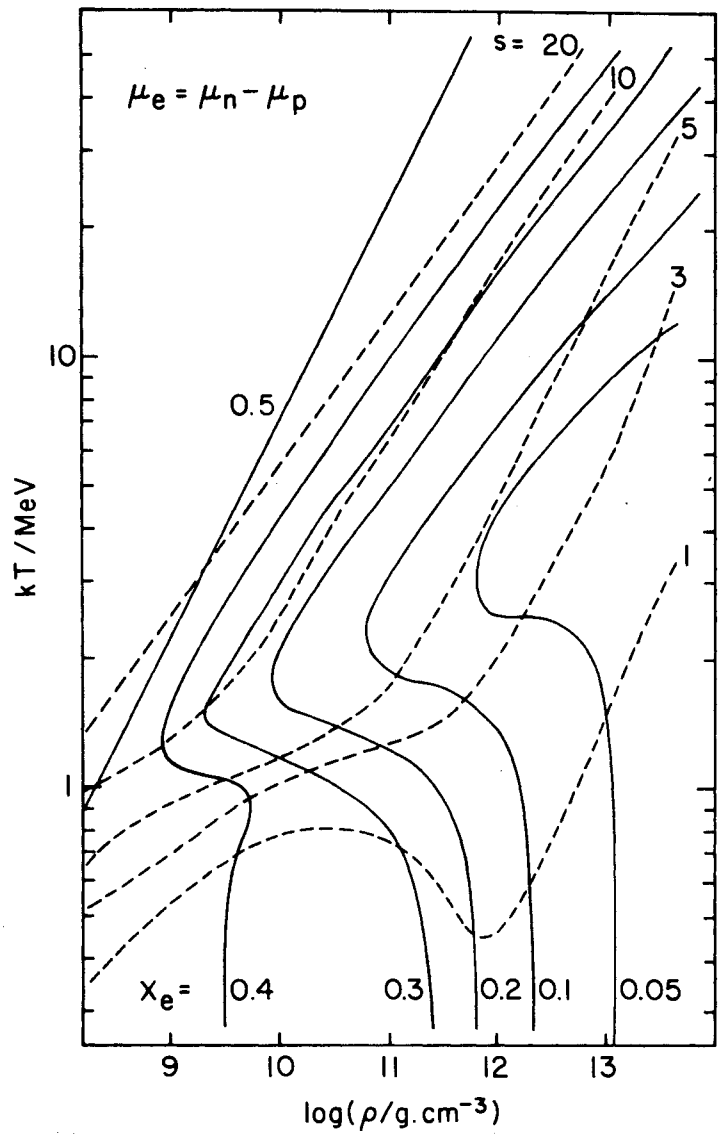

i) $s \gtrsim 6$ - Lepton gradients cannot drive convection since their effects on pressure variations are minor.
- For convective overturn to be possible the entropy gradient must be negative.

ii) $s \gtrsim 3$ - Core penetration cannot be mediated by lepton depletion in the mantle.

Current hydrodynamic work indicates that $s > 3$ is likely for the post-shock material. Furthermore, cooling times for the shocked material are of order seconds. Thus global core overturn cannot occur on dynamic times of several milliseconds. Leptonic convection is restricted to the dense mantle regions around 10^{12}g cm^{-3} to 10^{14}g cm^{-3}. These results imply that any enhancement of the neutrino emission due to convective overturn is not likely to be dramatic.

References

1. See S.A. Colgate's contribution to these proceedings; and S.A. Colgate and A.G. Petscheck, 1979 Los Alamos preprint.

2. S.W. Bruenn, J.R. Buchler, and M. Livio, Ap. J. Lett., 234, L183 (1979).

3. R.I. Epstein, M.N.R.A.S., 188, 305 (1979).

4. J.R. Wilson, Proceedings of the 9th Texas Symposium on Relativistic Astrophysics, Ann. N.Y. Acad. Sci., in press.

5. M. Livio, J.R. Buchler, and S.A. Colgate, 1979 Los Alamos preprint.

6. L. Smarr, J.R. Wilson, R. Barton, and R. Bowers, 1980 preprint.

7. D.Q. Lamb, J.M. Lattimer, C.J. Pethick, and D.G. Ravenhall, Phys. Rev. Lett., 41, 1623 (1978).

8. See for example, Ya. B. Zel'dovich and Yu. P. Raizer, Physics of Shock Waves and High-Temperature Hydrodynamics (1966, Adademic Press, New York).

9. H.A. Bethe, G.E. Brown, J. Applegate, and J.M. Lattimer, Nucl. Phys., A324, 487 (1979) see also the contribution of J. Cooperstein and T.J. Mazurek to these proceedings.

10. E.W. Kolb and T.J. Mazurek, Ap. J., 234, 1085 (1979).

11. J.M. Lattimer and T.J. Mazurek, B.A.A.S., 12, 439 (1980); T.J. Mazurek, in Proceedings of Neutrino 79, eds. A. Haatuft and C. Jarlskog (University of Bergen Press, Bergen).

12. S.W. Bruenn, J.R. Buchler, and M. Livio, Ap. J. Lett., 234, L183 (1979).

Magnetohydrodynamic Origin of Crab Nebula Radiation

C. F. Kennel[1], [2], [3]

F. S. Fujimura[1]

(1) Department of Physics, University of California
Los Angeles, CA 90024

(2) Institute of Geophysics and Planetary Physics,
UCLA

(3) Center for Plasma Physics and Fusion Engineering

Abstract

We review our efforts to construct a self-consistent model that relates pair production near the Crab pulsar to a relativistic wind outflow. The nebular radiation is observable only beyond a confining fast magnetohydrodynamic shock. We recently made two improvements in the model. (1) We found that the hot relativistic wind has asymptotic properties quite distinct from the classical cold wind model, (2) We integrated the Rankine-Hugoniot relation for highly magnetized shocks. Using these two new pieces of information, we find that outer gap pair production can account for the nebular radiation, but a polar gap model cannot. The nebular optical radiation can be generated by the post shock thermalized flow. If extremely energetic particles are accelerated at the shock, the MHD model can account quantitatively for the dependence upon photon energy of the apparent size of the x-ray nebula.

1. Introduction

The Crab nebula emits a spectrum of photons that extends from radio frequencies to gamma ray energies. The photons from RF to at least ten keV are polarized, and are therefore generated by the synchrotron radiation of highly relativistic electrons and or positrons in the nebular magnetic field. Both phenomenological and theoretical estimates place the nebular magnetic field strength in the range 10^{-3} - 10^{-4} Gauss. If so the Lorentz factors of the particles generating 10 keV photons are 2.5×10^7 and their synchrotron lifetime is comparable to the light propagation time across the nebula. Thus the energy of the particles producing the synchrotron radiation must be replenished. The observed lengthening of the Crab pulsar period yields a rotational energy loss rate that equals the sum of the nebular photon energy plus expansion energy loss rates, assuming the pulsar is a rotating neutron star.

The discovery of the Crab pulsar solved the problem of the nebular energy source. When Goldreich and Julian (1969) argued that rotating magnetized neutron stars could field emit charged particles, it became clear that the pulsar could also inject new particles in the nebula. And when Pacini (1967, 1968) suggested that rotating magnetized neutron stars radiated an electromagnetic wave, it appeared that the pulsar could also account for the nebular magnetic field. A self-consistent model that links the Crab pulsar to the particles and magnetic field in the nebula has therefore been an ambition of theoretical astrophysics since the discovery of the pulsar (Shklovsky, 1970).

This paper reports recent progress in making more quantitative the following nebular model. The pair production discharge models, originally suggested by Sturrock (1971) and Ruderman and Sutherland (1975) and since refined by many authors, estimate the number flux and mean energy of the positronic plasma injected by the pulsar into its exterior magnetosphere. This plasma is too dense to support a plasma wave of relativistic amplitude (Kennel, et al., 1973; Kennel, et al., 1979), and dense enough to use the magnetohydrodynamic approximation. The exterior magnetosphere is the relativistic wind first proposed for pulsars by Michel (1969). Knowledge of the pulsar plasma sources and magnetic field permits estimates of the parameters that scale the asymptotic properties of the wind (Kennel et al., 1979). The wind is confined by a fast MHD shock which stands where the wind dynamic pressure, given by the pulsar energy loss rate, equals the static pressure of the nebula, given from observations (Rees and Gunn, 1974). The wind is decelerated and heated by the shock. The observable nebular radiation is produced somewhat beyond the shock where the wind is further decelerated to non-relativistic speeds, and the absence of relativistic beaming renders the pattern of radiation emitted from a moving element of plasma more isotropic in the observer's frame of reference. The observed properties of the nebular synchrotron radiation can therefore be linked in principle to those of the pulsar pair production source.

Recent optical photopolarimetry studies of the portions of the Crab nebula immediately surrounding the pulsar (Schmidt, et al., 1979) support the above theoretical orientation. Baade (1942) had noticed a "hole" in the optical luminosity surrounding the point where the 1054 supernova occurred, and near where the pulsar is now known to exist. When foreground and background luminosity are removed, Schmidt, et al., find essentially zero radiation coming from the hole. The underluminous zone ends at a distance of 3×10^{17} cm from the pulsar. Most of the nebular optical radiation comes from a shell surround-

ing the pulsar. Polarization measurements reveal that the magnetic field in the shell is highly ordered and wound into a toroidal shape centered on the pulsar. Scargle's (1969) wisps, localized regions of enhanced synchrotron emission that vary on the time scale for light to traverse the hole, lie near the inner boundary of the shell. Much of the above is qualitatively consistent with a wind model. Radiation from the relativistic wind zone would be strongly forward shifted and therefore be observable only along the line of sight to the pulsar. It would be difficult to disentangle from a steady pulsar component. The underluminous zone does end where a shock is expected to stand. The toroidal magnetic field characteristic of winds should be preserved as the outflowing plasma traverses the shock. Radiation should be observable from regions where the decelerating post shock flow is non-relativistic.

Six calculations must be assembled to relate the nebular radiation to the pulsar. We must:

(1) Calculate the initial flow 4-speed and thermal energy density using pair production models
(2) Given the pulsar magnetic field and particle source, calculate the wind 4-speed and magnetic field at large distances from the pulsar
(3) Calculate the position of the shock using pressure balance arguments
(4) Given the position of the shock, calculate the flow 4-speed, density, temperature, and magnetic field immediately downstream, using the relativistic Rankine Hugoniot relations
(5) Calculate the radial dependence of the flow well downstream from the shock
(6) Calculate the synchrotron radiation from the downstream flow region.

The literature contains inconsistences concerning steps (2), (4), (5), (6). Since the flow expands enormously beyond the light cylinder, it will cool, and it has been thought that a zero-temperature approximation provides an adequate description of pulsar winds. Yet a cold wind has an asymptotic fast Mach number of unity,and less than unity elsewhere (Michel, 1969); consequently no fast MHD shock can stand in such a flow. Rees and Gunn (1974) argued that the pulsar provides the nebula with its magnetic field, yet they assumed the shock was essentially hydrodynamic. For pair-production winds, the asymptotic magnetic energy density exceeds the flow energy density. The flow downstream of a highly magnetized fast shock can remain relativistic, and so radiation emitted by the thermalized plasma downstream could remain difficult to observe, in contrast with hydrodynamic shocks.

We will review the impact of our recent repairs to steps (2) and (4) upon the self-consistent nebular model. We will find that polar gap pair production cannot account for the nebular radiation whereas "outer-gap" pair production can. The thermalized flow downstream of the shock can account for the nebular optical radiation. Moreover we can calculate the radiation from a highly energetic electron or positron convected in the downstream flow, and predict the observed weak dependence on x-ray energy of the apparent angular size of the nebula.

2) Pair Production Plasma Sources

2.1) Polar Gaps

Field-aligned currents are a necessary part of the coupling of the pulsar

to its exterior magnetosphere. In the absence of pair production, the carriers of field aligned currents can be provided by field emission from the neutron star surface (Goldreich and Julian, 1969), of electrons or ions depending upon the sign of the parallel electric field generated by the rotating magnetic field of the pulsar. In either case, the parallel electric field at the surface should adjust to produce an emission current consistent with the coupling to the exterior magnetosphere. However, since the parallel electric field required for ion emission is very large, a question remains pulsar polar caps can field-emit ions.

Sturrock (1971) pointed out that pulsars can find an easier way to carry the current. About 10^6 galactic γ rays fall on the polar cap each second (Ruderman and Sutherland, 1975). These photons can produce pairs in a strong magnetic field (Erber, 1966). The ambient parallel electric field accelerates one particle toward the star, the other away; the one accelerated away soon radiates photons because it follows a curved field line. The question is, can the curvature photons produce more pairs? If so, a cascade takes place, the plasma density increases, and the potential drop diminishes. Since the secondary pairs share the momentum of the outgoing curvature photon, they will all be created moving outward, and many could escape. This suggests that a positronic plasma may flow outwards from a polar cap sheath on open field lines that connect to the exterior wind zone. The outgoing plasma would have a field aligned pitch angle distribution, since energy in motion perpendicular to the magnetic field immediately disappears into synchrotron radiation.

Regions of the polar cap required by self-consistency to emit ions could solve their current starvation problems by producing pairs in unsteady spark discharges. Ruderman and Sutherland (1975) considered the unsteady discharges that short out the vacuum electric field in a "gap" that forms when the surface is unable to field emit ions. After a spark, the vacuum gap thickness h grows until it again reaches the mean free path for Erber pair production, at which point the spark strikes again. As the pulsar spins down, h must increase to maintain the potential drop to produce pairs. When h increases to about the radius of the polar cap, pair production should cease. Since coherent radio emission probably requires the presence of a moderately dense plasma, pair production threshold corresponds to the cut off of coherent radio pulses. The distribution of old pulsars has a cut off consistent with the calculated pair production threshold (Kennel, et al,, 1979).

It is possible to estimate some properties of the positronic plasma created near the magnetic poles. Kennel, et al., (1979) relate the polar gap pair production threshold function E to a pulsar's period P and period derivative $\dot{P}$:

$$E = 2.5 \times 10^{14} \dot{P} P^{-2.75} I_{44} (a_6)^{-5/6} \qquad (1)$$

where P is in seconds, $\dot{P}$ in sec/sec. I_{44} is the neutron star moment of inertia in units of 10^{44} gm-cm^{-2} and a_6 its radius in units of 10^6 cm. $E = 1$ defines pair production threshold; for the Crab $E \simeq 6 \times 10^7$. The ratio of the total energy loss rate, $\dot{W}_{TOT}$, $\simeq 5 \times 10^{38}$ ergs/sec, to the total energy invested in cresting pairs $\dot{W}_{PAIRS}$ is, for the Crab pulsar

$$\sigma = \frac{\dot{W}_{TOT}}{\dot{W}_{PAIRS}} \simeq 2 \times 10^4 \qquad (2)$$

$\dot{W}_{PAIRS}$, an all-important initial condition for the pulsar wind, may be written in the form

$$\dot{W}_{PAIRS} = J\,\gamma_*\,\mu_* \tag{3}$$

when J is the total number flux, γ_* is the Lorentz factor of the flow exiting the production zone, and μ_* is the specific enthalpy

$$\mu_* = \left(1 + \frac{\Gamma}{\Gamma-1}\,T_*\right) mc^2 \tag{4}$$

where T_* is the temperature in units of mc^2 and Γ is an effective adiabatic index.

How $\dot{W}_{PAIRS}$ is apportioned between J, μ_*, and γ_* depends on how many generations of pairs are produced and how much energy they lose to synchrotron radiation, factors difficult to estimate. $\gamma_*\mu_*$ can be bounded as follows. If hardly any pairs were produced the entire current threading the polar cap could be carried by a beam of primary particles that traverse the entire potential drop of the gap and acquire an energy $\gamma_p mc^2$; for the Crab, $\gamma_p \simeq 10^7$. In this condition, the number flux has the minimum value J_{GJ} necessary to carry the current required to produce the observed spin-down

$$J_{GJ} \simeq \frac{\Omega B}{2\pi e}\,Apc \tag{5}$$

where Ω is the spin frequency, B is the polar surface magnetic field, e the electronic charge in esu, and Apc is the area of the polar cap. With $B \simeq 10^{12}$, and $\Omega = 190$ r/s, $J_{GJ} \simeq 2 \times 10^{33}$ particles/sec

$E^{4/7}$ When pairs are produced, J must exceed J_{GJ}. Nonetheless, the value of calculated from the observed P and $\dot{P}$ constrains $\dot{W}_{PAIRS}$. Thus

$$\left(J/J_{GJ}\right)\left(\frac{\gamma_*\,\mu_*}{mc^2}\right) \lesssim \gamma_p \simeq 10^7 \tag{6}$$

The parameters σ and $\gamma_*\mu_*$ specify a wind solution in the exterior magnetosphere. Thus if polar gap pair production provided all the plasma for the relativistic wind leaving the pulsar, we would know that the wind σ would be $\simeq 2 \times 10^4$, and we would guess that $J \simeq 10^{3-4} J_{GJ}$ and therefore that $\gamma_*\mu_* \simeq 10^{3-4} mc^2$. We would also guess that some primaries, with $\gamma_p \simeq 10^7$, would escape as well.

2.2) Outer gap

Although E = 1 produces a pulsar threshold consistent with the observed distribution of P and $\dot{P}$ of old pulsars, other possibly more efficient pair production mechanisms with higher thresholds could operate in the Crab and other young pulsars. The entire question of pair production in pulsar magnetospheres has been thoroughly reviewed by Arons (1979). We will extract the simple estimates we need from the outer gap model discussed by Cheng et al (1976) and extended specifically to the Crab pulsar by Cheng and Ruderman (1977).

The existence of outer gaps well away from neutron star polar caps was first proposed by Holloway (1973). The charge density in a corotating magneto-

sphere is approximately

$$\rho_{GJ} \simeq - \frac{\vec{\Omega}.\vec{B}}{2\pi c} \tag{7}$$

If the rotation and dipole axes are misaligned, there are open field lines which intersect the surface $\vec{\Omega}.\vec{B} = 0$ within the light cylinder. These must carry a field-aligned currents that connect the neutron star to its exterior magnetosphere. Outflow of charge through the light cylinder then depletes the charge density near $\vec{\Omega}.\vec{B} = 0$ point on a field line. A large parallel electric field then accelerates particles of opposite sign charge from the $\vec{\Omega}.\vec{B} = 0$ surface towards the star. Very large potentials develop across the resulting gap. Pairs are again produced by curvature radiation from the escaping primaries. Because the outer gap is larger than the polar gap, its potential can be larger. Furthermore, because the outgoing pairs are produced in a much weaker magnetic field, they are more likely to retain their initial energies in the face of synchrotron losses.

The particle production rate in outer gaps is difficult to relate to the observed pulsar periods and their derivatives, because the location of the gap depends on the unknown obliquity of the dipole to spin axis and is in the outer magnetosphere where the magnetic field is distorted. Cheng and Ruderman (1977) use a detailed study of the Crab pulses to estimate that about 10% of the total energy loss rate is invested in outer gap pairs. These have an initial flow Lorentz factor of at least 300 and a perpendicular (thermal) γ of about 3×10^4. Thus, if such an outer gap supplies plasma to the exterior wind, the wind would have $\sigma \simeq 10\text{-}20$ and $\gamma_* \mu_* = 10^7\ mc^2$.

3) Relativistic Wind

Michel (1969) proposed the first model of a relativistic wind. When it is cold, $\gamma_* \mu_* = mc^2$, the wind depends on only one parameter, σ, where

$$\sigma = c \frac{(\phi R/c)^2}{J mc^2} \tag{8}$$

and ϕ is the magnetic flux per steradian. The asymptotic radial flow speed U_∞ is

$$U_\infty = \sigma^{1/3} \quad , \tag{9}$$

and the four-speed of a fast magnetosonic wave is given by

$$U_{F\infty}^2 = B_\phi^2 / 4\pi n \gamma^2 mc^2 = \sigma^{2/3} \tag{10}$$

where B_ϕ is the toroidal magnetic field and n is the proper density. Thus, the asymptotic fast Mach number is unity. A fast shock cannot stand in such a flow.

Recently, we have performed numerical calculations of the properties of hot relativistic winds (Fujimura and Kennel, 1980). Michel's σ generalizes naturally to

$$\sigma = c \frac{(\phi R/c)^2}{J \gamma_* \mu_*} \tag{11}$$

which we showed earlier (Kennel, et al. 1979) equals $\dot{W}_{TOT}/\dot{W}_{PAIRS}$. When $\gamma_* \mu_* > \sigma^{\frac{1}{2}} mc^2$ exceeds unity, the cold solution is a poor guide to understanding the wind. In this limit,

$$U_\infty \simeq \gamma_* \mu_* \tag{11}$$

$$U_F^2 \simeq \sigma \tag{13}$$

and the asymptotic Mach number based on the four-speeds is large. Therefore, hot relativistic winds can be confined by strong fast shocks.

4) Rankine-Hugoniot Relations

Rees and Gunn (1974) used hydrodynamic Rankine-Hugoniot relations to evaluate the shock jump conditions. For strong hydrodynamic shocks, the downstream flow speed is c/3. However, σ exceeds unity for all pair producing pulsars, so that the flow upstream of the shock is highly magnetized. Since the upstream fast magnetohydrodynamic wave 3-speed is close to c, the downstream flow velocity can be highly relativistic as well.

The Rankine-Hugoniot relations for a strong fast shock in a highly magnetized plasma in the limit $U_1 >> U_{F_1} >> 1$, lead to

$$U_2 = U_1/M \tag{14}$$

$$T_2 \simeq M/8 \tag{15}$$

where U_1 and U_2 denote the up and downstream flow four-speeds, U_{F_1}, the magnetosonic four-speed, and $M = V_1/U_{F1}$.

For hot relativistic winds, $U_1 = U_\infty \simeq \gamma_* \mu_*/mc^2$ and $M = U_\infty/\sigma^{\frac{1}{2}}$. Thus,

$$U_2 = \sqrt{\sigma} \tag{16}$$

$$T_2 = U_1/8\sigma^{\frac{1}{2}} \tag{17}$$

and, although the flow is strongly decelerated across the shock, it remains relativistic if $\sigma > 1$. The ratio of the particle to magnetic energy flux downstream is

$$\frac{4\pi n_2 \gamma_2^2 U_2}{B_{\phi 2}^2} = \frac{1}{2U_{F1}^2} = \frac{1}{2\sigma} \tag{18}$$

Thus the downstream flow remains magnetized. About $1/\sigma$ of the total energy flux crossing the shock is converted to thermal energy flux.

5) Radial Dependence of Downstream Flow

For a steady adiabatic spherical wind flowing perpendicular to a toroidal magnetic field below the fast magnetosonic speed

$$U(R) = U_2(R_{sh}^2/R^2) \tag{19}$$

$$B_\phi(R) = B_\phi(R_{sh})\,(R/R_{sh}) \tag{20}$$

$$T(R) = T_2 = \text{constant} \tag{21}$$

$$N(R) = N_2 = \text{constant} \tag{22}$$

This solution, which has a constant sum of pressure plus toroidal magnetic stress, would continue until it encounters the interface with the supernova remnant, where pressure boundary conditions are applied. Observations place this interface at about $R \lesssim 20\ R_{sh} \simeq 6 \times 10^{18}$ cm, and it is thought to expand at a speed of about 10^{-2} c (Rees and Gunn, 1974). A more accurate solution would include the effects of synchrotron energy losses, neutral matter entrained in the flow, and turbulent mixing at the interface. In addition, the flow is evolving since its creation only a thousand years ago. Nonetheless, the above solution provides a basis for certain assertions about the radiation from the deceleration zone. Let us therefore assemble the estimates made in sections (2-5). First of all,

$$\sigma = \dot{W}_{TOT}/\dot{W}_{PAIRS} \tag{23}$$

and for a hot relativistic wind upstream of the shock,

$$U(r) = \sigma^{1/2}\,(R_{sh}/R)^2 \tag{24}$$

$$T_2 = \frac{1}{8}\,\frac{\gamma_* \mu_*}{\sigma^{1/2}\, mc^2} \tag{25}$$

Finally, the toroidal magnetic field falls off as $1/R$ from the light cylinder at $R_{LC} = c/\Omega$, so that at the shock

$$B_\phi(R_{sh}) = B\,(a/R_{LC})^3\,\frac{R_{LC}}{R_{sh}} \tag{26}$$

where B is the surface field at the pulsar. The magnetic field makes a small jump at the shock, so that beyond it

$$B_\phi\ (R>R_{sh}) \simeq B(a/R_{LC})^3\,\frac{R_{LC}R}{R^2_{sh}} \tag{27}$$

For Crab parameters, $a = 10^6$ cm, $\Omega \simeq 190$ r/s, $B = 10^{12}\ B_{12}$ Gauss, $R_{sh} = 3\times10^{17}$ cm,

$$B_\phi\ (R>R_{sh}) \simeq 1.5\ B_{12}\,(R/R_{sh}) \times 10^{-4}\ \text{Gauss} \tag{28}$$

It takes a time T_F for the flow to reach the interface, where

$$T_F = \frac{\sigma^{1/4} R_{sh}}{c} + \frac{1}{c}\int_{\sigma^{1/4} R_{sh}}^{20\ R_{sh}} dR\,(R/R_{sh})^2 \simeq 10^3 \text{ years} \tag{29}$$

Thus when $\sigma^{1/4} < 10$, T_F equals the age of the nebula.

6) Optical Radiation

A polar gap wind source cannot account for the geometry of the nebular radiation. For $\sigma = 10^4$, the postshock flow would not become non-relativistic until it nears the boundary of the nebula. Much of the nebular radiation would be relativistically beamed and difficult to observe. Moreover its speed at 20 R_{sh} would be larger than that observed. It is evident that only a much smaller σ fits these constraints. The outer gap model does well on this score. A $\sigma = 10$ wind becomes non relativistic at $R = 1.7\ R_{sh}$ and has a speed of 10^{-2} C at $R = 20\ R_{sh}$.

Now, let us turn to the radiation. For $U_\infty = 10^7$, the downstream T_2 is 4×10^5. The critical frequency ν_c of the synchrotron radiation emitted by an electron or positron of energy Tmc^2 is

$$\nu_c = \frac{3}{2} T^2 \, fc \simeq 10^{14} B_{12} \, (R/R_{sh}) \text{ Hz} \qquad (30)$$

An isotropic Maxwellian distribution radiates synchrotron energy up to a few ν_c and then cuts off with increasing frequency. Thus the postshock flow radiates infrared to optical photons. The synchrotron lifetime τ of electrons or positrons with energy Tmc^2 is roughly

$$\tau = \frac{4 \times 10^8}{B^2 T} \text{ sec} = \frac{1000}{B_{12}^2} \left(\frac{R_{sh}}{R}\right)^2 \text{ years} \qquad (31)$$

Since the radiative lifetime is comparable with the flow time, nearly all the flow thermal energy is radiated into infrared and optical photons as the flow traverses the nebula. This is about $1/\sigma$, or 10%, of the total pulsar energy loss rate, in general agreement with observation. This also implies that the adiabatic downstream flow solution will have to be modified for radiative losses near the interface.

7) Apparent Size of the x-ray Nebula

The post shock thermalized flow cannot produce X and γ radiation because T_2 is too small. On the other hand, energetic particles should be accelerated by a $U_1 \simeq 10^7$ shock, and perhaps some primary particles from the pair production discharge cross the shock. Such superthermal particles should produce x-rays. Since their radiation lifetimes are less than the flow time T_F, the apparent size of the nebula will depend upon photon energy. We may estimate this dependence as follows. Suppose a superthermal particle transported by the flow arrives at $R_0 = \sigma^{1/4} R_{sh}$ with energy $\gamma_o mc^2$. We assume for simplicity that it has 90° pitch angle. Since in the absence of synchrotron losses it would conserve its first adiabatic invariant, its energy should tend to increase as $B^{1/2}$. With synchrotron losses, we have

$$U(R) \frac{d\gamma}{dR} = \frac{\gamma}{2B} U(R) \frac{dB}{dR} - KB^2\gamma^2 \qquad (32)$$

where $K = (4 \times 10^{+8})^{-1}$ sec^{-1}, the synchrotron lifetime constant. Let us now define $Z = R/R_o$, use the post-shock flow solution for U(R) and B(R).,

$$U = U_o Z^{-2} \tag{33}$$

$$B = B_o Z = \sigma^{\frac{1}{4}} B_{sh} Z \tag{34}$$

and solve the resulting differential equation for $\gamma(Z)$;

$$\frac{\gamma}{\gamma_o} = \frac{Z^{\frac{1}{2}}}{1 + \left(\frac{\gamma_o}{\gamma_c}\right)(Z^{11/2}-1)} \tag{35}$$

where γ_c is a critical injection γ

$$\gamma_c = \frac{11}{2} \frac{U_o}{KB_o^2 R_o} \simeq \frac{10^{10}}{B_{12}^2 \sigma^{3/4}} \left(\frac{R_{sh}}{3x10^{17}}\right) \tag{36}$$

and we estimated $U_o \simeq C$ and used equation (23). Particles with $\gamma_o > \gamma_c Z^{-11/2}$ will radiate most of their energy away before reaching the point Z, and their energy will be given by $\gamma \simeq \gamma_c Z^{-5}$. Thus, there will be no particles with energies exceeding $\gamma_c Z^{-5}$. For example, suppose the injection spectrum were a power law of the form

$$n_o = {}^{N}/_{\gamma_o^n} \quad ; \tag{37}$$

then using the methods in Tucker (1975), we can show that

$$n(\gamma,Z) \simeq \frac{N}{\gamma^n}\left(1 - {}^{\gamma}/_{\gamma_c Z^{-5}}\right)^{n-2} \quad , \gamma<\gamma_c Z^{-5} \tag{38}$$

$$= 0, \gamma>\gamma_c Z^{-5}$$

The maximum frequency emitted at the point Z will then scale as the critical synchrotron frequency based upon $\gamma_c Z^{-5}$, $\nu_c = \bar{\nu}_c Z^{-9}$ where

$$\bar{\nu}_c = \frac{3}{2} \gamma_c^2 f_{co} = 6.27 B_{12}^{-3} \sigma^{-5/4} \left(\frac{R_{sh}}{3x10^{17}}\right) x\ 10^{22} \text{ Hz} \tag{39a}$$

$$h\bar{\nu}_c = 260 B_{12}^{-3} \sigma^{-5/4} \left(\frac{R_{sh}}{3x10^{17}}\right) \quad \text{Mev} \tag{39b}$$

where f_{co} is the electron or positron cyclotron frequency at Z = 1. Thus $\bar{\nu}_c$ corresponds to 15 Mev γ-rays near Z = 1 for σ = 10, traverses the x-ray spectral region between Z = 2 and 4 and arrives at 10^{15} Hz optical photons beyond Z = 5. The ratio of a given frequency ν to ν_c at the point Z may be written as

$${}^{\nu}/_{\nu c} = ({}^{Z}/_{Z_\nu})^9 \tag{40}$$

where $Z_\nu = (\bar{\nu}_c/\nu)^{1/9}$. The point $Z = Z_\nu$ defines an outer radial boundary for synchrotron emission of photons of frequency ν, Z_ν then scales the angular size of the nebula.

For a 1 keV photon

$$Z_\nu = 4\ B_{12}^{-1/3}\ \sigma^{-5/36}\ (R_{sh}/_{3x10^{17}})^{1/9} \tag{41}$$

which corresponds to a radial distance

$$R = 1.2 \times 10^{18}\ B_{12}^{-1/3}\ \sigma^{1/9}\ (R_{sh}/_{3x10^{17}})^{10/9}\ \text{cm} \tag{42}$$

that subtends an angle ($\Delta\alpha$) at a distance of 2 kpc of

$$\Delta\alpha = 42''\ B_{12}^{-1/3}\ \sigma^{1/9}\ (R_{sh}/_{3x10^{17}})^{10/9} \tag{43}$$

Thus for $B_{12} = 1$, $\sigma = 10$ and $R_{sh} = 3 \times 10^{17}$, the angular size of the nebula should scale as

$$\Delta\alpha = 54''\ (\frac{1\ \text{Kev}}{h\nu})^{0.111} \tag{44}$$

Lunar occultation observations indicate that the FWHM of the apparent nebular size scales as (Ku, et al., 1976)

$$\Delta\alpha = 54''\ (\frac{1\ \text{Kev}}{h\nu})^{0.148} \tag{45}$$

Given the simplicity of the theory and the difficulty of the observations, we consider this agreement sufficiently encouraging to warrant further more detailed calculations of the post shock flow and the radiation from it. Much remains to be done. The frequency spectrum of the integrated nebular emission depends upon a combination of the nebular geometry and particle energy spectrum. A simple calculation, that assumes that a monoenergetic spectrum of fast particles is generated at the shock, predicts that the integrated x-ray spectrum would be proportional to $\nu^{-14/9}$, where ν^{-1} or $\nu^{-1.2}$ is observed. Use of the distribution function (38) with $n = 2$ produces a ν^{-1} x-ray spectrum, but a $\nu^{-\frac{1}{2}}$ RF spectrum, whereas $\nu^{-\frac{1}{4}}$ is observed. We have pretended that the wind is spherically symmetric, whereas in fact its magnetic field should be small near the rotational poles, small again in a neutral sheet near the rotational equator, and probably peak at latitudes of 10°-20°. The post shock flow solution must be amended to include radiation losses. The ideal interface between post shock flow and supernova remnant is undoubtedly a fiction, and considerable mixing probably occurs. All these faults need correction by more detailed calculations. Finally several interesting questions of relativistic plasma physics are raised. What is the spectrum of super-energetic particles generated in a highly magnetized relativistic shock ? Are such particles scattered by plasma turbulence in the post shock flow?

8) Conclusions

Integration of the hot relativistic wind equations, and a solution of the Rankine-Hugoniot relations for a highly magnetized relativistic shock permit

more consistent estimates pertinent to a magnetohydrodynamic model of the Crab nebula that links nebular radiation to pair production sources near the pulsar. We find that the wind must be hot when it exits the pulsar inner magnetosphere. An outer gap pair production model fits this criterion whereas a polar gap model does not. The pair production source parameters predicted by simple outer gap models then suggest that the optical nebula can be produced by synchrotron radiation in the thermalized post shock flow. If very energetic particles also are injected into the post-shock flow, we can account quantitatively for the dependence upon photon energy of the apparent size of the x-ray nebula. The model naturally accounts for the fact that the optical and x-ray nebula appear underluminous near the pulsar.

Acknowledgements

We are pleased to report several interesting conversations with D. Barbosa, and F. Coroniti. This work was supported by NASA NSG-7341 and NGL-05-007-190.

References

Arons, J., Space Sci. Rev., 24, 437, 1979

Baade, W., Ap. J., 96, 109, 1942

Cheng, A., M. Ruderman, and P. Sutherland, Ap. J., 203, 209, 1976

Cheng, A., and M. Ruderman, Ap. J., 216, 865, 1977

Erber, T., Rev. Mod. Phys., 38, 626, 1966

Fujimura, F., and C. Kennel, Hot Relativistic Winds, to be submitted, 1980

Goldreich, P., and W. Julian, Ap. J., 157, 869, 1969

Holloway, N., Nature, 246, 13, 1973

Kennel, C. F., G. Schmidt, and T. Wilcox, Phys. Rev. Letters, 31, 1364, 1973

Kennel, C., F. Fujimura, and R. Pellat, Space Sci. Rev., 407, 1979

Ku, W., H. L. Kestenbaum, R. Novick, and R. S. Wolff, Ap. J., 204, L 77, 1976

Michel, F., Ap. J., 157, 1183, 1969

Pacini, F., Nature, 216, 567, 1967

Pacini, F., Nature, 219, 145, 1969

Rees, M., and J. Gunn, Mon. Not. R. Astron. Soc., 167, 1, 1974

Ruderman, M., and P. Sutherland, Ap. J., 196, 51

Scargle, J., Ap. J., 156, 401, 1969

Schmidt, G. D., J. R. P. Angel, and E. A. Beaver, Ap. J., 227, 106, 1971

Shklovsky, I., Ap. J., 159, L 77, 1970

Sturrock, P., Ap. J., 164, 529, 1971

Tucker, W. H., Radiation Processes in Astrophysics, M.I.T. Press, Cambridge, Mass., 1975

VIII. High Energy Physics and Astrophysics

ON HIGH ENERGY NEUTRINO RADIATION OF QUASARS AND ACTIVE GALACTIC NUCLEI.

V.S.Berezinsky*) and V.L.Ginzburg**)

*)Institute for Nuclear Research, Academy of Sciences of the USSR, Moscow

**)P.N.Lebedev Physical Institute, Academy of Sciences of the USSR, Moscow

ABSTRACT

The nature of kerns in quasars and active galactic nuclei is still a controversy, though a massive black hole or a magnetoid (spinar) seem to be most plausible models of kern activity. It is difficult to distinguish between these models using only the observations of electromagnetic radiation. We suggest in this paper that high energy ($E \gtrsim$ I TeV) neutrinos can be a useful tool for solving the problem. The models of the structureless magnetoid and the black hole, surrounded by the dense gas shell or "gas" of X-ray photons, can be convincingly distinguished on the basis of the measured ratio of neutrino ($E_\nu \gtrsim$ I TeV) to gamma-ray ($E_\gamma \gtrsim$ 70 MeV) fluxes. The existence of a cocooned black hole (i.e. a black hole surrounded by the gas shell rare inside and dense outside) and the possibility of particle acceleration in the cavity are discussed in the paper.

I. INTRODUCTION

The nature of the kerns in quasars and active galactic nuclei is not yet understood. Two models are considered at present as the most plau - sible: a massive black hole and a massive superstar (spinar or magnetoid). A compact star cluster as a third possibility seems to be less probable. The possibility of the combined models, such as black hole inside magnetoid (Ozernoy I972), also should be mentioned. More generally the experimental predictions for the black hole models essentially de - pend on the amount of the gas in the vicinity of the black hole, which for the typical galactic nuclei can be characterized by the ratio M_g/M_h, where M_g is the mass of the gas and M_h is the mass of the black hole. For $M_g/M_h > I$ we have the "hidden" black hole, while for $M_g/M_h < I$ the depth of the matter at least in some directions is small and electromagnetic radiation (in particular, X-ray radiation), generated near the black hole, can escape from the galactic nucleus. The observations can reveal therefore the sources of the different types. The discussion of the models of the galactic nuclei is beyond the scope of this paper, a reader can find such a discussion as well as the references to the original works in the recent review (Ginzburg and Ozernoy I977, Lynden-Bell I977, Rees I977, Cavaliere I979); we want only to emphasize here, that it is most important, in our opinion, to understand, how the models of structureless magnetoid (i.e. one without a black hole inside) and of the black hole can be observationally distinguished. It is the diffi - cult problem, since all kinds of electromagnetic radiations (radio, optical, X-ray and even gamma-ray) are emitted from the relatively thin outer layer with the depth not in much excess of the radiation length $x_{rad} \lesssim 60\ g/cm^2$. Therefore for example, in the case of magnetoid with the radius $R_{Mg} \sim I0^{I6}$cm, the luminous mass is $M \lesssim 4\pi R_{Mg}^2 \cdot x_{rad} \sim 40\ M_\odot$, while the total mass of the magnetoid is $M_{Mg} \gtrsim I0^7 M_\odot$.

Because the principal difference of the magnetoid and the black hole models is related to the central parts of the system, it seems natural to suggest the neutrinos as the radiation which can help to distinguish between both models. The situation here is analogous to that well known for the Sun, which central temperature, density and chemical composition are directly related only to the neutrino radiation; the difference is that in the case of galactic nuclei the high energy ($E_\nu \gtrsim I$ TeV) neutrinos must be exploited. The high energy neutrino radiation from quasars

and galactic nuclei was already considered in the literature (Berezinsky I977, Eichler and Schramm I978). In the important paper by Silberberg and Shapiro I979 the propagation of high energy neutrino, gamma and X-rays was studied for the model of the black hole surrounded by gas with the density peaked at the center.

It should be emphasized that not every black hole model must differ by its neutrino radiation from the model of magnetoid, although such the difference exists for wide variety of the models. But it actually means that neutrino radiation of quasars and galactic nuclei is model dependent while in the case of electromagnetic radiation the dependence on the model is slurred over or absent at all (see especially, Cavaliere I979).

This paper is organized in the following way.

In Section 2 the existence of the black holes and their gravitational radiation is discussed. We don't see at present the realistic possibilities for the detection of the gravitational radiation from the massive black holes: one of the reasons is in too long duration of the gravitational signal. The situation is more favourable for high energy neutrino radiation: the estimated fluxes from the galactic nuclei can be detected by the future deep underwater muon and neutrino detector DUMAND (Roberts I978).

In Section 3 the neutrino and gamma radiations are studied phenomenologically for magnetoid and black hole models. It is shown, that for the models of structureless magnetoid the high energy neutrino flux is unavoidably accompanied by the flux of gamma radiation greater than some definite calculated value, while for the black hole model, neutrino radiation can be accompanied by the very small gamma-ray flux.

In all papers known to us, the neutrino radiation of the galactic nuclei was studied phenomenologically, i.e. the question how the accelerated particles are produced in the dense gas, was not considered at all.

In Section 4 we suggest a black hole in cocoon as the most plausible model providing the mixture of high energy particles with the dense gas. The possibility of the long time (quasi-stationary) existence of the cocoon and the acceleration of the particles in the "vacuum" cavity around the black hole are considered in this Section.

In Section 5 a bare black hole, i.e. one with a small depth of a surrounding gas, is considered and a ratio of gamma to neutrino flux is studied.

In Section 6 a possibility of a search for antimatter in Universe,

using high energy neutrino radiation, is discussed.

2. ON THE EXISTENCE OF THE BLACK HOLES AND THEIR GRAVITATIONAL RADIATION.

The discussion of the models of the black holes and their gravitational radiation is usually based on the general relativity. This is quite natural since general relativity is logically consistent theory which is in agreement with all known experimental data. Besides, the general relativity is very attractive just because of its internal beauty and simplicity, while the alternative theories of gravitation meet difficulties, they are complicated and less developed. At the proper conditions, the existence of the black holes within the framework of the general relativity is, in our opinion and contrary to some doubts in the literature, reliably justified. Moreover, for macroscopic black holes with $M \gtrsim M_\odot$, for example, there is no reason to expect that application of the general relativity is limited by some microscopic phenomena, such as the quantum effects or a possible existence of the fundamental length (Ginzburg I975, Ginzburg and Frolov I976).

At the same time, considering the fundamental problem of the nature of kerns in the quasars and galactic nuclei, one should keep in mind, that any known astrophysical object was not yet reliably identified with a black hole, and that general relativity is not experimentally tested in the strong gravitational fields (Ginzburg I979). It can be considered as experimentally confirmed only for the weak gravitational field, when $|\varphi| /c^2 \ll I$, for example, within the solar system with $|\varphi| /c^2 \lesssim GM /(R_\odot c^2) = 2.I2 \cdot I0^{-6}$, where φ is a Newton potential and G is a gravitational constant. The statement based on this agreement, that the theory is correct up to the horizon of events, is equivalent to the transition from the expression of I+y to $I/(I-y)=I+y+y^2+y^3+\ldots$, where $y=r_g/r$, $r_g=2GM/c^2$ and the Schwarzschild solution is implied.

Let,however, the general relativity be correct for the strong fields far away from the singularity, so that the macroscopic black holes can exist and beyond the horizon of events can be quantitatively described by the theory. Even in thiscase the question arises wheather the massive black holes can be formed in a considerable quantity under the real conditions existing in the Universe. The fact is, that a formation of a black hole in the process of collapse is very complicated and, to the best of our knowledge, only the accretion of the matter to the existing

black hole was considered in the literature, but not the process of the black hole formation. The account of angular momentum conservation, the instabilities and fragmentation, as well as the nuclear reactions can, probably, prevent the formation of a black hole during the available time ($\lesssim 10^{10}$ years).

What was said does not mean, that we are against the black hole models in astrophysics or moreover, against the general relativity. We just think, that the exclusive privilege given sometimes to the black hole model for the explanation of galactic nuclei phenomena is justified yet neither theoretically nor experimentally. A model of structureless magnetoid as an explanation of all, or maybe some of active galactic kerns, is at present not less acceptable. These conclusions emphasize the importance of the choice between the models, based on the observations, though the theoretical analysis, especially one connected with the formation of a massive black hole, is also of the great importance.

A massive black hole and a structureless magnetoid can, in principle, be distinguished by observations of their gravitational radiation*). In particular, a magnetoid can radiate practically no gravitational waves with the frequency higher than $\nu_{Mg}=1/P_{Mg} \lesssim 1.10^{-8}\,sec^{-1}$, where $P_{Mg} \gtrsim 1yr$ is the rotation period of the magnetoid, while a black hole surrounded by stars and gas can produce a bursts of gravitational radiation of the duration $\tau \sim r_g/c \sim 10^2 sec$ (at $M_h \sim 10^7 M_\odot$). The shorter bursts can be produced as a result of the tidal break up of the stars near the kern. According to some estimates, only small fraction of the total self-energy of the star $M_s c^2$ is transferred to gravitational radiation in these processes. Much more considerable amount of energy can in principle be released in the case of the group star accretion with the stars being on some particular trajectories, and in the process of asymmetric collapse, in which the considered black hole has been originated.

As a numerical example of detection possibility let us consider a burst with the energy output $W_g \sim M_\odot c^2 \approx 2.10^{54}$ erg at the distance $r \sim 100$ Mpc, which results in the energy density flux of order $1 erg/cm^2$. The detection of such flux with the duration of the burst $\tau \sim 10^2$ sec seems to be hopeless in the foreseen future (Braginsky and Rudenko 1978).

---

*) The production of gravitational radiation and its detection were reviewed by Braginsky and Rudenko 1978, Tyson and Giffard 1978, Press and Thorne 1972 .

Moreover, even the sources of short gravitational pulses, for which the threshold of detection is much lower, are difficult for identification because of the poor angular resolution of the gravitational antennas.

It can be concluded, therefore, that detection of gravitational radiation from the quasars and active galactic nuclei at the stages after their formation does not look realistic at least in the near future.

3. NEUTRINO RADIATION

Under astrophysical conditions the high energy neutrinos ($E_\nu \sim$ I-IOTeV) are generated mainly as a result of the high energy cosmic ray collisions with the atomic nuclei, via the decay of the produced charged π - and K-mesons. These processes are inevitably accompanied by the generation of gamma-radiation mainly throug the neutral pion decays, with the energy of gamma-quanta $E_\gamma \gtrsim$ 70 MeV.

In a magnetoid model, the neutrino flux $F_\nu(E)$ must be accompanied by the definite flux of gamma-rays $F_{\gamma,acc}$, because in this model both neutrinos and gamma-rays are produced outside the magnetoid, i.e. at the distance greater than magnetoid radius $R_{Mg} \gtrsim IO^{I5}$-IO^{I6}cm, where the medium is transparent for gamma-quanta with $E_\gamma \gtrsim$ 70 MeV. The transparency is a direct consequence of the experimental data which show, that the mean hydrogen depth at $r \gtrsim IO^{I5}$-IO^{I6}cm is obviously less than radiative length $x_{rad} \approx 60$ g/cm^2 *) and that the density of X-ray photons is small, so that the gamma-ray absorption due to the process $\gamma + \gamma_X \rightarrow e^+ + e^-$ is negligible.

---

*) This conclusion is based on:I) X-ray variability with $t \lesssim IO^5$sec (if the depth at $r > IO^{I5}$-IO^{I6} cm were considerably greater than the Thompson depth $x_{Th} \approx m_H/\sigma_T \approx 2.5$ g/cm^2, the variable flux of X-rays would diffuse through the outer region at $r > IO^{I5}$-IO^{I6}cm and loose its variability), 2) the low energy cut off in the X-ray spectra of some sources (e.g. NGC 4I5I) and 3) the rapid variation of polarization of optical continuum (e.g. 3C446), which would be destroyed in the case of large depth. The large electron density $n_e \gtrsim IO^8$cm^{-3} in the broad-line emission regions does not contradict to a small mean depth of the matter, implying that a filling factor is small ($\varepsilon \sim IO^{-9}$).

A flux of gamma-rays with $E_\gamma \gtrsim 70$ MeV, which accompanies the neutrino flux $F_{\nu_\mu}(>E)$ in the case of a small depth of the matter $x < x_{rad}$, is (Berezinsky 1979)

$$F_{\gamma,acc} = \lambda(\gamma) E^{\gamma} F_{\nu_\mu}(>E) \quad , \qquad (1)$$

where neutrino flux $F_{\nu_\mu}(>E)$ is the number of $\nu_\mu + \bar{\nu}_\mu$ -neutrinos with energy greater than E emitted by a source per I sec and $F_{\gamma,acc}$ is a flux of gamma-quanta with energy $E_\gamma \gtrsim 70$ MeV generated in a relevant process of π^0-decays. The Eq.(I) was obtained under assumption, that high energy protons, which produce both neutrino and gamma-radiations, have a power-law differential energy spectrum $\varphi_p(E)dE = A(E+I)^{-(\gamma+I)}dE$, where E is kinetic energy of proton; here and henceforth the energy and luminosity are given in GeV and GeV/sec respectively, if not stipulated otherwise. The values of $\lambda(\gamma)$ are given in Table I.

Table I

γ	I.2	I.4	I.6	I.8	2.0
$\lambda(\gamma)$	5.9	8.3	I2.2	I7.2	23.8

Since gamma-rays can be also produced by electrons, gamma-ray flux in magnetoid model must obey to inequality:

$$F_\gamma (\gtrsim 70 \text{ MeV}) > F_{\gamma,acc} = \lambda(\gamma)\, E^{\gamma}\, F_{\nu_\mu}(>E). \qquad (2)$$

If the observed gamma-ray flux with $E_\gamma \gtrsim 70$ MeV does not obey to inequality (2), a cosmic ray source has to be covered by a thick layer of gas with $x > x_{rad}$ or surrounded by the "gas" of X-ray quanta ($E_X \gtrsim$ I keV) with a sufficient space density. Both possibilities contradict to a structureless magnetoid and favour a black hole model.

For a cosmic ray source covered by a thick gas shell with $x \gg x_{rad}$, or by the dense X-ray gas, gamma-radiation can be absorbed, while the

neutrino flux is (Berezinsky I979, Berezinsky and Volynsky I979):

$$F_{\nu_\mu}(>E) = \frac{\varphi_\nu}{1-\alpha} \cdot \frac{\gamma-1}{\gamma} \cdot L_p E^{-\gamma} \qquad (3)$$

where L_p (in GeV/sec) is the cosmic ray luminosity of the source (i.e. energy relesed in the form of the accelerated protons per I sec.), $\alpha \approx 0.5$ is a fraction of the energy retained by a proton in a nuclear collision, and φ_ν is a dimensionless coefficient of $\nu_\mu + \bar{\nu}_\mu$ -neutrino generation, which values are given in Table 2 (the definition of φ_ν and its calculation are given in the paper by Berezinsky and Volynsky I979).

Table 2

γ	I.2	I.3	I.4	I.6	I.8	2.0
$10^3\varphi_\nu$	94.6	69.8	5I.9	29.7	I7.7	I0.9

As an illustration we shall give the following numerical example. Consider the kern of a quasar or of an active galactic nucleus with $L_p = I.I0^{49}$GeV/sec $\approx I.6.I0^{46}$erg/sec and $\gamma = I.3$ (the exponent of production spectrum of cosmic rays in our Galaxy:see Ginzburg and Ptuskin I976) at a distance r=I00 Mpc. According to Eq.(3), the flux of $\nu_\mu + \bar{\nu}_\mu$ -neutrinos with energy $E_\nu \geq I0^3$GeV is $F_\nu(>I0^3\text{GeV}) \approx 4.I0^{43}$neutrino/sec.

As a detector of these neutrinos we shall consider deep underwater DUMAND array, which construction is expected in the near future (Roberts I978). The detector is designed as a space grid of the photomultipliers, Ikm^3 in volume, submerged into water at 5 km depth. Undergoing nuclear collision in the water, muon neutrino (or antineutrino) effectively turns into muon, which at the discussed energies moves practically in the same direction as the parent neutrino. The pathlength of muon with energy $E_\mu \sim I0^3$GeV in the water is nearly 3 km. The trajectory of muon looks like a light jet, several meters in diameter. The light is emmited as a čerenkov radiation of the cascades, which are

initiated by electron-positron pairs and bremstrahlung photons produced by muon along its trajectory. The light is triggering many photomultipliers along I km muon pathlength in the array, so that direction of muon (and hence neutrino) trajectory can be found with a good accuracy $\delta\Theta \sim I^{\circ}$. Therefore, the DUMAND array will work as a neutrino telescope with a high angular resolution.

For the numerical example given above, DUMAND will detect about 30 muons with energy $E_{\mu} \gtrsim I0^{3}$GeV per year within an angle $\delta\Theta \sim I^{\circ}$ in the direction of the galactic nucleus. The background produced within this angle by atmospheric neutrinos is considerably lower.

Consider now the flux of accompanied gamma-radiation with $E_{\gamma} \gtrsim 70$ MeV. From Eq.(2), the gamma-ray flux density at the Earth (r=I00 Mpc) for $F_{\nu}(>I0^{3}\text{GeV}) \approx 4.I0^{43}\text{sec}^{-I}$ and $\gamma = I.3$ is $j_{\gamma}(\gtrsim 70\ \text{MeV}) > F_{\gamma,acc}/4\pi r^{2} = 2.I0^{-6}$ photons/cm^{2}sec; this value is almost an order of magnitude higher than the threshold of the detection of the existing satellite gamma-detectors. A gamma-ray flux lower than this predicted value provides the direct contradiction to the model of structureless magnetoid and gives support to the model of compact ($R < I0^{I5}$cm) cosmic ray source covered by gas shell with $x > x_{rad}$ or surrounded by the dense gas of X-ray photons.

The considered model of a "hidden" source of accelerated particles has also another signature: the thermal (or quasithermal) radiation with luminosity L_{th}, correlated with neutrino luminosity $L_{\nu_{\mu}} = \int E \cdot F_{\nu_{\mu}}(E)dE$, or with detected neutrino flux $F_{\nu_{\mu}}(>E)$

$$L_{th} \approx \frac{1}{4}\,\frac{1-\alpha}{\varphi_{\nu}}\,L_{\nu_{\mu}} \qquad (4)$$

$$L_{th} \approx \frac{1}{2}\,\frac{1-\alpha}{\varphi_{\nu}}\,\frac{\gamma}{\gamma-1}\,E^{\gamma}F_{\nu_{\mu}}(>E)$$

The Eq.(4) is primarily the consequence of a relation $L_{th} \approx \frac{1}{2} L_{p}$, since only around half of the proton energy lost in nuclear collisions is carried away by neutrinos, another half is transferred to the photons and electrons, being then thermalized inside the gas shell and finally emitted from the surface as a thermal radiation. Deriving the Eq.(4), we approximately estimated the minimum energy in neutrino pro-

duction spectrum.

The thermal optical radiation was observed from some quasars and active galactic nuclei. In our numerical example, $L_{th} \approx 8.10^{45}$ erg/sec is a possible value for a thermal component of a quasar radiation (one must keep in mind also the possibility of partical comptonization of the thermal radiation outside the gas shell).

4. BLACK HOLE IN COCOON.

How particle acceleration can occur under the dense ($x \gg x_{rad}$) gas shell?

The natural solution of this problem is given by a cocooned black hole model, i.e. by a system comprised of a black hole surrounded by a "vacuum" cavity with a dense gas shell outside. The cocooned black hole is somewhat similar to the cocooned pulsar considered by Milgrom 1976 and Milgrom and Pines 1978. In many aspects, however, the massive cocooned black hole as a model of an active galactic kern is different from the cocooned pulsar: in the latter case there is the outflow of the energy and radiation, supported by the internal energy (rotation) of the source, while in the former case the solution must be selfconsistent, namely, accretion to the black hole must produce radiation, which supports the cocoon in quasi-equilibrium state. There is also another difference which concerns the life time of the system. For an isolated young pulsar the life time of the cocoon is limited by the expansion of the shell, resulted in the transparency of the cocoon for all kinds of radiation; for a binary pulsar the life time of the cocoon can be prolonged due to outflow of the matter from the massive companion. The life time of a cocoon around a massive black hole depends on the accretion rate to the black hole, on the mass of the primordial shell and on the accretion rate of the gas and stars from the outer space; for the explanation of active nuclei phenomena the life time of about 10^6-10^8 years is needed.

Further on we shall discuss two problems of the cocooned black hole, namely, the problem of quasi-equilibrium state and the particle acceleration. We cannot give at present the detailed selfconsistent description of the cocoon around the massive black hole. Instead, we shall find the equilibrium state in a simple subsidiary model, in which a source of low energy electromagnetic radiation is surrounded by cocoon. Then, taking into account the instabilities and accretion to the black hole, we shall discuss qualitatively, to what physical state will de-

velop the found unstable equilibrium?

We had considered first the subsidiary model of the central source with the mass M_h and the luminosity L, surrounded by hydrogen shell of the mass M_g. The equilibrium state had been looked for as a solution of hydrostatic equation

$$-\frac{\partial P_{gas}}{\partial r} + \frac{L\,\sigma_T\,\rho(r)}{4\pi r^2 c\, m_H} - \frac{G\,M(r)\,\rho(r)}{r^2} = 0 \quad , \tag{5}$$

where M(r) is the mass of the system inside the radius r, σ_T is the Thompson cross-section and the other notations are obvious.

At first sight the quasi-equilibrium state of the "vacuum" cavity cannot be supported by gravitational and radiation forces only, since both forces have the same distance dependence ($\sim 1/r^2$). But in fact, the Eq.(5) has the equilibrium solution with the "vacuum" cavity, especially if conditions $M_g \gtrsim M_h$ or $M_g >> M_h$ take place.

The dynamical state of the gas shell cruicially depends on the luminosity of the central source L. There are three characteristic values of luminosity:

$$\begin{aligned} L_c &= 4\pi G c (M_h + M_g)\,\tilde{x} \quad , \\ L_{Edd,c} &= 4\pi G c (M_h + M_g)\,x_T \quad , \\ L_{Edd,h} &= 4\pi G c\, M_h x_T \quad , \end{aligned} \tag{6}$$

where $x_T = m_H/\sigma_T$ is the Thompson depth and

$$\tilde{x} = \int \frac{M(r)}{M_g + M_h}\,\rho(r)\,dr$$

is approximately the depth of the gas shell.

If $L > L_c$ the radiation force L/c exceeds the gravitational attraction of the shell to the central source, and the shell undergoes the steady expansion.

At $L_c > L > L_{Edd,t}$ the luminosity exceeds the Eddington limit for the total mass of the system $M_g + M_h$, this regime is characterized by a violent outflow of the gas from the outer surface and by a convection inside the shell.

The regime most favourable for the equilibrium occurs at $L_{Edd,t} > L \gtrsim L_{Edd,h}$, i.e. when the luminosity L is greater than Eddington limit for the central source, but less than the total Eddington limit of the system. In this case the radiation pressure exceeds the gravitational attraction in the vicinity of the central source, but it is less than gravitational force at the edge of the gas shell.

The equilibrium state has been found as the solution of Eq.(5) with $\partial S / \partial r > 0$ up to $r = r_c$, where the luminosity of the central source L becomes equal to Eddington limit for the mass $M(r_c)$. In fact, the Eq.(5) has the different form in three physical regions, namely, (i) where the pressure p(r) and gradient $\partial p/\partial r$ are small and can be neglected (the "vacuum" cavity), (ii) where the pressure p(r) is small, but gradient $\partial p/\partial r$ is large (the transition region) and, finally, (iii) the shell itself, where Eq.(5) is directly applied. In the vacuum cavity (i) and transition region (ii) electrons and protons have been considered separately as two ideal gases, taking into account the equation for the electric field $\mathcal{E}(r)$. The cruicial role in the supporting of the equilibrium state with $\partial p/\partial r > 0$ is played by the transition region (ii).

The calculations will be presented somewhere else.

The considered state has two kinds of instabilities. The first is Reyleigh-Taylor instability, which at $L \gtrsim L_{Edd,h}$ results in irregular tongue-like accretion to the central source. The second kind of instability develops in the gas shell and is connected with the positive gradient $\partial S / \partial r$ up to $r = r_c$; it results in the formation of the convective zone.

We expect that the simple model considered above can be used for the description of the cocooned black hole, when the luminosity induced by accretion is equal (or slightly over) the Eddington limit for the black hole $L_{Edd,h}$. The picture must be selfconsistent: the irregular accretion results, through the turbulence and the shock waves, in the heating of the gas near the black hole and in the generation of the radi-

ation which regulates the accretion rate $\dot{M}$ in such a way, that $\epsilon \dot{M} c^2 \gtrsim L_{Edd,h}$ with the efficiency $\epsilon \sim 0.1$. The vacuum cavity of the subsidiary model turnes, thus, into the turbulent rarefied plasma, where the accretion tongues, which power the system, are chaotically replaced by the jets of the gas driven out by the radiation. We conjecture the acceleration processes taking place under these conditions, with the energy density of cosmic rays being $\omega_p \sim \rho u^2/2$ and the cosmic ray luminosity $L_p \sim 1/3 \dot{M} c^2$.

The picture presented here is similar to the dissipative quasi-spherical accretion considered by Rees (1978). The quasi-spherical accretion in particular takes place if it is supplied by a tidal stellar disruption in the field of a black hole with a mass $M_h > 3.10^5 M_\odot$ (Gurzadyan and Ozernoy 1979). This situation might occur for the old bare black holes (see Section 5), while for the young black hole surrounded by the primordial massive ($M_g \gtrsim M_h$) rotating cloud, the infalling gas forms an accretion disc because of the necessity to loose the angular momentum; the black hole then acquires some angular mometum carried by the gas and becomes rotating even if it was at rest at the beginning (Lynden-Bell 1978)

The life time of the cocoon comprised of the massive black hole and the massive (primordial) gas shell can be roughly estimated from $\tau \sim M_g/\dot{M}$ and $L_{Edd,h} \approx \epsilon M c^2$ as

$$\tau \approx 4\left(\frac{\epsilon}{0.1}\right).10^7 M_g/M_h \text{ years.}$$

Consider now the problem of acceleration in a cocoon.

Till now we did not take into account the rotation and magnetic fields. Meanwhile they are essential and important phenomena: neglecting them it is hardly possible to understand predominance of nonthermal emission in quasars and active galactic nuclei.

In the disc accretion models, the rotation of the disc, generation (or amplification) of the regular magnetic field and the existence of the vacuum cavity around the disc provide the necessary conditions for particle acceleration. There is an extensive literature about mechanisms of acceleration for the disc accretion models. We shall shortly review the basic ideas of the proposed acceleration mechanisms.

As a result of disc accretion a black hole acquires the angular momentum and positive electric charge, which together induce the dipole magnetic field around the black hole. This field, being frozen into the

rotating disc, produce the high electric potential, in the same way it is produced in pulsar magnitosphere (Kaplan and Schwartzman I969, Harrison I969). According to Harrison's estimate, a black hole of $10^8 M_\odot$ can attain the potential up to 10^{20}V.

The other mechanism (Blandford I976, Lovelace I976) is connected with the perpendicular to the disc component of the magnetic field carried by the accreting gas from the outer space and amplified by the compression in the disc. The magnetic field lines, being involved into the Keplerian rotation of the disc, produce the electric field and particle acceleration almost in the same way as in pulsar.

The recconnections of the magnetic field lines in the disc can be another mechanism of particle acceleration (Kaplan and Schwartzman I976).

The acceleration is expected also for a spherical and quasi-spherical accretion due to the turbulence of the rarefied magnetized plasma.

5. NEUTRINO AND GAMMA RADIATION FOR A BARE BLACK HOLE

According to environment conditions and the epoch of formation, a black hole can be surrounded by different amount of the gas. A young black hole formed in the center of galaxy can develop into the cocooned black hole or, as extreme possibility, into a magnetoid with a black hole inside. As it consumes the gas around, the black hole turns into a bare one, with the accretion provided by stellar tidal disruption and by infall of the gas from the surrounding galaxy. Although, according to this scheme a cocooned and a bare black holes are the young and old objects respectively, this is not the only possibility: the direct formation of a bare black hole from a primordial gas cloud is also a possibility.

In this Section we shall consider the bare black holes, i.e. those with a small depth of the gas around ($x < x_{rad}$ or $x \ll x_{rad}$) and discuss the relations between neutrino and gamma radiation. There can be two types of accretion onto a bare black hole: disc accretion (when inflowing gas has a large angular momentum) and a quasi-spherical accretion (when gas has a small net angular momentum).

Consider first the quasi-spherical accretion to an old black hole supplied by stellar disruption.

The tidal radius, within which the captured solar-type stars are disrupted, is (Rees I978)

$$r_t \approx 9.10^{13} \ (M_h/10^8 M_\odot)^{1/3} \text{ cm} \qquad (7)$$

For massive black holes with $M_h \sim 10^7$-$10^8 M_\odot$ the tidal radius is not much larger than the radius of the last stable orbit for Schwarzschild black hole

$$r_{st} = 3\, r_g \approx 9.10^{13} (M_h/10^8 M_\odot)^{1/3} \text{ cm} \qquad (8)$$

Therefore, the gas is supplied directly to the region, where the mass is converted into kinetic energy and the radiation is produced through some dissipative processes. Consider X-rays isotropically generated within this region, with luminosity L_x in quanta with individual energies $\mathcal{E}_x \gtrsim 25$ keV. The gas of these photons absorbes gamma-quanta with $E_\gamma \gtrsim$ 70 MeV due to pair-production $\gamma + \gamma_x \rightarrow e^+ + e^-$, with the probability ($\sigma_p n_x r_t$) of absorption equal:

$$\sigma_p n_x r_t \approx \frac{\sigma_p L_x}{\pi c \bar{\mathcal{E}}_x r_t} \qquad (9)$$

where n_x and $\bar{\mathcal{E}}_x$ are the mean density and the mean energy of X-ray quanta respectively, and $\sigma_p \approx \frac{1}{2}\pi r_e^2 \approx 1.10^{-25} \text{cm}^2$ is an effective value of $\gamma + \gamma \rightarrow e^+ + e^-$ cross-section (r_e is a classical electron radius). At $L_x \sim 10^{45}$ erg/sec and $\bar{\mathcal{E}}_x \approx 5$ keV, $\sigma_p n_x r_t \sim 10^3$, i.e. the region within the tidal radius $r_t \sim 10^{14}$ cm is opaque for photons with $E_\gamma \gtrsim$ 70 MeV. Thus a neutrino flux generated in this region is not accompanied by gamma radiation. For the considered model of quasi-spherical accretion (a turbulent magnetized plasma in stellar disruption region) the particales are accelerated in situ and those with $E > 10^4$ GeV undergo, according to Eq.(9), several photopion collisions with X-ray quanta ($p + \gamma_x \rightarrow \pi + N$, the effective cross-section $\sigma \sim 2$-3.10^{-28}cm^2) before they leave the region. Therefore, we have come again to the picture of almost gamma-unaccompanied neutrino radiation.

The open disc models are much more uncertain: the pion production and gamma absorption depend on the angle between the trajectories of the colliding particles (the head-tail collisions are ineffective for the production of pions or e^+e^--pairs), depend on whether or not the trajectories of accelerated particles pass through this region etc. Thus it

seems, that these models can be constructed with the different ratio of gamma to neutrino flux.

6. SEARCH FOR ANTIMATTER.

It is well known that electromagnetic radiation carries no infcrmation by which kind of the material, matter or untimatter, it was generated. As it will be demonstrated in this Section high energy neutri - nos can tell us the difference.

What are the theoretical expectations for the presence of antimatter in the Universe?

In the standard grand unified theories the attemptswere made (Ignatiev et al I978, Yoshimura I978, Ellis et al I979, Weinberg I979) to explain the barion asymmetry as being the same in the whole Universe. According to these theories the Universe with the excess of barions had developed from early barion symmetric Big Bang due to violation of ba - rion number and CP violation in the decays of Higgs mesons. It demands, if CP violation was induced by spontaneous symmetry breaking, the phase of vacuum expectation value to be the same in the whole Universe. But if the potential part of Lagrangian for scalar field φ has a form $\lambda (\varphi^* \varphi - \eta^2)^2$, the phase δ of a vacuum expectation value $\varphi = \eta\, e^{i\delta}$, is acquired arbitrary and, in principle, must not be the same at the distances greater than event horizon. Then CP violation can be different in these regions (domains), this results in the different barion (or antibarion) excess in the domains and hence in the different barion density after the epoch of barion-antibarion annihilation. It must reveal itself now in anisotropy of the relict radiation. This conclusion is similar to the conclusions of the paper by Zeldovich et al I974, to which a reader is referred for a suggestion and analysis of domain structure of the Universe with different CP violation (see also the paper by Brown and Stecker I979 with the contrary conclusion in favour of domain structure). We can conclude therefore, that although a domain structure is somewhat natural to appear at the very early stage of the Universe, it is probably contradictive for the later stages.

Under these circumstances it is interesting to discuss the posiibilities of the experimental search for antimatter in the Universe.

Learned and Stecker (I979) suggested the high energy ν_μ and $\bar{\nu}_\mu$ - neutrinos produced in pp-collisions as the tracers of antimatter in the Universe. The suggested effects, such as y-distributions in ν_μN-interactions, depend on the ratio r of ν_μ-neutrino to $\bar{\nu}_\mu$-neutrino flux,

which is different for the sources from the matter ($r = I.03$) and antimatter ($r = 0.97$).

We would like to notice here, that for $p\gamma$ -neutrinos, produced in the collisions of high energy protons with low energy photons, there is much more distinctive effect, which can distinguish the matter and antimatter. The $p\gamma$ -neutrino production is dominant for bare black hole and magnetoid models of the quasars.

In $p\gamma$ - and $\bar{p}\gamma$ -collisions the pions (and decay neutrinos) are produced mostly at the threshold of pion production when a target photon has a minimal energy possible for a given proton energy. The neutrinos are produced according to the following scheme:

$$p + \gamma \to \pi^+ + n \quad \begin{array}{l} \hookrightarrow \mu^+ + \nu_\mu \\ \qquad \hookrightarrow e^+ + \bar{\nu}_\mu + \nu_e \end{array} \qquad \bar{p} + \gamma \to \pi^- + \bar{n} \quad \begin{array}{l} \hookrightarrow \mu^- + \bar{\nu}_\mu \\ \qquad \hookrightarrow e^- + \nu_\mu + \bar{\nu}_e \end{array} \tag{I0}$$

One can see from Eq.(I0), that the flux of $\bar{\nu}_e$-neutrinos must be overwhelmingly greater for an antiquasar than for quasar. On the other hand at very large energy $E_o = m_w^2/2m_e = 6.3.I0^6$ GeV ($m_w \simeq 80$ GeV is the mass of W-boson), $\bar{\nu}_e$-neutrinos produce the main effect in a detector in comparison with all other types of neutrinos, through the resonant $\bar{\nu}_e + e \to W^- +$ hadrons reaction: the number of resonant events in a detector is ~ 20 times higher than the number of other neutrino events (Berezinsky I977). For the detection of $\bar{\nu}_e$-neutrinos from an antiquasar at a distance $r \sim I00$ Mpc an underwater detector of $I0^{II} m^3$ is needed; such volume can be in principle, achieved in future with the help of acoustic technique .

CONCLUSIONS

A choice between a black hole and a structureless magnetoid as an energy power of quasars and active galactic nuclei is a difficult experimental task. Even the short time variations, like those discovered by HEAO-2 (Tananbaum et al I979), when X-ray flux from quasar 0X I69 abruptly decreased during the time $\tau \lesssim I0^4$ sec, cannot be decisive for

the choice of the model. In fact in this case, although the characteristic size $c\tau \lesssim 3.10^{14}$cm is less than magnetoid radius, the observed X-ray flux variation can be, probably, explained in magnetoid model as a local X-ray burst.

The measurement of high energy neutrino radiation can drastically change the situation because the model of the structureless magnetoid predicts the rigorous relation, given by Eq.(2), between the neutrino and gamma-ray fluxes. A violation of this relation for a galactic nucleus under observation could unambiguously reject the magnetoid model and support a black hole model as the most probable alternative.

On the other hand the black hole models can differ in the predictions of the ratio of gamma-ray to neutrino fluxes. A cocooned black hole and a massive ($M \gtrsim 10^7 M_\odot$) bare black hole with quasi-spherical accretion supplied by a stellar disruption can produce the high neutrino flux accompanied by low gamma-ray flux ($E_\gamma \gtrsim 70$ MeV). Meanwhile such prediction probably does not exist for all bare disc models.

The gamma-rays from the quasars and active galactic nuclei can be produced not only through π^0-decays, but also by the inverse compton scattering of the electrons (this mechanism of gamma-ray production was suggested for quasar 3C 273 as early as in 1964: see Ginzburg et al 1964) Throughout the present paper the contribution of the electrons to gamma-ray luminosity (with $E_\gamma \gtrsim 70$ MeV) was taken into account: for a magnetoid model it strengthens the inequality (2), for a cocooned black hole it can be responsible (together with the π^0-decays) for the observed gamma-radiation, generated outside the cocoon, and it is inessential for the bare black hole with the quasi-spherical accretion, since the conclusion about a small gamma-ray flux for this model is connected with the absorption of gamma-quanta with $E_\gamma \gtrsim 70$ MeV in active region, independently on the generation mechanism.

The aims and possibilities of high energy neutrino astronomy are not limited, of course, by the discussed task. Being produced exclusively in nuclear pp- and $p\gamma$ -collisions, neutrino radiation provides the direct information on nuclear component of cosmic rays (protons and nuclei) in the remote galaxies, while all kinds of electromagnetic radiation , including gamma-rays, can be generated also by electrons. Neutrinos with energy $E \gtrsim 10^{12}$ eV carry the information about very high energy processes in the most remote objects, from which gamma-rays with the same energy cannot reach the Earth bacause of the absorption in the Universe.

And finally, neutrinos provide the unique possibility for the exploration of the dense objects in the Universe, such as the cocooned black holes, the black holes surrounded by the dense "gas" of low energy photons etc.

Realization of such a feasible project as 10^9 tons DUMAND will give us the first possibility to look at the Universe in the high energy "neutrino light". The view can be unexpected, but we can count on the detection of the active galactic nuclei and on the solving the problem of the kern structure.

The authors are grateful to L.M.Ozernoy for a fruitful discussion.

REFERENCES

Berezinsky V.S. I977 Proc. Int. Conf. "Neutrino-77" (USSR), v.I,I77
Berezinsky V.S. and Volynsky V.V. I979 Proc. I6 Int. Cosmic Ray Conf. (Kyoto), V.IO,326
Berezinsky V.S. I979 Proc. Int. Symposium "DUMAND-79" (to be published)
Blandford R.D. I976 Mon. Not. I76,465
Braginsky V.B. and Rudenko V.N. I978 Phys. Reports 46, I67
Brown R.W. and Stecker F.W. I979 NASA Technical Report 8028I
Cavaliere A. I979 Proc. I6 I t. Cosmic Ray Conf. (Kyoto) I4,9I
Eichler D. and Schramm D.N. I978 Nature 275, 704
Ellis J., Gaillard M.K. and Nanopoulos D.U. I979 Phys. Lett. 80 B,360
Ginzburg V.L., Ozernoy L.M. and Syrovatskii S.I. I964 Doclady of USSR Academy of Sciences (in Russian) I54,557; in English: Proc. I Texas Symposium on Relativistic Astropyhsics I965,277
Ginzburg V.L. I975 JETPh Leters 22, 5I4
Ginzburg V.L. and Ptuskin V.S. I976, Rev. Mod. Phys. 48, 675; Sov. Phys. Uspekhi I8,93I
Ginzburg V.L. and Frolov V.P. I976 Astron. Journ. Lett. 2, 474
Ginzburg V.L. and Ozernoy L.M. I977 Ap.Sp.Sci 50,23
Ginzburg V.L. I979 Sov. Fiz. (Uspekhi) I28,435
GurzadyanV.G.and Ozernoy L.M. I979 Nature 280,2I4
Harrison E.R. I976 Nature 264,525
Ignatiev A.Yu., Krasnikov N.V.,Kuzmin V.A.,Tavkhelidze A.N. Phys.Lett. 76 B,436
Kaplan S.A. and Schwarzman V.F. I976 in "Origin and Evolution of galaxies and stars" (Ed.Pikelner S.B.) p.3I9, Nauka Publishing House, Moscow
Learned J.G. and Stecker F.W. I979 NASA Technical Report 7956
Lovelace R.V.E. I976 Nature 262, 649
Lynden-Bell D. I978 Physica Scripta I7,I85
Milgrom M. I976 Astr. and Ap. 5I, 2I5
Milgrom M. and Pines D. I978 Ap.J. 220,272
Ozernoy L.M. I974 Proc. Firts Europ. Astron. Meeting 3,65
Press W.H. and Thorne K.S. I972 Ann. Rev. Atsron. Atsroph. IO, 335

Rees M.J. I978 Physica Scripta I7, I93.
Roberts A. (Editor) I978 Proc. I978 DUMAND Summer Workshop, Scripps Institute, USA.
Silberberg R. and Shapiro M.M. I979 Proc. I6 Int. Cosmic Ray Conf. (Kyoto), IO, 357.
Tananbaum H. et al. I979 Ap. J.Leters 234,L 9.
Tyson J.A. and Giffard R.P. I978 Ann. Rev. Astron. Astroph. I6, 52I.
Weinberg S. I979 Phys. Rev. Lett. 42, 850.
Yoshimura M. I978 Phys. Rev. Lett. 4I, 38I.
Zeldovich Ya.B., Kobzarev I.Yu. and Okun L.B. I974 JETPh (in Russian), 67, 3.

NEUTRINO DATING OF THE GALAXY FORMATION EPOCH

V.S.Berezinsky*) L.M.Ozernoy**)

*)Institute for Nuclear Research, USSR Academy of Sciences, Moscow

**)Lebedev Physical Institute, USSR Academy of Sciences, Moscow

Abstract

High energy neutrinos, owing to their penetration capability, can serve as a probe of the remote past of the Universe. The possible investigations include search of pregalactic objects and of the "bright phase" in course of galactic evolution, i.e. comparatively short time interval when luminosities of galaxies were very high. If the bright phase took place at redshifts as large as $z \gtrsim 10$, the use of high-energy neutrinos is especially efficient because, in addition to an enhanced generation of ultra-high energy particles during the bright phase, there was a large density of relic photons; collisions of the former with the latter generate charged pions which produce, in a chain of decays, neutrinos.

The expected flux of neutrinos with energies $E_\nu > 10^{15}$ eV is evaluated for a case when the bright phase took place at $z \gtrsim 10$. The accompanying gamma-ray radiation produced due to interactions of cosmic rays with gas (both in galaxies and in intergalactic space) and with relic radiation does not exceed the observed intensity of isotropic gamma-ray background. The expected intensity of neutrino fluxes is such that it can be measured by means of an acoustic version of the DUMAND array widely discussed at present.

The paper also touches upon some topics of early evolution of galaxies and the acceleration of particles to ultra-high energies at the bright phase of galactic evolution.

1. INTRODUCTION

Range of redshifts between $z=10^3$ (decoupling epoch) and $z=3 - 4$ (which corresponds to the most distant quasars known so far) is one of the most intriguing in cosmology since various astronomical objects such as quasars, galaxies, groups and clusters of galaxies, etc. were formed in the Universe at that time. Unfortunately, the main theories for origin of galaxies based on adiabatic, whirl and entropic perturbations are still in a very rudimentary state to predict with any confidence the moment(s) of galaxy formation; there are also no data to investigate these problems experimentally.

Our knowledge of these remote cosmological epochs is extremely poor. In particular, very little is known about the earliest stages of the evolution of galaxies after their formation. But there is a common belief that galaxies being formed have undergone an appreciable evolution.

The usual concept of evolution includes the evolution of stellar population , which consists of an initial, relatively short, "bright phase" and of a much more prolonged, secular evolution.

During the last decade much attention was paid to the bright phase of galaxies beginning from the pioneering work of Partridge and Peebles (1967). They have estimated that the bright phase took place at the epoch with the redshift between 10 and 30 with an energy output of about $3 10^{61}$ ergs per galaxy. Schwarz , Ostriker and Yahil (1975) considered the bright phase, caused possibly by the cumulative effects of supernova explosions, at the redshifts between 2 and 10 with the energy output $\sim 10^{61}$ ergs per galaxy in the form of kinetic energy of supernova shells alone. Many arguments in favour of the bright phase are summa-

rized in the paper by Ozernoy and Chernomordik (1976).

The fact that quasars (i) are active phenomena in the galactic nuclei and (ii) undergo a pronounced secular evolution (Schmidt, 1972, 1978) makes it reasonable to suppose that evolution of galaxies includes, besides the evolution of stars, also evolution of galactic nuclei. Apparently, the latter consists of the secular evolution and of (one or a few) bright phase (s). The general scheme of the galactic evolution which includes evolution of stellar and non-stellar constituents, may look like as follows:

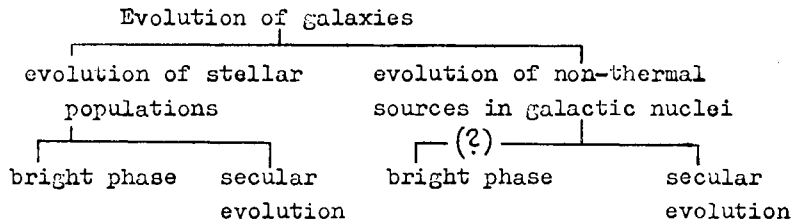

Secular evolution of stellar populations is a result, first of all, of a time-dependent rate of star formation which is given by the theory in the form $\nu(t) \sim \exp(-t/\tau)$. The characteristic evolution time, τ , which depends on the morphological type of a galaxy , is equal to $\tau_S \approx (3\text{-}4)10^9$ yr for our Galaxy (Fowler, 1972) and is considerably less for elliptical galaxies : $\tau_E \approx 10^8$yr (Gott and Thuan, 1976).

The bright phase of the evolution of stellar populations has the character of a burst, is related only to the old galactic population and apparently has a much shorter duration τ . Although there are yet no direct experimental data to characterize the bright phase quantitatively, one can judge about the rela-

tive roles of the bright phase and the secular evolution, using the iron production arguments. It is a well known fact that the observed abundance of iron could be hardly explained if the present rate of its production via supernova explosions kept the same during all the life time of the Galaxy. Therefore, if one managed somehow to limit the contribution of secular evolution, it would inevitably enhance the production activity during the bright phase.

The aim of this paper is twofold. Firstly, we are able to show that gamma-ray data allow to put rather severe constraints to evolution of galaxies. Secondly, we would like to demonstrate that high energy neutrinos are an excellent instrument to study such a remote past in the galactic evolution as their bright phase; in particular, the dating of the galaxy formation epoch is possible using neutrinos with energies $E_\nu > 10^{15}$ eV.

II. CONSTRAINTS TO THE SECULAR EVOLUTION OF GALAXIES

Recent measurements of the diffuse gamma rays with energies up to 200 MeV (Fichtel et al., 1977 and 1978) have an important consequence for the secular evolution of galaxies. The observed variation of gamma ray intensity with galactic latitude in the form $I(b) = C_1 + C_2/\sin b$ has allowed to separate the diffuse galactic component from the extragalactic one. The latter has been found to have a steep spectrum with the exponent of the differential spectrum $\gamma \approx 3.2$–3.4. The steepening of the spectrum begins at surprisingly low energy $E_\gamma \approx 35$ MeV. It results in a very low diffuse gamma-ray intensity at $E_\gamma > 200$ MeV:

$$\Phi_\gamma (> 200 \text{ MeV}) \approx (5\text{-}10)\ 10^{-7} \text{cm}^{-2} \text{s}^{-1} \text{sr}^{-1} \qquad (1)$$

To estimate the effect of secular evolution of galaxies similar to our own, we must subtract from Eq.(1) the non-evolutionary contribution of this type of galaxies plus contribution (including its evolutionary part) of all other galaxies. Let us calculate the present gamma emissivity F_γ (in sec^{-1}) of our Galaxy caused by nuclear collisions of cosmic ray (c.r.) protons with ambient gas

$$F_\gamma = 2c \frac{M_g}{m_H} \int_{E_{th}}^{\infty} n(E_p) \sigma_{\pi^0}(E_p) dE_p = 2c \frac{M_g}{m_H} \omega_p \sigma_{eff} \qquad (2)$$

where $M_g = 8\ 10^9\ M_\odot$ is the total mass of gas in the Galaxy, $\sigma_{\pi^0}(E)$ is the product of π^0-production cross-section and multiplicity, $n(E_p)$ is the density of c.r. protons in the Galaxy, which according to observations (e.g.Cummings et al., 1973) is taken as

$$n(E_p) = \omega_p (E_p + E_0)^{-2.6} cm^{-3} GeV^{-1} \qquad (3)$$

with $E_0 = 1$ GeV and $\omega_p = 4\ 10^{-10} GeV/cm^3$, and

$$\sigma_{eff} = \int_{E_{th}}^{\infty} (E_p + E_0)^{-2.6} \sigma_{\pi^0}(E_p)\, dE_p = 4.0\ 10^{-27} cm^2 \qquad (4)$$

Here and henceforth the energy of a particle E is measured in GeV, if not stipulated otherwise.

From Eq.(2) we get at $E_\gamma > 100$ MeV that $F_\gamma = 1.0\ 10^{42} sec^{-1}$, which can be compared with $F_\gamma = 1.3\ 10^{42} sec^{-1}$ at $E_\gamma > 100$ MeV derived by Strong et al.(1976). The account of the halo radiation can increase the Galactic gamma emissivity to $7\ 10^{42} sec^{-1}$ (Worral and Strong, 1977). Using the generation spectrum $F_\gamma(>E_\gamma) \approx 2\ 10^{41} (E+0.3)^{-1.75} sec^{-1}$ derived from the fit experimental data on pion production we get the diffuse flux produced by the galaxies like our own during their total life time $T \approx 1.3\ 10^{10} yr$

$$\Phi_\gamma(>200\,\mathrm{MeV}) = \frac{c}{4\pi} n_G T F_\gamma(>200\,\mathrm{MeV}) \approx 7\,10^{-7} \frac{n_G}{1\,10^{-75}\,\mathrm{cm}^{-3}}\ \mathrm{cm}^{-2}\mathrm{s}^{-1}\mathrm{sr}^{-1} \quad (5)$$

where n_G is the spatial density of spiral galaxies similar to our own. The value (5) is in a close agreement with estimations of Strong et al.(1977).

Eq.(5) is obviously the lower limit estimate of the contribution of galaxies like our own since, firstly, the decrease of the extragalactic component by Fichtel et al.(1978) increases the Galactic component of the flux and, secondly, the electron component, discrete gamma sources and possible gamma radiation of halo are not taken into account in Eq.(5). Moreover, the spectrum of the Galactic radiation according to Fichtel et al. (1977,1978) is much flatter than that of extragalactic component.

The proximity of the value (5) to the experimental value (I) puts into question the existence of any appreciable secular evolution of the galaxies like our own whereas, owing to the steep isotropic gamma spectrum, this discrepancy does not restrict the possibility of the bright phase at large redshifts. Recently Wheeler et al.(1980) expressed also some doubt about the secular evolution in production of metals. However, the creation of metals very early in the history of the Galaxy, during its bright phase, remains to be very probable possibility. To investigate the bright phase of galaxies, high energy neutrinos seem to be most attractive. The reason is that at large redshifts ($z > 300$ at $\Omega = 0.2$) the column density of the matter exceeds the radiation length $x_{rad} = 62.8\ \mathrm{g/cm}^2$ (for the hydrogen) so that the gamma-ray spectrum should have a cut-off at the energy $E_\gamma \sim 1\ \mathrm{MeV}/(1+z) \sim 3\ \mathrm{keV}$. Meanwhile high energy neutrinos survive even from much more remote cosmological epochs without any appreciable energy losses except due to redshift.

III. GENERATION OF HIGH ENERGY NEUTRINOS AT THE BRIGHT PHASE OF GALAXIES

High energy neutrinos are originated in the decays of pions produced in the interactions of ultra high energy protons with ambient gas or with low energy electromagnetic radiation. In this Section three problems will be discussed: (a) the possibilities of acceleration to the very high energies ($E \gtrsim 10^{17}$eV), (b) the characteristic features of the neutrino spectrum imposed by the interaction of high energy protons with the relic radiation, and (c) the value of neutrino flux generated as a result of this interaction.

a) Acceleration to the very high energies

During the bright phase not only the processes of acceleration associated with single objects such as existing at present (e.g. supernovae, galactic nuclei) proceeded more intensively, but also acceleration associated with numerous objects or phenomena which rapidly died out in the "young" ($1000 > z > 10$) Universe, could have taken place. The latter include (i) numerous, rapidly evolving massive stars, (ii) overlapping shock fronts of many supernovae explosions (Schwarz et al., 1975; Ozernoy and Chernomordik, 1978) and (iii) turbulence accompanying the early stages of galaxy formation.

According to observations, the acceleration of particles is a very common feature of practically all astrophysical objects, from planet magnetospheres to galactic nuclei. In general, it is connected with the cosmic ray generation in the presence of turbulence or/and with the transformation of gravitational energy into kinetic energy in the presence of magnetic fields. The observed spectrum of cosmic rays extends to the energies over 10^{20}eV. From astrophysical point of view the observed intensity of ultra high

energy cosmic rays is very large. In particular, supernovae and pulsars which seem to be the only reasonable sources of ultra high energy c.r. in our Galaxy and in the surrounding normal galaxies, cannot provide the observed c.r. intensity at energies $10^{19} \lesssim E \lesssim 10^{20}$eV even under the assumption that the generation spectrum is very flat (Berezinsky and Grigor'eva 1979). Unfortunately, there is at present no reliable theory of particle acceleration to ultra high energies. The theoretical arguments can so far only indicate the sources where there are conditions suitable for such an acceleration. These sources are compact spinning bodies (neutron stars, magnetoids) with large surface magnetic fields, accreting black holes and large- scale turbulence with the magnetic field. We shall present here in brief some general ideas about acceleration to ultra high energies.

(i) Acceleration by compact objects

Consider a spinning, compact, massive body with the surface magnetic field B_s. Such a body is a homopolar generator having an electric potential φ on its surface. The difference in the potentials between two points on the surface is determined explicitely by the surface characteristics and does not depend on the conditions outside the object (in its magnetosphere):

$$\varphi_2 - \varphi_1 = \int_1^2 \vec{E}\, d\vec{\ell} = \frac{1}{c}\int_1^2 (\vec{v} \times \vec{B}_s)\, d\vec{\ell} \qquad (6)$$

where the integration is carried out along a contour on the surface of the body having a radius R_s, $\vec{v} = \vec{\Omega} \times \vec{R}_s$ is the velocity on the surface, $\vec{E} = \vec{v} \times \vec{B}/c$ is the electric field, and $\vec{\Omega}$ is the angular velocity.

The maximum value of the potential on the surface (relative to the infinity) , $\varphi_m = \max(\varphi_2, \varphi_1)$, is

$$\varphi_m \geq \frac{1}{2}(\varphi_2 - \varphi_1).$$

If the points 2 and 1 are taken on the pole and on the equator, then

$$\varphi_m = \frac{1}{2c} B_s \Omega R_s^2 . \qquad (7)$$

To go through the potential difference (7), the particles have to go away up to a very large distance from the surface. Meanwhile they can move only strictly along the magnetic lines of force. Being ejected, for instance, from the equator, the particles are keeping inside the "light cylinder" radius $R_c = c/\Omega$. Taking into account only those regions of the compact object from which the magnetic force lines go beyond the light cylinder leads to an extra factor in Eq.(7) equal to $\Omega R_s/c$, so that

$$\varphi_m = \frac{1}{2c^2} H_s \Omega^2 R_s^3 . \qquad (8)$$

Formulae analogous to Eq.(8) are well known for pulsars as specific sources of acceleration. We would like to stress here that the potential difference through which a particle goes, does not depend on magnetosphere models and is determined only by conditions on the surface of a source.

The numerical estimates of Eq.(8) for a young pulsar ($R_s \sim 10^6$cm, $B_s \sim 10^{13}$G, $\Omega \sim 10^3 \text{sec}^{-1}$) and a magnetoid-- a magnetized, spinning, supermassive body-- ($R_s \sim 10^{16}$cm, $B_s \sim 10^6$G, $\Omega \sim 10^{-7}\text{sec}^{-1}$) result in the potential difference $\varphi_m \sim 10^{18}$-10^{21} V.

Harrison's (1976) estimate of the potential difference being generated in the vicinity of a massive black hole with an accretion disk yields a similar value $\varphi_m \sim 10^{20}$ V .

However, available models indicate that the energy losses in the magnetosphere of a source diminish greatly the final energy attained by a particle being accelerated, as compared with the potential difference (8) estimated above. At the same time, it would be rather imprudent, based on this ground, to dismiss compact objects as probable sources of particle acceleration to ultra high energies. After all, such particles are observed in the Galaxy where there are no reasonable alternatives to explain them. Most probably that further theoretical analysis of various models for compact objects will be able to overcome the above mentioned difficulty.

(ii) Acceleration by large-scale turbulence

Acceleration of particles by large-scale turbulence can be carried into effect both by reflection of particles from moving inhomogeneities in the turbulent medium and by multiple passages of particles through shock fronts generated by turbulence. Whereas generation of particles is related to the bright phase in galactic evolution, the probable source of particle acceleration is the turbulence which accompanies the very origin of galaxies. It is natural to expect such a developed turbulence at the stage of galaxy formation -- or as a product of primaeval whirl motions or as a result of evolution of potential (adiabatic or entropy) perturbations.

Maximum energy which can be acquired by a particle moving in the turbulent medium is determined from the condition that the Larmor radius of the particles becomes to be comparable with

the characteristic scale, ℓ, of turbulent motions, so that

$$E \sim eH\ell \,, \tag{9}$$

with H being the magnetic field on the scale ℓ. It is reasonable to suppose that even at an early stage of galactic evolution H is determined, by an order of magnitude, from the equipartion of kinetic and magnetic energies, i.e.

$$H \sim v(4\pi\rho)^{1/2}. \tag{10}$$

From Eqs.(9) and (10) we get

$$E \sim e(4\pi\rho)^{1/2} v\ell = 300\,(4\pi\rho)^{1/2} K \quad eV \tag{11}$$

where the r.h. side of Eq.(11) is expressed, for a convenience of following estimates, by means of the specific angular momentum of the turbulent medium $K = v\ell$.

Although Eq.(11) has a rather general character we shall use now a concrete theory for galaxy formation -- namely, the whirl theory which makes it possible to calculate main characteristics of both galaxies and systems of galaxies as a result of evolution of cosmological turbulence (for a review, see Ozernoy, 1978). This theory shows that at the epoch of galaxy formation ($z_f \sim 30$)

$$\rho = 5\,10^{-24}\left(\frac{W}{0.2}\right)^4 g\,cm^{-3}, \quad K \approx 2\,10^{29}\left(\frac{M}{10^{12}M_\odot}\right)^{2/3}\left(\frac{W}{0.2}\right)^{2/3} cm^2 s^{-1} \tag{12}$$

where $W = V_e/c \sim 0.1 - 0.3$ is the dimensionless amplitude of primaeval whirl motions, $M \sim 10^{12} M_\odot$ is the maximum galaxy mass, which corresponds to the characteristic scale of turbulence accompanied the formation of galaxies. Substituting Eq.(12) into Eq.(11) yields $E \sim 4\ 10^{20}$eV.

Obviously, particles can be accelerated to ultra high energies by turbulence of an other origin, for instance, by secondary turbulence, generated, say, by potential perturbations in the course of galaxy formation. However, only in the whirl theory for origin of galaxies there are turbulent motions of protogalactic medium at redshifts as large as $z \sim 30$.

b) Characteristic energies in the spectrum

We assume that generation of c.r. with total energy output W_{CR} per each galaxy and with differential spectrum $A(E+E_o)^{-(\gamma_g+1)}$ extended up to energies $E \gtrsim 10^{10}$GeV, took place during the bright phase. Let us restrict ourselves by $p\gamma$ - neutrinos produced by collisions of ultrarelativistic protons with photons of the black-body relic radiation:

$$P+\gamma \longrightarrow N+\pi \hookrightarrow \mu+\nu \hookrightarrow e+\nu+\bar{\nu} \quad .$$

The $p\gamma$ -neutrino production was considered by Berezinsky and Zatsepin (1970). At the threshold of pion production the energies of neutrinos and protons are related by

$$E_\nu \approx \xi E_p \qquad (13)$$

where $\xi \approx (m_\pi / 4m_p) \approx 4\ 10^{-2}$.

It is convenient to introduce two characteristic energies of protons at the epoch with redshift z:

$$\Theta_p(z) = \frac{\Theta_{p0}}{1+z} \quad , \qquad \Theta_{p0} = 4.0\ 10^8 \text{ GeV} \ ; \qquad (14)$$

$$\Theta_\pi(z) = \frac{\Theta_{\pi 0}}{1+z} \quad , \qquad \Theta_{\pi 0} = 6.1\ 10^{10} \text{ GeV} \ . \qquad (15)$$

At $E_p \gtrsim \Theta_p(z)$ protons are decelerated due to (e^+e^-) pair production: $p+\gamma \rightarrow p+e^+ + e^-$. At $E_p \gtrsim \Theta_\pi(z)$ the deceleration of protons is mainly due to photopion production: $p + \gamma \rightarrow \pi + X$. Owing to the threshold character of pion production, a sharp maximum appears in the neutrino differential spectrum. The energy of neutrinos at the maximum of the spectrum observed at z = 0 is equal to

$$E_m = \xi \frac{\theta_{\pi o}}{(1+z_f)^2} = 6.1\,10^6 \left(\frac{20}{1+z_f}\right)^2 \text{ GeV} \qquad (16)$$

where z_f is the galaxy formation epoch which has the bright phase in its beginning. The measurement of the maximum in the spectrum of the diffuse neutrino flux allows to determine directly the redshift of the galaxy formation epoch.

It can be shown (see Appendix) that the expected flux of neutrino with energies above E_m which is produced at the bright phase of galaxies "switched on" at $z = z_f$ and having the present spatial density n_G, is given by

$$\Phi_\nu = \frac{3\eta c}{4\pi} \frac{\gamma_g - 1}{1-\alpha^{\gamma_g}} (1+z_f)^{\gamma_g} \frac{n_G W_{CR}}{E_o} \left(\frac{\theta_{\pi o}}{E_o}\right)^{-\gamma_g}. \qquad (17)$$

Here α is the energy fraction conserved by a proton in $p\gamma$-collision; α is ranged between $\alpha_{th} = I - m_\pi/m_p = 0.85$ at the threshold and $\alpha = 0.5$ at very high energies; η is relative probability for production of charged to neutral pions in $p\gamma$-collisions, η being ranged between 1/3 at the threshold and 2/3 at very high energies.

Eqs.(16) and (17) demonstrate clearly that the neutrino dating is most efficient if the bright phase took place at a sufficiently large redshift $z_f \gtrsim 20$. If z_f is smaller the value of Φ_ν diminishes and the location of the maximum in the spectrum E_m shifts to higher energies where the efficiency of its detection is smaller due to impossibility to use the resonance reaction $\bar{\nu}_e + e^- \to W^- \to$ hadrons (see Sect.4).

c) Numerical estimates of the neutrino flux

For numerical estimates we use a c.r. spectrum which is similar to that observed in our Galaxy. The spectrum of galactic protons has $\gamma = 1.65$ in the energy interval from 1-3 GeV up to $(1\text{-}3)10^6$ GeV (e.g.Zatsepin and Volkova, 1977). Meanwhile, the energy dependence of the path length of c.r.in the Galaxy, observed in the energy interval 1-100 GeV/nucleon, implies that the diffusion coefficient depends on energy like $D(E) \sim E^{\delta}$, so that the generation spectrum of cosmic rays has an exponent $\gamma_g = \gamma - \delta$. The value of δ is still uncertain being 0.59 ± 0.09 according to Caldwell and Meyer (1977) or 0.30 ± 0.06 according to Lezniak and Weber (1978). As a conservative estimate, we will take $\gamma_g = 1.3 - 1.4$. To explain the observed both intensity and anisotropy of c.r. at $E \lesssim 10^{10}$ GeV this generation spectrum should be extended up to the energy $E \sim 10^{10}$ GeV (Berezinsky et al, 1979).

Of course, the shape of the c.r.spectrum in our Galaxy can serve only as a guide in choosing γ_g for the bright phase. The value of γ_g characterises the efficiency of c.r.acceleration to very high energies as compared with smaller energies. Then it is naturally to expect the smaller value of γ_g at the bright phase than for our Galaxy now. This point of view meets some confirmation in the rather flat gamma ray spectra observed from such powerful sources as 3C 273 and Cen A.

Diffuse flux of neutrinos produced at the bright phase of galaxies (Eq. 16) is estimated as

$$\Phi_\nu(>E_m) = 2\,10^{-15}\left(\frac{1+z_f}{20}\right)^{1.3} \frac{n_G}{10^{-75}\,cm^{-3}} \frac{W_{CR}}{3\,10^{60}\,ergs}\ cm^{-2}s^{-1}sr^{-1} \qquad (18)$$

at $\gamma_g = 1.3$

$$\Phi_\nu(>E_m) = 6\,10^{-14}\left(\frac{1+z_f}{20}\right)^{1.1} \frac{n_G}{10^{-75}\,cm^{-3}} \frac{W_{CR}}{3\,10^{60}\,ergs}\ cm^{-2}s^{-1}sr^{-1} \qquad (19)$$

at $\gamma_g = 1.1$

being very sensitive to the value of γ_g *. The estimate (19) should be considered as an upper limit only, since the flux of diffuse gamma rays accompanying the neutrino flux (19) is already approaching one experimentally detected.

Our calculations give the smaller fluxes then those derived in the model of Berezinsky and Zatsepin (1976). That model with γ_g =I.I, was constructed to explain the observed isotropic X - and gamma-rays by the c.r. generation burst at $z \approx 30$. As was marked by Berezinsky (1978) the model encounters a difficulty in connection with low energy ($E_\gamma \approx 35$ MeV) steepening of gamma spectrum discovered by Fichtel et al.(1977,1978).

Comparing the fluxes (18) and (19) with fluxes from other sources (see Fig.1) we note that flux of prompt neutrinos from the atmosphere is about $10^{-16}cm^{-2}\ s^{-1}sr^{-1}$ at the same energies, the resulting neutrino flux from normal galaxies is less than $3\ 10^{-18}cm^{-2}s^{-1}sr^{-1}$, whereas the flux of galactic neutrinos from the direction towards the Galactic centre is about $3\ 10^{-15}cm^{-2}s^{-1}sr^{-1}$ (it should be undertaken that the total neutrino flux from the

* The choice of γ_g much larger than in our Galaxy (Stecker,1978) would result in a great decrease of the expected neutrino flux from the bright phase of galaxies.

whole disc of the Galaxy which is obtained by multiplication of this value to comparatively small effective solid angle $\Omega_{eff} \approx 0.8\pi$ is much smaller than the expected neutrino flux produced at the bright phase of galaxies).

IV. DISCUSSION

a) Related X-ray and gamma ray emission

Neutrinos generated at the bright phase of galaxies must be accompanied by X-and gamma-ray radiation produced by the same c.r. This radiation is a sum of gamma-rays resulting from the decays of neutral pions produced in pp-interactions, and the electromagnetic cascade resulting from the interactions of cosmic rays with the relic photons (Strong et al.,1973, Berezinsky and Smirnov, 1975). The relative contributions of these two components depend on the exponent γ_g : at $\gamma_g > 1.3$ gamma radiation from $pp \to \pi^0 X$ prevails, while at $\gamma_g < 1.3$ the cascade radiation dominates. To estimate the former we have assumed the depth of the matter traversed by c.r. in a parent galaxy and metagalactic space to be equal $x \approx 5$ g/cm^2. The calculations have shown that gamma-ray fluxes accompanied the neutrino fluxes (18) and (19) are less than the observed diffuse flux at all energies up to $E_\gamma \approx 200$ MeV; the upper limit (19) is related to cascade radiation with the latter being limited by experimental data at 35 MeV $\lesssim E \lesssim$ 200 MeV.

It is interesting to note that total neutrino flux (18) increases with z_f, while relevant 100 MeV gamma-ray flux decreases with z_f if $\gamma_g > 1.2$; for $z_f > 300$ at $\Omega \geq 0.2$ the present (z=0) gamma-ray spectrum would suffer a cut-off at $E_\gamma \sim 3$ keV. It illustrates the efficiency of neutrinos, as compared with X- and gamma

rays, for investigations of very redshifted epochs. In particular, neutrino dating of the galaxy formation epoch seems to be more promising than gamma-ray dating (Ozernoy, 1976).

b) Prospects for neutrino detection

Neutrinos of the energies under consideration ($E_\nu \gtrsim 10^{15}$–10^{16}eV) are very effective to be detected since in the Weinberg-Salam model the resonance energy for the reaction $\bar{\nu}_e + e^- \to W^- \to$ hadrons is about 6 10^{15}eV which is of the same order of magnitude as the energy (16) of the maximum in the expected neutrino spectrum. Effective cross-section for the detection of $\bar{\nu}_e$ is about 3 10^{-32}cm^2 which is by two orders of magnitude greater than the typical cross-section for ν N-interactions.

To detect neutrino fluxes of the order of 10^{-14}cm^{-2}s^{-1}sr^{-1} (see Eqs.(18) and (19) with the rate of about 100 hadronic cascades per year, the detection volume $\sim 10^{11}$ m^3 is necessary which can be feasible with underwater acoustic technique (Askarjan and Dolgoshein, 1977; Bowen, 1977). The underwater installation DUMAND being projected at the present time (Roberts, 1978) with an effective area of about 1 km^2 will detect ultrahigh energy muons ($E_\mu > 10^3$TeV) produced by neutrino flux $\Phi_\nu = 1\ 10^{-14}$cm^{-2}s^{-1}sr^{-1} with a rate 2 muons per year or so. The energy of these muons is so high that they can be unmistakably idenified, while the backgroung is expected to be extremely low. Therefore, a 10^9m^3 detector can provide a suggestive evidence for the existence of the bright phase.

V. CONCLUSIONS

High energy neutrinos give a remarkable possibility to investigate the earliest stages of evolution of galaxies even at redshifts as large as several hundreds. The main results of the present work devoted to the analysis of this topic may be summarized as follows.

1. Evolution of galaxies can be divided into bright phase and secular evolution. Apparently, the bright phase was the characteristic feature not only of stellar populations, but also of non-stellar, active sources in the galactic nuclei.

2. New data about the isotropic gamma-ray background at energies of about 200 MeV make questionable the presence of any appreciable secular evolution in c.r.luminosities of galaxies. This may be considered as an evidence in favour of even more violent bright phase of galaxies.

3. Bright phase of galaxies is expected to be the most powerful source of high energy neutrinos produced by interactions of c.r. with relic black-body radiation.

4. Differential neutrino spectrum has a maximum at the energy which is determined only by the redshift of the c.r. producing epoch. This gives a unique possibility of neutrino dating of the galaxy formation epoch being especially effective if the bright phase of galaxies took place at $z_f \gtrsim 20$.

Appendix

Flux of ($p\gamma$)-neutrinos from the bright phase of galaxies

We calculate here the flux of ($p\gamma$)-neutrinos produced at the bright phase of galaxies (redshift z_f) on the assumption that each galaxy like our own goes through the bright phase generating cosmic rays (c.r.) with the spectrum $A(E + E_o)^{-(\gamma_g+1)}$ and with the c.r. energy output W_{CR}.

If c.r. did not undergo in the intergalactic space any energy losses except those due to redshift, their energy density ω_{Mg} and flux $\Phi_p(E)$ at the present time ($z = 0$) would be equal, respectively, to:

$$\omega_{Mg} = \frac{W_{CR} n_G}{1+z_f} , \qquad (A\ 1)$$

$$\Phi_p(E)\,dE = B\left(\frac{E}{E_o}\right)^{-(\gamma_g+1)} \frac{dE}{E_o} \quad \text{at } E \gg E_o \qquad (A\ 2)$$

where $$B = \frac{c}{4\pi}\gamma_g(\gamma_g-1)\frac{\omega_{Mg}}{E_o}(1+z_f)^{-(\gamma_g-1)} . \qquad (A\ 3)$$

In reality, the protons generated at redshift z_f with energies above $\Theta_\pi(z_f) = \Theta_{\pi o}/(1+z_f)^2$ have lost all their energy as a result of photopion reactions on relic photons: $p + \gamma_r \to \pi + al.$ The flux of neutrinos produced in pion decays can be easily found using (A 2):

$$\Phi_\nu(>E) = 3\eta \frac{\xi^{\gamma_g}}{1-\alpha^{\gamma_g}} \frac{B}{\gamma_g}\left(\frac{E}{E_o}\right)^{-\gamma_g} . \qquad (A\ 4)$$

Here ξ is the fraction of energy transferred by a proton to a neutrino in the reaction $P+\gamma \to \pi^{+} + X$; $\xi = m_{\pi}/4m_{p} \approx 0.04$ at the threshold energy E_{th} and $\xi \approx 0.05$ at $E \gg E_{th}$. The factor $(1 - \alpha^{\gamma_{\beta}})^{-1}$ accounts for multiple collisions of a proton with relic photons: the energy $\xi^{-1}E_{\nu}$ necessary to generate neutrino of the energy E_{ν} may be attained not only by a proton which acquires this energy as a result of acceleration, but also by a proton of a greater energy which decelerates down to the energy $\xi^{-1}E_{\nu}$ in the photopion collisions; α is a fraction of energy conserved by a nucleon in the reaction $P+\gamma \to \pi + a\ell$. :

$\alpha = \alpha_{th} = 1 - m_{\pi}/m_{p} \approx$ 0.85 at the threshold of pion production and $\alpha \approx 1/2$ at much higher energies. The factor η in Eq.(A4) is the relative probability for production of charged to neutral pions in the $p\gamma$ -collisions: $\eta = \eta_{th} = 1/3$ at the threshold and $\eta \approx 2/3$ at much higher energies. The coefficient 3 in Eq.(A4) accounts for production of three neutrinos in the chain of π -meson decays.

Note that the Eq.(A4) contains the exponent of the proton generation spectrum, which must be smaller (like in our Galaxy) than the exponent of the spectrum for protons confined within a galaxy; their spectrum is related to that of gamma or radio radiation produced inside of the galaxy. Neglecting this difference, one would underestimate greatly the high energy neutrino flux (see e.g.Stecker, 1979).

Substituting now Eqs.(A 1) -(A 3) into Eq.(A 4) we get Eq.(17). Detailed numerical computations of the spectrum and $(p\gamma)$-neutrino flux are contained in the paper by Berezinsky and Smirnov (1975).

FIGURE CAPTIONS

Fig.1. Diffuse neutrino fluxes as a function of energy.
The flux from our Galaxy is given for the direction to the Galactic centre, two lines correspond to different extrapolation of the $pp \to \pi X$ cross-section at very high energies. Dashed lines show the fluxes of decay atmospheric neutrinos from horizontal (a) and vertical (b) directions. Dotted - dashed line shows the flux of prompt atmospheric neutrinos. The bright phase neutrino spectra are shown for the case $z_f = 30$.

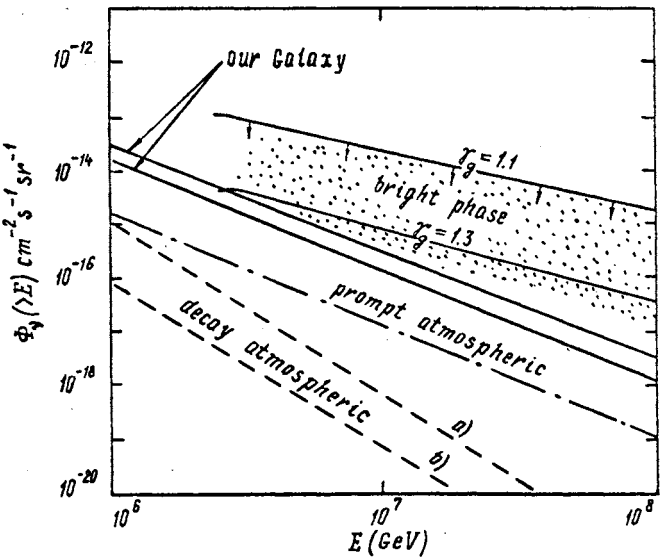
our Galaxy
$\gamma_g = 1.1$
bright phase
$\gamma_g = 1.3$
prompt atmospheric
decay atmospheric
a)
b)
10^{-12}
10^{-14}
10^{-16}
10^{-18}
10^{-20}
10^6
10^7
10^8
$E\,(GeV)$
$\Phi_\nu(>E)\ cm^{-2}\,s^{-1}\,sr^{-1}$

REFERENCES

Askarjan G.A. and Dolgoshein B.A.: 1977, Pis'ma Zh.Exp.Teor. Fiz.25, 232.

Berezinsky V.S.: 1978, Proc.Int.Conf."Neutrino-78" (ed. E.Fowler, Purdue, USA) p.23.

Berezinsky V.S. and Grigor'eva S.I.: 1979, Proc.16th Intern. Cosmic Ray Conf.(ICRC) 2, 81

Berezinsky V.S. and Zatsepin G.T.: 1970, Yadernaya Fizika II,200

Berezinsky V.S. and Smirnov A.Yu.: 1975, Astrophys.Sp.Sci.32,461

Berezinsky V.S. and Zatsepin G.T.: 1976, DUMAND-1976 (ed.A.Roberts),21

Berezinsky V.S., Syrovatskii S.I. and Mikhailov A.A. : 1979, Proc. 16th ICRC, 2, 86.

Bowen T. : 1977,Proc. 15th ICRC 6, 277.

Caldwell J.N. and Meyer P.: 1977, Proc.15th ICRC, 1,243

Cummings A.C., Stone E.C. and Vogt R.E.: 1973, Proc.13th ICRC 1, 335

Fichtel C.E., Hartman R.C., Kniffen D.A., Thompson D.J., Ögelman H.B. Ozel M.E. and Tumer T.: 1977, Astrophys.J. 217, L7.

Fichtel C.E., Simpson G.A. and Thompson D.J.: 1978, Astrophys.J. 222, 833

Fowler W.A.: 1972, in Cosmology, Fusion and Other Matters, Ed.by F.Reines.

Gott J.R. and Thuan T.X.: 1976, Astrophys.J., 204, 649

Harrison E.R.: 1976, Nature, 264, 52

Lezniak J.A. and Webber W.R.: 1978, Astrophys.J. 223, 676

Ozernoy L.M.: 1976, Comm.Grimea Astrophys.Observ. 54. 326 (in Russian)

Ozernoy L.M.: 1978, in The Large Scale Structure of the Universe (Proc.IAU Symp.No.79, Eds. M.S.Longair and T.Einasto), pp.427-438

Ozernoy L.M. and Chernomordik V.V.: 1976, Sov.Astr. -Astr.Zh., 20, 260

Ozernoy L.M. and Chernomordik V.V.: 1978, Sov.Astr. -Astr.Zh.22, 141

Partridge R.P. and Peebles P.J.E.: 1967, Astrophys.J. 147, 868

Roberts A. (editor): 1978, Proc.of DUMAND 1978 Summer Workshop

Schmidt M.: 1972, Astrophys.J. 176, 273

Schwarz J., Ostriker J.P. and Yahil A.: 1975, Astrophys.J., 202,1

Stecker F.W.: 1979, Astrophys.J. 228, 919

Strong A.W., Wolfendale A.W. and Wdowchyk J.: 1973, Nature, 241,109

Strong A.W., Wolfendale A.W. and Worral D.M.: 1976, J.Phys.A9, 1153

Strong A.W., Wolfendale A.W. and Worral D.M.: 1977,Proc.15th ICRC, 1, 91

Wheeler J.C., Miller G.E. and Scalo J.M.: 1980, Astron.Astrophys. 82, 152

Worral D.M. and Strong A.W.: 1977, Astron.Astrophys. 57,229

Zatsepin G.T. and Volkova L.V.: 1977, Proc.15th ICRC, 6,1

DUMAND AS A W^- FACTORY

K. O. Mikaelian*†
Department of Physics
Oklahoma State University
Stillwater, Oklahoma 74078

and

I. M. Zheleznykh
Institute of Nuclear Research
Academy of Sciences of the USSR
Moscow, USSR

ABSTRACT

$\bar{\nu}_e e$ annihilations leading to several new final states are considered for $\bar{\nu}_e$ energies between 10^{10} and 10^{18} eV interacting in the DUMAND detector. The rates are dominated by W^- production near its mass shell at $E_{\bar{\nu}} \approx 7 \times 10^{15}$ eV, which suggests viewing DUMAND as a W^- factory.

(Submitted for publication in the Proceedings of the 1980 International DUMAND Symposium held July 24-August 2 at Honolulu, Hawaii.)

*Work supported in part by the U.S. Department of Energy.

†Address after January 1981: Lawrence Livermore National Laboratory, Livermore, California.

1. Introduction

Since the early days of DUMAND, it has been clear[1] that the unique advantage of this project in high energy physics is its ability to look for processes initiated by very high energy neutrinos. Unless a completely new technological advance is made in accelerator physics (and none has really been suggested so far), accelerator neutrinos will in the foreseeable future be limited to energies of less than a few TeV. Cosmic neutrinos, either atmospheric or extra-terrestrial, will in that case be our only source of higher energy ($E_\nu \gtrsim$ 1-10 TeV) neutrinos. It must be noted, however, that at this Symposium and earlier it has been suggested[2] to build a "mini-DUMAND" (10^6 Tons) as a first stage of the project. The presumably small flux of very high energy ν's will be practically impossible to detect in such a "small" detector.

Besides the classic experiment of deep inelastic neutrino-nucleon scattering at high energies[1,3] (turnover of σ_T, shrinking y-distribution, etc.), there are other experiments which require high energy neutrinos because of higher thresholds; for example, neutrino production of weak bosons[4] and of Higgs bosons[5] off nuclear targets. Another class of reactions on which we report here is the annihilation of electron-antineutrinos on target electrons in the detector - $\bar{\nu}_e e$ annihilations.

Energy requirements are more severe in this class of reactions because the smallness of the electron mass m_e implies that one needs neutrinos of very high energy E_ν to achieve any useful center-of-mass energy $\sqrt{S}$, since $S = 2m_e E_\nu$, or

$$E_\nu(\text{TeV}) = S(\text{GeV}^2) \ . \qquad (1)$$

Since the charm threshold is at $\sqrt{s} \simeq 2$ GeV, the antineutrino energy $E_{\bar{\nu}}$ must be at least 4 TeV to excite the D-mesons, for example. Obviously, only a project like DUMAND can do any interesting $\bar{\nu}_e e$ physics.

We have made a systematic study of $\bar{\nu}_e e$ annihilations[6] and present here some results relevant to DUMAND. Earlier work has been done on the $\bar{\nu}_e e \to \pi^- \pi^o$ reaction[7] and on $\bar{\nu}_e e \to q\bar{q}$ as a probe of quark flavors.[8] In this paper we discuss several reactions with increasing thresholds. A natural dividing point is the W^- pole, so we first discuss annihilations below the W^- pole (Sect. 2), and in Sect. 3 we consider reactions with threshold above the W^- pole, which may also be called associated production, since they involve the production of a W boson in association with a γ, Z^o, or Higgs. The W^- pole itself was discussed[9] some time ago, and the applications of that large resonant cross section to DUMAND experiments have also been reported[10] in the literature.

2. $\bar{\nu}_e e$ Annihilations Below the W^- Pole

Below the W^- pole, which occurs at $\sqrt{s} = M_W \simeq 85$ GeV/c^2, and in order of increasing values for the threshold energies, the reactions are:

$$\bar{\nu}_e e \to \bar{\nu}_e e \qquad \text{(i)}$$

$$\bar{\nu}_e e \to \bar{\nu}_\mu \mu \qquad \text{(ii)}$$

$$\bar{\nu}_e e \to \text{hadrons } (\pi\text{'s, etc.}) \qquad \text{(iii)}$$

$$\bar{\nu}_e e \to \rho^-, K^{*-}, \ldots\ldots \qquad \text{(iv)}$$

$$\bar{\nu}_e e \to \bar{\nu}_\tau \tau \qquad \text{(v)}$$

followed by $\bar{\nu}_e e \to$ heavy hadrons like strange, charm, bottom quarks etc. All of the above reactions proceed by first converting $\bar{\nu}_e e$ into a virtual W^- which then decays into the particular final state (see Fig. 1), except the first reaction, to which we must add the exchange of the neutral intermediate vector boson Z^0.

Complete expressions for these processes, valid for all energies, are rather long and given in ref. 6. Since we are here below the W^- pole, the appropriate approximation is $S \ll M_W^2$, in which case the results simplify, and we shall quote only the total cross sections in this limit. The opposite limit, $S \gg M_W^2$, will be treated in Sect. 3. The electron mass is neglected throughout this paper.

In this "low" energy region, meaning $E_{\bar{\nu}} \ll M_W^2/2m_e \simeq 7 \times 10^3$ TeV, we find

$$\sigma(\bar{\nu}_e e \to \bar{\nu}_e e) = \frac{G_F^2 S}{3\pi}\{\frac{1}{4} + \sin^2\theta_W + 4\sin^4\theta_W\}$$

$$\simeq 3.7 \times 10^{-39}(\text{cm}^2)E_{\bar{\nu}} , \qquad (2)$$

where we set $\sin^2\theta_W = .23$, and $E_{\bar{\nu}}$ is in TeV.

For reaction (ii), setting $m_\mu = 0$, we get

$$\sigma(\bar{\nu}_e e \to \bar{\nu}_\mu \mu) = G_F^2 S/3\pi \simeq 5.3 \times 10^{-39}(\text{cm}^2)E_{\bar{\nu}}/\text{TeV} . \qquad (3)$$

The same expression also describes $\bar{\nu}_e e \to \bar{\nu}_\tau \tau$ if $m_\tau^2/S \ll 1$, since both proceed via W^- decay only. The full expression, keeping m_τ finite, is given by

$$\sigma(\bar{\nu}_e e \to \bar{\nu}_\tau \tau) = \frac{G_F^2 S}{3\pi}(1 + m_\tau^2/2S)(1 - m_\tau^2/S)^2 \quad . \tag{4}$$

We now turn to hadroproduction. Using the quark-parton picture, Fig. 1c, we describe $\bar{\nu}_e e \to$ hadrons as $\bar{\nu}_e e \to q\bar{q} \to$ hadrons, and define a ratio in analogy with e^+e^- reactions:

$$R_W = \frac{\sigma(\bar{\nu}_e e \to \text{hadrons})}{\sigma(\bar{\nu}_e e \to \bar{\nu}_\mu \mu)} \quad . \tag{5}$$

If we neglect the Cabibbo or Kobayashi-Maskawa mixing angles, then $R_W = 3$ below the charm threshold, $R_W = 6$ above the $s\bar{c}$ threshold, and $R_W = 9$ above the $b\bar{t}$(?) threshold. Adding $\tau \to$ hadrons with B.R. $\simeq$ 65% brings R_W close to 10 in the standard 6-lepton and 6 x 3_c-quark model, 3_c being the color factor.

We close this Section by discussing resonance production of vector mesons like ρ^-, K^{*-}, F^{*-}, etc. In terms of the decay widths of the vector meson V into $\bar{\nu}_e e$ and any final state F, we can write

$$\sigma(\bar{\nu}_e e \to V \to F) = 24\pi \frac{\Gamma_{V\to\bar{\nu}_e e}\Gamma_{V\to F}}{(S-m_V^2)^2 + m_V^2\Gamma_V^2} \quad . \tag{6}$$

In Fig. 2 we illustrate V production by ρ^- and F^{*-}, taking $\Gamma_{F^*} = 1/10$ GeV rather arbitrarily, since it is not known at this time. The leptonic decay widths $\Gamma_{V\to\bar{\nu}_e e}$ can be obtained using vector meson dominance, as has been done in ref. 6.

Numerical results are given in Fig. 2 which shows the total cross sections as a function of neutrino energy both below and above the all-dominant W^- pole. We next discuss the region above this pole.

3. $\bar{\nu}_e e$ Annihilations Above the W^- Pole

In addition to new channels opening up as the neutrino energy is increased and new thresholds are crossed, we have, of course, reactions (i) - (v) still occurring but at a different rate, and we discuss them first. Vector meson production, reaction (iv), will take place only if there are ultraheavy mesons as predicted in some technicolor theories.[11] Eq. (6) still holds, of course. Similarly hadron production, reaction (iii), when normalized to the $\bar{\nu}_\mu \mu$ cross section and expressed as R_W in Eq. (5), remains the same, viz. ~ 10 in the standard channel, assuming that the top-quark threshold lies below M_W. The rates for heavy lepton production and muon production, reactions (ii) and (v), become identical as long as we are appreciably above the heavy lepton threshold, as seen in Fig. (2). However, instead of increasing linearly with $E_{\bar{\nu}}$ as they were below the W^- pole, now they decrease with $E_{\bar{\nu}}$:

$$\sigma(\bar{\nu}_e e \to \bar{\nu}_\mu \mu) = \sigma(\bar{\nu}_e e \to \bar{\nu}_\tau \tau) = \frac{G_F^2 M_W^4}{3\pi S}$$

$$\simeq 2.8 \times 10^{-31} (\mathrm{cm}^2)/E_{\bar{\nu}} \qquad (7)$$

where we set $M_W = 85\ \mathrm{GeV}/c^2$, and $E_{\bar{\nu}}$ is again in TeV.

The elastic cross section , $\bar{\nu}_e e \to \bar{\nu}_e e$, changes in a different manner: from a linear increase with $E_{\bar{\nu}}$ below the pole it goes over to a constant value for energies substantially above the pole. This behavior is caused by Z^o exchange (see Fig. 1) and is not duplicated by any of the other processes. The value of the asymptotic limit is:

$$\sigma_{asymp}(\bar{\nu}_e e \to \bar{\nu}_e e) \quad \frac{G_F^2 M_Z^2}{8\pi}\{1 + (1-4\sin^2\theta_W)^2\}$$

$$\simeq 1.9 \times 10^{-35} cm^2. \qquad (8)$$

Since the asymptotic amplitude is a purely neutral current term, we conclude that in the same limit, i.e. $S >> M_W^2, M_Z^2$, Eq. (8) describes also the elastic scattering of $\bar{\nu}_\mu$ and $\bar{\nu}_\tau$ on electrons. One can also show that the scattering of neutrinos ν_e, ν_μ and ν_τ on electrons is also given by Eq. (8) in the high energy limit.[12]

We now turn to reactions whose thresholds lie at or above the W-pole:

$$\bar{\nu}_e e \to W^- \qquad (vi)$$

$$\bar{\nu}_e e \to W^- \gamma \qquad (vii)$$

$$\bar{\nu}_e e \to W^- Z^0 \qquad (viii)$$

$$\bar{\nu}_e e \to W^- H \qquad (ix).$$

The resonant cross section[9] can be written as

$$\sigma_{res}(\bar{\nu}_e e \to W^- \to F) = \frac{24\pi}{M_W^2} \frac{\Gamma_{W\to e\nu}\Gamma_{W\to F}}{(\Gamma_{W\to all})^2} \qquad (9)$$

for any final state F. In the standard model with three lepton doublets and nine quark doublets, $\Gamma_{W\to all} = \sum_F \Gamma_{W\to F} = 12\Gamma_{W\to e\nu}$, and we get

$$\sigma_{res}(\bar{\nu}_e e \to W^- \to anything) = 2\pi/M_W^2 \simeq 3.4 \times 10^{-31} cm^2 . \qquad (10)$$

Analytical expressions for the remaining reactions (vii), (viii) and (ix) are rather complicated and we refer to references 6 and 13. At very high energies they all decrease like $1/E_{\bar{\nu}}$ or $1/E_{\bar{\nu}}\ \ell n E_{\bar{\nu}}$: e.g. Higgs boson production $\bar{\nu}_e e \to W^- H$ has a rate four times less than $\bar{\nu}_\mu \mu$ production. The total cross sections for reaction (vi) to (ix) are shown in Fig. 2 (we have set $m_H = 30\ \mathrm{GeV}/c^2$ in Fig. 2). Clearly the maximum rates are reached soon after the thresholds are crossed, after which they start decreasing.

Multiparticle final states like $W^- e^+ e^-$, $W^- Z^o H$, etc., are also energetically possible at these high energies and may, in fact, exhibit a mild logarithmic growth with energy. They are, however, of higher order in the coupling constants and hence will be suppressed until we reach energies well beyond cosmic ray energies. We have not considered such possibilities.

4. Conclusions

Fig. 2 shows the results of our detailed calculations: the cross sections are dominated by the W^- pole, which makes us view the DUMAND project partly as a W-factory, in analogy with Z^o-factories now under serious study at SLAC and CERN. Unless specific final states can be distinguished, the earlier calculations[10] based only on resonance production are quite adequate.

Except for $\bar{\nu}_e e \to \bar{\nu}_\mu \mu$, identification of final states will be difficult because other reactions can mimic the ones considered here. For example, elastic scattering can be confused with neutral current scattering because the high energy scattered electron may be misidentified as a hadronic jet. $W^- Z^o$ will look like two hadronic jets (charm production?). Similarly for $W^- H$. If, however, muons can be correctly identified as such, then $\bar{\nu}_e e \to \bar{\nu}_\mu \mu$ will be observable because a single muon, originating deep within the ocean and unaccompanied by any hadronic debris is hard to duplicate. The same

applies to τ production when the τ decays into μ's.

Several processes that we have considered require extremely energetic neutrinos, and the cosmic ray flux being a steep function of energy we naturally conclude that there will be very few events of this type in DUMAND (unless there is an anomalously large flux of antineutrinos!). As a comparison, we mention that the deep inelastic scattering cross section levels off (actually grows very slowly) at about $10^{-34} cm^2$ for $E_\nu \gtrsim 100$ TeV. Against this background one must measure the $\bar{\nu}_e e$ rates reported here. The presence of the W^- pole makes this task possible, but certainly not easy.

References

1. D. Cline, Proceedings of the 1976 DUMAND Summer Workshop at Honolulu, p. 265.
2. J. G. Learned, Proceedings of the 1979 DUMAND Summer Workshops at Khabarovsk and Lake Baikal, p. 324.
3. T. K. Gaisser and A. Halprin, Proceedings of the 15th Int'l. Cosmic Ray Conference, Plovdiv, MN 265 (1977).
4. R. W. Brown et al., Proceedings of the 1978 DUMAND Summer Workshop at La Jolla, p. 13.
5. K. O. Mikaelian and R. J. Oakes, ibid, p. 89.
6. K. O. Mikaelian and I. M. Zheleznykh, Physical Review D (in press).
7. D. K. Ershov and I. M. Zheleznykh, Comm. on Physics (Lebeden Inst.), 4, 37 (1972).
8. E. A. Tainov and I. M. Zheleznykh, Proceedings of the 1979 DUMAND Summer Workshops at Khabarovsk and Lake Baikal, p. 188.
9. S. L. Glashow, Phys. Rev. 118, 316 (1960).
10. V. S. Berezinsky, D. Cline and D. N. Schramm, Phys. Lett. 78B, 635 (1978).
11. See, e.g. S. Dimopoulos and L. Susskind, Nucl. Phys. B155, 237 (1979).
12. At lower energies the neutrino scattering rates are different from the antineutrino rates.
13. R. W. Brown, D. Sahdev and K. O. Mikaelian, Phys. Rev. D20, 1164 (1979).

Figure Captions

Fig. 1. Feynman diagrams for processes initiated by $\bar{\nu}_e e$ collisions.

Fig. 2. Total cross sections for $\bar{\nu}_e e$ annihilation into $\bar{\nu}_e e$, $\bar{\nu}_\mu \mu$, $\bar{\nu}_\tau \tau$, ρ^-, F^{*-}, W^-, $W^-\gamma$, W^-H and W^-Z^o, as a function of the anti-neutrino energy $E_{\bar{\nu}}$.

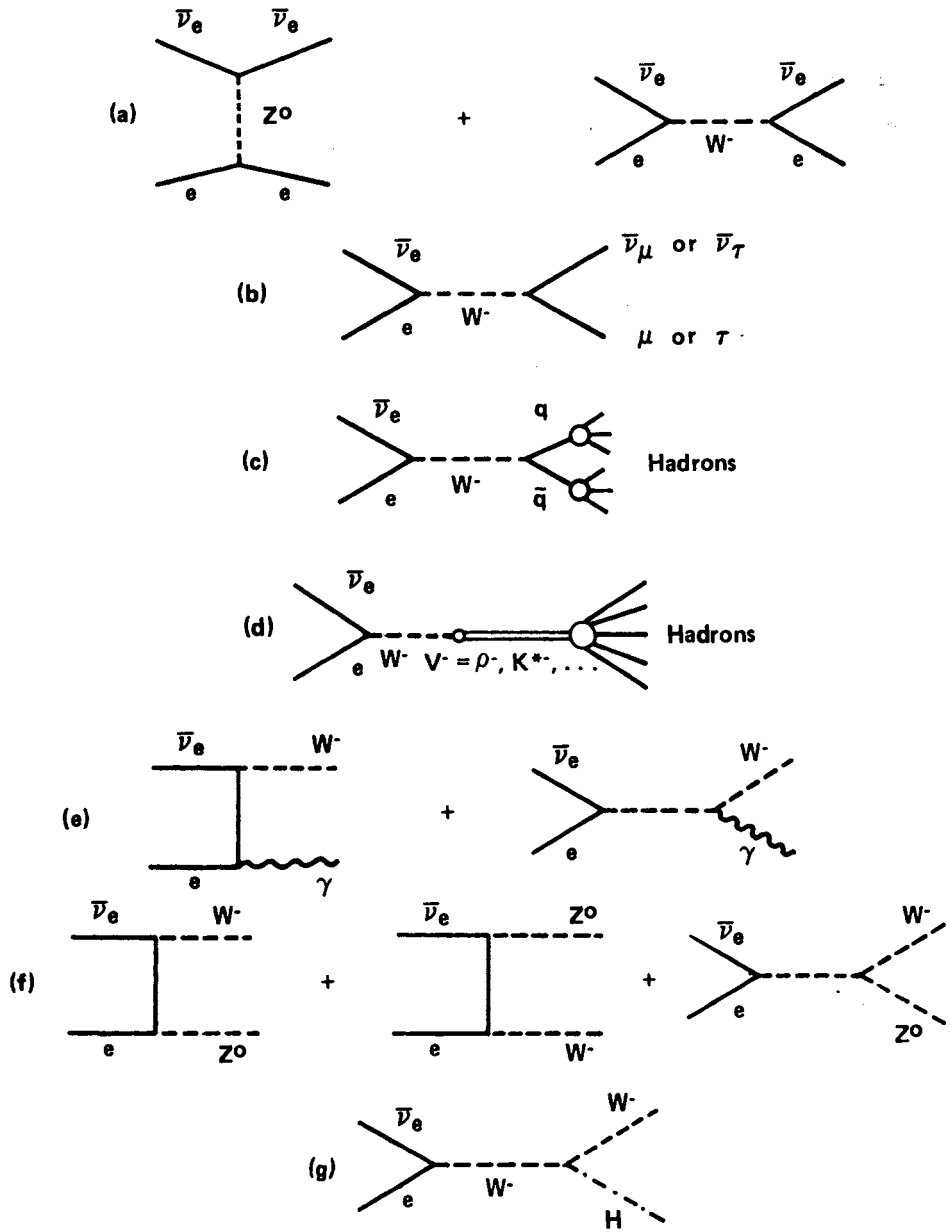
(a)
$\bar{\nu}_e$
$\bar{\nu}_e$
Z^o
e
e
+
$\bar{\nu}_e$
$\bar{\nu}_e$
W^-
e
e
(b)
$\bar{\nu}_e$
W^-
e
$\bar{\nu}_\mu$ or $\bar{\nu}_\tau$
μ or τ
(c)
$\bar{\nu}_e$
q
W^-
e
$\bar{q}$
Hadrons
(d)
$\bar{\nu}_e$
e
W^-
$V^- = \rho^-, K^{*-}, \ldots$
Hadrons
(e)
$\bar{\nu}_e$
W^-
e
γ
+
$\bar{\nu}_e$
W^-
e
γ
(f)
$\bar{\nu}_e$
W^-
e
Z^o
+
$\bar{\nu}_e$
Z^o
e
W^-
+
$\bar{\nu}_e$
W^-
e
Z^o
(g)
$\bar{\nu}_e$
W^-
e
W^-
H

Figure 1

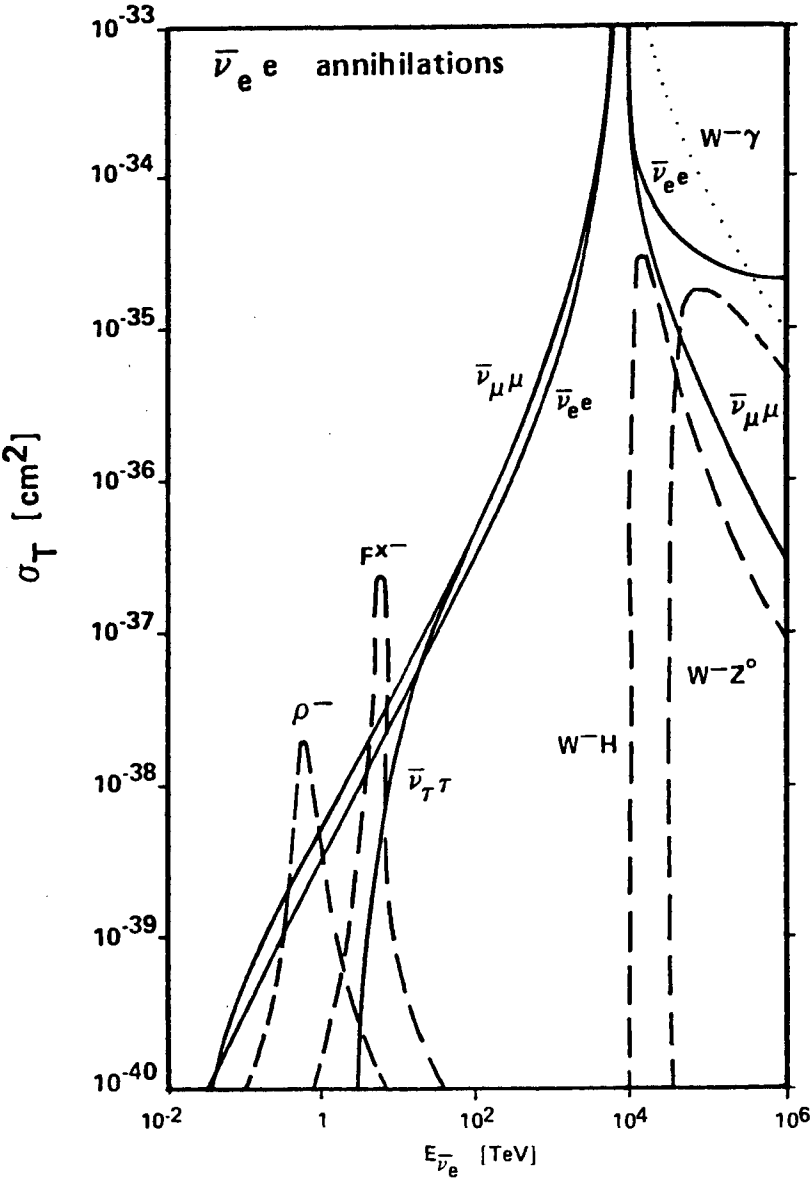
$\bar{\nu}_e$ e annihilations
10^{-33}
10^{-34}
10^{-35}
10^{-36}
10^{-37}
10^{-38}
10^{-39}
10^{-40}
σ_T [cm^2]
10^{-2}
1
10^2
10^4
10^6
$E_{\bar{\nu}_e}$ [TeV]
W$^-\gamma$
$\bar{\nu}_e$e
$\bar{\nu}_\mu\mu$
$\bar{\nu}_e$e
$\bar{\nu}_\mu\mu$
F^{x-}
ρ^-
$\bar{\nu}_\tau\tau$
W$^-$H
W$^-$Z$^\circ$

Figure 2

Heavy Weak Bosons, Cosmic Antimatter and DUMAND:

I: Looking for Heavier Weak Bosons with DUMAND

R.W. Brown*

Physics Department

Case Western Reserve University

Cleveland, Ohio 44106

and

F.W. Stecker

Laboratory for High Energy Astrophysics

NASA Goddard Space Flight Center

Greenbelt, Maryland 20771

Abstract: We discuss a possibly unique opportunity afforded by a facility like that of DUMAND. A number of different theoretical developments indicate that one or more heavier weak bosons may coexist with the "standard" weak boson. If this is true, a broad program may be laid out for a search for the heavier W's via change in the total cross section for $\nu N \to \nu X$ due to the additional propagator, a concomitant search via the annihilation $\bar{\nu}_e e^-$, and a subsequent search (discussed in the following paper) for significant antimatter in the universe involving the same annihilation, but being independent of possible neutrino oscillations. The program is likely to require detectors sensitive to higher energies, such as acoustic detectors.

*Research supported in part by the National Science Foundation, Grant No. PHY80-08548

I. INTRODUCTION

There are reasons to believe that a number of weak bosons exist:

1) We may very well have different generations gauge bosons just as exist for quarks and leptons.(1)
2) The increased interest and success in thinking about substructure "prequarks," "preons", or "rishons" may lead to heavier composite systems of all spins.(2)
3) Superunification investigations have recently led to a natural composite picture.(3)
4) Heavy "right-handed" W's may arise if parity is spontaneously broken.(4)
5) Heavy "right-handed" W's may arise in a gauge hierarchy of grand unified theories.(5)

These are not all of the contexts in which heavier W's arise. There is the general question about which gauge group is involved in the weak interaction field theory.

It is quite likely that only higher energy facilities like DUMAND could be used in a search for these new particles, in contrast to the up-and-coming search for the "standard" W . For clarity in presenting our program, we will assume that two W's exist, W_1 and W_2, with masses

$$M_1 \simeq M_W = \frac{37.4}{\sin\theta_W} \simeq 80 \text{ GeV}/c^2 \quad , \qquad (1)$$

$$M_2 \gtrsim 3M_W \quad .$$

In section 2, we shall discuss how the presence of the second W changes the hallmark of the standard DUMAND W search, the propagator bendover in

$$\nu N \to \mu X \quad . \qquad \text{(i)}$$

The "W^- factory" idea for DUMAND,(6)

$$\bar{\nu}_e e^- \to W^- \quad , \qquad \text{(ii)}$$

can be extended to the heavier W_2 case. There are, in fact, some advantages in doing so, relative to the lighter W. We discuss this in section 3.

The final step in our program addresses the profound question of whether or not large regions of antimatter exist in the universe. Neutrino astronomy with heavier W's playing a key role can answer this question and is discussed in section 4 and the companion paper II.

The new issue of neutrino oscillation and mass does not becloud our program. Rather, the possible existence of right-handed (left-handed) neutrinos (antineutrinos) adds to its attractiveness. We shall comment on the relevance of this issue in each section.

II. INELASTIC NEUTRINO SCATTERING

The propagator due to the W-boson should be clearly visible in deep inelastic y-distributions for reaction (1).[7] For our present purposes, we have investigated how the <u>total</u> cross section changes due to <u>two</u> W's. The old, single bendover will be seen to have additional structure. The y-distribution discussion will be included in an amended edition of this paper.

We can draw upon recent work[8] on doubling weak bosons, for a representative calculation. Our philosophy is quite different, however. Rather than concentrate on the lighter W_1, and its phenomenology, the emphasis is on the heavier W_2. In the event that $M_1 \simeq M_W$, the search for more involved structure in weak interactions will require higher energies and a focus on W_2.

Define

$$\kappa \equiv \left(\frac{M_2}{M_W}\right)^2 \quad , \quad \epsilon \equiv 1 - \left(\frac{M_1}{M_W}\right)^2 \quad . \tag{2}$$

Implementing (1),

$$\kappa >> 1 \quad , \quad \epsilon << 1 \, . \tag{3}$$

Then the leptonic decay widths $(W_1 \to \ell \nu)$ are

$$\frac{\Gamma_1^\ell}{M_1} \simeq \frac{\Gamma_W^\ell}{M_W} \simeq 0.3\% \quad ,$$

$$\frac{\Gamma_2^\ell}{M_2} \simeq \epsilon\kappa \, \frac{\Gamma_W^\ell}{M_W} \quad . \tag{4}$$

We further stipulate

$$\kappa\epsilon \simeq 1 \quad , \tag{5}$$

although larger values of $\kappa\epsilon$ will still leave us with sufficiently small total widths ($\Gamma = 12 \, \Gamma_W^\ell$ for the usual single-boson 3-generation model).

The standard propagator is now replaced:

$$\frac{1}{1+z} \to \frac{1}{1+z} \, \frac{2z+R}{z+R} \tag{6}$$

where

$$z \equiv Q^2/M_W^2 \ , \ Q^2 = -\ (\text{4-momentum-transfer})^2 \ .$$

With a numerical integration over the parton form of the deep inelastic differential cross section, the question of how much the total cross section is changed can be answered. Noting $\kappa = \infty$ corresponds to the old standard, we look at the deviation from the single-boson total cross section in Fig. 1 for the case $\kappa = 10$. The deviation scales in s/M_W^2 . For $M_W = 80$, the cosmic ray energy is

$$E = 3.4 \frac{s}{M_W^2} \text{ TeV} \ , \ \text{TeV} = 10^{12}\text{eV} \ . \tag{7}$$

The asymptotic value for Fig. 1 is .36 .

The conclusion is that a 20% increase shows up around the next scale

$$s/M_W^2 = \kappa \ . \tag{8}$$

(Remember that the first propagator effect takes place around $s/M_W^2 = 1$.)

We comment on this result by way of a list of points for future study:

1) As we increase κ without decreasing ε , the deviation can be larger.
2) It appears that acoustic detectors are not crucial for this stage of our program. For very large κ , the deviation is small, anyway.
3) The y-distributions should be examined in detail for bins in the TeV range, in the 10 TeV range, and so forth.
4) What if there are neutrino oscillations? Suppose that neutrinos oscillate into antineutrinos. In that case, their helicity is then wrong for the V-A charged currents. However, V+A currents and associated (heavy) weak bosons B then come into play. We would see a new incoherent contribution to deep inelastic events at the higher energies if B's exist. If the neutrinos oscillate among the generations $(e,\mu,\tau,\ldots)$, the final lepton signature is changed. But the τ and μ signatures are both viable. In any case, the total neutrino flux is not so small that oscillations are a problem.
5) It will be of interest to extend the calculations[9] for the reaction,

$$\nu N \to \ell\, B_i X \tag{iii}$$

where the B_i are actually produced. For larger $\varepsilon\kappa$, we could have significantly larger cross sections than in the standard model.
6) Sequential W's should also be considered.[10]
7) The ratio examined here is insensitive to many details such as scaling violations.
8) Finally, we emphasize again that it is possible that DUMAND could distinguish between various weak-EM gauge models.

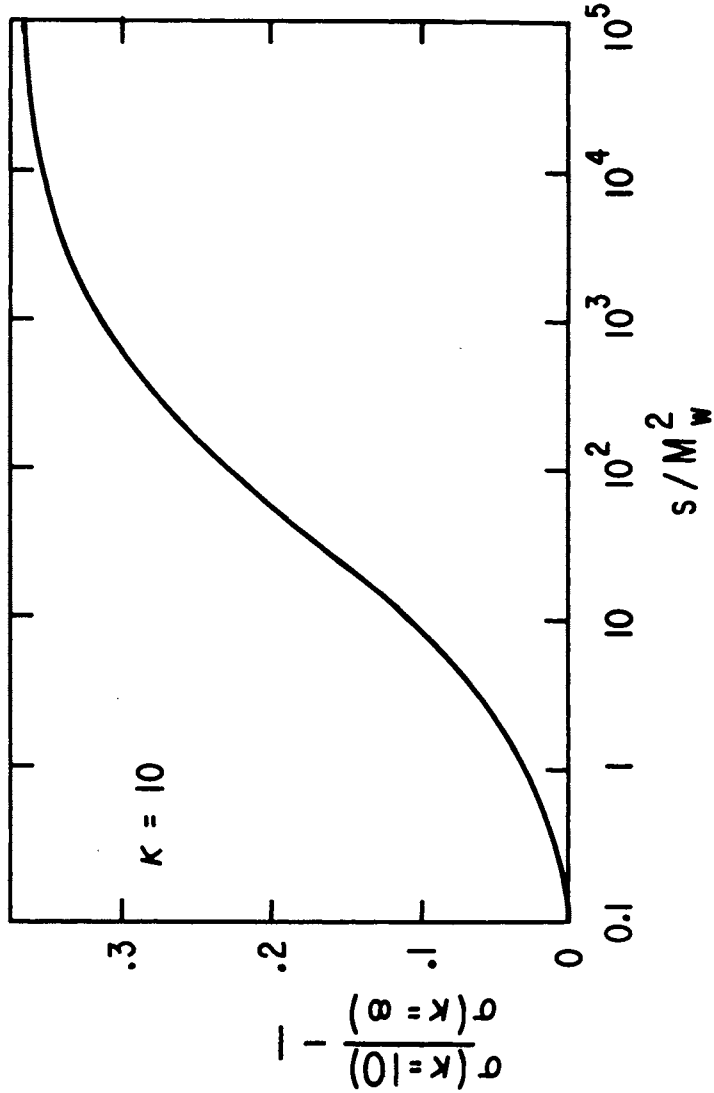

Fig. 1. Increase in the total νN inelastic cross section due to a second weak boson with $\kappa = 10$.

III. NEUTRINO-ELECTRON ANNIHILATION

The resonance reaction (ii) has been the subject of a proposal for a DUMAND cosmic ray experiment.(11) However, for a standard weak-boson mass, there may be severe background problems from the general reaction (i). We note that the cosmic neutrino must now have energy

$$E = 6.26 \frac{s}{M_W^2} \text{ PeV} \quad ,$$

$$\text{PeV} = 1000 \text{ TeV} = 10^{15} \text{ eV} \quad , \tag{9}$$

for $\bar{\nu}_e e^-$ c.m. energy $\sqrt{s}$.

If there is a heavier W, on the other hand, the background flux will have dropped off and we are back in business. The heavier of any forest of resonance spikes will stand out. It is here where acoustic detector developments are helpful. If we have a detection system which is (increasingly) sensitive to higher energies, then the new mass scales in weak interactions and lower backgrounds are at hand. (See paper II.)

If the flux and detector energy-dependence is negligible over the boson resonance width, the relevant quantity for the event rates is

$$\int \sigma_{res} \, dE = \frac{1}{2m_e} \int \sigma \, ds = \frac{1}{2m_e} \, 24\pi^2 \, \frac{\Gamma_i^\ell}{M_i} \tag{10}$$

for narrow total width Γ_i . We see that heavier bosons may very well have an increase in rates for a given flux and detection efficiency. The fact that acoustic detectors may be increasingly sensitive to higher energies and that the backbody process (see paper II) yields a shoulder in the flux of $\bar{\nu}_e$ makes an even stronger case here.

Even if there are only extragalactic neutrinos left above a certain energy, there are showers to be expected from deep inelastic scattering (by the same neutrinos). However, this background is small:

$$\frac{\int \sigma_{back} \, dE}{\int \sigma_{res} \, dE} \simeq \frac{<\sigma_{back}>\Delta S}{24\pi^2 \, \Gamma_i^\ell / M_i} \simeq \frac{<\sigma_{back}>}{2\pi^2 / M_W^2} \frac{\Gamma_i}{12\Gamma_i^\ell} \kappa_i \quad ,$$

$$\kappa_i = \left(M_i / M_W \right)^2 \tag{11}$$

For

$$2\pi^2 / M_W^2 = 1.2 \times 10^{-30} \text{ cm}^2 \quad , \quad <\sigma_{back}> \simeq 3 \times 10^{-34} \text{ cm}^2 \quad ,$$

$$\Gamma_i = 12 \, \Gamma_i^\ell \quad , \quad \kappa_i = 10 \tag{12}$$

the number is 2.7×10^{-3} .

If the $\bar{\nu}_e$ oscillate into other neutrino states, then we lose events. But an important point is that the counterpart left-handed $\bar{\nu}_e$ [arising, perhaps, from ν_{e_L} transitions into $(\bar{\nu}_{e_L})$] will then produce the "right-handed" W_R and we can rephrase everything in terms of W_R sequences.

IV. SEARCH FOR ANTIMATTER

The third leg of this program for DUMAND involves the symbiotic relation between the existence of a heavy W and the fact that high energy $\bar{\nu}_e$'s may come from large scale, distant antimatter sources. If the existence of heavier W's can be established by the propagator effect, say, of section 2, then we can turn the resonance analysis discussed in section 3 around. The $\bar{\nu}_e$ flux can be determined-the expected number of events is a strong function of the acoustic detection characteristics-and the possibility of important extragalactic sources explored.

We leave the discussion of the third leg to the companion paper (II) where the event rates are discussed but we reiterate that any oscillation $\bar{\nu}_e \leftrightarrow \nu_e$ will not wash out this test for antimatter, since helicity is preserved. Thus sources of ν_{e_L} will not contaminate the $(\bar{\nu}_e)_R$ flux. Even better, the existence of additional W_R's will provide more signature for this important test of antimatter in the universe.

REFERENCES

1. This is not yet an orthodox grand-unified-field-theory view, but experiment and superunified view are our bias here.

2. J.C. Pati, A. Salam, and J. Strathdee, Phys. Lett. 59B, 265 (1975); H. Harari, Phys. Lett. 86B, 83 (1979); M.A. Shupe, Phys. Lett. 86B, 87 (1979); and H. Terazawa, Proc. XIX Int'l Conf. on High Energy Physics [ed. by S. Homma, M. Kawaguchi, and H. Miyazawa (Phys. Soc.of Japan, Tokyo, 1979)], p. 617.

3. E. Cremmer and B. Julia, Phys. Lett. 80B, 48 (1978). See the recent study by J. Ellis, M.K. Gaillard, L. Maiani, and B. Zumino, LAPP-TH-15, April, 1980.

4. See the references in R.N. Mohapatra and G. Senjanović, Phys. Lett. 79B, 283 (1978). A recent discussion is by T.G. Rizzo, Phys. Rev. D21, 1214 (1980).

5. Q. Shafi and C. Wetterich, CERN. Th. 2667, May 1979.

6. See R.W. Brown in Proc. of Workshop on Production of New Particles in Super High Energy Collisions [ed. by V. Barger and F. Halzen (U. of Wisconsin, Madison, Wisc., 1980)].

7. A. Roberts, 16th International Cosmic Ray Conference, FERMILAB-Conf-79/32-EXP.

8. V. Barger, W.Y. Keung, and E. Ma, Phys. Rev. Lett. 44, 1169 (1980); Phys. Rev. D22, 727 (1980).

9. R.W. Brown, D. Sahdev, J. Stroughair, and K.O. Mikaelian, in Proc. of DUMAND 1978 Summer Workshop, ed. A. Roberts (La Jolla, 1979).

10. V. Barger, W.Y. Keung, and E. Ma, Phys. Lett. 94B, 377 (1980). See also E.H. Degroot, G.J. Gounaris and D. Schildknecht in Phys. Lett. 85B, 399 1979); Zeit. Phys. C5, 127 (1980).

11. V.S. Berezinsky, D. Cline, and D.N. Schramm, Phys. Lett. 78B, 635 (1978).

Heavy Weak Bosons, Cosmic Antimatter and DUMAND:

II: Looking for Cosmic Antimatter with DUMAND

F.W. Stecker

Laboratory for High Energy Astrophysics

NASA Goodard Space Flight Center

Greenbelt, Maryland 20771

and

R.W. Brown*

Physics Department

Case Western Reserve University

Cleveland, Ohio 44106

Abstract: We discuss various means for using high energy neutrino astronomy to directly test for the existence of cosmic antimatter on a significant cosmological scale. The best future hope for such a test may lie in studies of the ultrahigh energy diffuse neutrino background using acoustic detectors, particularly if high mass Glashow resonances exist. Point source studies are also discussed.

*Research supported in part by the National Science Foundation, Grant No. PHY80-08548

I. Why Look for Cosmic Antimatter with DUMAND?

In a previous paper[1] we have argued the plausibility of expecting a domain structure of baryon and antibaryon excesses to emerge from the early evolution of the big-bang from spontaneous symmetry breaking at the GUT (grand unified theory) level when horizon effects are taken into account. Further work[2,3] has been encouraging, and we feel that a domain type baryon symmetric cosmology provides at least a viable alternative theory to the present orthodox picture where antimatter is assumed to be absent on the macroscopic and astronomical scale.

We therefore feel that one should seriously consider the possibility that we live in a universe where roughly half of the distant galaxies which we see may consist of antimatter. Evidence for such a structure has been given[1,4-6] which we consider to be highly suggestive, but definitive tests remain to be explored. In this regard, we consider that neutrino astronomy is likely to play a key role in the future. This conclusion stems from the basic fact that the photon is its own antiparticle whereas the neutrino is not. Thus, at all wavelengths of the electromagnetic spectrum galaxies and antigalaxies look alike, but such is not the case when one looks with "neutrino telescopes."[7]

The basic physics argument regarding the question of a baryon symmetric versus an asymmetric cosmology hinges on the manner in which CP violation is incorporated into unified gauge theories (and into nature). If the CP violation is spontaneous, it will arise with random sign changes in causally independent regions[2,3] and the universe will naturally split into domains of baryon and antibaryon excesses with no preferred direction of CP symmetry nonconservation. Aside from philosophical and aesthetic considerations, other motivations for considering the CP violation occurs spontaneously have come from problems involving fundamental gauge theory itself.[8]

The basic scenario envisioned for a viable baryon symmetric cosmology is then outlined in Figure 1. This scenario has profound implications for much of astrophysics including the problems of helium synthesis, galaxy formation[5,10] and a viable explanation of the cosmic X-ray background radiation[4,5] as shown in Figure 2. Thus, results of a significant neutrino search for cosmic antimatter would have profound implications for our understanding of the large scale evolution and structure of the universe.

II. Looking for an Antimatter Signature in the Diffuse Cosmic Neutrino Background

In order to discuss the possibility of looking for an antimatter signature in the diffuse cosmic neutrino background, we will draw heavily on calculations of diffuse cosmic neutrino fluxes reported previously.[11] A production mechanism of particular importance in this context because of its large inherent charge asymmetry involves the photoproduction of charged pions by ultrahigh energy cosmic rays interacting with the universal 3K blackbody background radiation[12]. The most significant reactions are

$$\begin{aligned} p + \gamma &\rightarrow n + \pi^+ \\ \bar{p} + \gamma &\rightarrow \bar{n} + \pi^- \end{aligned} \qquad (1)$$

SIMPLEST BARYON SYMMETRIC BIG-BANG SCENARIO

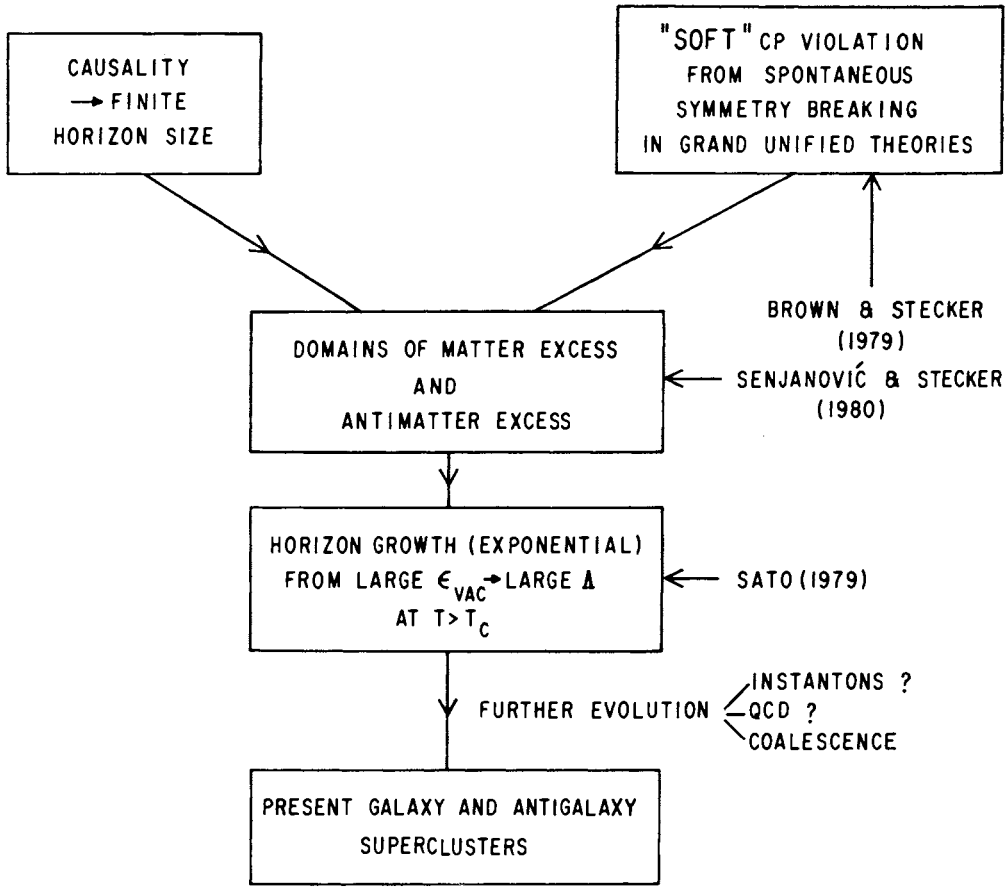

Fig. 1

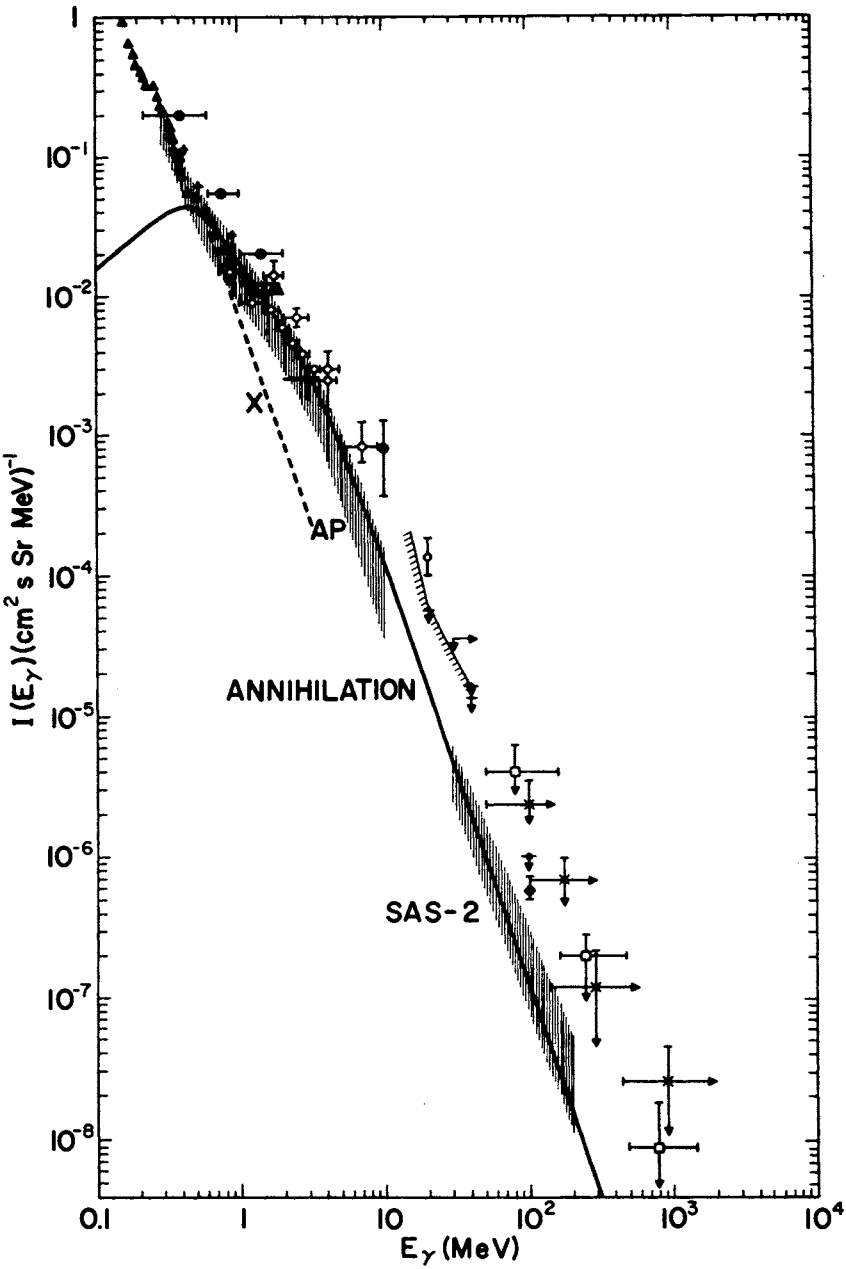

Fig. 2. The cosmic gamma-ray background spectrum predicted for matter-antimatter annihilation in a baryon symmetric big-bang cosmology shown together with Apollo 15 (AP) and SAS-2 satellite data (shading) and upper limits from balloon data. A separate x-ray background component (X) is also shown.

which occur in the astrophysical context principally through the resonance channels

$$\begin{aligned} p + \gamma &\to \Delta^+ \\ \bar{p} + \gamma &\to \bar{\Delta} \end{aligned} \tag{2}$$

because of the steepness of the ultrahigh energy cosmic ray spectrum.[13]

The principal charged pion decay modes are, of course,

$$\begin{aligned} \pi^+ &\to \mu^+ + \nu_\mu \\ &\quad \hookrightarrow e^+ + \bar{\nu}_\mu + \nu_e \\ \pi^- &\to \mu^- + \bar{\nu}_\mu \\ &\quad \hookrightarrow e^- + \nu_\mu + \bar{\nu}_e \end{aligned} \tag{3}$$

The four leptons resulting from pion decay split the pion rest energy almost equally and there is no asymmetry in ν_μ versus $\bar{\nu}_\mu$ production. However, the π^+ decays produce ν_e's where as the π^- decays produce $\bar{\nu}_e$'s . Thus, if one can distinguish ν_e's and $\bar{\nu}_e$'s in one's detector, in principle the diffuse neutrino background can tell us the ratio of ultrahigh energy protons to antiprotons in the universe. (The universe is transparent to ν_e's and $\bar{\nu}_e$'s coming from all observable distances.) It has been pointed out that there is a significant and potentially useful way of distinguishing $\bar{\nu}_e$'s from ν_e's, namely through their interactions with electrons.[14] The ν_e's have an enhanced cross section through formation of weak intermediate vector bosons such as the W^-

$$\bar{\nu}_e + e^- \to W^- \quad , \tag{4}$$

the Glashow resonance effect.[15] For electrons at rest in the observer's system, the resonance occurs for cosmic $\bar{\nu}_e$'s energy

$$E^W = M_W^2/2m_e = 6.3 \times 10^3 \text{ TeV} \tag{5}$$

for $M_W \simeq 80$ GeV corresponding to $\sin^2\theta_W \simeq 0.23$.

For our purposes here, we will not restrict ourselves to this W above, but we will also entertain the possibility of higher mass intermediate vector bosons, B^- (see Brown and Stecker, these proceedings, paper I).

$$\bar{\nu}_e + e^- \to B^- \tag{6}$$

and resonance energies

$$E^B = M_B^2/2m_e > E^W \tag{7}$$

The cosmic and atmospheric fluxes for $\bar{\nu}_e$'s , based on the calculations in Rerefence 11, are shown in Fig. 3. Assuming that there is no significant enhancement in the flux from production at high redshifts, the integral $\bar{\nu}_e$ spectrum from $\nu\bar{p}$ interactions is expected to be roughly constant at 10^{-18} to 10^{-17} $\bar{\nu}_e$'s cm^{-2} sr^{-1} up to an energy of $\sim 2 \times 10^7$ TeV (2×10^{19} eV) above which it is expected to drop steeply. Fig. 3 shows the estimated upper limit (UL) and lower limit (LL). It is expected that the largest competing background flux of $\bar{\nu}_e$'s will be prompt $\bar{\nu}_e$'s from the decay of atmospherically produced charmed mesons. The estimated upper and lower limits for this flux are also shown in Fig. 3 the position of the W^- resonance is indicated by an arrow. It can be seen that a cosmic $\bar{\nu}_e$ signal may be heavily contaminated by prompt atmospheric $\bar{\nu}_e$'s at the resonance energy E^W . The cosmic flux is expected to dominate the higher energies so that the existence of higher mass boson B^- may be critical to any proposed test for cosmic antimatter using diffuse fluxes. In the following discussion, we will assume that such bosons exist. (It may be possible to test for their existence independently using DUMAND (see Brown and Stecker, these proceedings) or future colliding beam accelerators.)

The total cross section is

$$\sigma(\nu_e e^- \to B^- \to \text{all}) = 24\pi \frac{\Gamma \Gamma_\ell}{(s-M_B^2)^2 + \Gamma^2 M_B^2} \tag{8}$$

where Γ is the total width Γ_ℓ the width for a leptonic channel and s is the square of the center-of-mass energy of the $\bar{\nu}_e e^-$ system. The integrated cross section is

$$\int \sigma_{res} ds = 24\pi^2 \frac{\Gamma_\ell}{M_B} \tag{9}$$

Assuming three generations of quarks and leptons, $\Gamma \simeq 12\ \Gamma_\ell$. QCD corrections give a more exact relation

$$\Gamma \simeq 9\ \Gamma_\ell \left(1 + \frac{\alpha s}{\pi}\right) + 3\ \Gamma_\ell \simeq 12.43\ \Gamma_\ell \tag{10}$$

For the W^- resonance

$$\Gamma_\ell = \frac{G_F}{\sqrt{2}} \frac{M_W^3}{6\pi} = 0.226 \text{ GeV} \tag{11}$$

and

$$\int \sigma_W ds = 2.58 \times 10^{-28} \text{cm}^2 \text{ GeV}^2$$

The background event rate per electron (and nucleon) from $\sigma^{\nu_\mu N}$ integrated over the width of the resonance energy

$$\Delta E^W = \frac{M_W \Gamma}{2m_e} \tag{12}$$

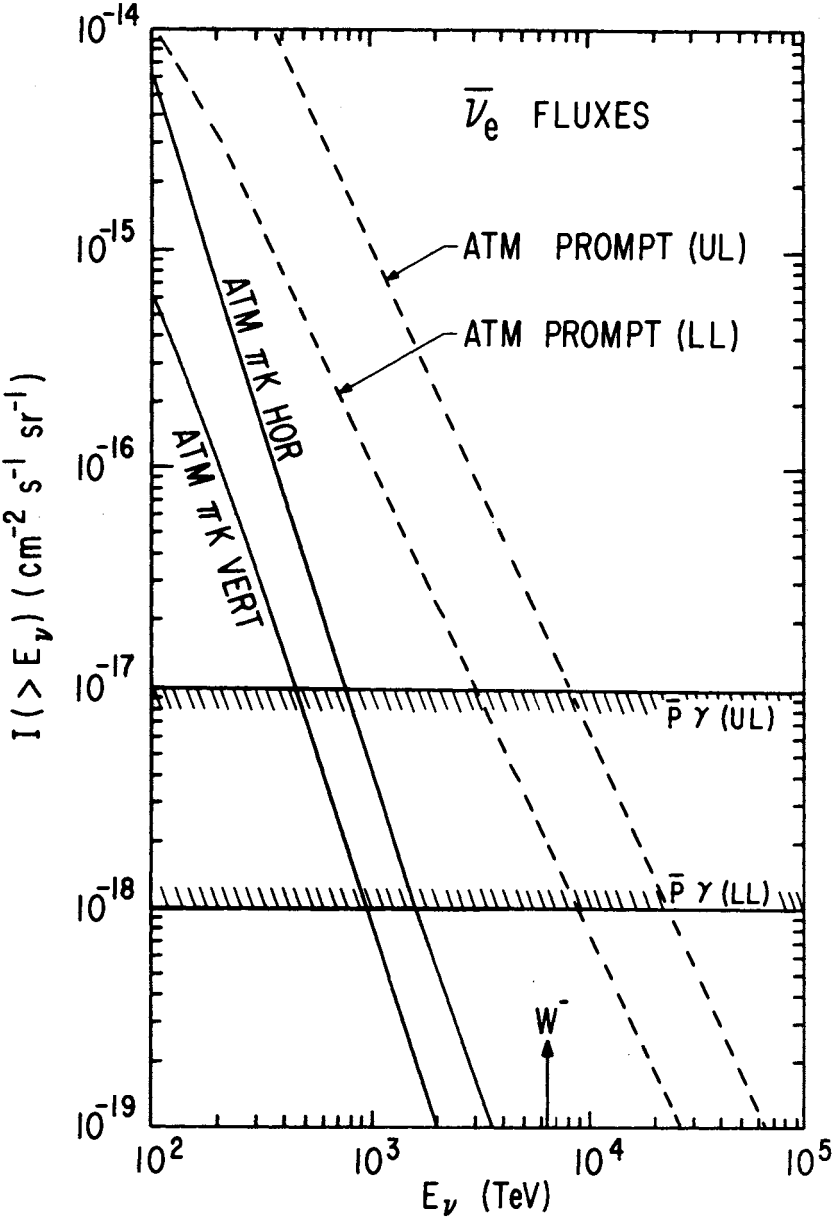

Fig. 3. Cosmic and atmospheric $\bar{\nu}_e$ Fluxes.

provides the "noise" over which the resonance "signal" must be seen. The "signal/noise" ratio is then

$$R = \frac{\int_{\Delta E_W} \sigma_W dE}{\int_{\Delta E_W} \sigma^{\nu N} dE} = \frac{\frac{1}{2m_e}\int \sigma_W ds}{<\sigma^{\nu N}> \frac{M_W \Gamma}{2m_e}} = 24\pi^2 \left(\frac{\Gamma_\ell}{\Gamma}\right) \Big/ M_W^2 <\sigma^{\nu N}> = 3.6 \times 10^3 \qquad (13)$$

For the generalized Glashow resonance B^- where $M_B^2 \equiv \kappa M_W^2$, $\kappa > 1$, we find (see Brown and Stecker, these proceedings)

$$R = \frac{3.6 \times 10^3}{\kappa} \qquad (14)$$

The event rate expected for $\bar{\nu}_e$ induced B^- events is quite low using the "conservative" extimates for the $\bar{\nu}_e$ flux shown in Figure 3. For example, with

$$I^{\bar{p}}_{\bar{\nu}_e} = 10^{-26}\ \text{cm}^{-2}\ \text{s}^{-1}\ \text{sr}^{-1}\ \text{GeV}^{-1}$$

$$\text{and with} \int_{-\Gamma/2}^{\Gamma/2} \sigma_B dE = \frac{1}{2m_e}\int \sigma_B ds \simeq 3 \times 10^{-24}\text{cm}^2\ \text{GeV} \qquad (15)$$

where we have assumed a factor of 10 increase over $\int \sigma_W dE$) we find an event rate

$$r_{B^-} = 4\pi I_{\bar{\nu}_e} N_e \int \sigma_{B^-} dE \simeq 1\ \text{event/yr} \qquad (16)$$

for a 10^{11} ton acoustic detector. (Note: Acoustic detectors can be much more effecient at ultrahigh energies than optical detectors.[17]) However, two points may be noted regarding this low event rate: 1) It may be possible that $I_{\bar{\nu}_e}$ is significantly higher (perhaps $\sim 10^{-25}\,\text{cm}^2\ \text{s}^{-1}\text{sr}^{-1}\text{GeV}^{-1}$) due to cosmic ray production at high redshifts,[18] and 2) No significant signal is expected otherwise (within the level given by equation (15)) unless there is significant $\bar{\nu}_e \leftrightarrow \bar{\nu}_\mu$ mixing. Such a significant $\bar{\nu}_e \leftrightarrow \bar{\nu}_\mu$ mixing is not supported by present data.[19] Also, owing to the very low probability for helicity flipping,[20] $\bar{\nu}_e \leftrightarrow \nu_e$ oscillations, if they occur, will not produce a significant left-handed signal (See Brown & Stecker, these proceedings).

An acoustic deep underwater neutrino detector may provide the best hope for testing for cosmic antimatter by studying the diffuse background neutrinos. The practical threshold for such devices appears to be in the neighborhood of $10^3 - 10^4$ TeV[17], where the W^- resonance occurs. For higher mass resonances B^-, the relevant neutrino resonance energy $E^B \propto M_B^2$ and the effective detection volume $V_{\text{eff}} \propto M_B^6$. Considering that the incident flux is ixpected to be roughly constant up to energies $\sim 2 \times 10^7$ TeV, one gains much in looking for higher mass Glashow resonances at higher energies. Acoustic detectors of effective volume $>>10$ km^3 (10^{10} tons) may be economically feasible and consequently event rates of $\sim 10^2 - 10^4\ \text{yr}^{-1}$ may be attained in time.

III. Looking for Antimatter Signatures in Cosmic Point Sources

The asymmetry in the production of charged pions in matter versus antimatter sources is reflected in cosmic-ray pp and $\bar{p}\bar{p}$ interactions as well as $p\gamma$ and $\bar{p}\gamma$ interactions. Through the principal decay mode (equation (3)), this asymmetry is again reflected in a $\nu_e - \bar{\nu}_e$ asymmetry and thus in the characteristics of events produced in deep underwater neutrino detectors. For ν-sources, these effects may be measurable at energies $\sim$ 1-10 TeV with optical detectors. The details of this possibility have been discussed by Learned and Stecker.[7]

The possibility that $p\gamma$ and $\bar{p}\gamma$ in interactions in cosmic sources would produce significant fluxes of $\bar{\nu}_e$'s , detectable through the $\bar{W}$ resonance, has been suggested by Berezinsky and Ginzburg (these proceedings) as a way of looking for cosmic antimatter. Hopefully, this interesting suggestion will be explored in more detail as our understanding of the nature of cosmic-ray production in compact objects increases. The relevant interactions here would involve $\sim 10^5$ TeV cosmic rays and ultraviolet photons in sufficient quantities.

Another possible $\nu_e - \bar{\nu}_e$ asymmetry which may provide a future test for cosmic antimatter involves lower energy (30-50 MeV) neutrinos produced during the gravitational collapse of astrophysical objects. Neutrinos from gravitational collapse events are expected to exhibit significant $\nu_e - \bar{\nu}_e$ asymmetries[21] which can be used to determine whether the collapsing object consists of matter or antimatter by separately determining the fluxes of ν_e's and $\bar{\nu}_e$'s . However, the bursts expected from a stellar collapse in a neighboring supercluster will be 10^8 times weaker than the $\bar{\nu}_e$ burst previously reported[22], making detection of extragalactic antimatter collapses very difficult unless the masses involved are on a much larger scale.

IV. Conclusion

Neutrino telescopes can be used to distinguish between matter and antimatter sources of cosmic neutrinos and thus provide a direct test of baryon symmetric cosmologies. Perhaps the most promising form of test may lie in studies of ultrahigh energy photomeson-produced neutrinos using acoustic detectors. A two-stage program is suggested in which the existence of heavy Glashow resonances $\bar{B}$ is first independently established.

References

1. R.W. Brown and F.W. Stecker, Phys. Rev. Lett. 43, 315 (1979).
2. K. Sato, Nordita Preprint (1980).
3. G. Senjanović and F.W. Stecker, Physics Letters B, in press.
4. F.W. Stecker, D.L. Morgan, Jr. and J. Bredekamp, Phys. Rev. Lett. 27, 1469 (1971).
5. F.W. Stecker, Nature 273, 493 (1978).
6. F.W. Stecker and R.W. Brown, Proc. Neutrino 79 Intl. Conf., Ed. A. Haatuft and C. Jarlskog, Univ. of Bergen, Norway 2, 409 (1980).
7. J. Learned and F.W. Stecker, Proc. Neutrino 79, ibid. 2, 461 (1980); see also Proc. 1979 DUMAND Summer Workshops, Ed. J. Learned, 274 (1980).
8. M.A.B. Bég and H.S. Tsao, Phys. Rev. Lett. 41 278 (1978); R.N. Mohapatra and G. Senjanović, Phys. Lett. 79B, 283 (1978); H. Georgi, Hadronic J 1, 155 (1978); G. Segré and A. Weldon, Phys. Rev. Lett. 42, 1191 (1979); S.M. Barr and P. Langacker, Phys. Rev. Lett. 42, 1654 (1979).

9. F.W. Stecker, Phys. Rev. Lett. 44, 1237 (1980), see also F.W. Stecker, these proceedings.
10. F.W. Stecker and J.L. Puget, Astrophys. J. 178, 57 (1972).
11. F.W. Stecker, Proc. 1978 DUMAND Summer Workshop, Ed. A. Roberts, Scripps Inst., La Jolla 2, 267 (1979); F.W. Stecker, Astrophysical Journal 228, 919 (1979).
12. The authors thank V.S. Berezinsky (private communication) for bringing this to our attention.
13. F.W. Stecker, Phys. Rev. Lett. 21, 1016 (1968); Astrophys. and Space Science 20, 47 (1973).
14. L.G. Dedenko, V.A. Kuz'min, E.A. Tainov and I.M. Zhelezhnykh, Proc. 1978 DUMAND Summer Workshop, ibid. 2, 81 (1979). V.S. Berezinsky, D. Cline and D.N. Schramm, Phys. Lett. 78B, 635 (1978); K.O. Mikaelian and I.M. Zhelezhnykh, preprint OSU-106 (1980).
15. S.L. Glashow, Phys. Rev. 118, 316 (1960).
16. D. Albert, W.J. Marciano and D. Wyler, preprint COO-2232B-190 (1979).
17. T. Bowen and J.G. Learned, Proc. 16th Int'l Cosmic Ray Conf Kyoto, Japan 10, 386 (1979); H. Bradner and J. Learned, Proc 1978 DUMAND Summer Workshop 1, 227 (1979).
18. V.S. Berezinsky and G.T. Zatsepin, Proc. 1976 DUMAND Summer Workshop, Ed. A. Roberts, Fermilab, p. 215 (1977); See, however, the caveat in F.W. Stecker, Proc. Neutrino 79 Intl. Conference Ed. A. Haatuft and C. Jarlskog Univ. of Bergen, Norway 2, 475 (1980), also Astrophys. J. 228, 919 (1979).
19. A. De Rújula, M. Lusignoli, L. Maiani, S.T. Petcov, and R. Petronzio, Nuc. Phys. B168, 54 (1980).
20. S.L. Shapiro S.A. Teukolsky and I Wasserman, Cornell Preprint CESR-746 (1980).
21. D. Schramm, Proc. 1976 DUMAND Summer Workshop, ibid. p. 87 D.K. Nadyozhin and I.V. Otroshenko, Astron. Zh 57, (1980).
22. K. Lande, G. Bozoki, W. Frati, C.K. Lee, E. Fenyves and O. Saavedra, Nature 251, 485 (1974).

IF INTERMEDIATE WEINBERG-SALAM BOSON WILL NOT BE FOUND ...

V.S.Berezinsky and A.Yu.Smirnov

Institute for Nuclear Research, Academy of Sciences of the USSR.

60th October Anniversary Prospect 7a, Moscow II73I2, USSR.

Abstract

Presented in the paper simple electroweak $SU_2 x U_I x U_I'$-model has a usual fermion sector and a charged W-boson with the mass arbitrary ranged from I00 to 400 GeV. The model is in agreement with all available 4-fermion experimental data. The characteristic observational features appeared in resonant production of ultra heavy intermediate bosons are discussed.

The status of the Weinberg-Salam-Glashow (WSG) model [I] approaches the rank of the full weight theory. This position is a result of the simple structure of the model and its agreement with all available 4-fermion experimental data. More specifically, there are two statements: (I) WSG is the simplest model (i.e. one with the minimal fermion and boson sectors and the smallest number of the free parameters) among those which can correctly describe the observed structure of neutral currents (NC), and inversely, (2) WSG-model can be uniquely derived from phenomenological 4-fermion effective Lagrangian, including NC, if some extra minimizing assumptions are accepted [2].

In the above discussion the indirect confirmation of WSG-model was implied, its direct examination consists in the search for $W^{\pm}$, Z^{0}-bosons with the masses $m_W \approx 80$ GeV and $m_Z \approx 90$ GeV predicted by WSG-model. The future pp, $p\bar{p}$ and e^+e^- - colliding beam experiments [3-6] are to accomplish this goal. The experiments envisage the search for intermediate bosons with the masses as heavy as 300 GeV. In connection with this it is appropriate to ask, whether the absence of W-boson with $m_W < 100$ GeV is theoretically inconceivable? Can the models with the masses as heavy as those anticipated in experimental projects be constructed? In this paper we shall consider more restricted problem of the existence of W-boson with $m_W > 200$ GeV in the framework of the unified gauge models.

We shall present here (i) the simple electroweak $SU_2 \times U_I \times U_I'$-model which agrees with all available 4-fermion data and in which the W-boson mass ranges from 100 to 400 GeV, and (ii) a discussion of the detection of very heavy intermediate bosons.

The general analysis of the common and necessary features of the models with the very heavy W-bosons can be found in ref. [7-9].

i) Description of the model. It has a standard (as in WSG-model) fermion sector with the left components of leptons and quarks transforming as the weak isodoublets and the right components- - as isosinglets. The interaction of charged intermediate bosons with fermions is introduced in a standard way. The interaction of the neutral gauge bosons $W_{3\mu}$, B_μ and B'_μ with NC is described by the Lagrangian

$$\mathcal{L} = i(g \cdot J_3^\mu \cdot W_{3\mu} + \tfrac{1}{2} g_B \cdot Y^\mu \cdot B_\mu + \tfrac{1}{2} g'_B \cdot Y'^\mu_1 \cdot B'_\mu) \ . \qquad (I)$$

In eq.(I) $W_{3\mu}$ is the neutral component of SU_2 triplet, coupling with the current $J_3^\mu = \sum_i \bar{\Psi}_i \gamma^\mu T_3 \Psi_i$ where Ψ_i are the left doublets and T_3 is the generator of SU_2 group. Neutral bosons B_μ and B'_μ associated with Abelian subgroups are coupling with the currents Y^μ and Y_1^μ of the weak hypercharges Y and Y_1, which are related to the electric charge Q as $Y+Y_1 = 2(Q-T_3)$. The hypercharge (Y and Y_1) assignments differ on Higgs sector and coincide ($Y=Y_1$) on fermion sector, providing thus the cancellation of anomalies [IO] .

The Higgs sector (see below) is more complicated than one in WSG-model, with the structure being changed as the masses of the gauge bosons increase. Further on we shall restrict ourselves by the case $m_W \geqslant 200$ GeV, when $\alpha_W = g^2/4\pi >> \alpha_{em}$, though our model includes, of course, the case of lighter intermediate bosons down to the masses of WSG-model.

We shall turn now to the description of NC.

Since the weak constant $\alpha_W >> \alpha_{em}$, one of the couplings g_B or g'_B must be small*). Without loss of generality we can consider the case $g'_B << g, g_B$, when photon is almost a pure state of a gauge field B'_μ . Then within the accuracy $\sim \alpha_{em}/\alpha_W$ the last term in eq.(I) can be neglected. The remaining part of the Lagrangian (I) is equivalent to $SU_2 \times U_1$ -model with two heavy neutral bosons. In the low energy limit Lagrangian (I) produces 4-fermion NC Lagrangian (2) together with the relations given below by eqs.(3)-(6):

$$\mathcal{L}_{eff}^{NC} = 8 \frac{G_F}{\sqrt{2}} \Big\{ (J_{3\mu} - \sin^2\theta_W J_\mu^{em})^+ (J_{3\mu} - \sin^2\theta_W J_\mu^{em}) + \frac{1}{4} \times \cos^4\theta_W Y_\mu^+ Y_\mu \Big\} \qquad (2)$$

where J_μ^{em} is electromagnetic current and

---

*) When both $g_B << g$ and $g'_B << g$ hold, our model gives approximately the predictions of WSG-model with the very small $\sin^2\theta_W$, which is in contradiction with the experimental data.

$$tg^2\theta_W = -\frac{g_B}{g}\,\frac{m_{B3}^2}{m_B^2} \qquad (3)$$

Although $\sin^2\theta_W$ enters the first term in r.h.s. of eq.(2) in the same way as in WSG-model, θ_W in our model is not mixing angle of gauge fields: it is a formal parameter defined by eq.(3) with m_{B3}^2 and m_B^2 being the elements of nondiagonal mass matrix $\hat{M}^2$ in the basis of the gauge fields W_3^μ and B^μ :

$$\hat{M}^2 = \begin{pmatrix} m_3^2 & m_{B3}^2 \\ m_{B3}^2 & m_B^2 \end{pmatrix}. \qquad (4)$$

Parameter x in the Lagrangian (2),

$$x = \left(\frac{g_B}{g}\right)^2 \frac{\det \hat{M}^2}{m_B^4}\,, \qquad (5)$$

is a measure of the difference between $\mathcal{L}_{eff}^{NC}$ of our model and the corresponding NC Lagrangian of WSG-model, given by the first term in r.h.s. of eq.(2)*).

Therefore, we have two free parameters, $\sin^2\theta_W$ and x (accuracy of proximity to WSG-model), for the description of NC data. At x=0.I and $\sin^2\theta_W$=0.20 the difference between the Lagrangian (2) of our model and the corresponding WSG-Lagrangian is small; the comparison of calculated and measured chiral amplitudes are given in Table I

Table I

amplitudes	d_L	u_L	u_R	e_L	e_R
experiment.	-0,43 ± 0,07	0,35 ± 0,07	-0,16 ± 0,06	-0,26 ± 0,06	0,28 ± 0,06
theoret.	-0.444	0.356	-0.176	-0.270	0.264

*) x=0, i.e. det $\hat{M}^2$=0, results in the massless combination of W_3^μ and B^μ, and it brings us back to the WSG-model.

Consider now the Higgs sector.

The essential feature of our model is the unique connection between x and the ratio of m_3 to m_W (the mass of the charged W-boson):

$$\frac{m_3^2}{m_W^2} = \frac{I}{\cos^4\theta_W}\left(I + \frac{I}{x}\,tg^2\theta_W\right) \qquad (6)$$

As the Lagrangian (2) approaches the corresponding WSG-Lagrangian, i.e. as x diminishes, the ratio m_3/m_W increases. In the framework of the Higgs mechanism of the mass generation, the large ratio m_3/m_W can be obtained introducing the Higgs multiplet of a large isospin I. The maximum electric charge Q_m in the I-spin multiplet is bounded /II/ by inequality $2I \geq Q_m \geq m_3^2/m_W^2$. At x=0.I and $\sin^2\theta_W$ =0.2 we obtain $m_3^2/m_W^2 \approx 2.5$ and hence Q_m=3 . Then the Higgs sector of our model includes I=3/2 multiplet ($\Phi^{+++}, \Phi^{++}, \Phi^{+}, \Phi^{o}$), the usual isodoublet (φ^{+}, φ^{o}) and isosinglet χ^{o}. This Higgs structure provides the intermediate boson masses obeing the relation (6).

As far as high order corrections can be neglected, the 4-fermion predictions of the model don't depend on the masses of $W^{\pm}$ - and B-bosons. If the model is specified by a choice $m_B=m_W$, one can find from eqs. (4) and (5) the coupling g_B and the masses of the physical neutral bosons Z_I and Z_2, i.e. those which diagonalize the mass matrix (4), using as before, x=0.I and $\sin^2\theta_W$=0.2 :

$$g_B = 0.064g\,, \quad m_{Z_I} = 0.72m_W\,, \quad m_{Z_2} = I.74m_W \qquad (7)$$

The numerical coefficients in eq.(7) increase with the increasing of the ratio m_B/m_W .

The above consideration is valid when α_W and m_W are small enough. At $m_W \gtrsim$ 300 GeV the naive perturbation parameter $\xi = \alpha_W/2\pi$ exceeds 0.I and the high order terms become appreciable. The account of them break the agreement of the Lagrangian(2) with the experimental data (see the calculations of ref. [8]). In the considered model it results in the limitations $\alpha_W \leq 0.8$ and $m_W \leq 400$ GeV imposed by g^4-terms. At α_W=0.5 (m_W=3I0 GeV) eq.(7) gives m_{Z_I} =220 GeV and m_{Z_2} =540 GeV.

(ii) Detection of superheavy intermediate bosons. The cross-section of $W^{\pm}$-boson resonant production in quark-antiquark collision is shown in fig.I as a function of c.m.-energy for the different masses of W-bosons. As m_W increases the following features appear:

I) The total width of W-boson decay increases as m_W^3 and reaches Γ =I50 GeV at m_W=300 GeV and α_W=0.5, i.e. Γ/m_W becomes ½ .

2) The position $(s/m_W^2)_r$ of resonance peak is shifting to the left from the value s/m_W^2 =I as m_W increases:

$$(s/m_W^2)_r = (I+ \Gamma^2/m_W^2)^{-½}$$

3) The maximum cross-section in the resonance peak diminishes as I/m_W^2 .

The account of high order terms, which is necessary at $m_W \gtrsim 300$ GeV, conserve the same tendencies, and the resonant curves seem to converge to some limiting form, being defined by the Fermi constant G_F alone. This limiting curve is similar to the one in 4-fermion theory with unitary cut-off (eg. see [I2]).

In fig. 2 are shown the resonant cross-sections of $e^+e^- \to Z^0 \to \mu^+\mu^-$ for m_{Z_I} =220 GeV and m_{Z_2} =540 GeV, i.e. for the case m_W=3I0 GeV and α_W=0.5 .The resonant curves are modified in a way described above, as the masses increase.

In summary, the models with large masses of intermediate bosons (m_W > 200 GeV) are conceivable as far as 4-fermion data are concerned. In the sugggested $SU_2 \times U_I \times U_I'$-model the price we pay for the large masses is the complicated Higgs sector with the multicharged (Q=3) particles. The experimental consequences of these models are the linear rise of weak cross-sections (e.g. in νN-scattering) up to (2-5).I0^{-33} cm^2 at $\sqrt{s} \sim$ 200-300 GeV, and the broadening of the resonance peaks ($\Gamma \sim m_W$) in pp- and $p\bar{p}$-scattering.

References

[I] S.Weinberg Phys. Rev. Lett. I9 (I967) I264
A.Salam in: Elementary particle physics (Almquist and Wiksells, Stockholm, I968) p. 367
S.L.Glashow Nucl.Phys. 22 (I96I) 579 .
[2] V.S.Mathur and T.Rizzo Phys.Rev. D I9 (I979) 309, see also ref [9]
[3] C.Rubbia (CERN proposal) Invited talk at EPS Geneva Conf. (I979).
[4] Isabelle proposal BNL report (I97I).
[5] J.B.Adams et al Proc. of LEP Summer Study, CERN 79-0I (I979).
[6] D.Cline Proc. Int.Conf. "Neutrino-78", Purdue, USA (I978) 723 .
[7] V.S.Berezinsky and A.Yu.Smirnov Nuovo Cim. Lett. I9 (I977) 303 .
[8] V.S.Berezinsky and A.Yu.Smirnov Proc. Int. Conf. "Neutrino-78", Purdue, USA (I978) C 254 .
[9] V.S.Berezinsky and A.Yu.Smirnov Yadernaya Fiz. (in Russian) 3I (I980) I55I .

[I0] M.S.Chanowitz, J.Ellis and M.K.Gaillard Nucl. Phys. B I28 (I977) 506 .
[II] D.A.Ross and M.Veltman Nucl.Phys. 95 B (I975) I35 .
[I2] C.C.Chiang and B.B.Dao Nuovo Cim. Lett. I8 (I977) 575
N.Dombey Nature 279 (I979) 675 .

Figure captions

Fig. 1 Cross-section of $\bar{u}+d \to W^- \to e+\bar{\nu}$ as a function of c.m.-energy for WSG-model and for the cases m_W=200 GeV and m_W=300 GeV. The dashed line shows cross-section of $\bar{u}+d \to e+\bar{\nu}$ in 4-fermion theory with a unitary cut off.

Fig. 2 Cross-section of $e^+ + e^- \to Z \to \mu^+ + \mu^-$ for WSG-model and for the $SU_2 \times U_I \times U_I'$-model with m_{Z_I} = 220 GeV and m_{Z_2} = 540 GeV.

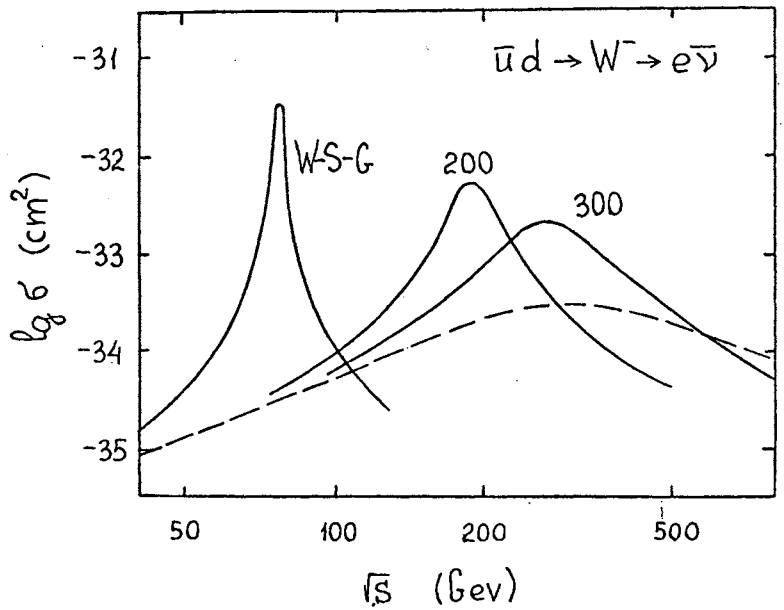
$\bar{u}d \to W^- \to e\bar{\nu}$
W-S-G
200
300
$\log \sigma$ (cm^2)
-31
-32
-33
-34
-35
50
100
200
500
$\sqrt{s}$ (Gev)

Fig. I

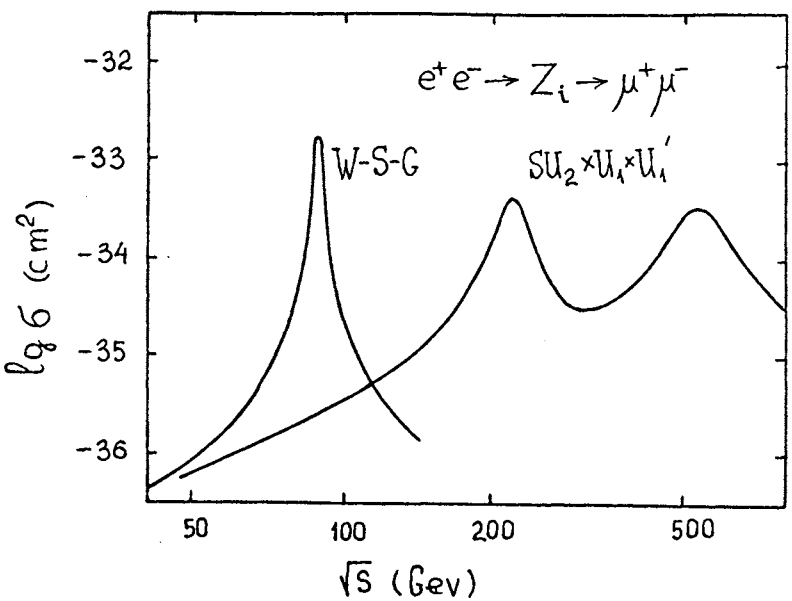
$e^+e^- \to Z_i \to \mu^+\mu^-$
W-S-G
$SU_2 \times U_1 \times U_1'$
$\log \sigma$ (cm^2)
-32
-33
-34
-35
-36
50
100
200
500
$\sqrt{s}$ (Gev)

Fig. 2

SS 433: A Possible Neutrino Source?

David Eichler

University of Maryland

One currently popular model for SS433 invokes an accreting neutron star in a binary system. The gravitational energy released by the accretion apparently goes mainly into the beams, rather than photons that escape the system. That the beams precess coherently suggests that they are guided by magnetic field lines that are grounded in the solid crust of the neutron star. The accreting matter, then, falls to the surface on one set of field lines, and the beams exit on another set. Assuming steady state, matter must flow across field lines. The pressure at which the solid crust liquifies is many orders of magnitude greater than the pressure at which magnetic field lines at the surface of the neutron star ($B \simeq 10^{12}$ gauss) would buckle, suggesting that the accreting matter crosses the field lines above the crust. The final beam velocity ($v=.27c$) is close to the escape velocity from the neutron star surface, suggesting that the fluid switches field lines and lifts off near the surface.

The flow from accretion field lines to beam field lines, in this model, is an important aspect of SS433; however, it is heavily obscured by the accreting matter. Freely falling, spherically symmetric accreting matter would have a column density at a radius R of

$$\int \rho \, dR = 2 \times 10^4 L_{41} (R_{NS}/R)^{1/2} \text{ g cm}^{-2} \qquad (1)$$

where L_{41} is the power in units of 10^{41} erg s^{-1}. (See reference 1 for an estimate of the power and many other parameters.) The effect of radiation pressure is to increase the column density for a given acretion rate at a given radius. This heavy obscuration is no doubt why the energy released by the accretion does not escape as photons. Here, however, we propose that particle acceleration within the high density parts of the flow is not unexpected, and would manifest itself via high energy neutrino production. The neutrinos, of course, would escape, carrying information concerning the site of their production.

It is not unlikely that the flow within the beam is highly variable near its point where it is collimated. One could list a variety of instabilities that might cause such variation. If the flow is unsteady shocks form, and if they are collisionless and of high Mach number they are presumed here to give rise to energetic particles. This scenario is certainly consistent with observations of active galactic nuclei and quasars which display radio jets. That high Mach number collisionless shocks spontaneously produce energetic particles is illustrated by the earth's bow shock, and the assumptions about it here follow simply from scaling up the parameters of the bow shock in the context of simple shock acceleration theory[2].

One concern is that shocks in fluid of large optical depth will be radiation dominated rather than collisionless, and would

thus not produce high energy particles. However, for shocks that form in narrow beams, it is the optical depth across the beam that is the more significant quantity. Indeed it can be shown that the Thompson upscattering of photons that is necessary to produce a radiation dominated shock cannot occur unless the shock is at least $\sim 3\ c/v_s$ photon mean free paths wide, where v_s is the shock velocity. Assuming a beam velocity of .27c, and an opening angle of 1/10 radian, the density $\rho(R)$ of the beam at a radius R from the neutron star is given by

$$\rho(.27c)^3(R/10)^2/2 = L_{41} \times 10^{41}\text{erg/s}. \qquad (2)$$

Assuming a photon scattering grammage G_{ph} of one Thompson scattering depth (as free-free absorbtion here can be neglected) shocks in the beam would be collisionless at

$$R = 2(v_s/c)L_{41}\cdot 10^{12}\text{cm}. \qquad (3)$$

If the neutron star has a dipolar surface field and the field is frozen into the beam material, the magnetic field decreases as R^{-3} out to roughly 10^7cm, where the magnetic stress dominates the beam motion, and thereafter decreases as R^{-2}. Assuming a surface field, at $R=10^6$cm, of 10^{12} gauss, we choose a field beyond 10^7 cm of

$$B = 10^9(10^7\text{cm}/R)^2 \text{ gauss}. \qquad (4)$$

At the radii we are concerned with, this is in principle strong enough to contain particles ranging up to ~ 100 Tev in energy. The maximum energy up to which protons can be accelerated is generally limited by p-p collisions. The condition is that the proton loss time, roughly $G_{cr}/\rho c$, (where G_{cr} is the stopping grammage for relativistic protons) exceed the acceleration time, which can be shown to be on the order of $3Ec/eBv_s^2$. Assuming the material to be just tenuous enough to disallow radiation dominated shocks,

$$R/10 = 3cG_{ph}/v_s, \qquad (5)$$

proton energies would not exceed

$$E_m = eBR(v_s/c)^3 G_{cr}/100G_{ph} \qquad (6)$$

This equation is for reference; obviously, if ρ is lower than that given by (5), E_m can be higher. The other limiting factor on the maximum proton energy, that they not diffuse off to the side of the shock in less than one acceleration time, is a weaker condition than (6) for $v_s/c \approx 1/10$. However, it should be kept in mind that independent of the density, the latter limit constrains the proton energy not to exceed $eBRv_s/10c$.[2]

Note that the column density across the width of the beam is small compared to that along the axis of the beam out to infinity and probably small compared to that of the surrounding accretion column. If the radius of the shock is comparable to c/v_s photon

scattering lengths, photons generated within should be well hidden.

At a distance of 3 Kpc, a luminosity in UHE neutrinos ($E \gtrsim 1$ Tev) of only 10^{35} erg s^{-1} is detectable by DUMAND. This is perhaps only 10^{-6} of the beam power of SS433. More than this amount of power must be dissipated in the line emitting region ($R \sim 10^{15}$cm) to account for the H_α emission.[1] There is likely to be more power being dissipated at smaller scales. It should be noted however, by combining equations (2) through (6), that when L_{41} is of order unity, it is difficult to accelerate protons beyond 1 Tev; the most favorable conditions for a detectable neutrino signal is where L_{41} is of the order 10^{-2}. Under this circumstance, collisionless shocks can form in a high enough magnetic field and low enough densities to allow particle acceleration up to 100 Tev. An UHE neutrino signal from SS433 is still nothing more than a hope, but it would certainly not be a complete surprise, and would indicate that the compact object has a surface field of about 10^{12} gauss.

A strong signal from SS433 could serve as a probe of the density at which they are produced. An absence of electron neutrinos would imply that the muon collision time was less than its decay time, or that $n > 10^{16}$ cm^{-3}. At lower densities, the cutoff in electron neutrinos would be at a correspondingly higher energy, where the muon decay time is longer due to its higher time dilation factor. (Of course, if neutrinos oscillate, this information would be erased.) The spectrum of neutrinos would reflect that of the energetic protons, which might indicate the

size of the production site relative to the proton gyroradius.

SS 433 is a good example of a very powerful accreting object whose remarkable energy budget was unnoticed for many years of X-ray astronomy because the point of energy release lies beneath an optically thick accretion column. There may be many other similar objects that have not yet been discovered. If it is a detectable neutrino source, on the other hand, other objects like it would be detected at once by DUMAND, which is a 4π detector. The most interesting neutrino sources in the sky may be, as was the case with SS433 a few years ago, phenomena that have not yet been thought of.

1. Begelman, M, Sarazin, C, Hatchett, A. Mckee, C. and Arons, J., 1980, Ap. J. 238, 722 (1980).

2. Eichler,D. 1981, Ap.J., 244 (in press).

DUMAND as a τ Detector

John G. Learned
Hawaii DUMAND Center
2505 Correa Road
Honolulu, Hawaii 96822

ABSTRACT

It is pointed out that τ leptons produced with enough energy ($\gtrsim$300 TeV) to travel significant distances before decaying would be uniquely identifiable in a DUMAND array because of their relatively light ionization followed by spectacular decay, usually without emerging muon. Also because τ's never range out, DUMAND will have an effective volume for ν_τ detection that grows with energy making DUMAND a more effective ν_τ than ν_μ detector above $\sim 3 \times 10^{17}$ eV. At $\gtrsim 10^{20}$ eV τ's may traverse the whole earth!

I. DUMAND as a Clean τ Detector

DUMAND may be an excellent instrument for detecting very high energy τ leptons. The τ lifetime is known to be $<2\times10^{-12}$ s[1] and straightforward calculation[2] of the lifetime for its weak decay gives 3×10^{-13} s, which is hard to escape. The mean distance before decay is then

$$L = E\tau c/mc^2$$

or

$$L/E = 1m/18.6\ TeV$$

Thus a τ of energy 300 TeV would travel ~16m, a potentially observable distance in DUMAND. In order to reach DUMAND from production (by a neutrino) at a 2 km distance it would need $\sim4\times10^{16}$ eV, and in order to survive from production in the atmosphere, at a distance of ~20 km overhead, it would need an initial $\sim4\times10^{17}$ eV.

The τ arriving at DUMAND from whatever source would have a unique signature:

a) Low rate of energy loss relative to a muon of the same energy. The τ with mass 1.784 GeV will have loss rate[3], in water of

$$-dE/dx \simeq .3 + E/1000 \quad TeV/km$$

as shown in figure 1.

Thus a τ with just the critical energy (300 TeV) will typically travel ~16 m before decay, giving up ~5 GeV and appearing as a nice near minimum ionizing rate <1 TeV muon, but then decaying in a 300 TeV blaze of glory. A muon starting with 300 TeV would typically give up 1,600 GeV in this distance and even neglecting fluctuations would give up ~500 GeV. It will "never" look like a τ and is distinguished in loss rate by > two orders of magnitude.

In general when a particle suddenly stops in a collision we can measure an energy and compare that with the previously observed loss rate. For muons of high energy (>> 1 TeV)

$$E\mu/\langle dE/dx\rangle\mu \simeq 3.3\ km$$

whereas for τ's it should be observed to be

$$E\tau/\langle dE/dx\rangle\tau \simeq 1000\ km,$$

The difference being just the ratio of masses squared (285). Since the Monte Carlo program has been predicting resolutions in energy of <100% we get easy and complete particle seperation by this measure alone.

b) To add further to the identification, most of the time (80%) the τ

will decay to hadrons or electrons and neutrinos[1]. Thus it will typically end in a cascade with no high energy muon emerging. Muons almost always range out, while τ's never last long enough to ionize to a stop. More precisely, the quantity

$$(dE/dx)_{min} \bullet c\tau/mc^2 = 1320 \text{ for a muon}$$

and $$= 5\times10^{-5} \text{ for a } \tau.$$

Thus a τ is a charged particle that suddenly stops (the probability that a 1000 TeV muon does not survive for at least 1 km is negligible[4].) No other charged particle has this property: other known short lived particles will interact strongly and cascade to a halt within 10 meters of production.

c) Because of the foregoing, this phenomena will only take place for energies above ~20 TeV. Low energy τ's don't go anywhere. Emerging from neutrino interactions, low energy τ's would be indistinguishable (in DUMAND) from electromagnetic and/or hadronic debris. On the upper side in energy, if a τ has more than $\sim5\times10^{16}$ eV it won't be likely to stop in 1 km and we don't see any decay. Thus there are a band of energies for which the golden τ signature applies: namely from $\sim10^{15}$ to 5×10^{16} eV as the τ arrives at DUMAND.

d) A further tag, more difficult to utilize, is the rate of change of dE/dx over the array. For a large DUMAND array (~1 km) high energy muons will on average decrease their dE/dx by ~1/4 between entrance and exit, while τ's will show no significant change.

e) Another tipoff to a throughgoing τ comes from fluctuations in dE/dx. For example a burst of energy too large to have come from a muon of that average dE/dx could signal a τ. A 10^{17} eV τ traversing the array would appear like a 3.5×10^{14} eV muon. However the τ will frequently deposit 3.5×10^{14} eV in a single burst in the array and continue apparently unaffected whereas the muon would be drastically reduced in average dE/dx after such a burst. Calculations are needed to estimate what τ seperation can be achieved by studying these fluctuations, but my guess is that with adequate sampling fairly high seperations are achievable.

In summary, with these five tools to discern μ's from τ's I believe that DUMAND will be useful to detect and identify τ's of energy more than ~300 TeV, the obvious question is are there any such τ's?

II DUMAND as a ν_τ Detector

It is obvious that since the calculated ν_μ flux from the atmosphere would not produce a significant rate of interactions above 300 GeV then we cannot anticipate significant numbers of ν_τ interactions from atmospheric cosmic rays. Only an unanticipated and large increase in direct production above 100 TeV could give an observable atmoshpheric ν_τ flux.

Extraterrestrial neutrino source models do not suggest significant ν_τ fluxes, in comparison to ν_μ and ν_e fluxes. However if neutrinos do oscillate they certainly will have reached equilibrium after travelling astronomical distances, even for the highest energies. As shown in Figure 2, the range of a τ exceeds the range of a μ above $\sim 3 \times 10^{17}$ eV and thus the effective volume for a DUMAND detector for neutrino detection will be larger for ν_τ's than ν_μ's (and ν_e's) above that energy. Indeed the target volume grows to earth dimensions by 10^{20} eV, by which energy I estimate the effective target volume for DUMAND to be $\sim 10^{12}$ tons for ν_τ's. Thus if neutrino oscillations exist (with significant mixing angles) the sensitivity to τ neutrinos will make a substantial addition to DUMAND's neutrino flux sensitivity at ultra high energies.

References

1) Particle data book, April 1980.

2) $\tau_\tau \simeq (m\mu/m\tau)^5 \bullet \tau_\mu \bullet 1/5 = 3.2 \times 10^{-13}$ s

3) The radiation length for muons in water is ~15.5 km. The radiation length for τ's will be ~4,400 km, because the radiation length scales as mass squared. The critical energies are 3.1 TeV and 895 TeV respectively. See D. M. Ritson, Techniques of High Energy Physics, Interscience, New York (1961), p.45.

4) M.G.K. Menon and P.V.R. Murthy, Prog. in Cosmic Ray Physics 9, 1967.

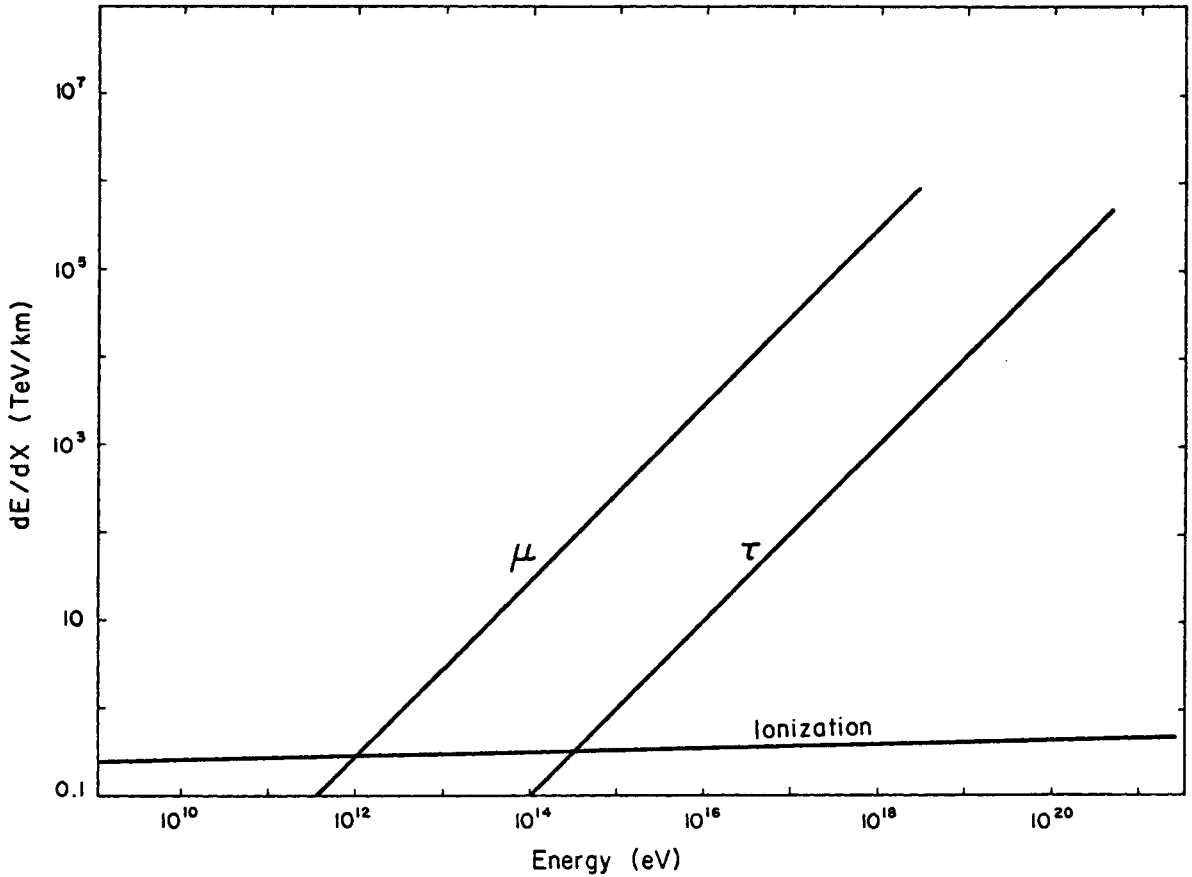

Fig. 1. The energy loss rate of muons and taus in water. The ionization loss rate applies to both particles. Muons begin to radiate at a rate which increases linearly with energy above ∿1 TeV, and taus above ∿300 TeV.

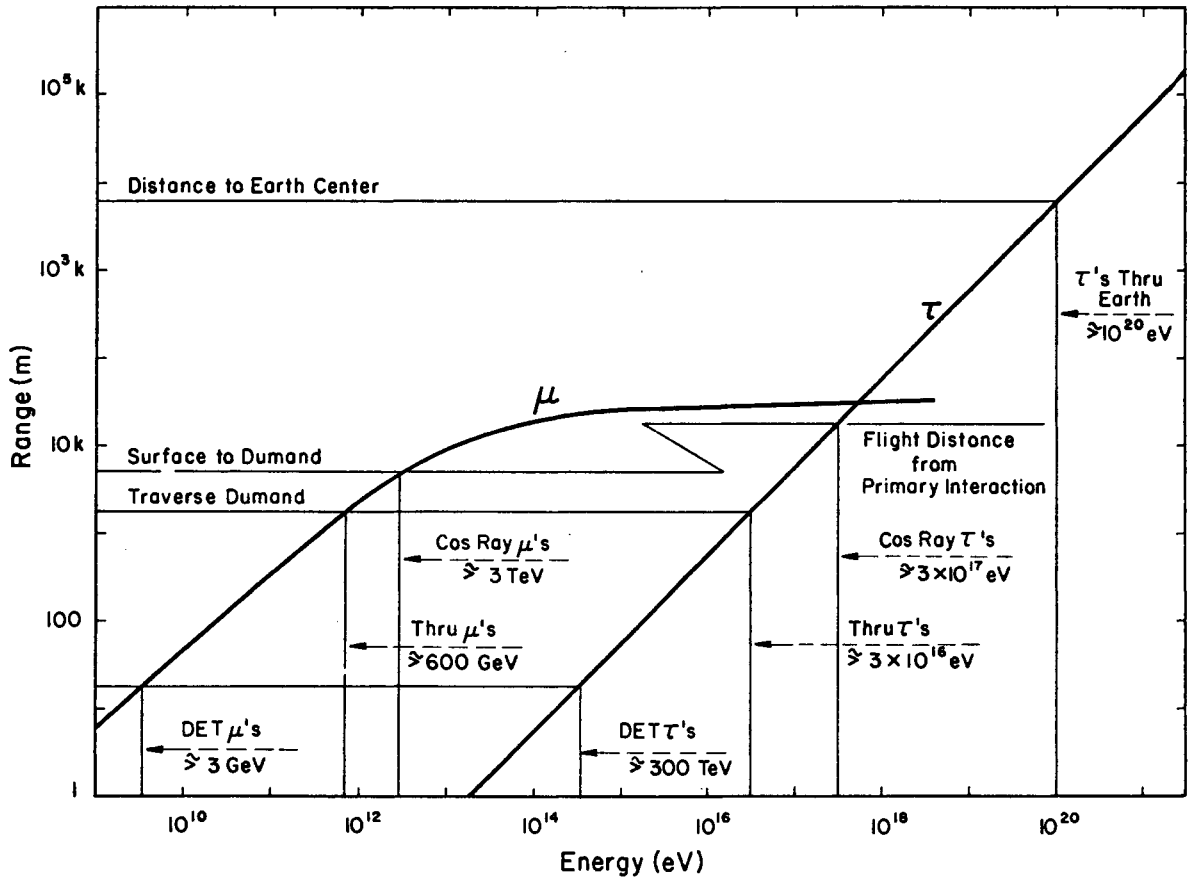

Fig. 2. The range energy relation in water for muons, which almost always come to "rest" before decay, and for taus, which always decay before stopping. Energy thresholds to travel various significant distances are indicated. It is seen that above 3 x 10^{17} eV taus have longer range than muons, while above 10^{20} eV taus may traverse the whole earth.

GAMMA RAY ASTRONOMY AT VERY HIGH ENERGIES

Jonathan E. Grindlay[1]
Harvard-Smithsonian Center for Astrophysics
60 Garden Street
Cambridge, Massachusetts 02138

ABSTRACT

Gamma ray astronomy at very high energies ($\gtrsim$1 TeV) has yielded significant detections of several sources. These results are reviewed and their astrophysical significance as well as relevance to DUMAND is discussed. Several more recent results from both the high energy gamma ray domain as well as x-ray studies are also mentioned in this context. A proposed scheme for renewed observations of gamma ray sources at $\gtrsim$1 TeV with increased sensitivity is described as a worthwhile and yet simple complement to a DUMAND experiment.

---

[1]Alfred P. Sloan Fellow

1. INTRODUCTION

The relatively drawn out birth of gamma ray astronomy has been delayed most by the high backgrounds and low signal levels encountered at gamma ray energies as well as early theoretical estimates of source fluxes which were too optimistic. However, now that the exploratory phase of the topic has detected more than 25 sources--from the lowest energies (~1 MeV) to the highest (~1-10 TeV) and from objects (where identified) as close as the dense ρ Oph cloud of gas and protostars to quasars as distant as 3C273--detailed astrophysical studies will be possible. The development of neutrino astronomy may well undergo a similar evolution.

Perhaps the closest parallels can be drawn between very high energy gamma ray astronomy and neutrino astronomy as envisioned with DUMAND. Both make use of ground-based detection schemes with large geometric areas (though very different effective areas), are limited by cosmic ray-induced backgrounds and can identify cosmic sources from anisotropies in candidate event rates with modest (though quite different) spectral and angular resolution. Very high energy gamma ray astronomy has made considerable progress, which we shall review briefly, but is now in a state of suspension in the United States. Stimulus from the DUMAND program may help to revive a more sensitive program of gamma ray observations.

2. SUMMARY OF VERY HIGH ENERGY GAMMA RAY OBSERVATIONS

It is somewhat surprising how little known are the results, and the methods, of very high energy gamma ray astronomy. Cosmic gamma rays at energies $\gtrsim 10^{12}$ eV have been definitely detected from at least three sources: the pulsar in the Crab nebula, the active radio galaxy Centaurus A (NGC 5128), and the x-ray (binary ?) source Cygnus X-3. These detections are at the highest photon energies, by several orders of magnitude, of any celestial source and provide direct evidence that high energy cosmic rays are produced in a wide range of different objects. Recent reviews of the results and methods used have been given by Grindlay (1976) and Porter and Weekes (1978); we shall briefly summarize these here.

At energies of ~1 TeV, a cosmic gamma ray interacting with the Earth's atmosphere produces an extensive air shower (EAS) of (almost entirely) electromagnetic cascades. The number of electrons in this cascade reaches a maximum at an atmospheric depth of ~300 g cm^{-2} (or ~8 km altitude) where several hundred electrons are expected with energies above the ~100 MeV threshold for production of Cerenkov radiation. The optical Cerenkov photons radiated by these electrons are collimated within ~1-2 degrees about the primary direction so that they are detectable at ground level out to radii of ~100-200 m from the EAS axis. The resulting optical photon density is ~40 m^{-2} in a pulse of duration ~5 nsec. This photon density is very nearly linearly

proportional to the primary gamma ray energy. The simplest detector system for very high energy gamma rays need then only be a light collecting mirror, photomultiplier, and fast-pulse electronics system (amplifier, discriminator, and scaler). Scaled up versions of such systems, either single reflector/detectors or multiple systems operated in coincidence, were used in the many early searches for gamma rays from objects such as the Crab nebula (e.g., Chudakov et al. 1965, Fazio et al. 1972). The upper limits for continuum emission from the Crab at energies of $\sim 10^{11}$ eV (using the large 10 m aperture reflector on Mt. Hopkins) to $\sim 10^{12}$ eV were astrophysically significant for the corresponding limits on the magnetic field in the nebula ($\gtrsim 5 \times 10^{-4}$ gauss). The magnetic field estimates were derived from Compton-synchrotron models (e.g., Rieke and Weekes 1969, Grindlay and Hoffman 1971) in which the gamma rays are produced by inverse Compton scattering of synchrotron photons (optical through x-ray) by their "parent" (synchrotron-radiating) electrons.

Whereas these early experiments did not actively discriminate against the proton (or heavier) cosmic ray-induced EAS, which are otherwise very similar to gamma-ray events when detected by a single detector, several active discrimination techniques have been developed. These have been reviewed in some detail by Porter and Weekes (1978). We shall only mention one such method, the so-called "double beam" technique (Grindlay 1971, 1975a) which lead to the detection of $\sim 10^{12}$ eV gamma rays from two of the sources listed above: the Crab pulsar (Grindlay et al. 1976) and Cen A (Grindlay et al., 1975). By this technique cosmic ray-initiated EAS are selectively identified (with ~80 percent efficiency) by simultaneous detection of the spatially resolvable Cerenkov emission of the electrons at the EAS maximum vs. the penetrating muons relatively close to the detector. These separate components of the Cerenkov light can be identified by a spaced array (~100 m separations) of detectors with narrow (~0.5 degree) fields of view which are pointed to the mean angular positions of the light from the EAS maximum (electrons) and penetrating muons, respectively. The reduced cosmic ray background after rejection of events with detectable muon components, as well as the decreased solid angle for the initial detection at the EAS maximum, combine to yield a factor of ~6 increase in sensitivity over a conventional system. An even larger sensitivity increase is likely for a proposed imaging detection scheme which will be described below (cf. Section 4).

Coincidence arrays of coaligned Cerenkov detectors have also yielded positive results recently. Cygnus X-3, the third certain detection at very high energy gamma rays mentioned above, has been detected by the Soviet group in the Crimea in a long series of observations (Vladimirsky et al. 1973, Neshpor et al. 1979) and has just recently been confirmed by Danaher et al. (1981) using a similar detector system at Mt. Hopkins. The Cyg X-3 gamma ray flux is modulated at the same 4.8-hour period as the x-ray flux and, in fact, the Soviet period determination was for a time more

precise than the x-ray period. The fact that a refined x-ray period was in close agreement with the gamma ray value gave further credence to the Soviet results (Grindlay 1976). A coincidence system was operated by the Iowa State group and resulted in a probable detection of the Crab pulsar (Erickson et al. 1976). Finally, a coincidence array Cerenkov detector system in India, currently the largest in operation, has recently yielded positive detections of both the Crab pulsar (Gupta et al. 1977) and the Vela pulsar (Bhat et al. 1979).

3. RECENT DEVELOPMENTS AND IMPLICATIONS FOR NEUTRINO ASTRONOMY

The positive detections of several gamma ray sources at ~1 TeV require, of course, that at least electrons are accelerated to still higher energies in these objects. It is likely that protons and heavier nuclei are also accelerated in these same objects. Very little spectral information is available so that source radiation mechanisms cannot be specified uniquely. The most complete information is available for the Crab pulsar where the combination of all the positive detections and upper limits (see Porter and Weekes 1978) stronly suggest a flat spectrum with (energy) index $\simeq 1.3$ that is probably a separate spectral component from that seen at gamma ray energies $\lesssim$100 MeV. It is possible that this component is due to curvature radiation from electrons accelerated along the (strong) magnetic field lines near the neutron star and that the lower energy spectrum is due to secondary cascades produced when most of this radiation is annihilated in photon-photon interactions (Sturrock 1971). In this picture the ~1 TeV gamma ray, and lower energy photon spectrum (through ~1 GeV), are produced in electromagnetic processes and not nuclear (e.g., p-p) interactions. Thus, secondary emissions and subsequent decays to neutrinos are not expected. However, the same strong fields that accelerate electrons away from the star will accelerate ions toward the star (polar caps). Neutrino production would then occur at the stellar surface where the very high densities will cause the primary particle energy to be rapidly diffused among particles of a hadronic cascade. The resulting neutrino flux would appear at lower energies and may be a substantial fraction of the incident particle luminosity.

Another possibility for the Crab (and presumably Vela) pulsars is that the very high energy gamma rays are instead produced near the light cylinder. This was suggested by Grindlay et al. (1976) because of the variability in pulse phase and amplitude observed. Such variability is difficult to understand if the radiation is produced near the stellar surface where particle fluxes must be locked rigidly to the strong magnetic field lines. It is interesting that after repeated observations with COS-B, the lower energy (~100 MeV) gamma ray spectrum has also now shown similar variability: during one COS-B observation of the Crab only a single pulse (rather than the main pulse plus

interpulse) was detected (Swanenburg 1980). The x-ray pulses have also shown variability (Ryckman et al. 1975), though much less dramatic, whereas no variations in amplitude or phase have yet been reported for the optical pulses (e.g., Horowitz et al. 1972). This overall behavior suggests to us the following qualitative model, which must be explored in detail: the highest energy gammas arise farthest from the star (perhaps near the light cylinder) where their parent cosmic rays (and electrons) are most able to perturb the confining magnetic field. The particles themselves may be accelerated in a spark gap (e.g., the Ruderman-type models) or perhaps in the shock which must exist at the discontinuity produced at the light cylinder as the primary gammas travel inwards toward the star into increasing magnetic fields. The radiation becomes increasingly stable in phase (and amplitude) as the cascade proceeds and synchrotron radiation from the secondaries in the rigid stellar field accounts for most of the energy loss. In this picture, neutrino production from p-p interactions of the "primary" cosmic rays in lower density regions (in which pions can decay) near the light cylinder might be significant.

The flux of ~1 TeV gamma rays from Cen A (Grindlay et al. 1975) also has important implications for possible neutrino production. Again the distinction between purely electromagnetic and nuclear production models cannot yet be made. If the gammas arise from p-p collisions, then a comparable flux (~50 eV cm^{-2}) of energetic neutrinos should be produced and could be detected by DUMAND (Eichler 1979). On the other hand, a Compton-synchrotron model (Grindlay 1975b) could also account for the gamma ray flux if a component of the x-ray spectrum from Cen A is due to synchrotron emission. Such a model alone would not require an accompanying neutrino flux (although again this cannot be ruled out if cosmic ray protons are accelerated through a dense medium).

Some support for this model has been obtained recently with the discovery that indeed synchrotron radiation is responsible for at least some of the x-ray flux. Schreier et al. (1981) have found that the x-ray jet in Cen A, which was discovered with the EINSTEIN X-ray Observatory, is coincident in extent and shape with a radio jet which they have found at the VLA. The relative spectra make it very likely that a single synchrotron spectrum extends from the radio to the x-ray (~2 KeV). It thus would seem reasonable that if continuing particle acceleration to the required high energies (~100 TeV) occurs in the jet, it also occurs in the nucleus as required for the Compton-synchrotron models.

Further observations, and correlated radio-x-ray and gamma ray variability (or limits) are required to establish the origin of the gamma ray flux. We note that a lower limit to the high energy neutrino flux can be derived from the known column density of matter to the central x-ray source (assumed coincident, or exterior to, the gamma ray source). This column density is

derived from the low energy absorption of the x-ray spectrum and is approximately 10^{23} cm^{-2}. Thus, photo-pion production should yield a neutrino luminosity of $\gtrsim 10^{-5}$ times the high energy gamma ray luminosity ($\simeq 10^{41}$ erg s^{-1}).

Finally, a similar physical system on a much-reduced scale might be embodied in SS433. X-ray jets (or lobes) have been discovered by EINSTEIN recently for this unusual source also (Seward et al. 1980) and again a synchrotron model is viable. If so, the required cosmic ray acceleration in the diffuse lobes might interact with relatively more dense material in the shock formed by the collimated matter beams from the central object. Neutrinos would then be produced although (in this scenario) with low fluxes. The beams themselves are sub-relativistic and thus not directly able to yield a neutrino flux.

4. FUTURE DEVELOPMENTS

Very high energy gamma ray astronomy is now at a standstill in the United States with no active program of observations, despite the promising results obtained. The Soviet and Indian groups continue to be active in the field, though using "conventional" techniques as mentioned above. A new and much more sensitive detection scheme has been proposed by T.C. Weekes at Mount Hopkins (SAO) and a collaboration including V. Stenger and J. Learned from the DUMAND team. This would make use of an array of photomultipliers at the focus of the 10 m reflector (and, eventually, other large reflectors in coincidence) to image the Cerenkov light flash. The arrival detection could be determined quite accurately ($\lesssim 0.3°$) anywhere within a moderately large field of view by analysis of the ellipticity of the light flash images. This allows a generalization of the double beam method by, essentially, measuring the angular distribution of each event individually. Protron primaries can be distinguished from gamma ray events and at lower primary energies than with the double beam method since more information is available. The method is, however, limited, of course, by fluctuations from event to event. This must be studied more carefully with simulations but can probably be overcome ultimately by multiple sampling of the Cerenkov light pool by an array of large reflectors with imaging detectors. The simultaneous observation of source and background increased angular resolution, and, background rejection combine to yield an overall factor of ~20 sensitivity increase.

Another significant development is the theoretical realization (based on EAS simulations by Turver) that the ~10-100 GeV energy band can be observed with a greatly reduced cosmic ray background. This is due to the fact that the Cerenkov light production of proton-initiated EAS decreases sharply below its asymptotic fraction (~0.4) of that for gamma ray initiated events as the primary energy decrease below ~100 GeV. This would, in turn, enable complete overlap with satellite experiments such as Gamma Ray Observatory which would have comparable sensitivity

below 10 GeV. Gamma ray observations at the greatly increased sensitivities available with an imaging Cerenkov detector could detect sources at much fainter fluxes so that (scaling from the history of x-ray astronomy) hundreds of sources would likely be detectable. These would, in turn, provide enormous stimulus to searches for accompanying neutrino emission by DUMAND.

REFERENCES

Bhat, P. et al. 1979, Proc. 16th International Cosmic Ray Conference, Kyoto, 1, 138.

Chudakov, A., Dadykin, V., Zatsepin, V. and Nesterova, N. 1965, Trans. Consultants Bureau, 26, 99.

Danaher, S., Fegan, D., Porter, N. and Weekes, T. 1981, preprint.

Eichler, D. 1979, Ap.J., 232, 106.

Erickson, R., Fickle, R. and Lamb, R. 1976, Ap.J., 210, 539

Fazio, G., Helmken, H., O'Mongain, E., Rieke, G. and Weekes, T. 1972, Ap.J.(Letters), 175, L-117.

Grindlay, J.E. 1971, Nuovo Cimento, 2B, 119.

Grindlay, J.E. 1975a, Phys. Rev. D, 11, 517.

Grindlay, J.E. 1975b, Ap.J., 199, 49.

Grindlay, J.E. 1976, Proc. Symposium on Gamma Ray Astronomy and Galactic Structure, Goddard Space Flight Center, NASA publication CP-002, pp. 81-98.

Grindlay, J. and Hoffman, J. 1971, Astrophysical Letters, 8, 209.

Grindlay, J., Helmken, H., Hanbury Brown, R., Davis, J. and Allen, L.R. 1975, Ap.J.(Letters), 197, L-9.

Grindlay, J., Helmken, H. and Weekes, T. 1976, Ap.J., 209, 592.

Gupta, S., Ramana Murthy, P., Sreekantan, B., Tonwar, S. 1977, Proc. 15th International Cosmic Ray Conference, Plovdiv, 1, 114.

Horowitz, P., Papaliolios, C., and Carleton, N. 1972, Ap.J., 172, 251.

Neshpor, Yu, Stepanian, A., Fomin, V., Gerasimov, S., Vladimirsky, B. and Ziskin, Yu, Astrophys. and Space Sci., 61, 349.

Porter, N.A. and Weekes, T.C. 1978, Smithsonian Astrophysical Observatory, Special Report No. 381.

Riecke, G. and Weekes, T. 1969, Ap.J., 15, 577.

Ryckman, S. et al. 1975, IAU Circular No. 2760.

Seward, F., Grindlay, J., Seaquist, E., and Gilmore, W. 1980, Nature, 287, 806.

Schreier, E., Feigelson, E., and Burns, J. 1981, preprint.

Sturrock, P.A. 1971, Ap.J., 164, 529.

Swanenburg, B.N. 1980, Talk at 10th Texas Symposium, Baltimore.

Vladimirsky, B., Stepanian, A., and Fomin, V. 1973, Proc. 13th International Cosmic Ray Conference, Denver, 1, 456.

Rapporteur Talk: Astrophysics and Cosmology

David Eichler

University of Maryland

There was a very diverse group of astrophysical papers presented at this meeting, and I will not attempt to review all of them. The list of possible astrophysical neutrino sources has not really changed since the DUMAND meeting two years ago, with the exception of SS433, which is discussed below. Also, the relationship between UHE neutrino astronomy and gamma ray astronomy was discussed extensively at that meeting. In this discussion, I will concentrate on the new ideas that have surfaced since then. At the risk of acting too opinionated, I will also mention points that were not made at this conference that I thought perhaps should have been.

First, there are the curious relationships between neutrino physics, neutrino astronomy, and cosmology. As we have heard, the neutrino may have a mass of order 10 eV. While I am not qualified to comment on the experimental side of the problem, I do agree with Schramm and Steigman, who argued here that there is much astrophysical motivation for believing in such a neutrino mass. In fact, the possibility of neutrino masses in the 1 to 100 eV range was discussd by Cowsik and McClelland[1] in 1972, and their motivation was largely astrophysical. The point is simply that there appears to be a significant amount of matter outside (the visible part of) galaxies, probably more than is inside them, and there are difficulties with assuming that this mass is in the form of baryons. The nucleosynthesis arguments restrict the baryon content of the universe to not much more that what is inside galaxies, and there are other (perhaps weaker) astrophysical arguments against putting the unseen component in the form of baryons. The Helium abundance argument

for the low baryon density standard cosmological model was controverted by Stecker. If there is still some disagreement among observers concerning the cosmological Helium abundance (or agreement among them that it is too low for the standard model), it should be remembered that the older arguments concerning the difficulties of post-big-bang deuterium production[2,3] still remain on firm ground. In the spirit of connecting neutrino asstronomy with cosmology, it should be remembered that the Reines experiment plays a role in the argument against post-big-bang deuterium production, since it rules out such production by very high energy spallation reactions.

Another connection between neutrinos and cosmology is the fact that extragalactic neutrinos represent the only direct way of determining whether the universe is baryon symmetric (Stecker and Brown, these proceedings and references therein). Stecker has in fact argued that local, acausal CP violation in the early universe could create a domain structure of matter and antimatter cells. The present domain size suggested by Stecker on astrophysical grounds, $\sim 10^8$ pc, has yet to be derived in any way from first principles.

Much attention was given to UHE gamma ray astronomy, and its relation to neutrino astronomy. As pointed out by Shapiro, Silberberg, and myself, gamma rays may not escape many of the dense, compact environments where UHE neutrino production has been hypothesized to occur, e.g. quasars, active galactic nuclei. On the other hand, gamma rays can be produced by processes that yield no neutrinos.

The possibility of "hidden" neutrino producing regions, from which photons do not directy escape, has been given added credibility by the discovery of SS433. The power of this remarkable object is estimated by some theorists[4] to be as high as 10^{41} erg s^{-1}, making it more than 1000 times as

powerful as the brightest known stellar object in the galaxy. That it remained undiscovered until recently is presumably because the enormous quantity of accreting material that powers the object is opaque to the photons generated within it. The enormous power of SS433 is further cause for optimism: If its luminosity is indeed as high as 10^{41} erg s^{-1}, only 10^{-6} of its power need emerge in the form of UHE neutrinos to be detected by DUMAND.

While neutrino and UHE gamma ray astronomy intersect only partially, one point concerning the latter cannot be overemphasized: It is in the interest of the DUMAND project that UHE gamma ray astronomy be developed, because it may turn up sources that are almost certainly from pion decay, which could then be considered highly probable neutrino sources. For example, we suggested that supernovae occurring in or near dense clouds in the galaxy could be UHE neutrino sources Recently there has been some speculation[5] that the point gamma ray sources ($E \approx 100$ Mev) detected by Cos B are indeed from supernova remnants in regions of young star formation. Clearly they should be studied at ultrahigh gamma ray energies. Emission above 1 Tev depends so sensitively on the slope of the cosmic ray spectrum that extrapolations from lower energies are extremely unreliable. However, UHE gamma-ray observations would eliminate the need for them.

I hope, therefore, that this meeting provided a forum (even though that was not the primary purpose) for publicizing the virtues of UHE gamma ray astronomy. As Sturrock has noted on various occasions, the pulsed UHE gamma rays from the Crab pulsar set interesting constraints on pulsar models, As noted here by Grindlay, there is much room for improvement in the sensitivity in UHE gamma ray detection. One source that may be lying just below current sensitivity is DC emission from the Crab nebula due to inverse Compton scattering. Detailed models of the Crab nebula, such as the one presented

here by Kennel, generally make predictions concerning this DC emission, so they are subject to observational tests, and are possibly constrained already by existing upper limits.

I am not qualified to review the discussion of neutrinos from gravitational collapse. My impression, however, is that the waiting time for collapses in our galaxy is still on the order of twenty years, and that there is still no hope of detecting neutrinos from extragalactic stellar collapse. One justification, however, for waiting patiently for the next stellar collapse in our galaxy is that observing the width of the neutrino pulse at earth could serve as a measurement of the neutrino rest mass.

There has been discussion of a mini-DUMAND. Learned reminded us that the proton decay experiment will have an effective neutrino collection mass, at neutrino energies above 1 Tev, of about 10^6 tons. This is about an order of magnitude better than Reines' South Africa experiment. Sensitivity can be enhanced further if there is energy resolution, as the extraterrestrial contribution is most likely to stand out above 1 Tev, where the atmospheric contribution is negligible. The basic principle of neutrio detection is particularly applicable to mini-DUMAND's: The more mass the better.

1. Cowsik, R. and McCelland, J,. 1972, Phys. Rev. Lett., 29, 669.
2. Epstein, R.I., Lattimer, J.M. and Schramm, D.N., 1976, Nature, 263, 198.
3. Eichler, D. 1979, Ap. J., 229, 39.
4. Begelman, M.C., Sarazin, C.L. Hatchett, S.P., Mckee, C.F., Arons, J., 1980, Ap. J. 238, 722 (1980).
5. Montemerle, T. 1979, Proc. of the 16th ICRC at Kyoto, OG1-20.

Appendix I

APPENDIX I

DUMAND 1980 ATTENDEES

Prof. O. C. Allkofer
Inst. fur Kernphysik
University of Kiel
Olshausenstrasse 40-60
23 Kiel, WEST GERMANY

Dr. Jim Andrews
Oceanography Department
University of Hawaii at Manoa
2565 The Mall, PSB 312
Honolulu, Hawaii 96822

Mr. John F. Babson
Department of Physics and Astronomy
University of Hawaii at Manoa
2505 Correa Road, WAT 434
Honolulu, Hawaii 96822

Dr. E. Bellotti
INFN and University - Milan
Istituto di Fisica dell Universita
16, Via Celoria
20133 Milano, ITALY

Mr. Grant Blackinton
University of Hawaii at Manoa
2525 Correa Road, HIG 154
Honolulu, Hawaii 96822

Dr. Theodore Bowen
Department of Physics
University of Arizona
Tucson, Arizona 85721

Dr. Hugh Bradner
Scripps Institution of Oceanography
IGPP, A-025
University of California, San Diego
La Jolla, California 92093

Mr. Tim Brown
Department of Physics and Astronomy
University of Hawaii at Manoa
2505 Correa Road, WAT 435
Honolulu, Hawaii 96822

Dr. Robert Burman
MP Division, MS846
Los Alamos Scientific Lab
P. O. Box 1663
Los Alamos, New Mexico 87545

Dr. Ugo Camerini
Department of Physics
University of Wisconsin
1150 University Avenue
Madison, Wisconsin 53706

Dr. David Cline
Department of Physics
University of Wisconsin
Madison, Wisconsin 53706

Dr. Stirling Colgate
Los Alamos Scientific Lab
MS-210
P. O. Box 1663
Los Alamos, New Mexico 87545

Prof. Marcello Conversi
Inst. Naz. Fis. Nucl.
Viale Regina Elena, 299
I-00161 Roma, ITALY

Dr. John P. Craven
Marine Programs
University of Hawaii at Manoa
Holmes 401
Honolulu, Hawaii 96822

Mr. E. Creutz
Bishop Museum
P.O. Box 19000-A
Honolulu, Hawaii 96819

Prof. Ray Davis
Brookhaven National Laboratory
Physics Department
Upton, New York 11973

Dr. David Eichler
University of Maryland
310 Dennis Avenue
Silver Spring, Maryland 20901

Dr. Jerry Elbert
Department of Physics
University of Utah
Salt Lake City, Utah 84103

APPENDIX I

DUMAND 1980 ATTENDEES

Dr. Bradley Filippone
Argonne National Lab., Bldg. 203
9700 S. Cass Avenue
Argonne, Illinois 60439

Dr. Peter Grieder
Physikalisches Institut
University of Bern
Sidlerstr. 5
CH-3013 Bern, SWITZERLAND

Dr. Jonathan Grindlay
Center for Astrophysics
Harvard University
60 Garden Street
Cambridge, Massachusetts 02138

Prof.Dr. Claus Grupen
Department of Physics
Siegen University
Holderlinstrasse 3,
5900 Siegen 21, WEST GERMANY

Mr. W. Paul Guinn
Department of Physics and Astronomy
University of Hawaii at Manoa
2505 Correa Road, WAT 109
Honolulu, Hawaii 96822

Dr. Arthur Halprin
Department of Physics
University of Delaware
Newark, Delaware 19711

Dr. Francis Halzen
Department of Physics
University of Wisconsin
1150 University Avenue
Madison, Wisconsin 53706

Dr. Tatsuro Hayashi
Hamamatsu TV Co.
1126-1 Ichino-cho
Hamamatsu City, 435 JAPAN

Prof. An-Xiang Huo
High Energy Physics Institute
Academia Sinica
P.O. Box 918 Peking
THE PEOPLE'S REPUBLIC OF CHINA

Dr. Yin-Lin Jiang
Institute of High Energy Physics
Academia Sinica
P.O. Box 918 Peking
THE PEOPLE'S REPUBLIC OF CHINA

Dr. Demosthenes Kazanas
Code 660
NASA, Goddard Space Flight Center
Greenbelt, Maryland 20771

Dr. Charles F. Kennel
Department of Physics
University of California
Los Angeles, California 90024

Prof. Takashi Kitamura
Inst. for Cosmic Ray Research
University of Tokyo
Midori-cho, Tanashi-shi
Tokyo 188, JAPAN

Mr. Alan Koide
Department of Physics and Astronomy
University of Hawaii at Manoa
2505 Correa Road, WAT 224
Honolulu, Hawaii 96822

Dr. William R. Kropp
Department of Physics
University of California
Irvine, California 92717

Dr. Kenneth Lande
Department of Physics
University of Pennsylvania
Philadelphia, Pennsylvania 19104

Prof. John G. Learned
Department of Physics and Astronomy
University of Hawaii at Manoa
2505 Correa Road, WAT 329
Honolulu, Hawaii 96822

Prof. Ernest Ma
Department of Physics and Astronomy
University of Hawaii at Manoa
2505 Correa Road, WAT 438
Honolulu, Hawaii 96822

APPENDIX I

DUMAND 1980 ATTENDEES

Dr. John W. MacKenty
Institute for Astronomy
2680 Woodlawn Drive, C-102
Honolulu, Hawaii 96822

Dr. Robert March
Department of Physics
University of Wisconsin
Madison, Wisconsin 53706

Dr. T. J. Mazurek
Department of Physics
State University of New York
Stony Brook, New York 11794

Dr. Don McGibney
Department of Physics and Astronomy
University of Hawaii at Manoa
2505 Correa Road
Honolulu, Hawaii 96822

Mr. Frank McHale
Dillingham/Hawaiian Dredging
614 Kapahulu Avenue
Honolulu, Hawaii 96815

Dr. Karnig Mikaelian
Department of Physics
Oklahoma State University
Stillwater, Oklahoma 74078

Prof. Saburo Miyake
Director, Cosmic Ray Laboratory
University of Tokyo
Midori-cho, Tanashi-shi
Tokyo 188, JAPAN

Mr. Dan O'Connor
Department of Physics and Astronomy
University of Hawaii at Manoa
2505 Correa Road, WAT 436
Honolulu, Hawaii 96822

Dr. Keith Olive
University of Chicago
5640 S. Ellis Ave.
Chicago, Illinois 60637

Dr. Sandip Pakvasa
Department of Physics and Astronomy
University of Hawaii at Manoa
2505 Correa Road, WAT 440
Honolulu, Hawaii 96822

Dr. Antares Parvulescu
University of Hawaii at Manoa
2525 Correa Road, HIG 441
Honolulu, Hawaii 96822

Mr. Joseph Pavlat
c/o Compumotor Corporation
P. O. Box 2928
Petaluma, California 94952

Dr. Fred Reines
Department of Physics
University of California
Irvine, California 92717

Dr. Leo Resvanis
Physics Laboratory
University of Athens
104 Solonos Street
Athens 144, GREECE

Dr. Arthur Roberts
Department of Physics and Astronomy
University of Hawaii at Manoa
2505 Correa Road, WAT 330
Honolulu, Hawaii 96822

Prof. Ray Sawyer
Center for Theoretical Physics
University of California
Santa Barbara, California 93106

Dr. David Schramm
University of Chicago
AAC-100
5640 S. Ellis
Chicago, Illinois 60637

Dr. Maurice Shapiro
Code 4020
Naval Research Lab
Washington, D. C. 20375

APPENDIX I

DUMAND 1980 ATTENDEES

Dr. Rein Silberberg
Lab for Cosmic Ray Physics
Naval Research Lab
Code 4028
Washington, D. C. 20034

Prof. Gary R. Smith
Department of Physics
University of Manitoba
Winnipeg, Manitoba
R3T3T3 CANADA

Dr. Henry W. Sobel
Dept. of Physics
University of California
Irvine, California 92717

Dr. Floyd W. Stecker
Code 660
Goddard Space Flight Center
Greenbelt, Maryland 20771

Dr. Gary Steigman
Bartol Research Foundation
University of Delaware
Newark, Delaware 19711

Dr. Richard Steinberg
Department of Physics
University of Pennsylvania
Philadelphia, Pennsylvania 19104

Dr. Victor J. Stenger
Department of Physics and Astronomy
University of Hawaii at Manoa
2505 Correa Road, WAT 230
Honolulu, Hawaii 96822

Dr. Alan Stockton
Institute for Astronomy
2680 Woodlawn Drive, C-217
Honolulu, Hawaii 96822

Dr. P. A. Sturrock
Institute of Plasma Research
Stanford University
Stanford, California 94305

Mr. Andrew Szentgyoizgyi
Department of Physics
University of Wisconsin
1150 University Avenue
Madison, Wisconsin 53706

Dr. Howard Talkington
Code 52
Naval Ocean Systems Center
San Diego, California 92152

Ms. Tina Tanaka
Department of Physics and Astronomy
University of Hawaii at Manoa
2505 Correa Road, WAT 205
Honolulu, Hawaii 96822

Mr. Geoffrey Taylor
Department of Physics and Astronomy
University of Hawaii at Manoa
2505 Correa Road, WAT 225
Honolulu, Hawaii 96822

Mr. Jack D. Thomson
Engineer Mgr., SEACO, Inc.
146 Hekili Street
P. O. Box 1171
Kailua, Hawaii 96734

Dr. Ira Wasserman
Space Science Bldg.
Cornell University
Ithaca, New York 14853

Dr. J. Craig Wheeler
Department of Astronomy
University of Texas
Austin, Texas 78712

Mr. A. G. Wright
EMI Electron Tubes
Bury Street, Ruislip
Middlesex, HA4 7TA,
ENGLAND

Dr. Ron Zaneveld
School of Oceanography
Oregon State University
Corvallis, Oregon 97331